



# Durham E-Theses

---

## *Analytical studies on channel forming proteins*

Ennaceur, Susan Mary

---

### How to cite:

Ennaceur, Susan Mary (2006) *Analytical studies on channel forming proteins*, Durham theses, Durham University. Available at Durham E-Theses Online: <http://etheses.dur.ac.uk/2620/>

---

### Use policy

The full-text may be used and/or reproduced, and given to third parties in any format or medium, without prior permission or charge, for personal research or study, educational, or not-for-profit purposes provided that:

- a full bibliographic reference is made to the original source
- a [link](#) is made to the metadata record in Durham E-Theses
- the full-text is not changed in any way

The full-text must not be sold in any format or medium without the formal permission of the copyright holders.

Please consult the [full Durham E-Theses policy](#) for further details.



Department of Chemistry

# Analytical Studies On Channel Forming Proteins

Susan (Sue) Mary Ennaceur

The copyright of this thesis rests with the author or the university to which it was submitted. No quotation from it, or information derived from it may be published without the prior written consent of the author or university, and any information derived from it should be acknowledged.

For the degree of Doctor of Philosophy  
2006



29 NOV 2006

Let's face it, I have often felt like screaming during my Ph.D and oh would I have done so with such sheer joy, but for fear of being taken away by men in white coats and there are many of those lurking in the chemistry department.

I have often thought that the best relief would have been to find a hill to run down whilst screaming at the top of my voice. The hill would have had to be cardiac hill for all the times I arrived up in biology out of breath and for all the frustration felt when things just would not work out the way I hoped they would, but running down that hill would only have scared away the squirrels that Stuart hates so much.

The elation experienced when projects went beyond my dreams was such that the balance always swayed towards the positive side and to have the company of the sweetest, nicest and most fantastic people, I have ever had to work with and probably ever will, was an experience that I could never forget.

To all those, who were patient, tolerant and just so helpful towards me and to those who have become my friends, I give thanks with all my heart.

Thank you!

Sue

**Title of Ph.D thesis: Analytical studies on channel forming proteins.**

**Sue M. Ennaceur**

**Abstract.** Antimicrobial peptides have shown great potential as pharmaceutical agents, they are being considered for their ability to fight bacterial and fungal infections and even to destroy cancerous cells by disrupting the cell membranes of their targets. A clear understanding of the mechanism behind their activity and how this is related to their structure is therefore essential if these peptides are to be considered as precursors for the next generation of a new range of drugs.

This research project has been involved in the development of a series of analogous model amphiphilic cyclic peptides, which were designed to adopt a  $\beta$ -sheet conformation on inserting into lipid membranes. The model peptides were examined using a wide range of analytical techniques; these studies have enabled both the propensity of these peptides to adopt transmembrane  $\beta$ -sheet structures to be established and to gain some understanding of their behaviour under different environments. Circular dichroism and its sister technique linear dichroism have shown both the structure and the orientation of the peptide backbone on insertion into lipid membranes. Calorimetric studies have demonstrated the extent of the cyclic peptide disruption on the phase transition of saturated and unsaturated phospholipid membranes and electron microscopy has revealed the ability of one of the model peptides to form fibrous structures on precipitation from a solution of the fluorinated alcohol, hexafluoroisopropanol (HFIP) in water.

A natural  $\beta$ -sheet forming protein, the C-terminal domain of the autotransporter protein BrKA from *Bordetella pertussis* was overexpressed to provide a comparison for the model  $\beta$ -sheet peptides. Attempts were made to grow highly ordered 2D arrays of the protein in phospholipid membranes for structural analysis by both transmission electron microscopy and atomic force microscopy.

The effect of the fluorinated alcohol HFIP, which was used to solubilise the amphiphilic peptides, was examined on phospholipid systems. The study was considered to afford some understanding towards the integration of small molecules into membranes.



## Declaration

I, Sue M. Ennaceur, hereby certify that this Ph.D thesis “Analytical studies on channel forming proteins.” has been written by me, that it is the recorded work carried out by me from October 2002 until October 2005 and that it has not been submitted in any previous application for a higher degree.

Date...17/04/06.....Signature of candidate.....S.M. Ennaceur ✓

The copyright of this thesis rests with the author. No quotation from it should be published in any format, including electronic and the internet, without the author's prior written consent. All information derived from this thesis must be acknowledged appropriately.

# Chapter I

<b>I. General Introduction.....</b>	<b>29</b>
<b>I.1. Antimicrobial peptides as pharmacological agents. ....</b>	<b>33</b>
<b>I.2. The activity and specificity of these peptides. ....</b>	<b>35</b>
<b>I.3. The structures and conformations adopted by antimicrobial peptides..</b>	<b>35</b>
<b>I.4. Antimicrobial peptides with <math>\beta</math>-barrel structures. ....</b>	<b>38</b>
I.4.1. $\alpha$ -Hemolysin. ....	38
I.4.2. Protegrin-1. ....	40
I.4.3. Gramicidin S. ....	40
I.4.4. Defensins.....	41
<b>I.5. Antimicrobial peptides with helical structures. ....</b>	<b>42</b>
I.5.1 Gramicidin A. ....	42
I.5.2 Magainins.....	43
I.5.3. Cecropins. ....	44
I.5.4. Melittin.....	45
I..5. Alamethicin.....	45
<b>I.6. Lipid membrane composition and peptide-lipid interactions. ....</b>	<b>47</b>
<b>I.7. Antimicrobial activity and mode of action. ....</b>	<b>51</b>
I.7.1 Effect of structure on activity. ....	57
<b>I.8. References.....</b>	<b>60</b>

## Chapter II

<b>II.1. The design and preparation of model amphiphilic cyclic peptides. ....</b>	<b>66</b>
<b>II.1.1. Design of a pore forming peptide template.....</b>	<b>66</b>
<b>II.1.2. Peptide synthesis and purification.....</b>	<b>69</b>
II.1.2.1. Peptide synthesis.....	69
II.1.2.3. Cyclisation. ....	71
II.1.2.4. Cleavage. ....	71
II.1.2.5. Purification. ....	71
<b>II.1.3. Determination of peptide concentration. ....</b>	<b>74</b>
<b>II.1.4. Peptide analysis. ....</b>	<b>75</b>
II.1.4.1. Solvent carrier system. ....	77
II.1.4.2. Derivatives.....	77
II.1.4.3. Detergents .....	78
II.1.4.4. Matrix-Assisted Laser Desorption Ionisation (MALDI). ....	78
 <b>II.2 The analysis of amphiphilic cyclic peptide interactions with phospholipid membranes.....</b>	 <b>83</b>
<b>II.2.1. Circular dichroism spectroscopy.....</b>	<b>83</b>
II.2.1 1. Introduction to the technique. ....	83
II.2.1.2. Evaluation of secondary structure content of a peptide.....	85
II.2.1.3. The dependence of the peptide structure on its environment. ....	87
II.2.1.4. Circular dichroism study of amphiphilic synthetic peptides. ....	88
II.2.1.5. Conformation of the template peptide in aqueous solution. ....	89

II.2.1.6. Conformation of the template peptide in a buffer-salt solution.....	90
II.2.1.7. Conformation of the template peptide in a TFE buffer solution. ....	91
II.2.1.8. Conformation of amphiphilic peptides in unilamellar lipid vesicles..	93
<b>II.2.2. Linear dichroism .....</b>	<b>98</b>
II.2.2.1 Introduction to the technique .....	98
II.2.2.2. The peptide transition moments need to be determined for interpretation of the template peptide-lipid LD signal. ....	100
<b>II.2.3. Differential scanning calorimetry (DSC). ....</b>	<b>104</b>
II.2.3.1. Introduction to the technique. ....	104
II.2.3.2. DSC analysis of peptide-lipid systems. ....	106
II.2.3.3. Peptide-DMPC systems. ....	107
II.2.3.4. Peptide-DPPC systems. ....	109
<b>II.2.4. Transmission Electron Microscopy. ....</b>	<b>111</b>
<b>II.2.5. Chapter summary. ....</b>	<b>115</b>
 <b>II.3.1. Materials and Methods. ....</b>	 <b>117</b>
<b>II.3.1.1. Materials. ....</b>	<b>117</b>
<b>II.3.2. Methods. ....</b>	<b>118</b>
II.3.2.1. Peptide synthesis.....	118
II.3.2.2. Allyl ester deprotection and cyclisation. ....	123
II.3.2.3. Peptide cleavage from the resin and side chain deprotection. ....	124
II.3.2.4. Purification. ....	124
II.3.2.5. Determination of peptide concentration. ....	125
II.3.2.6. Analysis by mass spectrometry. ....	127
II.3.2.7. Positive electrospray ionisation. ....	127

II.3.2.8. MALDI MS. ....	127
II.3.2.9. Preparation of Tetrakis(triphenylphosphine) Palladium(0) .....	127
II.3.2.10. Preparation of the quaternary ammonium ion .....	128
II.3.2.10.1. Preparation of trimethylamine anhydride. ....	128
II.3.2.10.2. Preparation of N-trimethyl-1,2-diaminoethane. ....	128
II.3.2.10.3. [2-(acetylamino)ethyl]trimethylammonium iodide. ....	129
II.3.2.10.4. Derivatization of peptides. ....	130
<b>II.3.3. Analytical methods. ....</b>	<b>130</b>
II.3.3.1. Unilamellar vesicles of phospholipids. ....	130
II.3.3.2. Circular dichroism (CD). ....	130
II.3.3.3. Linear Dichroism. ....	131
II.3.3.4. Differential Scanning Calorimetry. ....	131
II.3.3.5. Transmission Electron Microscope. ....	132
<b>II.4. References. ....</b>	<b>133</b>

## Chapter III

<b>III.1. Two dimensional (2D) crystallisation of membrane proteins.....</b>	<b>139</b>
<b>III.1.1. Properties of membrane proteins.....</b>	<b>142</b>
III.1.1.1. Quantities. ....	142
III.1.1.2. Purity. ....	142
III.1.1.3. Aggregation. ....	143
<b>III.1.2. The purification process.....</b>	<b>143</b>
<b>III.1.3. 2D crystallisation. ....</b>	<b>145</b>
III.1.3.1. Lipids used in reconstituted membrane environments.....	146
III.1.3.2. Role and choice of detergent. ....	148
III.1.3.3. The ionic strength and pH of buffer solutions.....	151
III.1.3.4. The temperature profile and the duration of dialysis. ....	152
III.1.3.5. The mechanism of crystal formation from detergent solution. ....	153
III.1.3.6. Other methods for 2D crystallization. ....	155
<b>III.1.4. Electron microscopy analysis. ....</b>	<b>157</b>
III.1.4.1. Scanning electron microscopy. ....	157
III.1.4.2. Transmission electron microscopy. ....	159
III.1.4.3. Sample preparation for electron microscopy. ....	160
III.1.4.4. Electron diffraction. ....	161
<b>III.1.5. Other techniques used for crystallographic studies. ....</b>	<b>162</b>
III.1.5.1. Atomic Force Microscopy.....	162
III.1.5.2 Imaging conditions. ....	163
III.1.5.3. X-ray diffraction.....	164

<b>III.2. Natural <math>\beta</math>-barrel pore forming models for structural analysis: the <i>Bordetella pertussis</i> autotransporter BrKA C-terminal protein.</b>	<b>165</b>
<b>III.2.1. Introduction.</b>	<b>165</b>
<b>III.2.2. The outer membrane C-terminal domain of BrKA.</b>	<b>168</b>
III.2.2.1. The BrKA C-terminal protein.	169
III.2.2.2. Generation of a His-tagged BrKA C-terminal protein.	174
III.2.2.3. Protein folding.	177
III.2.2.4. Concentration determination.	178
III.2.2.5. Structural analysis.	179
III.2.2.6. Optimisation of folding process.	181
III.2.2.7. Structural analysis after optimisation of folding conditions.	182
<b>III.2.3.1. Two-dimensional (2D) trials of BrKA C-terminal domain.</b>	<b>184</b>
III.2.3.2. Preparation and imaging.	184
III.2.3.3. Lipid sheets.	185
III.2.3.4. Striated domains.	187
III.2.3.5. Stacks.	190
III.2.3.6. Fourier transform processing of digital images.	193
III.2.3.7. Pore structures.	197
III.2.3.8. Extended regions of ordered protein-lipid arrays.	198
III.2.3.9. Other systems for 2D crystal trials.	202
<b>III.2.4.1. The M protein.</b>	<b>202</b>
III.2.4.2. 2D crystallisation.	203
<b>III.2.5. 2D trials on synthetic amphiphilic peptides.</b>	<b>206</b>
<b>III.2.6. Examination of protein-lipid arrays by AFM.</b>	<b>207</b>
III.2.6.1. Supported lipid bilayers.	207

III.2.6.2. Electrostatic repulsion. ....	209
III.2.6.3. AFM imaging performed on BrKA-DMPC samples. ....	210
III.2.6.4. AFM imaging performed on M protein-DMPC samples. ....	214
<b>III.2.7. Further work. ....</b>	<b>215</b>
 <b>III.3. Materials and Methods. ....</b>	 <b>217</b>
<b>III.3.1. Materials. ....</b>	<b>96</b>
<b>III.3.2. Protein analysis. ....</b>	<b>218</b>
III.3.2.1. Circular dichroism. ....	218
III.3.2.2. UV titrations. ....	218
III.3.2.3. Electron Microscopy. ....	218
III.3.2.4. Atomic Force Microscopy. ....	218
III.3.2.5. Supported EPC, DMPC and DPPC bilayers ....	219
III.3.2.6. Protein-lipid sample preparation. ....	219
<b>III.3.3. Methods. ....</b>	<b>220</b>
III.3.3.1. Unilamellar vesicles of phospholipids. ....	220
III.3.3.2. Lipid preparation for 2D crystallisation trials. ....	220
III.3.3.3. Dialysis tube preparation. ....	220
III.3.3.4. Dialysis procedure. ....	221
III.3.3.5. YT media. ....	221
III.3.3.6. Agar plates. ....	221
III.3.3.7. Standard 15 % SDS-Polyacrylamide gel. ....	221
III.3.3.8. Agarose gel. ....	222
III.3.3.9. BrKA C-terminal protein expression. ....	223
III.3.3.10. Protein expression. ....	223



III.3.3.11. Cell harvesting.....	223
III.3.3.12. Protein purification.....	224
III.3.3.13. Subcloning of BrKA C-terminal domain into a pET 19b Vector. ....	224
III.3.3.14. Purification of constructs. ....	224
III.3.3.15. Subcloning.....	225
III.3.3.16. Separation of fragment by agarose gel electrophoresis.....	226
III.3.3.17. Purification of target fragments.....	226
III.3.3.18. Ligation of recombinant pET 19b-BrKA C-terminal clone. ....	227
III.3.3.19. Transformation into competent cells.....	227
III.3.3.20. Expression and cell harvesting.....	227
III.3.3.21. Purification.....	228
III.3.3.22. Protein refolding.....	228
III.3.3.23. Determination of protein concentration. ....	229
III.3.3.24. 2D crystallisation procedures. ....	230
III.3.3.25. Modified crystallisation procedures. ....	230
III.3.3.26. The M protein crystallisation procedures.....	231
III.3.3.27. The 2K4Y03 peptide crystallisation procedure.....	231
III.3.3.28. Elimination of excess lipid.....	231
<b>III.4. Appendix.....</b>	<b>232</b>
<b>III.5. References.....</b>	<b>236</b>

## Chapter IV

<b>IV.1. Analytical studies of the interactions of the perfluorinated alcohol, hexafluoroisopropanol, with phospholipid membranes. ....</b>	<b>247</b>
<b>IV.1.1. Introduction.....</b>	<b>247</b>
<b>IV.1.2. Investigation of the effects of HFIP on phospholipid membranes. .</b>	<b>249</b>
<b>IV.1.3. (Fluorescence) Marker Release experiments. ....</b>	<b>251</b>
<b>IV.1.4. Differential Scanning Calorimetry.....</b>	<b>254</b>
<b>IV.1.5. Small Angle X-ray Scattering, SAXS.....</b>	<b>257</b>
IV.1.5.1. Description of the technique. ....	257
IV.1.5.2. X-ray scattering data collection and processing. ....	259
IV.1.5.3. SAXS from HFIP-DMPC systems.....	261
IV.1.5.4. SAXS from HFIP-DOPC systems. ....	264
<b>IV.1.6. HFIP-Phosphatidylcholine Monolayer experiments. ....</b>	<b>265</b>
IV.1.6.1. Monolayer technique.....	265
IV.1.6.2. Experimental procedure. ....	268
IV.1.6.3. Monolayers of DMPC over HFIP-H <sub>2</sub> O subphases. ....	269
IV.1.6.4. Monolayers of DOPC over HFIP-H <sub>2</sub> O subphases. ....	273
<b>IV.1.7. Light Scattering Analysis of the effects of HFIP on the size of DMPC and DOPC liposomes. ....</b>	<b>277</b>
IV.1.7.1. A brief description of the technique.....	277
IV.1.7.2. Particle sizing of DMPC-HFIP systems.....	278
IV.1.7.3. Particle sizing of DOPC-HFIP systems. ....	280

<b>IV.1.8. Transmission Electron Microscopy, TEM.....</b>	<b>281</b>
IV.1.8.1. TEM imaging of the effects of HFIP on DMPC liposomes.....	282
<b>IV.1.9. Conclusion. ....</b>	<b>287</b>
 <b>IV.2. Materials and Methods.....</b>	 <b>291</b>
<b>IV.2.1. Materials. ....</b>	<b>291</b>
<b>IV.2.2. Methods.....</b>	<b>291</b>
IV.2.2.1. <sup>19</sup> F NMR experiments. ....	291
IV.2.2.2. Marker release experiments. ....	292
IV.2.2.3. Differential Scanning Calorimetry, DSC. ....	292
IV.2.2.4. Small Angle X-ray Scattering, SAXS.....	293
IV.2.2.5. Monolayer experiments.....	293
IV.2.2.6. Light Scattering Analysis.....	294
IV.2.2.7. Transmission Electron Microscopy. ....	294
<b>IV.3. References.....</b>	<b>296</b>

## Chapter V

<b>V. General conclusion.....</b>	<b>300</b>
V.1. Chapter II.....	300
V.2. Chapter III.....	301
V.3. Chapter IV.....	302

# Table of figures

## Chapter I

Figure I.1. Diagram of the gram-negative cell wall.....	31
Figure I.2. Hydrogen bonding between, (a) antiparallel $\beta$ -strands and (b) parallel $\beta$ -strands.....	24
Figure I.3. NMR determined structure of the E. coli OmpA porin transmembrane domain in dodecylphosphocholine micelles (PDB entry 1G90).....	25
Figure I.4. Ribbon representation of the active form of $\alpha$ -hemolysin. View of the stem, head and rim (a) and through the channel (b). ....	27
Figure I.5. Secondary structure of Gramicidin S.....	28
Figure I.6. Representation of NMR determined structure of magainin 2 in lipid micelles.....	31
Figure I.7. Structure of the $\alpha$ -amino-isobutyrate residue, AIB. ....	33
Figure I.8. Ribbon representation of the helix structure of Alamethicin .....	34
Figure I.9. Dimyristoyl phosphatidyl choline, DMPC.....	35
Figure I.10. Typical structure of a phosphatidyl glycerol lipid.....	36
Figure I.11. Representation of lipid phase transition from gel to fluid state.....	37
Figure I.12. (a) shows a typical monolayer structure; (b) and (c) show respectively positive curvature and negative curvature strain on a membrane produced by lipids with bulky (b) and small (c) headgroups. ....	39
Figure I.13. Schematic representation of cationic peptide attraction to negatively membrane surface. ....	41

Figure I.14. Model for peptide interaction with the membrane surface.....	42
Figure I.15. Representation of a peptide transmembrane channel. ....	42
Figure I.16. Representation of peptide aggregation and pore formation in the lipid bilayer. ....	43
Figure I.17. Representation of channel formation by gramicidin A. ....	45
Figure I.18. Schematic representation of cyclic $\beta$ -sheet peptides with (a) and without (b) a disulphide bridge. ....	46
Figure I.19. Cyclic peptides stacking as a continuous $\beta$ -sheet.....	46

## **List of tables**

### **Chapter I**

Table I.1. Comparison of gram-negative and positive cell walls.....	32
Table I.2. Transition temperatures of different phosphatidyl choline and phosphatidyl ethanolamine molecules. ....	50

## Table of figures

### Chapter II

Figure II.1.1 Cyclic peptide template.....	67
Figure II.1.2. Aspartic acid residue with $\alpha$ -allyl ester and Fmoc $\alpha$ -amino protecting groups.....	69
Figure II.1.3. Solid support (tentagel) rink amide resin .....	70
Figure II.1.4. The Fmoc protected Pseudoproline dipeptide Tyrosine(tBu)-Serine.....	70
Figure II.1.5. UV absorption of the purified cyclic 6Y01 peptide in TFE.....	72
Figure II.1.6. HPLC profile for the cyclic peptide 2K4Y03. ....	73
Figure II.1.7. Plot of the corrected absorption against the volume of peptide solution added to the cell.....	74
Figure II.1.8. The quaternary ammonium ion. ....	77
Figure II.1.9. Diagram showing the ionisation process in MALDI MS.....	79
Figure II.1.10. MALDI mass spectrum of the 6Y01 peptide with a major peak corresponding to the linear peptide with allyl ester protection group and a minor peak showing fragmentation of the peptide with loss of the final dipeptide, valine-serine. ....	80

Figure II.1.11. MALDI mass spectrum showing a major peak for the 2K4Y03 cyclic hydrophobic peptide and a minor peak indicative of peptide fragmentation with loss of the final dipeptide valine-serine.....	81
Figure II.2.1. Diagram showing the generation of a CD spectrum. ....	83
Figure II.2.2. Circularly polarized light, where K is the propagation direction...84	
Figure II.2.3 Diagram showing typical CD spectra for different types of protein secondary structure. <sup>31</sup> .....	86
Figure II.2.4. CD spectra of the template peptide 6Y01 in a 4 % TFE solution of pure water.....	89
Figure II.2.5. CD spectra of the peptide 6Y01 measured over arrange of concentrations from 40 to 60 $\mu$ M in a 10 mM Tris-150 mM NaCl solution with 4 % TFE at pH 7.4.....	90
Figure II.2.6. CD spectra of peptide 6Y01 at a concentration of 50 $\mu$ M in 10 mM Tris-150 mM NaCl buffer with 15 % TFE (v/v) at pH 7.4. ....	91
Figure II.2.7 CD spectrum of the peptide 6Y01 at 50 $\mu$ M concentration in a 10 mM Tris-150 mM NaCl buffer with 30 % TFE (v/v) at pH 7.4. ....	92
Figure II.2.8. CD spectrum of the peptide 6Y01 at 50 $\mu$ M in EPC (1 mM) and Tris (10 mM)-NaCl (150 mM). ....	93
Figure II.2.9. CD spectrum of the peptide 2W4Y02 at 50 $\mu$ M in EPC (1 mM) and Tris (10 mM)-NaCl (150 mM) with 4 % TFE.....	94
Figure II.2.10. CD spectrum of the peptide 2K4Y03 at 50 $\mu$ M in EPC (1 mM) ..... and Tris (10 mM)-NaCl (150 mM) with 4 % TFE.....	95
Figure II.2.11. Diagram showing the generation of a LD spectrum. ....	98

Figure II.2.12. Diagrams of <b>(a)</b> a liposome and <b>(b)</b> a shear deformed liposome.	99
Figure II.2.13. Diagram showing the alignment of molecules in solution by sheer flow gradient in a Couette cell, which is basically a spinning cylinder within a concentric sleeve. ....	99
Figure II.2.14. Showing the orientation direction in the peptide-lipid system.....	99
Figure II.2.15. Showing <b>(a)</b> the orientation of the $\beta$ -sheet transition moments polarizations relative to the peptide backbone and <b>(b)</b> the tyrosine transition moment polarizations. ....	100
Figure II.2.16. Linear dichroism spectrum of amphiphilic cyclic peptide 6Y01 in EPC liposomes. ....	101
Figure II.2.17. Diagram showing the peptide backbone orientation relative to the lipid bilayer for negative and positive LD signals. ....	102
Figure II.2.18. Multilamellar liposome. ....	104
Figure II.2.19. DSC thermogram of fully hydrated dimyristoyl phosphatidyl choline, DMPC, showing the lipid pre-transition, $T_p$ centred on 12 °C and the main transition, $T_m$ on 23 °C. ....	105
Figure II.2.20. Showing the tilted lipid monomers in the gel phase, below the pre-transition temperature.....	105
Figure II.2.21. Showing the disordered lipids in the fluid phase, above the main transition temperature of the lipids. ....	106
Figure II.2.22. DSC thermograms of fully hydrated DMPC-6Y01 peptide mixtures .....	107



Figure II.2.23. DSC thermograms of hydrated DPPC-6Y01 peptide with peptide to lipid molar ratios of: 0 (A), 0.05 (B), 0.1 (C) and 0.2 (D). .....	109
Figure II.2.24. TEM image of the negatively stained 2K4Y03 peptides showing filamentous structures. ....	111
Figure II.2.25. TEM image of the negatively stained 2K4Y03 peptides showing large areas of fibrous structures with a range of thicknesses. ....	112
Figure II.2.26. TEM image of the negatively stained 2K4Y03 peptides showing individual, bundles and twisted strands of fibre like structures. ....	113

## List of tables

### Chapter II

Table II.1.1. Series of amphiphilic cyclic peptides synthesised.....	68
Table II.3.1. Optimised RP-HPLC conditions for the synthetic peptides.....	125
Table II.3.2. Calculation of the extinction coefficient for the analogous cyclic peptides for UV absorption at a wavelength 280 nm.....	126

## Table of figures

### Chapter III

Figure III.1.1. schema of membrane proteins in a lipid bilayer. ....	140
Figure III.1.2. Representation of membrane protein solubilisation by detergent molecules.....	141
Figure III.1.3. Diagram of the interaction between the histidine residues on a tagged protein with a $\text{Ni}^{2+}$ ion on a Ni-NTA column. ....	143
Figure III.1.4. Diagram of the structure of histidine with its imidazole ring .....	144
Figure III.1.5. Diagram of membrane protein crystals in cross section. ....	146
Figure III.1. 6. Typical structure of a phosphatidyl choline lipid (DMPC).....	147
Figure III.1.7. Structure of zwittergent 3-12. ....	149
Figure III.1.8. Diagram of monomer–micelle equilibrium in aqueous solution.	149
Figure III.1.9. Structure of Triton X-100 .....	150
Figure III.1.10. Structure of DDM, n-dodecyl- $\beta$ -D-maltoside.....	151
Figure III.1.11. 2D crystallisation of membrane proteins anchored to functionalised fluorinated lipid spread at the air-water interface.....	156
Figure III.1.12. Diagram of the main parts of a scanning electron microscope.	158
Figure III.1.13. Diagram showing the different signals and information that can be obtained in a scanning electron microscope. ....	159

Figure III.1.14. Diagram showing the main features of contact mode AFM. ....	162
Figure III.2.1. Diagram of the primary structure of an autotransporter. ....	166
Figure III.2.2. Diagram showing insertion of outer membrane protein C-terminal domain into outer membrane.....	167
Figure III.2.3. Expression of prokaryotic outer membrane proteins. ....	169
Figure III.2.4. Structure of Sodium dodecyl sulfate (SDS).....	171
Figure III.2.5. SDS-page showing the change in protein production following a range of different expression conditions.. ....	172
Figure III.2.6. SDS Page showing the concentration of protein. ....	173
Figure III.2.7. SDS Page showing the reference markers SDS7(1) and the pure fractions of eluted protein (2 and 3). ....	174
Figure III.2.8. Diagram outlining the steps in a generic ligation process. ....	175
Figure III.2.9. SDS-page showing total cell protein expression at different temperatures.. ....	175
Figure III.2.10. SDS-page showing the high level of purity of eluted protein ..	176
Figure III.2.11. SDS-page showing the pure fractions and the flowthrough from the BrKA C-terminal protein after elution from a $\text{Ni}^{2+}$ affinity column .....	177
Figure III.2.12. Plot of protein absorbance against change in concentration (dilution) of the protein. ....	178
Figure III.2.13. CD spectrum of BrKA C-terminal protein.....	179

Figure III.2.14. SDS-page of the folding solutions.. .....182

Figure III.2.15. CD spectrum of the refolding.BrKA C-terminal protein .....183

Figure III.2.16. TEM image of a DMPC lipid sheet with protein arrays .....185

Figure III.2.17. TEM image showing “worm” like features after varying the dialysis conditions.....187

Figure III.2.18a. TEM image of ordered striated areas.. .....188

Figure III.2.18b. TEM image of distinct patches of striated domains.....190.

Figure III.2.19. TEM images of stacked planar structures obtained after a two fold increase in the dialysis rate. ....191

Figure III.2. 20. TEM images showing extensive stacking of disk structures. ..191

Figure III.2.21. TEM images of disk like structures stacked with different orientations. ....192

Figure III.2.22. TEM images of non stacked disk like structures along side groups of stacked structures. ....193

Figure III.2.23. Inverse Fourier Transform of a filtered Fourier Transformed image of stacked structures .....194

Figure III.2. 24. Image of a large area of protein-lipid structures with a variety of clearly defined domains .....195

Figure III.2.25. Power spectrum showing the effect of filters and inverse Fourier Transform of filtered Fourier Transform image.....195

Figure III.2.26. TEM images of non stacked disk structures merging into a sheet like layer following a further increase in the rate of dialysis. ....	196
Figure III.2.27. TEM image of pore like structures. ....	197
Figure III.2.28. Diagram of “the drop spreading method” for detecting residual detergent.....	199
Figure III.2.29. TEM image showing domains in lipid sheets of different periodicities perpendicular to each other.....	200
Figure III.2.30. TEM image of juxtaposed lipid sheets covered with protein arrays. ....	201
Figure III.2.31. TEM image of crystalline arrays of the M protein in sheets of the saturated lipid, DMPC.....	203
Figure III.2.32. TEM image of a long vesicular structure packed with crystalline arrays of the M protein. ....	204
Figure III.2.33. TEM image of large lipid sheets again packed with clearly crystalline arrays of the M protein .....	205
Figure III.2.34. AFM image of a supported DOPC bilayer .....	207
Figure III.2.35. AFM image of a supported DMPC bilayer .....	208
Figure III.2.36. Cross section of the line drawn on DMPC bilayer surface.....	208
Figure III.2.37. Force curves were recorded for all samples .....	209
Figure III.2.38. AFM performed on a BrKA-DMPC sample incubated at 4 °C overnight on a freshly cleaved mica support.....	210

Figure III.2.39. AFM image of a BrKA C-terminal protein sample showing features with a tetrameric appearance protruding from the membrane.....	211
Figure III.2.40. Cross section analysis of a supported BrKA-DMPC sample, from which an area of the sample has been scrapped away with the probe tip. ....	212
Figure III.2.41. Spot like depressions in a supported DMPC membrane visualised after removal of sample upper surface. ....	213
Figure III.2.42. Striated domains, <b>a</b> and <b>b</b> recorded using AFM on M protein-DMPC samples.....	214
Figure III.3.1. Diagram depicting the pET 11a vector cloning and expression regions with NdeI and BamHI cloning sites underlined in red.....	225.
Figure III.3.2. Diagram depicting the pET 19b vector cloning and expression regions with NdeI and BamHI cloning sites and N-terminal His Tag sequence underlined in red.....	225
Figure III.3.3. Elution of BrKA C-terminal protein from the nickel affinity column.....	228

## **List of tables**

### **Chapter III**

Table III.3.1. Digestion preparation of the BrKA construct and the pET 19b vector with the restriction enzymes BamHI and NdeI.....	226
Table III.3.2. Calculation of the extinction coefficient ( $\epsilon_{280\text{ nm}}$ ) for the BrKA C-terminal domain.....	229

# Table of figures

## Chapter IV

Figure IV.1.1. [1,1,1,3,3,3-hexafluoroisopropanol] (HFIP).....	247
Figure IV.1.2. $^{19}\text{F}$ NMR spectra of HFIP-DMPC and HFIP-DOPC preparations performed in $\text{D}_2\text{O}$ at 376 MHz: A, 1 % HFIP; B, $[\text{HFIP}]/[\text{DOPC}] = 2:1$ ; C, $[\text{HFIP}]/[\text{DMPC}] = 2:1$ and D, $[\text{HFIP}]/[\text{DMPC}] = 1:1$ .....	249
Figure IV.1.3. Expanded section of $^{19}\text{F}$ NMR spectra recorded in $\text{D}_2\text{O}$ at 376 MHz of: A, a 1% solution of HFIP and B, a 1:1 molar ratio of HFIP/DMPC. ....	250
Figure IV.1.4. Release of encapsulated CF ( $>35\text{mM}$ ) from EPC liposomes .....	253
Figure IV.1.5. DSC thermograms showing the effect of HFIP on fully hydrated MLVs of DMPC.....	254
Figure IV.1.6. The variation of phase transition temperature, $T_m$ .....	255
Figure IV.1.7. Diagram showing suggested location of HFIP in phospholipid bilayers. ....	256
Figure IV.1.8. Diagram of the basic components of an SAXS diffractometer. ....	257
Figure IV.1.9. Diagram showing the production of X-rays. ....	258
Figure IV.1.10. The X-ray patterns for HFIP-DMPC systems were measured over a range of HFIP/DMPC molar ratios.....	261
Figure IV.1.11. SAXS data for the HFIP-DMPC systems was collected over a range of HFIP/DOPC molar ratios. ....	264

Figure IV.1.12. Diagram of a pressure-area isotherm for DMPC over a pure H <sub>2</sub> O subphase. ....	266
Figure IV.1.13. diagram of a Langmuir-Blodgett trough.....	267
Figure IV.1.14. Pressure-area isotherm of DMPC over HFIP-H <sub>2</sub> O subphases..	269
Figure IV.1.15. plot of collapse pressures and collapse areas against HFIP concentration in the subphase. ....	270
Figure IV.1.16. Plot of area, A <sub>0</sub> against HFIP concentration in the subphase. ..	271
Figure IV.1.17. Pressure-area isotherms of DOPC recorded over a range of HFIP-pure water subphases.....	273
Figure IV.1.18. Plot of collapse pressures and areas against HFIP concentration in the subphase for DOPC monolayers recorded at 20 °C. ....	275
Figure IV.1.19. Plot of lift off area, A <sub>0</sub> against HFIP concentration in the subphase for DOPC monolayers recorded at 20 °C. ....	276
Figure IV.1.20. Diameter of DMPC liposomes determined, as a function of HFIP concentration in the sample solution, by laser correlation spectroscopy.DMPC concentration was 2 mM. ....	278
Figure IV.1.21. Diameter of DOPC liposomes determined, as a function of HFIP concentration in the sample solution, by Light Scattering Spectroscopy.....	280
Figure IV.1.22. TEM images of DMPC liposomes in pure water .....	282
Figure IV.1.23. DMPC liposomes in a 0.05 M HFIP- pure water solution imaged by TEM at magnifications of x 46 000.. ....	283



Figure IV.1.24. DMPC liposomes in a 0.38 M HFIP- pure water solution imaged by TEM at magnifications of: <b>a</b> , x 22 000 and <b>b</b> , x 46 000. . . . .	284
Figure IV.1.25. TEM images of HFIP (0.38 M) - pure water mixtures (mag. <b>a</b> , x 46 000 and <b>b</b> , x 100 000). . . . .	285
Figure IV.1.26. Schematic model describing a mechanism for the interaction of HFIP with DMPC membranes. . . . .	289

## List of tables

### Chapter IV

Table IV.1.1. Table listing numerical values ( $\text{\AA}^{-1}$ ) calculated for the area under the first-order and second-order reflections, the position, width and height of the reflections for scattering data collected on HFIP-DMPC systems.....	262
Table IV.1.2. Showing data for the compressional modulus, $\kappa$ of DMPC and DOPC monolayers over a range of HFIP-water subphases.....	274
Table IV.1.3. Showing the effective diameter and the polydispersity of the DMPC liposome-HFIP samples over a range of HFIP concentrations.....	279

# Chapter I

## I. General Introduction.

Protection against bacterial infections is widely regarded as a commodity of modern life; we rely on antibiotics to give constant respite from a whole host of illnesses.

Over the past decade though, a significant threat to our dominance over bacteria has become apparent, as a growing number of pathogenic organisms are becoming resistant to conventional antibiotics; amongst which a decreasing sensitivity of common bacterial infections, such as *Streptococcal pneumoniae*, a widespread cause of bacterial sinus and ear infection, to the antibiotic penicillin.<sup>1,2,3,4</sup>

A general abuse of established antibiotic drugs is being blamed for the emergence of plasmid-born resistance genes in bacteria and therefore of the decreasing efficiency of available antibiotics to fight bacterial infections. The use of antibiotics in food producing animals (fluoroquinolones; avoparcin) are thought to be responsible for resistant strains of bacteria, such as *Salmonella*, *Campylobacter*, *Enterococci* and *Escherichia coli*, which can be transferred to humans through the food chain.<sup>5</sup>

The increasing use of disinfectants in domestic and personal hygiene products also reduces the number of harmless bacteria and increases the number of resistant strains.

Antimicrobial agents find their way, often in high concentrations, to sewage effluents and from there, to the water systems.

The natural consequence of bacterial cell exposure to antimicrobial agents is an irreversible resistance to antibiotics. Bacteria have very short generation times from minutes to hours, which enable them to adapt rapidly to changes in their environment; modifications to bacterial genes allow bacteria to alter the specific target that antibiotics recognise and attack.<sup>6</sup>

Resistant strains of bacteria have a high epidemic potential, which is of particular concern in the field of hospital infection control, as resistant strains of bacteria

are far more expensive to treat and may require drugs that are more toxic than the common antibiotics.

Antibiotic agents have been developed to exploit the significant cellular and molecular physiological differences between eukaryotic and prokaryotic cells and thus to target exclusively bacterial cells over animal cells; avoiding or reducing the risk of toxicity to the host.

Bacterial cells are enclosed by a wall structure, as well as membranes, with a net like arrangement of cross linked sugar chains (N-acetyl glucosamine and N-acetyl muramic acid), the peptidoglycan layer, which confers rigidity to the bacterial cell allowing it to survive in media in which the cytoplasm may be hypertonic.

This cell wall is the target of  $\beta$ -lactam antibiotic drugs (penicillin) and glycopeptides (vancomycin), which irreversibly bind the enzyme transpeptidase that forms the cross linkage between the polymer chains for the former and the enzyme binding site (D-alanyl-D-alanine) on the sugar chains for the latter. Both classes of drugs act therefore by crippling the production of bacterial cell wall, which protects the cell from the environment.

Other antibiotic agents interfere with protein synthesis (tetracycline, aminoglycosides and macrolides) and metabolic processes such as the synthesis of vitamin K that are essential for bacterial survival, as well as inhibiting DNA and RNA synthesis (quinolones).<sup>7,8,9</sup>

The effectiveness of an antibiotic drug relies on its ability to penetrate the organism cell and to reach its target site in high enough concentrations and to remain in location long enough to kill the organism. Both  $\beta$ -lactams and glycopeptides exhibit time dependent killing and activity restricted towards specific types of bacteria.

The complexity of the cell wall and therefore the ease with which an antibacterial drug can penetrate the cell varies greatly depending on which of the two broad classifications of bacteria are considered; the cell walls of gram negative bacteria (*Salmonella*; *Neisseria* and *Yersinia*) have a more complex structure than those of gram positive organisms (*Bacillus*; *Staphylococcus* and *Streptococcus*).

Gram-negative cells are enclosed by the cytoplasmic or inner membrane, beyond which is the periplasmic space and then a thin peptidoglycan layer strongly bound to the outer membrane by a lipoprotein.

The outer membrane of gram-negative bacteria is very distinctive, as it contains not only lipids and proteins, but also lipopolysaccharides, LPS, which are composed of lipid A and a polysaccharide chain and are located on the outside face of the membrane.

LPS gives gram-negative bacteria a hydrophilic character and protects the cell against any hydrophobic molecules that could approach the outer membrane. These molecules are also toxic (endotoxins) to mammals, when released from the bacterial membrane on death of the cell.<sup>10</sup> Glycoproteins (e.g. vancomycin) have restricted activity against these organisms as they are unable to penetrate the outer membrane of gram-negative bacteria (Fig. I.1).

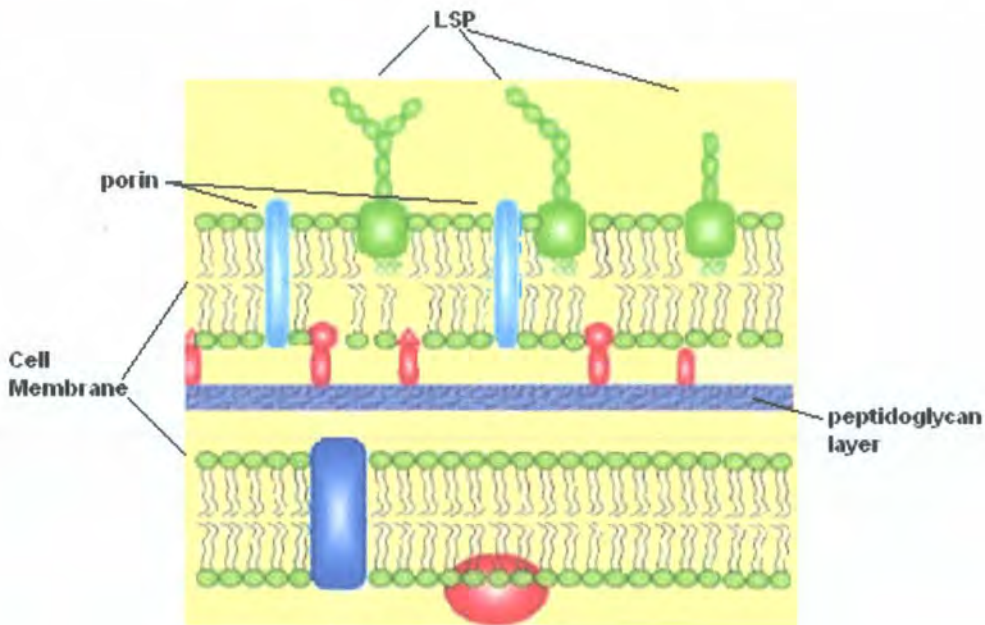


*Figure I.1. Diagram of the gram-negative cell wall.*

Gram-positive bacteria only have a plasma membrane and no outer membrane, but their cell wall is much denser than that of gram-negative bacteria; the plasma

membrane is protected and supported by peptidoglycan, which can reach up to 20 layers in thickness and constitute from 60 % to 90 % of the cell wall.

Interwoven in the cell wall are teichoic acids (polymers of glycerol; phosphates; ribitol, a sugar alcohol and depending on the species of bacteria, a lipid anchor). The negatively charged teichoic acid network acts, as a barrier for the cell against positively charged molecules. The outer surface of the peptidoglycan wall is studded with proteins, which can have a variety of functions, depending on the species of bacteria.<sup>11</sup>

A summary of the properties of gram positive and gram negative cell walls has been tabulated below.

Property	Gram Positive	Gram Negative
Thickness of wall	20-80 nm	10 nm
Number of layers in wall	1	2
Peptidoglycan content	60% - 90%	10-20%
Teichoic acid in wall	+	-
Lipid and lipoprotein content	0-3%	58%
Protein content	0%	9%
Lipopolysaccharide	0	13%
Sensitive to penicillin	+	- (less affinity)
Digested by lysozyme	+	- (less affinity)

*Table I.1. Comparison of gram-negative and positive cell walls.*

Bacterial cells eventually develop resistance towards the antibiotic drugs to which they are repeatedly exposed and especially towards those that have a slow rate of activity, which fail to completely eliminate the organism. These factors allow the more resistant bacterial strains to develop and to transmit their genes to other bacterial species. Bacterial resistance can manifest itself in a number of ways, from modifications to the drug's site of action to generation of enzymes that break the antibiotics down. The  $\beta$ -lactam antibiotics are attacked by  $\beta$ -lactamases, enzymes that hydrolyse the  $\beta$ -lactam ring, which is necessary for their activity.

Methicillin resistant *Staphylococcus aureus* (MRSA) or “the super bug” as it is more familiarly known, is a term used to describe *Staphylococcus aureus* organisms that have become resistant to an increasing number of common antibiotics. A number of modifications have been made to antibiotic drugs to stop bacterial resistance such as the inclusion of clavulonic acid in the preparation of augmentin which prevents action by lactamases. But it is only a matter of time before a bacterial counter attack is developed against all our common drugs, as a consequence of their specific mode of action and the speed with which they attack; therefore it has become essential to explore alternative routes, in order to remain safely ahead of the pathogenic hordes that could destroy the protected life we now enjoy.<sup>12,13</sup>

### **I.1. Antimicrobial peptides as pharmacological agents.**

A great variety of biologically active antimicrobial peptides have been discovered right across the evolutionary spectrum, from bacteria themselves to insects, plants and mammals.<sup>14</sup> The importance of these peptides in host-defence mechanisms, against microbial species, has become increasingly evident since the 1980s. Host defence peptides, from 15 to 40 amino acids in length, have evolved throughout the natural world to contend with invaders, as part of an active defence system. In mammals these antibacterial peptides are innate immune substances that act as the primary line of defence in the fight against invading pathogenic microorganisms.<sup>2,15</sup>

Interest in antimicrobial peptides appeared as early as 1939, when antibacterial compounds, showing biological activity against pneumococcal infection in mice, were isolated in soil *bacilli*.<sup>12</sup> The antimicrobial peptides tyrocidine and gramicidin were purified and crystallized from *Bacillus brevis* only a few years later. Tyrocidine was too toxic for use as an antibiotic, but gramicidin actually found use as a topical agent, before the availability of Penicillin.

Cecropins and defensins were the first antimicrobial peptides from animals, to be characterized structurally from 1981 to 1983.<sup>13,16</sup> Protegrin-1 (PG-1) was discovered in porcine leukocytes and exhibited remarkable antimicrobial activity, including the protection of cells from infection by HIV.<sup>1,30</sup> The peptide melittin was isolated from bee venom; the peptide magainin from amphibian skin secretions and alamethicin, a small 20 amino acid residue peptide, was found in the fungus *Trichoderma viride*.<sup>17</sup>

The production of antimicrobial peptides and proteins is extremely common in bacteria.<sup>15</sup> Bacteria are present everywhere throughout nature and within an extensive range of habitats, in water and in soil, on plants, as well as on and within mammals.<sup>18</sup>

In order to gain advantage over their competitors, these microorganisms produce antibiotic substances that inhibit or kill target cells of competitor organisms, but from which they are themselves immune. The most efficient of these substances are the Bacteriocins, which are potent antagonists; these are bacterial peptides ribosomally made or derived from gene encoded precursors.

Bacteriocins have evolved to fit both in size and specificity, the different cell wall architectures of the gram-negative and gram-positive bacteria.

The antimicrobial peptides produced by gram-positive bacteria, lactococcins and lantibiotics, are small, less than 10 kDa and have a wider activity range than those of gram-negative bacteria; they act through membrane perturbation and pore formation.<sup>19</sup> The activity of gram-negative antimicrobial peptides is much more specific and needs receptor binding domains for receptor-mediated antagonist activity.

Many conventional antibiotics disable or kill bacteria over a period of days, whereas antimicrobial peptides are both fast and lethal, killing almost instantaneously (within minutes). Their action is different to that of common drugs as it is directed towards the target cell membrane, causing disruption, which can result in cell leakage and death. Interest in the development of peptide based antibiotics is growing as bacterial resistance is thought unlikely to develop, as a result of the short exposure time of the target cells to the antimicrobial peptides.

However, a significant difficulty that would need to be addressed is that many antimicrobial peptides are also highly haemolytic and lack the high selectivity required for use as antibiotic drugs.<sup>20</sup>

## **I.2. The activity and specificity of these peptides.**

A potential antibiotic drug must have the ability to destroy pathogens while displaying relative non-toxicity to the host organism and being capable of reaching the infection site even when deeply buried within tissue.

One approach is to custom-design peptides with structural features likely to favour peptide insertion or disruption of the lipid bilayer of cell membranes and to study these peptide-lipid interactions. This can be achieved through a clear understanding of the structural organisation of membrane proteins and the complex intermolecular interactions of these proteins with their target cell membranes. The antibacterial and haemolytic activities of a peptide or protein are closely tied to its structure. Toxicity can be significantly reduced and antimicrobial activity improved by adjusting the structural features of the peptide.

## **I.3. The structures and conformations adopted by antimicrobial peptides.**

Peptides and proteins that interact with and penetrate the membranes of target cells possess membrane compatible amphipathic secondary structures such as  $\alpha$ -helix or  $\beta$ -sheet.<sup>21</sup> The formation of these secondary structures enables the hydrogen potential of the amide groups in the peptide sequence to be fulfilled (Fig. I.2) and to contain any non-saturated hydrogen bonds within a hydrophobic unit; avoiding energetically unfavourable exposure of polar groups to the lipid bilayer interior.



The majority of membrane proteins are located in the cytoplasmic membrane and consist of either individual or bundles of transmembrane  $\alpha$ -helices, spanning the membrane, whereas membrane proteins from the outer membrane of gram-negative bacteria and a large number of those from mitochondria and chloroplast outer membranes, form monomeric, dimeric or trimeric transmembrane  $\beta$ -barrels.<sup>22,23</sup>

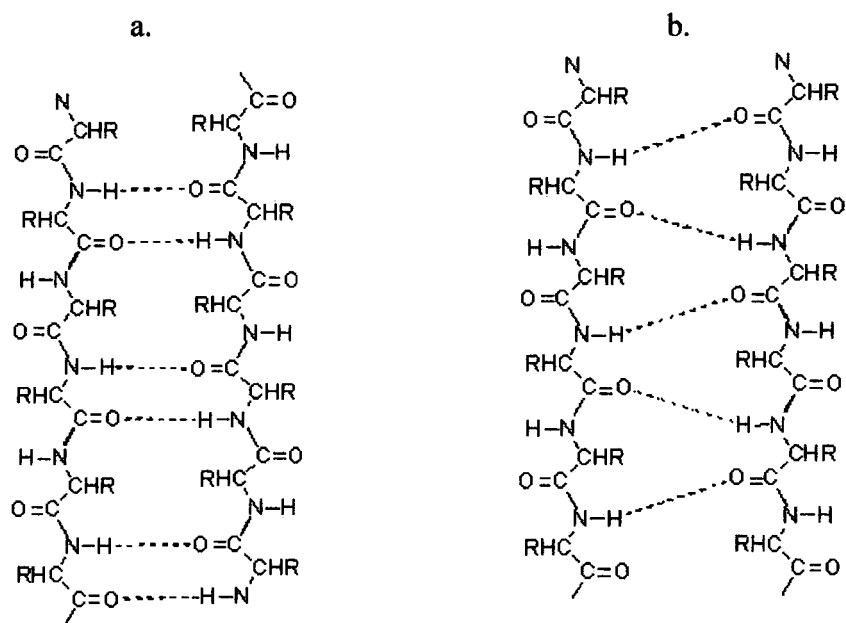


*Figure I.2. Hydrogen bonding between, (a) antiparallel  $\beta$ -strands and (b) parallel  $\beta$ -strands.*

The  $\beta$ -barrel structure forms a stable scaffold of  $\beta$ -sheet strands (Fig. I.3) in which the amino acid residues are connected by main chain hydrogen bonds, allowing the protein to remain correctly folded in the harsher external conditions of the outer membrane. The  $\alpha$ -helical bundles of the cytoplasmic membrane form less stable structures as they are only connected *via* side chain interactions.<sup>24</sup>

A range of  $\beta$ -barrel proteins have been characterised ranging from as few as 8 strands (OmpA and OmpX porins) and up to 22 strands (Ion transporters FhuA and FepA) per barrel; they exist either as single barrel structures or as oligomers often in trimer conformations.<sup>25</sup>

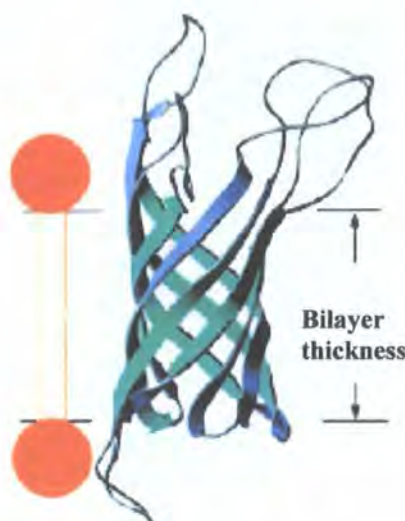


Figure I.3. NMR determined structure of the *E. coli* OmpA porin transmembrane domain in dodecyl phosphocholine micelles (PDB entry 1G90).

The construction of a  $\beta$ -barrel appears to be governed by a number of rules which have been deduced from compiling known  $\beta$ -barrel structures. These could be used both to predict  $\beta$ -barrel formation from a protein sequence and provide guide lines for engineering these structures.<sup>26</sup>

Secondary structure and structure-function relationships of a whole array of antimicrobial peptides have been examined using a wide range of techniques; these studies have provided considerable insight into the factors that enable and direct specific biological activity. Antibacterial peptides, which have well characterised structures and activities, include the  $\beta$ -sheet forming cytotoxin,  $\alpha$ -hemolysin; cyclic gramicidin S and members of the family of defensins as well as the  $\alpha$ -helical peptides: gramicidin A; magainins; cecropins; melittins and alamethicin, which is one of the most extensively examined peptides in peptide-lipid interaction studies.

Profile studies on these peptides have revealed a very high diversity in structure in relation to activity, which makes prediction or deduction of activity on the

basis of characteristics like length, charge or presence of disulphide bridges very difficult.

Peptides like magainins, cecropins and defensins, also have such a rapid response against bacterial cytoplasmic membranes that it has not been possible to determine whether they have other cellular targets

## **I.4. Antimicrobial peptides with $\beta$ -barrel structures.**

### **I.4.1. $\alpha$ -Hemolysin.**

The  $\beta$ -barrel structure is also used to form hydrophilic transmembrane channels in the membranes of target cells by many bacterial pore-forming toxins.

The protein  $\alpha$ -hemolysin (Figure I.4) is a cytotoxin secreted by the gram-positive bacteria, *Staphylococcus aureus*, which becomes biologically active on formation of a membrane-bound polymeric  $\beta$ -barrel on the surface of target cells.<sup>23</sup>

X-ray crystallographic and atomic force microscopic structural studies performed on  $\alpha$ -hemolysin have shown that the protein adopts a heptameric conformation in the presence of lipid and detergent micelles.

Polymorphism of the protein oligomer has also been observed by atomic force microscopy, where the protein has been clearly shown to form arrays of hexamers on supported phospholipid bilayers.<sup>23,27</sup>

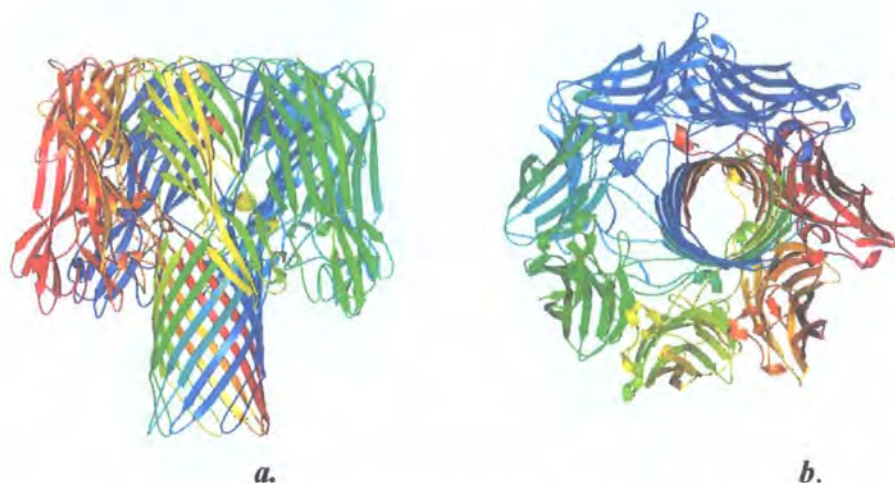


*Figure I.4. Ribbon representation of the active form of  $\alpha$ -hemolysin.  
View of the stem, head and rim (a) and through the channel (b).  
(PDB entry 7AHL)*

The protein complex as determined by X-ray crystallography (Fig I.4) has an overall size of about 10 x 10 nm and is shaped like a mushroom with a “head”, “rim” and “stem” part. The “head” is largely hydrophilic and with the “rim” protrudes by 4.8 nm from the membrane surface. The “head” is composed of seven  $\beta$ -sandwiches and amino linkers from each of the individual peptides. The “rim” is a 3 stranded  $\beta$ -sheet and the “stem” a 14 strand (two strands from each peptide) anti-parallel  $\beta$ -barrel with a height of 5.2 nm.<sup>28</sup>

The surface of the “rim” domain as well as being in contact with the lipid surface has solvent exposed aromatic residues. The peptide is released from the bacteria in a water soluble form, which binds to the target membrane causing the local concentration of peptide to increase. Once a sufficient level is reached, the toxin will fold into an oligomeric conformation and insert spontaneously into the membrane, forming channels of 1-2 nm in diameter.



The toxin has shown a high selectivity towards sensitive cells, such as Rabbit erythrocytes, which suggests that membrane binding may also be a receptor mediated process. Many membrane peptides and proteins undergo a conformational change upon binding to a target membrane surface.<sup>28,29</sup>

#### I.4.2. Protegrin-1.

The antimicrobial peptide, Protegrin-1 (PG-1), which forms an integral part of the porcine innate immune system, adopts a  $\beta$ -sheet structure on binding to target membranes. The 18 residue peptide has a roughly cylindrical shape which is folded into  $\beta$ -sheets and linked by two disulphide bridges. The peptide has demonstrated potential, *in vitro* as a potent pharmaceutical agent against the bacteria, *E. coli* and *Listeria monocytogenes* and the fungus *Candida albicans*, as well as potentially affording some protection against the HIV infection.<sup>30</sup>

Another  $\beta$ -barrel antimicrobial species, which has been successfully used as a topical antibacterial substance, is the cyclic peptide gramicidin S.

#### I.4.3. Gramicidin S.

The cyclic decapeptide, Gramicidin S is one of a series of peptides isolated from *Bacillus brevis*.<sup>12,31</sup>

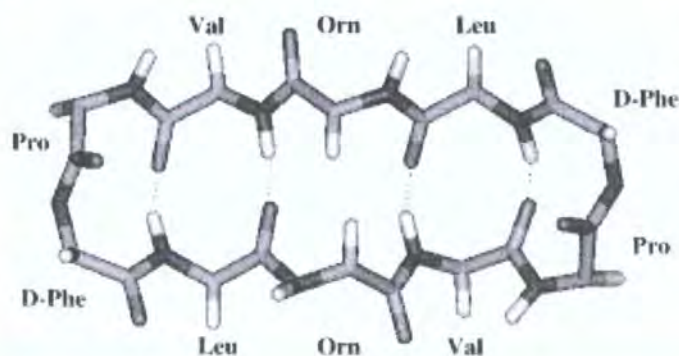


Figure 1.5. Secondary structure of Gramicidin S.

Gramicidin S adopts a very stable antiparallel  $\beta$ -sheet conformation with four intermolecular hydrogen bonds (Fig. I.5) and also shows the characteristic amphiphilic structure, with the segregation of polar and non polar surfaces, which is of prime importance for antimicrobial activity.

Gramicidin S is thought to bind to the cell membrane surface and penetrate to some extent into the bilayer, before the strain which results from this process, leads to pore formation and rupturing of the membrane. This antimicrobial peptide is a very efficient, but non specific killer, which can not distinguish between healthy cells and bacterial organisms; it therefore exhibits significant haemolytic activity as well as antimicrobial activity. Gramicidin S has at present limited use as a pharmaceutical agent, but the peptide has shown some sensitivity towards the lipid composition of membranes and research is being carried out to enhance this characteristic in favour of bacterial activity and consequently to reduce its toxicity.<sup>32</sup>

Other non selective peptides include the family defensins, which are amongst the most characterized of the  $\beta$ -sheet forming antimicrobial peptides.

#### **I.4.4. Defensins.**

This family of small cationic antimicrobial peptides, which have sequences between 29 to 35 amino acids in length, form part of the mammalian host defence system in mucosal surfaces and mammalian phagocytes.<sup>12</sup> They adopt a  $\beta$ -sheet conformation with 3 intermolecular disulphide bonds, giving the peptides stable cyclic structures.

The 3D conformations of two closely related defensins HNP-1 and HNP-3 have been determined by 2D NMR and X-ray crystallography respectively; these peptides form amphiphilic dimers, consisting mostly of antiparallel  $\beta$ -sheets with several tight turns. Defensins have a non selective behaviour; their biocidal activity is not restricted to microbial targets, but acts against prokaryotic and eukaryotic targets alike.<sup>33</sup>

They have a broad spectrum of activity and are biologically active against both gram-negative and positive bacteria as well as yeasts.<sup>34</sup>

Molecular mechanisms work along side these peptides to regulate localised production, storage and delivery to microbial targets and subsequent clearance from the cell with the help of plasma proteins, which avidly bind and mop up human defensins.

## **I.5. Antimicrobial peptides with helical structures.**

The majority of helical antimicrobial peptides are cationic as well as amphipathic and possess a broad spectrum of activity.

### **I.5.1 Gramicidin A.**

The  $\beta$ -helical antimicrobial peptide is a small linear 15 residue polypeptide with alternating L- and D- amino acids, which forms channels in phospholipid bilayers specifically for the transport of monovalent cations.

Gramicidin A, in its most stable conformation, adopts a right handed helical structure which traverses the membrane as a dimer, in a head to tail fashion. The peptide forms ion channels by association of two monomers through 6 intermolecular hydrogen bonds; the size of these channels has been estimated to a length of 3 to 4 nm and an inner diameter of 0.3-0.4 nm.<sup>57</sup> The carbonyl oxygens on the polymer backbone are thought to form the ion-conducting pathway, as gramicidin A does not contain any polar or hydrophilic residues.<sup>1</sup> The high aromatic content of the peptide, 4 tryptophan residues, is thought to stabilise the channels by locating at the membrane interface.<sup>35</sup>

Detailed structure-function studies on cecropins and magainins have highlighted the role of the helical structural motif and of appropriately positioned cationic residues in the activity of these peptides.

### I.5.2 Magainins.

This class of antimicrobial peptides (Fig.I.6) were isolated in 1987, from the granular gland in the skin of the African claw frog, *Xenopus laevis*. Magainins, which have between 21 to 26 amino acid residues, have a strongly basic character and dissolve readily in aqueous solutions.

These cationic peptides largely adopt right handed  $\alpha$ -helical conformations on association with lipid membranes.

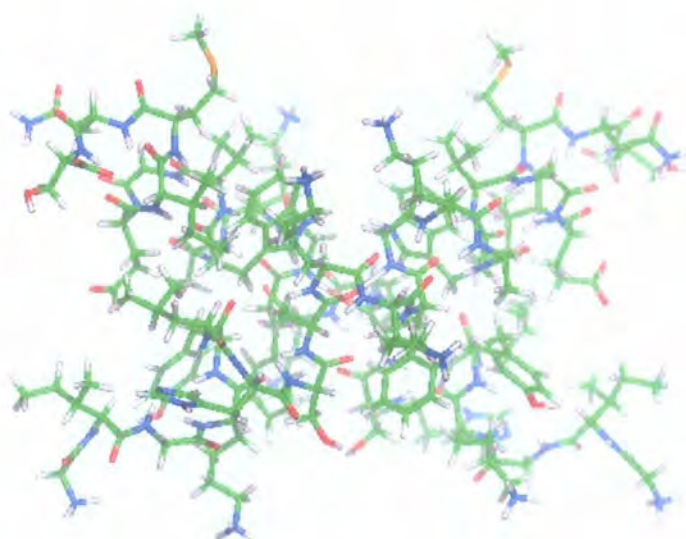


*Figure I.6. Representation of NMR determined structure of magainin 2 in lipid micelles (PDB entry 1DUM).*

Magainins show a broad spectrum of antimicrobial activity at low concentrations, in the range of 10 to 100  $\mu\text{g ml}^{-1}$ , against bacteria, fungi, and protozoa.<sup>36</sup> In contrast, these peptides must be present in high concentrations, in excess of 1  $\text{mg ml}^{-1}$  to lyse mammalian cells. Magainins are therefore selectively toxic towards micro-organisms and have also been shown to lyse tumour cells without killing healthy vertebrate cells. One explanation for this selective behaviour relates to the specific binding between the peptide and cholesterol



molecules, abundant in eukaryotic, but not in bacterial cells, which could inhibit formation by the peptide of the active lytic conformation.<sup>37</sup>

### **I.5.3. Cecropins.**

Cecropins are a group of very potent antimicrobial peptides, with sequence lengths between 35 to 39 residues, which form amphipathic helices without cysteines. These peptides were initially discovered in insects, in the pupae of the cecropia moth and then in other species, including mammals. The structure of cecropin A has two amphipathic helical regions connected by a flexible hinge region.<sup>38</sup> One face of the structure has basic residues along its length, whereas the other is much more hydrophobic.

The activity of cecropins is very selective; they do not attack mammalian cells or even yeast, but show strong antibiotic activity at micromolar concentrations, against both gram-negative and gram-positive bacteria. Cecropins interact with bacterial cells, through the formation of pores in the membrane bilayers; these carry current under a voltage gradient and allow the passage of ions. The diameter of the pores, 0.5 to 4 nm, suggests that at least 4 peptide monomers could aggregate to form a pore. Cecropins have also shown some indication that they could also exhibit anticancer activity.<sup>37</sup>

Novel antibiotic polypeptides have been synthesised from cecropin-melittin hybrid peptides and have shown a large improvement on the antimicrobial activity of the native cecropin. These mixed peptides, composed of one melittin and one cecropin domain, adopt the helix-bend-helix conformation of cecropin.<sup>37</sup>

#### I.5.4. Melittin.

Melittin is a cationic 26 residue toxin, isolated from the venom of *Apis mellifera*, honey bee, which adopts an extended  $\alpha$ -helical conformation with two helical domains arranged in a bent configuration with hydrophobic residues located on the inside of the bend. The peptide C-terminal segment of 6 residues is highly cationic and appears to play an important role for antimicrobial activity, whereas the highly hydrophobic N-terminal segment of 20 residues is essential for insertion or partitioning of the peptide into membranes. The peptide is thought to interact with target membranes by aligning parallel to the normal of the bilayer and inserting into the glycerol region of lipid head group.<sup>12,14</sup>

Melittin has a monomeric unstructured conformation at low concentrations in aqueous media, but will adopt a tetrameric structure with a dimer of dimers type conformation in lipid bilayers.<sup>39,40</sup>

#### I.5. Alamethicin.

Alamethicin is a member of a family of membrane active peptides of fungal origin, peptaibols, which have linear sequences of 10 to 21 residues in length. These peptides are characterised by an acetylated N-terminus, a high percentage of the “unnatural”  $\alpha$ -amino-isobutyrate, AIB residues (Fig. I.7), which favour the formation of a helical structures and a C-terminal amino alcohol instead of a carboxylic acid group.<sup>20,37</sup>

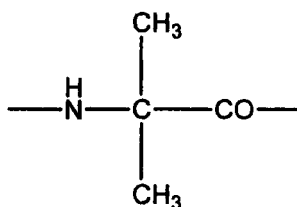


Figure I.7. Structure of the  $\alpha$ -amino-isobutyrate residue, AIB.

Alamethicin, with a sequence of 20 amino acids, is one of the larger members of this group and is known to affect the permeability of the membranes by forming voltage-dependent channels, even in the absence of an applied voltage. Alamethicin is rich in hydrophobic amino acids; it has eight  $\alpha$ -amino-isobutyric acid residues and adopts helical polymeric structures that self assemble in membranes. A proline residue at position 14 of the amino acid sequence gives the peptide its typical helix-bend-helix conformation.<sup>41</sup>

The channels formed by alamethicin (Fig. I.8) in target membranes are thought to be between 0.3 and 1 nm in diameter and to be composed of helical groups of up to 8 monomers each.



*Figure I.8. Ribbon representation of the helix structure of Alamethicin (PDB entry 1amt).*

Alamethicin is a toxin that exhibits very little selectivity for microbial membranes and consequently in its natural non modified form could only have limited use as a pharmacological agent.<sup>1,37</sup>

At present, several hundreds of natural antimicrobial peptides with linear and cyclic structures have been characterized; their interactions with natural and model membranes have been studied using an array of physical techniques, with the purpose of designing novel peptides or adapting natural peptide sequences for use as potential antimicrobial agents.

## I.6. Lipid membrane composition and peptide-lipid interactions.

The specificity of antimicrobial peptide activity towards a target cell, which is dependant on the complexity of the structure and composition of the membrane bilayer, can be enhanced by adapting the peptide structure to provide a greater discrimination between prokaryotic and higher eukaryotic membranes.<sup>14,49,42</sup>

There main differences, between the prokaryotic and eukaryotic membranes are in composition and arrangement of their lipids.<sup>20</sup>

The outer leaf of mammalian cell membranes is principally composed of electrically neutral zwitterionic phospholipids (Fig. I.9), phosphatidylcholines and sphingomyelins, whereas the inner leaf of the bilayer mostly contains aminophosphatides.<sup>51</sup>

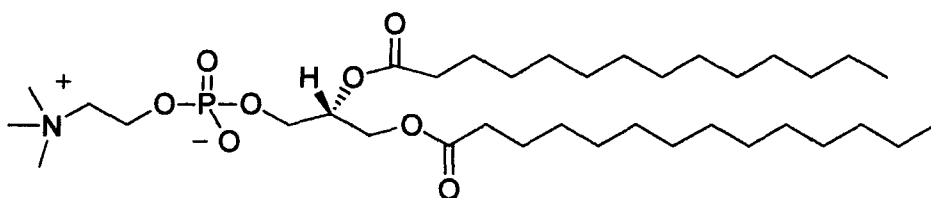


*Figure I.9. Typical structure of a phosphatidyl choline lipid, dimyristoyl phosphatidyl choline, DMPC.*

Eukaryotic cell membranes are also abundant in cholesterol which could afford some protection from antimicrobial activity, as they affect the ordering and packing and hence the physical state of the bilayer.<sup>43,44</sup>

The structure and composition of the cell envelope differs considerably in gram-negative and gram-positive bacteria, though both bacterial strains have negatively charged membranes.

Gram-negative bacteria have a very distinctive and highly asymmetrical outer membrane structure with an outer surface composed of negatively charged lipopolysaccharides, LPS and an inner surface, similar in composition to gram positive membranes and consisting mainly (70 to 80 %) of unsaturated phosphatidyl ethanolamine and to a lesser extent (20 to 30 %) of negatively charged phosphatidyl glycerol (Fig. I.10) and cardiolipin.<sup>45</sup>

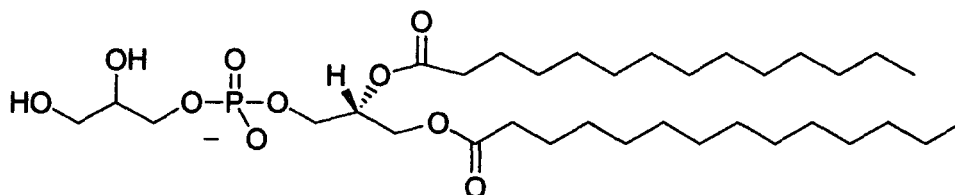


*Figure I.10. Typical structure of a phosphatidyl glycerol lipid.*

The teichoic acid molecules interwoven into the fabric of the gram-positive cell wall contribute, along with the phosphatidyl glycerol lipids, towards the negatively charged surface of this strain of bacteria.

Synthetic lipid bilayers have been developed to mimic microbial and eukaryotic cell membranes. A range of phosphatidyl choline molecules with different characteristics, saturated, mono and polyunsaturated lipids with different chain lengths, have been used as models for mammalian blood cell membranes, as they are abundant in the outer leaf of the outer membrane of eukaryotic cells.<sup>35</sup>

The unsaturated phospholipids, dioleoyl phosphatidylcholine, DOPC and negatively charged, dioleoyl phosphatidylglycerol, DOPG are commonly used as models for the negatively charged cytoplasmic membranes of bacteria.

The physical state of the lipid bilayer is also an important factor for peptide-lipid interactions and for bilayer integrity.

Lipids, at a given temperature, will undergo a phase transition (Fig. I.11) from an ordered gel state, in which the lipid monomers are closely packed to a less ordered liquid crystalline state.

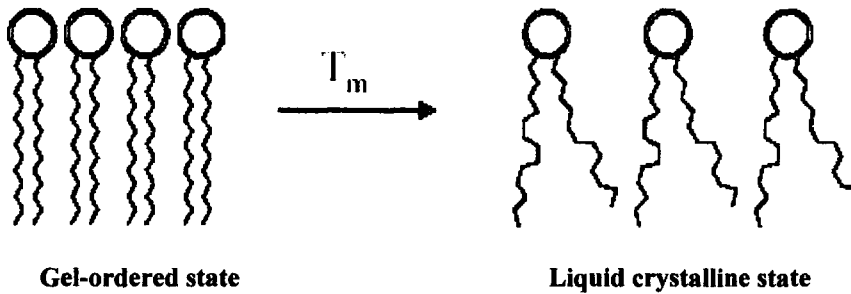


*Figure I.11. Representation of lipid phase transition from gel to fluid state.*

The temperature,  $T_m$ , at which this happens depends on the composition of the lipid, the length and the degree of saturation of the carbon chains (Table I.2.) as well as the size of the lipid head group.<sup>46,47</sup>

The unsaturated phosphatidylcholine lipids are in the fluid state below room temperature with transition temperatures that decrease considerably depending on the degree of saturation and chain length of the lipid, whereas the fully saturated lipids have transition temperatures that increase significantly with chain length; the commonly used DMPC and DPPC with chain lengths of 14 and 16 carbons respectively, have transition temperatures of 23 °C and 41 °C.

The unsaturated phosphatidyl ethanolamine molecules, found largely in bacterial cell membranes, have an unsubstituted quaternary ammonium group and a much smaller head groups than the bulky phosphatidylcholine molecules; these phosphatidyl ethanolamine lipids display much higher values of  $T_m$ , around 20 °C higher than their phosphatidylcholine counter parts.<sup>46</sup>

<b>Lipid molecules</b>	<b>Abbreviation</b>	<b>Chain length and saturation</b>	<b><math>T_m</math> (°C)</b>
Dimyristoyl phosphatidylcholine	DMPC	(14:0, 14:0)	23
Dipalmitoyl phosphatidylcholine	DPPC	(16:0, 16:0)	41
Distearoyl phosphatidylcholine	DSPC	(18:0, 18:0)	54
Palmitoyl-oleoyl phosphatidylcholine	POPC	(16:0, 18:1)	-7
Dioleoyl phosphatidylcholine	DOPC	(18:1, 18:1)	-20
Dipalmitoyl phosphatidyl ethanolamine	DPPE	(16:0, 16:0)	63
Palmitoyl-oleoyl phosphatidyl ethanolamine	POPE	(16:1, 18:1) (Trans)	23

*Table I.2. Transition temperatures of different phosphatidylcholine and phosphatidyl ethanolamine molecules.*<sup>47</sup>

The intrinsic curvature of the membrane is also thought to have an influence on antimicrobial activity, with highly curved membrane structures being implicated in a number of antimicrobial peptide pore forming mechanisms; the peptides themselves on interacting with the membrane, will cause strain on the bilayer, which can in turn be counteracted by the curvature of the target membrane.<sup>48,51</sup>



Molecules with large polar headgroups like phosphatidyl choline tend to adopt structures with positive curvatures, whereas molecules with smaller headgroups, like the phosphatidyl ethanolamines found predominately in bacterial membranes, preferentially adopt structures with negative curvature (Fig. I.12). Curvature, as well as the charge and physical state of a membrane bilayer, could also therefore have a significant role in antibacterial activity.

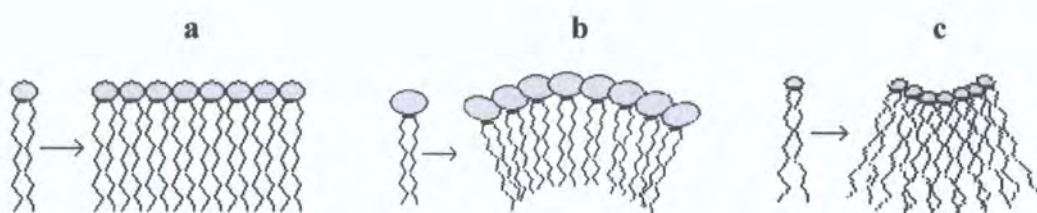


*Figure I.12. (a) shows a typical monolayer structure; (b) and (c) show respectively positive curvature and negative curvature strain on a membrane produced by lipids with bulky (b) and small (c) headgroups.*

## **I.7. Antimicrobial activity and mode of action.**

The mechanism behind antimicrobial peptide activity and the rapidity with which these peptides can strike a target cell are two factors that make bacterial resistance against antimicrobial peptides much less likely. Rapid disruption to the cell membrane is a very effective attack against a target cell, as the cell can not protect itself against such an unspecific and rapid onslaught. Although the molecular mechanism behind this peptide induced cell lysis is still not fully understood, several methods have been proposed to explain the activities of a range of antimicrobial peptides; these include formation of pores, which would span the entire membrane bilayer, detergent like activity towards the membrane and creation of defects in the membrane induced by a peptide lying parallel to the membrane and covering its surface, in a carpet fashion.<sup>49,50,51,52</sup>



Peptides, with very different sequences and structures, may still follow the same mechanism of pore formation or membrane disruption. On the other hand peptides with very similar structures and only slight differences in hydrophobicity or in the relative size of their hydrophobic domains may display very different activities.<sup>45</sup>

The relationship between structure and activity has been investigated through numerous studies using a whole range of physical techniques including calorimetric, spectroscopic, microscopic and diffraction studies. Several common antimicrobial peptide structural features have been identified as having a major role in antimicrobial activity and to influence the way in which a peptide will interact with a cell membrane.<sup>36</sup>

A high degree of hydrophobicity is clearly a requirement for peptide-lipid interactions and although peptides can achieve a hydrophobic compatible conformation by forming characteristic structures, such as  $\alpha$ -helical and  $\beta$ -barrel motifs, the primary sequence of the antibacterial peptide must contain a large number of hydrophobic residues for rapid peptide partitioning into membranes. The fine tuning of peptide hydrophobicity, through the choice of amino acid residues in the peptide sequence, has been observed to have a strong affect on the peptide antimicrobial activity; increasing or decreasing the hydrophobicity of a peptide by changing amino acid residues has lead to peptide activity becoming more selective.<sup>53</sup>

The overall charge of an antimicrobial peptide is another important factor for selective binding to anionic bacterial membranes (Fig. I.13).<sup>51</sup>

Strong basic residues, such as arginine or lysine are important for peptide interactions with negatively charged head groups at the surface of bacterial membranes, as they are involved in an initial electrostatic attraction to the anionic bilayer.

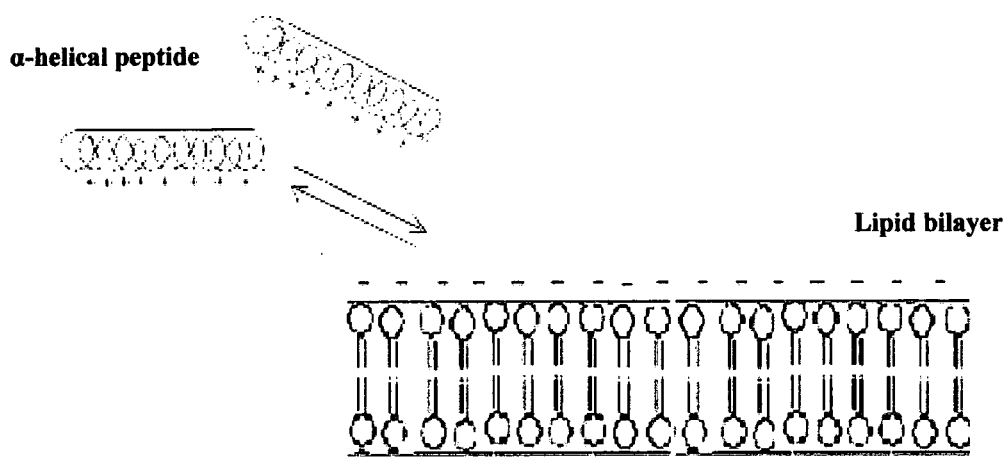


*Figure I.13. Schematic representation of cationic peptide attraction to negatively charged membrane surface.*

Cationic peptides, such as the magainin family of peptides, only become biologically active on binding to negatively charged groups on the surface of bacterial membranes; some cationic peptides need this electrostatic attraction to interact with a membrane because they have such a low degree of hydrophobicity that they can not interact in sufficiently high concentrations with a neutral zwitterionic membrane to become active.<sup>1</sup>

This attraction serves to increase the local peptide concentration at the membrane surface, but the actual disruption of membranes depends on the hydrophobic interactions of peptide with lipid regardless of whether the membrane is neutral or ionic. Other cationic peptides like the toxin melittin are already highly hydrophobic and are therefore non-selective in their behaviour towards membranes.

Once the peptide monomers interact with the membrane surface in high enough concentrations, they will aggregate and penetrate to form anion selective pores.

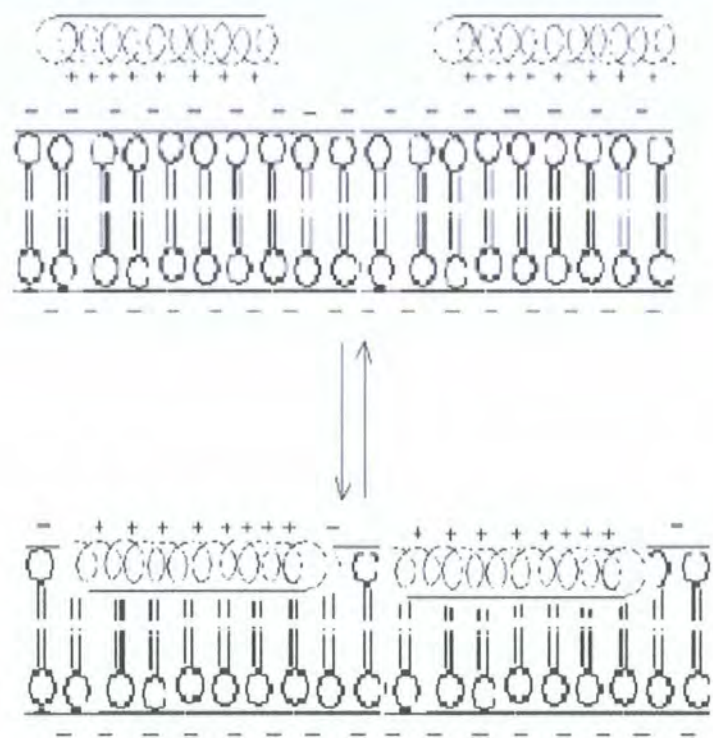


Figure I.14. Model for peptide interaction with the membrane surface.

The pores structures formed in this manner are thought to be unstable causing the peptides to translocate in to the membrane bilayer, disrupting its integrity even further.

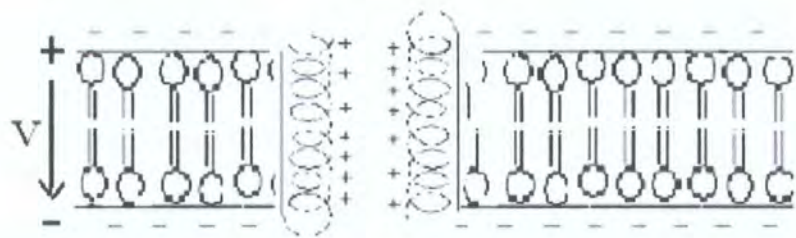
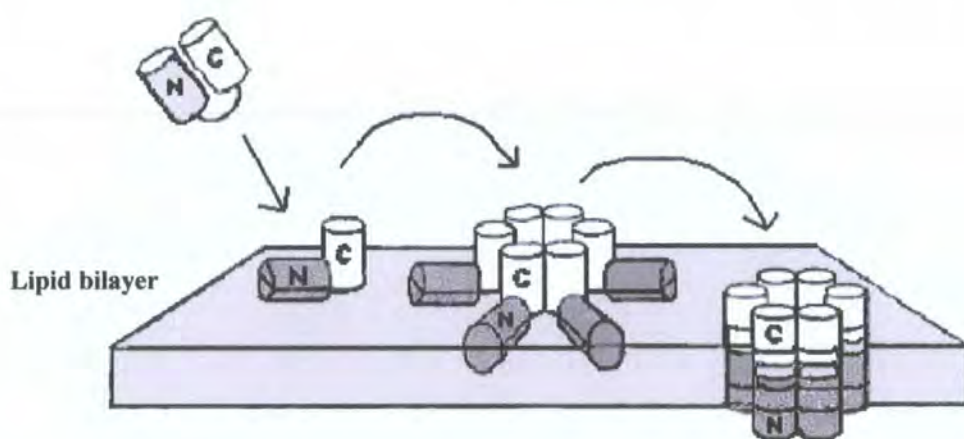


Figure I.15. Representation of a peptide transmembrane channel.

The amino acid side chains in the peptide sequence also play a significant role in the orientation of a peptide in the membrane. The charged and the polar groups prefer to be located on the outside of the membrane, exposed to the aqueous medium where they can interact with charged lipid head groups; the positively charged residues will favour the cytoplasmic surface of the membrane more than the negatively charged residues. The aromatic residues have a preference for the lipid carbonyl portion of the bilayer and are thought to help anchor the peptide to the membrane.<sup>54,55</sup> The hydrophobic aliphatic side chains favour the lipid hydrocarbon chains and therefore, any hydrophobic residues exposed to the aqueous medium, will provide a driving force for peptide insertion into the membrane (Fig. I.16).<sup>56</sup>

These preferences promote amphipathicity, a partitioning of the peptide structure into distinct regions: a hydrophilic side facing the aqueous environment either at the membrane surface or inside the transmembrane channels and a hydrophobic surface facing the acyl chains of the membrane bilayer.

This partitioning is the mechanism behind pore formation; the peptide monomers assemble into large oligomeric structures with their hydrophilic faces oriented towards each other, thus creating a hydrophilic water filled pore excluded from the hydrophobic surrounding media that allows the passage of ions.<sup>37,57</sup>



*Figure I.16. Representation of peptide aggregation and pore formation in the lipid bilayer.*

This is very similar to the mechanism proposed for the activity of  $\beta$ -sheet type antimicrobial peptides such as  $\alpha$ -hemolysin, in which monomer peptides are thought to aggregate on the lipid bilayer, to form oligomeric structures with 3 distinct regions: a hydrophobic domain inserted into the lipid environment, a rim or hinge region in contact with the surface and a hydrophilic domain protruding from the bilayer.<sup>27</sup>

The insertion of peptide monomers and polymeric structures into target membranes, may induce positive curvature strain in the lipid bilayer by expanding the polar head group region and causing irreversible membrane disruption.<sup>51</sup> This peptide induced positive curvature strain, would to some extent depend on the properties of the target membrane as a membrane with intrinsic negative curvature could reduce this effect.

The stress created in the bilayer by peptides lying parallel to the membrane surface in a so called “carpet mechanism” is also the disruptive force behind membrane dissolution into micellar structures at critical peptide concentrations.<sup>45</sup>

Another constraint that antimicrobial peptides may face, on inserting into a lipid membrane, is the hydrophobic mismatch between the length of the membrane spanning segments of the protein (Fig. I.17) and the hydrophobic thickness of the bilayer. Lipids can modulate the activity of membrane proteins by changing their hydrophobic thickness. In the case of a positive mismatch, a protein can be induced to form an oligomeric complex to shield any exposed groups from the polar environment. The protein backbone and the side chains could also be induced to tilt away from the bilayer normal, which would effectively reduce the protein length.<sup>56</sup>

A negative mismatch is overcome by peptides like gramicidin A through formation of extended structures and by translocation mechanisms; for example by formation of a head to head helical dimer.<sup>58,57</sup> Protein stretching and disordering of the alkyl chains have also been observed with some proteins facing a negative mismatch.<sup>56</sup>



The inside of the helical coil formed by gramicidin A constitutes a polar environment through which metabolites can either enter or leak from the cell.

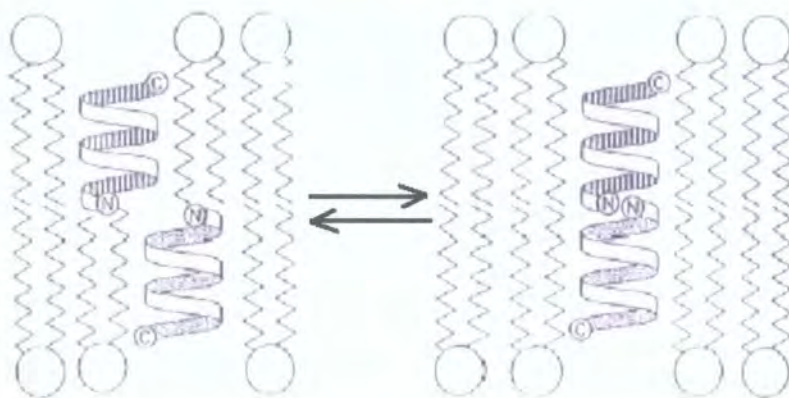


*Figure I.17. Representation of channel formation by gramicidin A.*

### **I.7.1 Effect of structure on activity.**

Antimicrobial activity may be induced by a conformational change in the peptide structure; peptide monomers may have a non active conformation, such as a random coil or even an  $\alpha$ -helical structure, which changes to an active structure on binding to a target membrane.<sup>38</sup> This change in conformation, which activates the antibacterial peptide, could be triggered by a range of different conditions, such as an increase in local concentration of the peptide; by a change in pH of the surrounding medium, interaction of the peptide with an acidic membrane or by a change in salt concentration.<sup>59,60,61</sup>

A structural design that has important effects on antibacterial activity is whether the peptide has a linear or cyclic structure. Cyclic antimicrobial peptides adopt mainly amphipathic  $\beta$ -sheet structures and have a higher affinity for antibiotic activity than their linear counterparts.

Cyclic structures can be achieved through (Fig. I.18) disulphide bridge formation or through backbone cyclisation.<sup>62</sup>

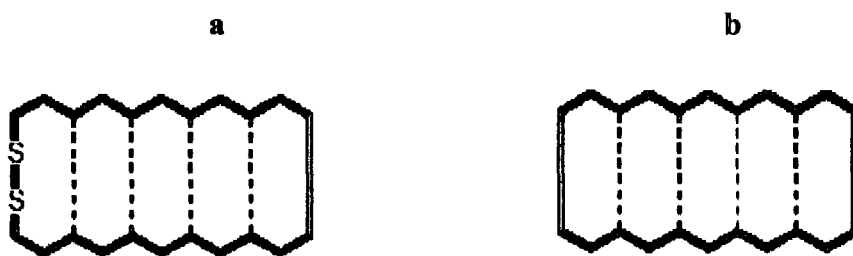


*Figure I.18. Schematic representation of cyclic  $\beta$ -sheet peptides with (a) and without (b) a disulphide bridge.*

The disulphide cross-links in the cyclic peptides create structural constraints that impart a high degree of stability to these structures and help preform the active  $\beta$ -structure, in both aqueous medium and phospholipid membranes. The cyclic structure gives greater conformational rigidity to the peptide than the linear structure as the peptide can form intramolecular hydrogen bonds as well as inter peptide  $\beta$ -sheets through the aggregation of monomers. The ring size of a cyclic peptide may also have a significant effect on the antibiotic activity, with larger rings showing broader activity than smaller rings.<sup>63,64</sup>

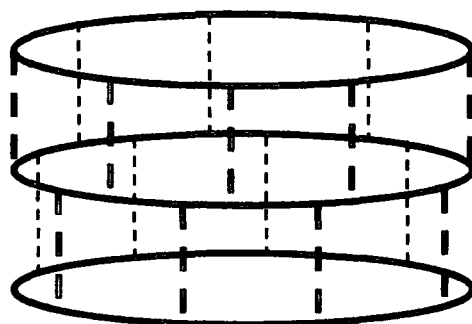


*Figure I.19. Cyclic peptides stacking as a continuous  $\beta$ -sheet.*

The cyclic monomer peptides can associate in a target membrane by stacking to form a contiguous  $\beta$ -sheet or tubule structure with partitioning of the hydrophobic groups towards the inside of the tubule structure. The backbone hydrogen bonding between the monomer rings gives a major stabilising force to the oligomeric structure in the membrane.

Antibacterial activity is affected by such a large range of factors, that the design of simple model systems to study the behaviour of antibacterial peptides with target membranes, would be invaluable towards gaining a thorough understanding of the relationship between structure and antibacterial activity.

Well behaved  $\beta$ -barrel forming peptide systems are very important as these peptides are difficult to manipulate and tend to aggregate readily. The  $\beta$ -barrel conformation is also the most commonly encountered conformation in prokaryotic outer membrane proteins which are important targets for drug uptake into the cell.<sup>65,66</sup>

Synthetic model antibacterial peptides could also incorporate some protection against digestion by proteases, by using chemically modified or non natural amino acids, such as  $\beta$ -amino acids.<sup>67,68,69</sup>



## I.8. References.

- 
- 1 R. M. Epand, H. J. Vogel, *Biochim. Biophys. Acta*, **1462**, 1999, 11-28.
  - 2 K. Lohner, E. J. Prenner, *Biochim. Biophys. Acta*, **1462**, 1999, 141-156.
  - 3 F. Service, *Science*, **270**, 1995, 724-727.
  - 4 J. Davies, *Nature*, **383**, 1996, 219-220.
  - 5 The hazards of the use of antibiotic in food producing animals, World health organisation (WHO) meeting, 13<sup>th</sup> to 17<sup>th</sup> of October 1997, Berlin, Germany.
  - 6 Antimicrobial resistance, an ecological perspective, Report from the American Academy of microbiology, American society for microbiology, 1999.
  - 7 H. Rahman and L. Smith, Infectious diseases, D. Armstrong and J. Cohen, Mosby, London, pp. 1-7, 1999.
  - 8 G. L. Mandell and W. A. Petri, Jr., Antimicrobial agents, Penicillins, Cephalosporins and other  $\beta$ -lactam Antibiotics, Godman & Gilman's The Pharmacological Basis of Therapeutics, 9th edition, eds. J. G. Hardman, L. E. Limbird, McGraw Hill, New York, pp. 1073-1101, 1996.
  - 9 F. Van Bambeke, Infectious diseases, D. Armstrong and J. Cohen, Mosby, London. pp. 7-8, 1999.
  - 10 T. Gutschmann, S. O. Hagge, A. David, S. Roes, A. Bohling, M. U. Hammer and U. Seydel, *J. Endotoxin Res.*, **11**, 2005, 167-173.
  - 11 Cell structure, function and metabolism, eds N. Cohen, Hodder & Stoughton Ltd, Kent, 1991.

- 
- 12 Antimicrobial peptides, Ciba foundation symposium 186, J. Wiley and Sons, Ltd., 1994.
- 13 R. E. W. Hancock and M. G. Scott, National Academy of Science colloquium, Virulence and defence in Host-pathogen interactions: common features between plants and animals, 9<sup>th</sup> to 11<sup>th</sup> December 1999, The Arnold and Mabel Beckman centre in Irvine, CA.
- 14 N. Sitaram, R. Nagaraj, *Biochim. Biophys Acta*, **1462**, 1999, 29-54.
- 15 C. Gray, Y. Strandberg, L. Donaldson, R. L. Tellam, *Aust. J. Exp. Agr.*, **45**, 2005, 757-761.
- 16 J. J. Schneider, A. Unholzer, M. Schaller, M. Schafer-Korting and H. C. Korting, *J. Mol. Med. JMM.*, **83**, 2005, 587-595.
- 17 R. W. Williams, R. Starman, K. M. P. Taylor, K. Gable, T. Beeler, M. Zasloff and D. Covell, *Biochemistry*, **29**, 1990, 4490-4496.
- 18 M. Suarez, M. Haenni, S. Canarelli, F. Fisch, P. Chodanowski, C. Servis, O. Michielin, R. Freitag, P. Moreillon and N. Mermoud, *Antimicrob. Agents Ch.*, **49**, 2005, 3847-3857.
- 19 P. Singleton, *Bacteria in biology, biotechnology and medicine*, 5th edition, J. Wiley and sons, Ltd., 1999.
- 20 A. Angelova, R. Ionov, M. H. L. J. Koch, G. Rapp, *Archives of Biochemistry and Biophysics*, **378**, 2000, 93-106.
- 21 A. Fersht, *Structure and Mechanism in Protein Science*, 4th edition, Freeman, New York, 1999.

- 
- 22 J. D. Lear, H. Gratkowski and W. F. Degrado, *Biochem. Soc. Trans.*, **29**, 2001, 559-564.
- 23 M. Montoya, E. Gouraux, *Biochim. Biophys. Acta*, **1609**, 2003, 19-27.
- 24 M. Bannwarth and G. E. Schulz, *Biochim. Biophys. Acta*, **1610**, 2003, 37-45.
- 25 G. E. Schulz, *Curr. Opin. Chem. Biol.*, **10**, 2000, 443-447.
- 26 L. K. Tamm, A. Arora and J. H. Kleinschmidt, *J. Biol. Chem.*, **276**, 2001, 32399-32402.
- 27 L. Song, M. R. Hobaugh, C. Shustak, S. Cheley, H. Bayley, J. E. Gouaux, *Science*, **274**, 1996, 1859-1866.
- 28 Y. Fang, S. Cheley, H. Bayley, J. Yang, *Biochemistry*, **36**, 1997, 9518-9522.
- 29 D. M. Czajkowsky, S. Sheng and Z. Shao, *J. Mol. Biol.*, **276**, 1998, 325-330.
- 30 W.T. Heller, A. J. Waring, R. I. Lehrer, T. A. Harroun, T. M. Weiss, L. Yang and H. W. Huang, *Biochemistry*, **39**, 2000, 139-145.
- 31 E. J. Prenner, R. N.A.H. Lewis, R. N. McElhaney, *Biochim. Biophys. Acta*, **1462**, 1999, 201-221.
- 32 PENCE research program, Medical Microbiology and immunology, University of Alberta, Canada, [www.nce.gc.ca/media/success/pence](http://www.nce.gc.ca/media/success/pence).
- 33 M. Sawai, H. P. Jia, L. Lui, V. Aseyev, J. M. Wiencek, P. B. McCray, T. Granz, W. R. Kearney and B. F. Tack, *Biochemistry*, **40**, 2001, 3810-3816.
- 34 C. Treffers, L. Y. Chen, R. C. Anderson and P. L. Yu, *Int. J. Antimicrob. Ag.*, **26**, 2005, 165-169.

- 
- 35 Y. Kobayashi, K. Fukada, *Biochim. Biophys. Acta*, **1371**, 1998, 363-370.
- 36 R. Maget-Dana, *Biochim. Biophys. Acta*, **1462**, 1999, 109-140.
- 37 B. Bechinger, *J. Membrane Biol.*, **156**, 1997, 197-211.
- 38 S.E. Blondelle, K. Lohner, M. Aguilar, *Biochim. Biophys. Acta*, **1462**, 1999, 89-108.
- 39 H. Vogel, *FEBS Lett.*, **134**, 1981, 37-42.
- 40 S. H. White, W. C. Wimley, A. S. Ladokhin and K. Hristova, *Methods Enzymol.*, **295**, 1998, 62-87.
- 41 T. Kikukawa, T. Arais, *Archives of Biochemistry and Biophysics*, **405**, 2002, 214-222.
- 42 S. Stankowski and G. Schwarz, *FEBS Lett*, **250**, 556-560.
- 43 F. Nicol, S. Nir, F. C. Szoka, *Biophys. J.*, **78**, 2000, 818-829.
- 44 S. Komura, H. Shirotori, P. D. Olmsted and D. Andelman, *Europhys. Lett.*, **67**, 2004, 321-327.
- 45 K. A. Henzler Wildman, D-K. Lee and A. Ramamoorthy, *Biochem.*, **42**, 2003, 6545-6558.
- 46 M. Polikandritou Lambros, E. Sheu, J. S. Lin, H. A. Pereira, *Biochim. Biophys. Acta*, **1329**, 1997, 285-290.
- 47 R. R. C. New, *Liposomes, a practical approach*, Edt.D. Rickwood and B. D. Hames, 1988, IRL Press, Oxford University Press.

- 
- 48 J. M. Sanderson, *Org. Biomol. Chem.*, **3**, 2005, 201-212.
- 49 Y. Shai, *Biochim. Biophys. Acta*, **1462**, 1999, 55-70.
- 50 T. C. B. Vogt and B. Bechinger, *J. Biol. Chem.*, **274**, 1999, 29115-29121.
- 51 K. Matsuzaki, *Biochim. Biophys. Acta*, **1462**, 1999, 1-10.
- 52 A. H. A. Clayton, W. H. Sawyer, *Eur. Biophys. J.*, **28**, 1999, 133-141.
- 53 A. C. Gibbs, T. C. Bjorndahl, R. S. Hodges and D. S. Wishart, *J. Am. Chem. Soc.*, **124**, 2002, 1203-1213.
- 54 C. M. Bishop, W. F. Walkenhorst and W. F. Wimley, *J. Mol. Biol.*, **309**, 2001, 957-988.
- 55 P. Braun and G. Von Heijne, *Biochemistry*, **38**, 1999, 9778-9782.
- 56 J. A. Killian, *FEBS Lett.*, **555**, 2003, 134-138.
- 57 B. A. Wallace, *BioEssays*, **22**, 2000, 227-234.
- 58 S. Morein, R. E. Koeppe II, G. Lindblom, B. de Kruijff, J. A. Killian, *Biophys. J.*, **78**, 2000, 2475- 2485.
- 59 Z. Oren, J. C. Lerman, G. H. Gudmundsson, B. Agerberth and Y. Shai, *Biochem. J.*, **341**, 1999, 501-513.
- 60 I. Nagaoka, S. Hirota, S. Yomogida, A. Ohwada and M. Hirata, *Inflamm. Res.*, **49**, 2000, 73-79.

- 
- 61 E. J. M. Van Kan, D. N. Ganchev, M. M. E. Snel, V. Chupin, A. Van der Bent and B. de Kruijff, *Biochemistry*, **42**, 2003, 11366.
- 62 T. M. Weiss, L. Yang, L. Ding, A. J. Waring, R. I. Lehrer and H. W. Huang, *Biochemistry*, **41**, 2002, 10070-10076.
- 63 C. Branden and J. Tooze, *Introduction to Protein Structure*, Garland Publishing, Inc. London. 1991.
- 64 E. G. Hutchinson, R. B. Sessions, J. M. Thornton and D. N. Woolfson, *Protein Science*, **7**, 1998, 2287-2300.
- 65 H. Stahlberg, D. Fotiadis, S. Scheuring, H. Remigy, T. Braun, K. Mitsuoka, Y. Fujiyoshi and A. Engel, *FEBS Lett.*, **504**, 2001, 166-172.
- 66 S. H. Gellman, *Curr. Opin. Chem. Biol.*, **2**, 1998, 717-725.
- 67 R. P. Cheng, S. H. Gellman and W. F. Degrado, *Chem. Rev.*, **101**, 2001, 3219-3232.
- 68 D. Barrett, A. Tanaka, K. Harada, E. Watabe, K. Maki and F. Ikeda, *Bioorg. Med. Chem. Lett.*, **11**, 2001, 1843-1849.
- 69 R. F. Epand, T.L. Raguse, S. H. Gellman and R. M. Epand, *Biochemistry*, **43**, 2004, 9527-9535.

## Chapter II

### II.1. The design and preparation of model amphiphilic cyclic peptides.

#### II.1.1. Design of a pore forming peptide template.

The development of synthetic peptide chemistry has lead to major advances in peptide structural analysis, providing an invaluable tool for studying the relationship between peptide structure and biological activity. A clearer understanding of this relationship has enabled the production of more active and less toxic pharmaceutical agents.<sup>1</sup>

A class of synthetic cyclic  $\beta$ -sheet type peptides was designed with the potential to mimic antibacterial activity by forming stable transmembrane pores in lipid bilayers.<sup>2</sup> The design was chosen following a bioinformatics exercise performed using non-homologous  $\beta$ -barrel membrane proteins from the protein data bank.

A sequence analysis was carried out on regular  $\beta$ -hairpins with similar structures and an analysis of amino acid preference for certain positions of the hairpins was performed; four residues: three tyrosine and a leucine residue were found to be highly conserved and were subsequently used in the design of the cyclic amphiphilic peptides. The sequence of the  $\beta$ -turns was also selected following this strategy which provided the asparagine-glycine-asparagine tripeptide turn for all our cyclic peptides.

The remaining residues were chosen so as to give the peptide an overall amphipathic structure, which would favour peptide insertion into a lipidic environment.

The cyclic peptide template was designed with a symmetrical sequence in order to simplify both the synthesis process and the subsequent study of peptide interactions with lipid membranes, as direction of insertion would then not be an issue.

The final template sequence contained 34 residues with alternating polar and non polar residues, creating an amphipathic partitioning of the amino acid side chains with all the polar residues situated along one face of the peptide.

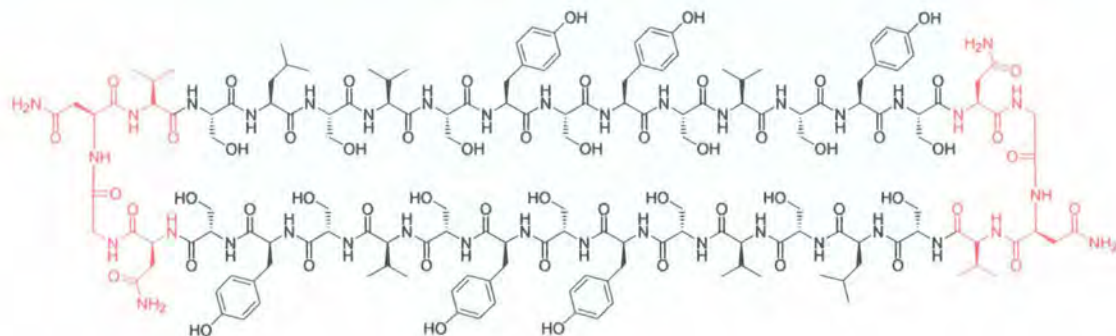


*Figure II.1.1 Cyclic peptide template.*

The alternating polar residues were all identical, serine residues and the hydrophobic residues contained eight  $\beta$ -branched residues, six valine and two leucine residues, which are thought to promote  $\beta$ -type conformations in peptides.<sup>4</sup>

A series of analogous peptides (Table II.1.1) were synthesised using the design of the template and only exchanging opposing pairs of tyrosine residues on either side of the template by pairs of tryptophan, cysteines or lysine residues. A pair of appropriately placed cysteine residues can give extra stability to the peptide structure by formation of a disulphide bridge and lysine residues can reduce the tendency of a peptide to aggregate, thereby increasing the ease with which the peptides can be manipulated and subsequently analysed.



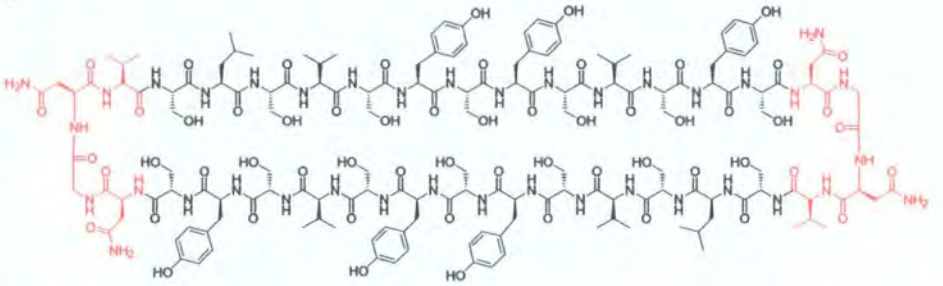
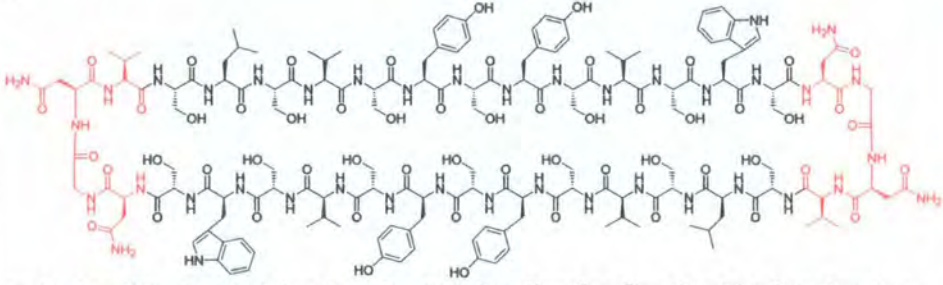
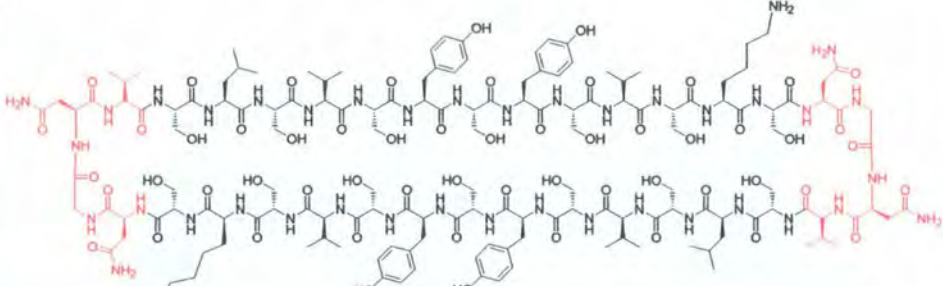
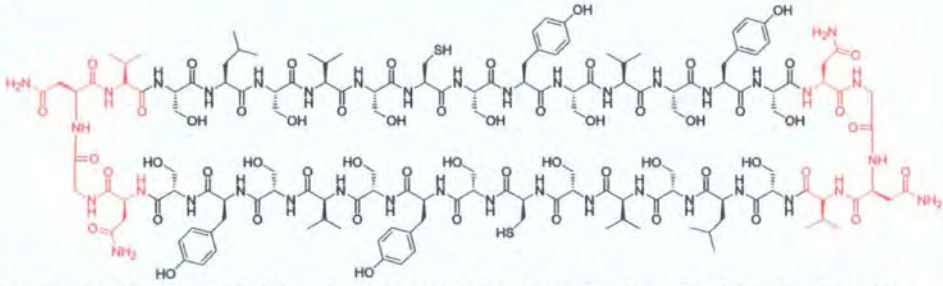
Synthetic amphiphilic peptide structures and names:	Ref. code
<p>1</p>  <p><b>cyclo-Asn-Gly-Asn-Val-Ser-Leu-Ser-Val-Ser-Tyr-Ser-Tyr-Ser-Val-Ser-Tyr-Ser-Asn-Gly-Asn-Val-Ser-Leu-Ser-Val-Ser-Tyr-Ser-Tyr-Ser-Val-Ser-Tyr-Ser</b></p>	6Y01
<p>2</p>  <p><b>cyclo-Asn-Gly-Asn-Val-Ser-Leu-Ser-Val-Ser-Tyr-Ser-Tyr-Ser-Val-Ser-Trp-Ser-Asn-Gly-Asn-Val-Ser-Leu-Ser-Val-Ser-Tyr-Ser-Tyr-Ser-Val-Ser-Trp-Ser</b></p>	2W4Y02
<p>3</p>  <p><b>cyclo-Asn-Gly-Asn-Val-Ser-Leu-Ser-Val-Ser-Tyr-Ser-Tyr-Ser-Val-Ser-Lys-Ser-Asn-Gly-Asn-Val-Ser-Leu-Ser-Val-Ser-Tyr-Ser-Tyr-Ser-Val-Ser-Lys-Ser</b></p>	2K4Y03
<p>4</p>  <p><b>cyclo-Asn-Gly-Asn-Val-Ser-Leu-Ser-Val-Ser-Cys-Ser-Tyr-Ser-Val-Ser-Tyr-Ser-Asn-Gly-Asn-Val-Ser-Leu-Ser-Val-Ser-Cys-Ser-Tyr-Ser-Val-Ser-Tyr-Ser</b></p>	2C4Y04

Table II.1.1. Series of amphiphilic cyclic peptides synthesised.

## II.1.2. Peptide synthesis and purification.

### II.1.2.1. Peptide synthesis.

The cyclic peptides were synthesised in parallel following the solid phase strategy originally developed by Merrifield from 1959 to 1963.<sup>3</sup> The synthesis was carried out in a fully automated procedure using a programmable peptide synthesiser in which the peptide chain was assembled in a step wise process.

The first amino acid, an  $\alpha$ -allyl ester and Fmoc (9-Fluorenylmethoxycarbonyl)  $\alpha$ -amino protected aspartic acid residue was attached to the solid support through its side chain and each subsequent residue was added to the growing chain, in a head to tail fashion or C to N terminal direction.

The coupling of the first amino acid was repeated to ensure maximum attachment to the resin, as the degree of amino acid anchorage would effect the subsequent peptide yield. All amino acids were used in a 5 fold molar excess to again ensure a high degree of peptide coupling.

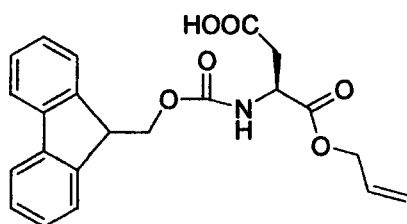


*Figure II.1.2. Aspartic acid residue with  $\alpha$ -allyl ester and Fmoc  $\alpha$ -amino protecting groups*

Fmoc chemistry was used to protect the  $\alpha$ -amino end of the peptide as it can easily be removed under mild basic conditions such as a 20 % by volume solution of piperidine in dimethylformamide, DMF at room temperature;

these conditions are completely orthogonal to the acidic conditions required for the side chain deprotection of tert-butyl and Boc groups as well as the cleavage of the peptide chain from the solid support.<sup>4,5,6</sup>

The support used in the peptide synthesis was a modified rink amide resin, compatible with Fmoc chemistry, which transfers an amine group to the aspartic acid residue attached to the resin during the cleavage process, transforming this group into an asparagine residue which forms part of the  $\beta$ -turn in the final peptide.

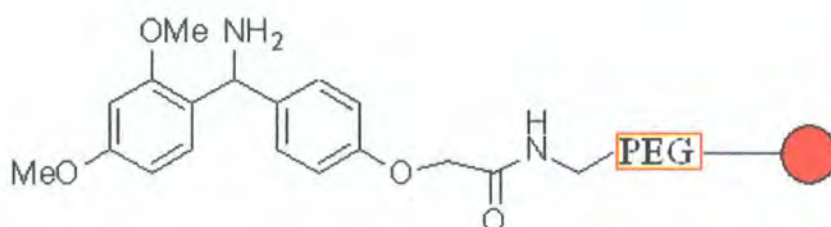


Figure II.1.3. Solid support (tentagel) rink amide resin

Pseudoproline dipeptides:<sup>5</sup> tyrosine-serine, leucine-serine, tryptophan-serine and valine-serine were used to minimize any problems associated with peptide aggregation, branching instead of linear synthesis and incomplete coupling. The use of dipeptides also reduces considerably the length of the synthesis.

The serine residue is regenerated from the oxazolidine by trifluoroacetic acid deprotection.

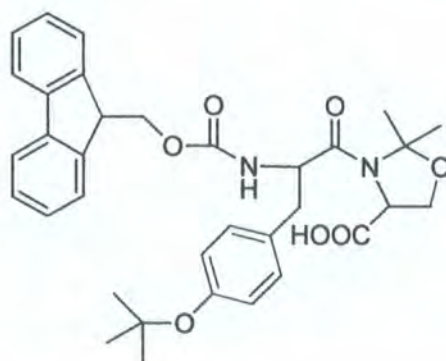


Figure II.1.4. The Fmoc protected Pseudoproline dipeptide Tyrosine(tBu)-Serine.

### II.1.2.3. Cyclisation.

The peptide was cyclised *in situ* while still attached to the solid support, following removal of the  $\alpha$ -allyl ester protection to regenerate the  $\alpha$ -carboxylic group of the first amino acid residue. The  $\alpha$ -allyl ester can be removed selectively in presence of the Fmoc, Boc and *t*-butyl-based protection groups, with a palladium(0) catalyst, such as Pd (Ph<sub>3</sub>P)<sub>4</sub>.<sup>7,8</sup>

The peptide was then cyclised by coupling the deprotected  $\alpha$ -carboxy group of the first amino acid with the deprotected  $\alpha$ -amino group of the last amino acid in the peptide chain.

### II.1.2.4. Cleavage.

Side chain deprotection of the Boc and *t*-butyl-based groups as well as regeneration of the serine residues from the oxazolidine are carried out during the cleavage of the finished cyclic peptide from the solid support.

The deprotection and cleavage reactions require a highly acidic solution, 95 % TFA, with a range of scavengers to neutralise any reactive cationic species generated from the break down of protecting groups such as from the tert-butyl groups and the rink amide linkers. Scavengers such as water and 1,2-ethanedithiol (EDT) can provide protection, to electron rich tyrosine and cysteine residues, from modification by reactive cations. Trialkylsilanes are also used as non-odorous substitutes for EDT and are efficient against stabilized cations produced from the rink amide linkers.

### II.1.2.5. Purification.

The crude peptide was purified by Reverse Phase High Performance Liquid Chromatography, RP-HPLC.

The peptide was dissolved in hexafluoroisopropanol, HFIP and loaded on to a pre equilibrated analytical C8 column; the peptide was eluted from the column in

a solvent system containing a high proportion of fluorinated alcohols, TFE and HFIP. This system was necessary to contend with the highly hydrophobic character of the cyclic peptides as they show a very low degree of solubility in most common solvents with the exception of fluorinated alcohols.

The solvent system and running conditions had to be optimised extensively because of difficulties with the peptides interacting or “sticking” to the hydrophobic stationary phase of the column, as the peptide would flow straight through the column. Peptide affinity for different stationary phases was tested by using columns with different packing such as C18 or a diphenyl packing, but the peptides did not appear to adhere to these columns over the range of conditions tried. The addition of a small amount of water to the solvent system helped increase the amphiphilic cyclic peptide affinity for the analytical C8 column.

The wavelength selected for monitoring sample elution from the column was 274 nm as this showed the aromatic side chain absorption from the tyrosine and tryptophan residues with minimal interference from both amide and solvent absorption.

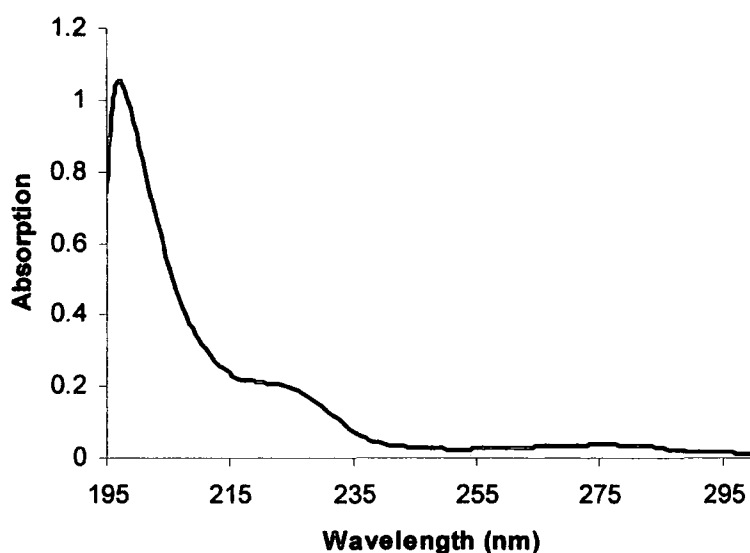


*Figure II.1.5. UV absorption of the purified cyclic 6Y01 peptide in TFE.*



A range of solvent combinations, gradients and flow rates were tried in order to maximum peak separation and hence peptide separation and purification from other components and by products. The solvent system, which produced the best result was a multi solvent system composed of the fluorinated alcohols in which the peptides are readily soluble, HFIP and TFE in a 1:9 (v/v) ratio, acetonitrile with 0.1 % TFA and a small amount of water (10 % v/v) which gave a much better peak separation.

The eluate, corresponding to the area under each peak produced, was carefully collected for analysis.

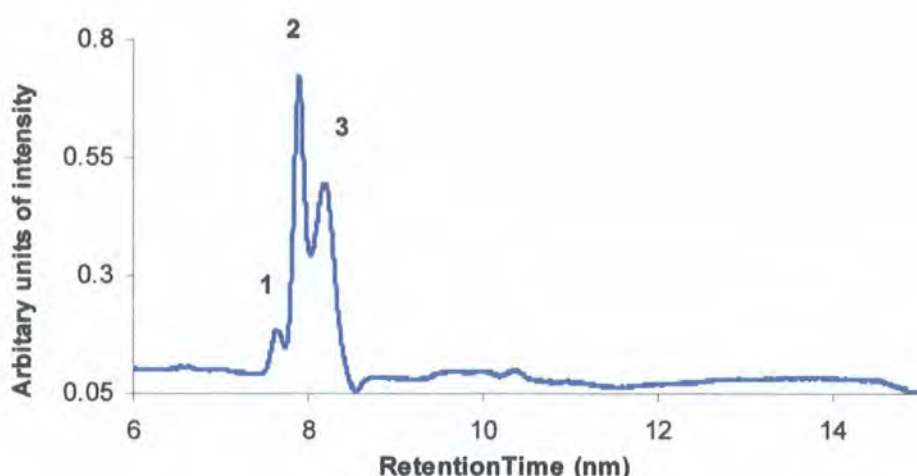


*Figure II.1.6. HPLC profile for the cyclic peptide 2K4Y03.*

The analogous amphiphilic cyclic peptides eluted from the column with different retention times, which appeared to reflect the hydrophobic character of the peptides, with the more hydrophobic of the series interacting with the column over a longer period of time; the peptides, which had no charged residues, such as the peptides with six tyrosine residues (6Y01) or four tyrosine and two tryptophan residues (2W4Y02) eluted from the column much later, at 12.6 minutes, than the peptide with two lysine and four tyrosine residues (2K4Y03) which eluted from the column at only 7.6 minutes.

### II.1.3. Determination of peptide concentration.

Peptide concentration was calculated following UV titrations; set volumes of peptide in trifluoroethanol were added by increments to a sample cell and the UV absorption, which was measured for each increase in peptide volume, was then plotted (after taking into account corrections for the change in TFE volume) against the change in the volume of peptide solution.

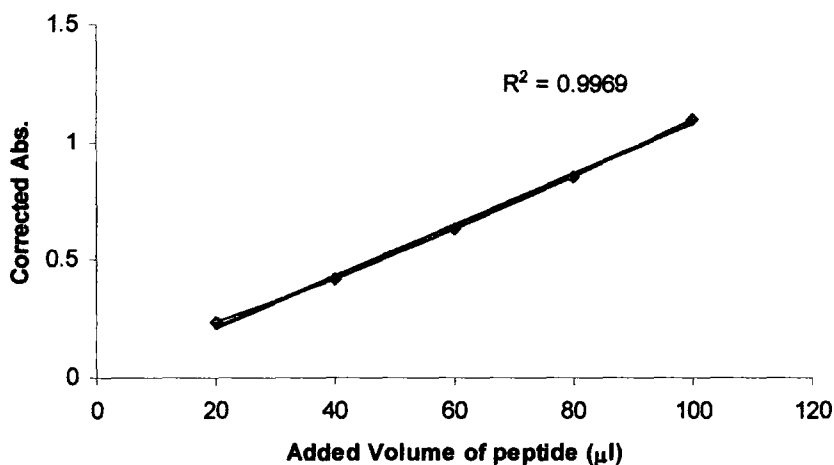


*Figure II.1.7. Plot of the corrected absorption against the volume of peptide solution added to the cell.*

A plot which produced a straight line would then validate the direct relationship between increase in peptide volume and the corrected absorption for a given peptide concentration and could subsequently be used with the Beer Lambert law to calculate peptide concentration:

$$C = A_{\text{corr}}/(\epsilon \cdot L) \text{ and } A_{\text{corr}} = A \cdot (V_o + V)/V_o$$

*Where C is the conc. of the peptide in solution; A is the peptide absorption at a given wavelength; A<sub>corr</sub> is the corrected absorption after taking into account the change in volume of solution in the cuvette; L is the path length (L=1 cm); ε is the extinction coefficient of the peptide at a given wavelength and is calculated by summing up the number of residues in the peptide that absorb at that given wavelength; V<sub>o</sub> is the initial volume (in μl) of solution in the sample cuvette and V is the added volume of peptide solution (in μl).<sup>9</sup>*

#### II.1.4. Peptide analysis.

Mass analysis of the peptide proved to be a difficult as well as a lengthy process because of both the low solubility in most solvents and the lack of ionisation shown by the cyclic hydrophobic peptides.<sup>10</sup>

The purified peptides were initially processed for mass spectral analysis by positive mode electrospray ionisation (ESI<sup>+</sup>) mass spectrometry, which is a widely used atmospheric pressure ionisation technique for mass measurements of proteins and peptides.<sup>11</sup>

Briefly a sample dissolved in a volatile solvent is injected into a capillary; a high voltage (3-4 kV) is applied to the tip of the capillary creating a strong electric field, which disperses the sample emerging from the capillary into an aerosol of highly charged droplets. A gas, usually nitrogen flowing along the out side of the capillary tube directs the sample spray towards the mass analyser. A stream of warm nitrogen gas helps evaporate the solvents molecules from the sample ions; some of which will then pass through the sampling cone and aperture into the analyser, where they are separated according to their mass-to-charge (m/z) ratios. A detector amplifies the ion current and sends the signal to a data system, which out puts the data as spectra of the ion m/z values plotted against their intensities, from which the number components, the molecular weight and the relative abundance of each component can be obtained.

Electrospray analysis can be quite difficult to interpret as peptides with molecular weights greater than 1 kDa may give rise to multiple charged molecular related ions such as (M+nH)<sup>+</sup>, which produce a whole series of ions each differing by a single charge from its neighbours:<sup>12,13</sup>

$$\frac{m}{z} = \frac{M + nH}{n}^{+}$$

*Where m/z are measured mass to charge ratios; n is the integer number of charges on the ion, H<sup>+</sup> is the mass of a proton and M is the molecular ion.*



The ion may also form adducts with several different cations and compounds such as TFA, which is included in low concentrations to help the ionisation process; the combinations of  $n\text{Na}^+$  ions and  $n\text{K}^+$  ions as well as any other adducts can be quite daunting to interpret. Fragmentation of sample ions also occurs, resulting in very complex and difficult spectra. Further more plasticizers frequently leach from sample vial lids and eppendorf tubes, contaminating the sample solution and producing strong signals, which mask the sample signal.

Positive electrospray ionisation, performed on the amphiphilic cyclic peptide (6Y01), produced a weak, but consistent signal showing a series of multi charged ions from 5  $\text{Na}^+$  to 9  $\text{Na}^+$  ions giving the correct mass ( $3590 \text{ g mol}^{-1}$ ) for the peptide.

The sampling cone voltage (40 to 100 V) can also be optimised for each sample, but a balance has to be maintained between low voltage with the lower energy producing less fragmentation in the sample and an increase in voltage with the higher energy enhancing protonation and hence producing a stronger signal. Changing the cone voltage did not enhance the signal for the cyclic peptide, but increased the extent of fragmentation.

Calibration and test measurements were carried out using a commercially available cyclic peptide, Valinomycin, which is less hydrophobic than the template cyclic peptides.<sup>16</sup>

Analysis of very hydrophobic peptides is difficult due to their very low solubility in solvents other than fluorinated alcohols, like TFE and especially HFIP. The fluoride ion was initially suspected of interfering with the ionisation and detection process of the mass spectrometer; therefore to eliminate this possibility, a soluble protein, human serum albumin (HSA) was dissolved in both methanol and HFIP before being submitted for electrospray analysis; the spectra of both samples gave comparable results.

#### II.1.4.1. Solvent carrier system.

The choice of mass spectroscopy solvent carrier systems was also given a great deal of consideration.<sup>11,14</sup> The polar solvent systems, methanol, acetonitrile and water, routinely used in the process are not suitable for very hydrophobic peptides, as these tend to aggregate and precipitate out of solution.

The solvent system had to be adapted to suit the hydrophobic character of the cyclic peptides; a range of solvents in various ratios, such as TFE, HFIP, chloroform and the addition of different concentrations of formic acid and TFA, were examined for compatibility as carrier solutions. Systems with a high proportion of HFIP produced better signals, although the less noxious solvent TFE was generally preferred

#### II.1.4.2. Derivatives.

Several other solutions were proposed for addressing the problem of low solubility, such as derivatisation of the peptides with a quaternary ammonium ion (Figure II.1.8), and although the modified peptides were readily soluble in aqueous solvents, they gave complex mass spectrum signals with extensive fragmentation, which could not be interpreted unambiguously.<sup>15</sup>

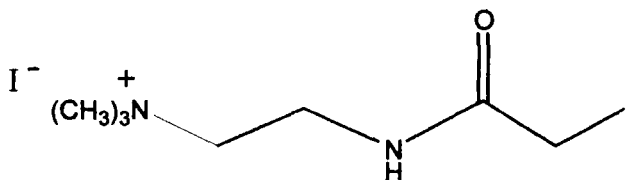


*Figure II.1.8. The quaternary ammonium ion, [2-(acetylamino)ethyl]trimethylammonium iodide.*

### **II.1.4.3. Detergents**

The efficiency of low concentrations of detergents, such as sodium dodecyl sulphate (SDS), Triton X-100 and 3-(3-cholamidopropyl)dimethylammonio-2-hydroxy-1-propanesulphide (CHAPS) in solubilising the cyclic hydrophobic peptides was examined using a range of detergent concentrations, from 0.3 % to 1 % (w/v) and of solvents, including water, methanol, ethanol and fluorinated solvents, but all the detergent solutions were found to interfere quite severely with the ion formation in ESI<sup>+</sup> mass spectrometry. Although another widely used mass spectrometry technique, Matrix-Assisted Laser Desorption Ionisation (MALDI), is more tolerant of the presence of detergents and electrolytes in sample solutions,<sup>12,16,17,18,19,20</sup> no signal was produced for the cyclic peptide in detergent solutions by either mass spectral techniques used, ESMS or MALDI MS.

### **II.1.4.4. Matrix-Assisted Laser Desorption Ionisation (MALDI).**

MALDI mass spectroscopy has proven to be a very efficient tool for analysing hydrophobic peptides and proteins and has scope and versatility for optimisation of sample preparation methods.<sup>21,22,23,24</sup> A sample is pre-mixed with a low molecular weight, UV absorbing matrix before being bombarded with a pulsed laser beam (N<sub>2</sub>;  $\lambda$  337 nm) to induce sample ionisation. The matrix, which is in vast excess effectively transforms the laser light into excitation energy to ionise the sample, as direct ionisation would cause the sample to fragment or decompose.

Ions from both the sample and matrix molecules are sputtered from the surface of the mixture (Fig. II.1.9) and accelerated with the same electrical potential difference (in a stationary electric field) towards a detector. Ions allowed to drift in the electric field, separate according to their mass-to-charge ratio with lighter ions drifting more quickly than heavier ions.

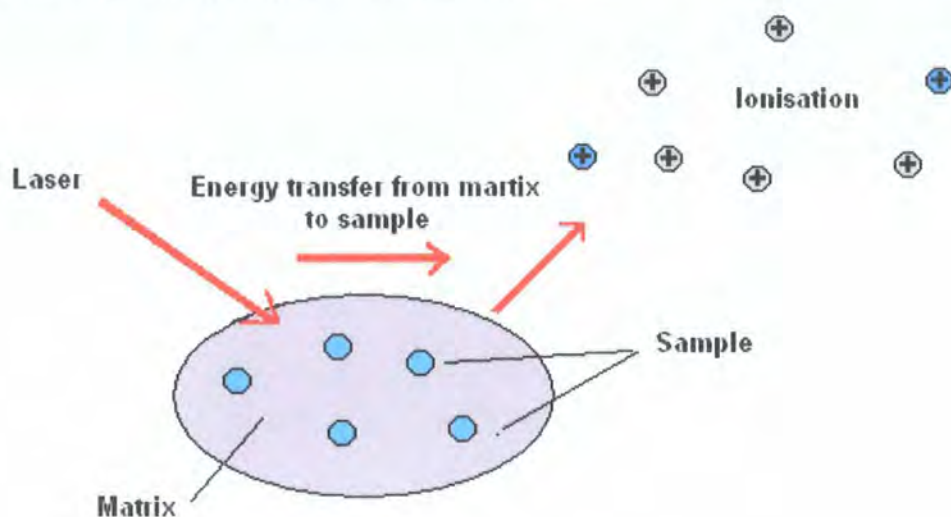


Figure II.1.9. Diagram showing the ionisation process in MALDI MS.

The time of flight taken for a molecule of mass,  $m$  and charge,  $z$  to drift towards the detector is proportional to the square root of the mass of the ion:  $t \propto (m/z)^{1/2}$ ; hence the signal output can be converted to a typical mass spectrum of mass-to-charge ratio versus intensity.

An extensive range of matrices is available for use with a whole range of molecules; Sinapinic acid; 2-(4-hydroxy-phenylazo)-benzoic acid (HABA);  $\alpha$ -cyano-4-hydroxycinnamic acid, ( $\alpha$ CHCA) and 2,5-dihydroxybenzoic acid (DHB) matrices are in general suitable for use with peptides and proteins, but their effectiveness depends on the individual characteristics of the sample to be analysed. A range of conditions, matrices, peptide-matrix ratios and solvents were examined for the cyclic hydrophobic peptide mass measurements by MALDI mass spectroscopy

The best results were obtained with the HABA matrix and to a lesser extent with the sinapinic acid matrix.

Both the peptide and the matrix had to be dissolved in HFIP with 0.1 % TFA, before premixing and spotting onto the MALDI sample plate to dry.<sup>25</sup> When either the sample or the matrix were dissolved in any of the other solvents tried, including TFE, the signal was broader and of a much lower intensity. As the ratio of matrix to protein can also severely affect the signal resolution, a range of ratios were investigated for both HABA and sinapinic acid matrices with the hydrophobic samples; a range of molecular ratio from 1:140 to 1:14,000 were tested; the best results were obtained for matrix to peptide molecular ratios from 1:1400 to 1:3000.

The MALDI spectra of the cyclic amphiphilic peptides showed peaks with the correct mass for the linear versions of the peptides with allyl ester protection group still attached. The same increase in mass was observed for all analogue peptides in the series; peptides 2W4Y02 and 2K4Y03 for which two of the original tyrosine (Y) groups had been replaced by two tryptophan (W) and two lysine (K) groups respectively.

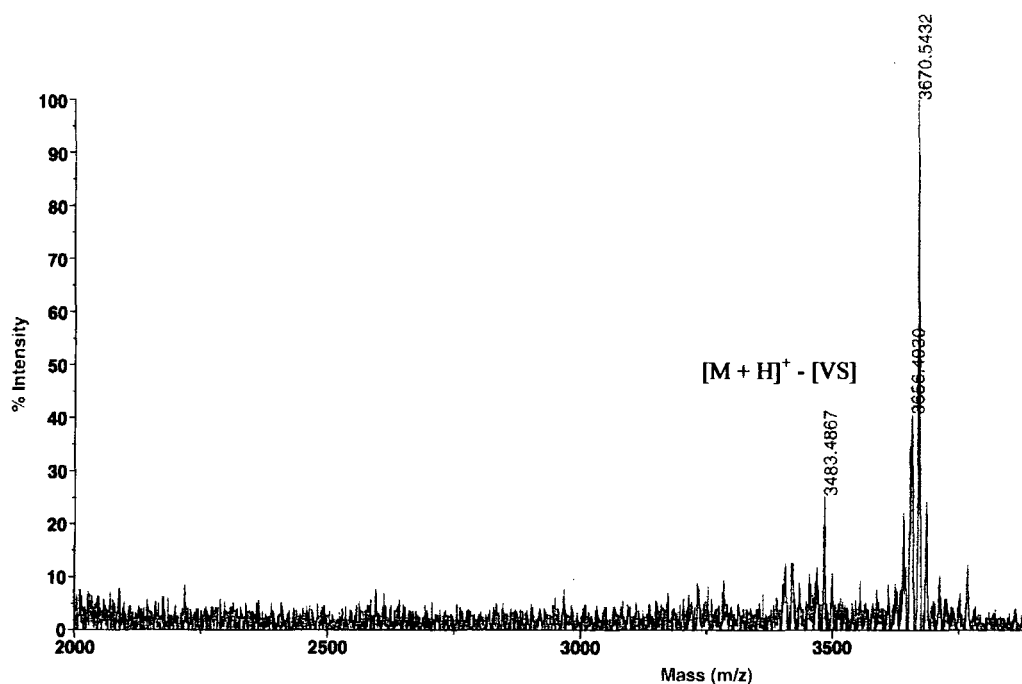


*Figure II.1.10. MALDI mass spectrum of the 6Y01 peptide with a major peak corresponding to the linear peptide with allyl ester protection group and a minor peak showing fragmentation of the peptide with loss of the final dipeptide, valine-serine.*

The synthesis process for the peptides was re-examined and the reactivity of the catalyst was found to be at fault; a fresh batch of catalyst was synthesised and particular care was taken in storing the compound, to prolong its shelf life.<sup>26</sup>

Following allyl ester deprotection and cyclisation, performed with fresh reagents, MALDI MS gave the correct mass for the cyclic 2K4Y03 peptide, but only produced a board and low intensity signal for the more hydrophobic peptides. The 2K4Y03 peptide with the two charged lysine residues was more soluble and behaved better in solution than its more hydrophobic analogues.<sup>27,28,29</sup>

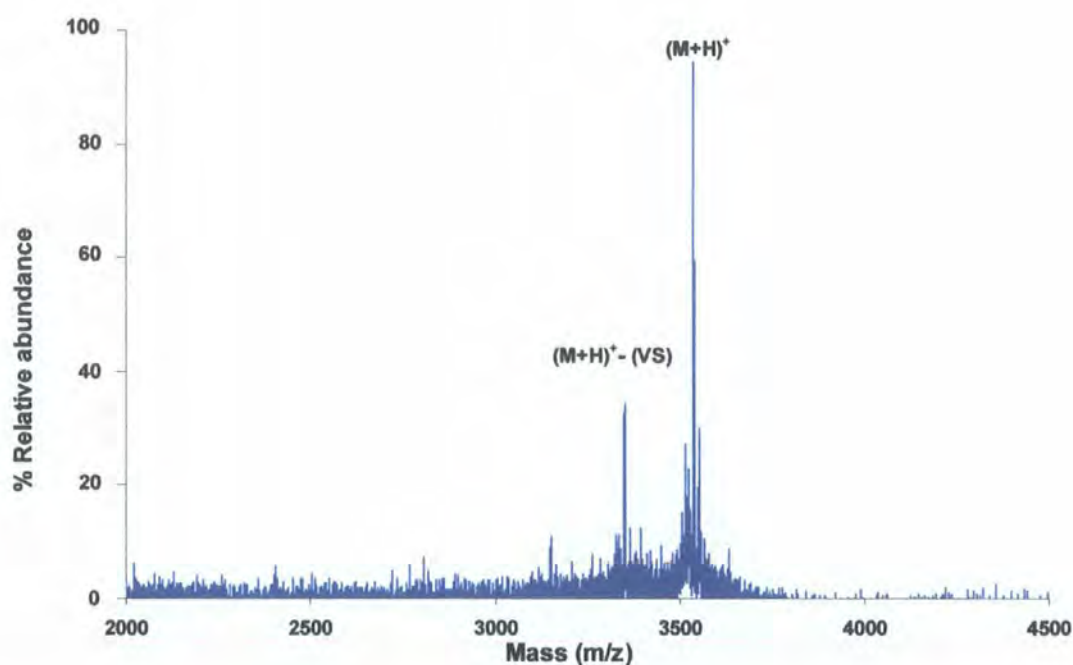


*Figure II.1.11. MALDI mass spectrum showing a major peak for the 2K4Y03 cyclic hydrophobic peptide ( $M_r$ : 3520) and a minor peak indicative of peptide fragmentation with loss of the final dipeptide valine-serine.*

Analysis by MALDI mass spectroscopy of the amphiphilic cyclic peptides needs to be further optimised, especially for the more hydrophobic cyclic peptides by exploring other solvent mixtures including the use of high concentrations of

formic acid (70 %), which has given good results with integral membrane proteins.<sup>25</sup>

A wider range of matrix to protein ratios could also be tried as well as other methods such as the use of a temperature leap system in which the sample and matrix are maintained at 4 °C overnight and then heated to 37 °C for an hour before analysis. This method has been quite successful for keeping hydrophobic proteins in solution and producing well resolved spectra.<sup>30</sup>

## II.2 The analysis of amphiphilic cyclic peptide interactions with phospholipid membranes.

A range of analytical techniques including spectroscopy, calorimetry and microscopy were employed in order to gain comprehensive structural information on the amphiphilic cyclic peptides as well as some understanding of their interactions and behaviour in different environments, aqueous and lipidic.

### II.2.1. Circular dichroism spectroscopy.

#### II.2.1 1. Introduction to the technique.

Circular dichroism (CD) spectroscopy has become a well established and very useful tool in protein and peptide structural studies, providing qualitative information about peptide and protein secondary structure and the structural relationship with the immediate environment. A signal is produced in circular dichroism spectroscopy from the difference in absorption,  $A$ , of a molecule between left and right circularly polarized light:  $CD = \Delta A = (A_L - A_R)$ .

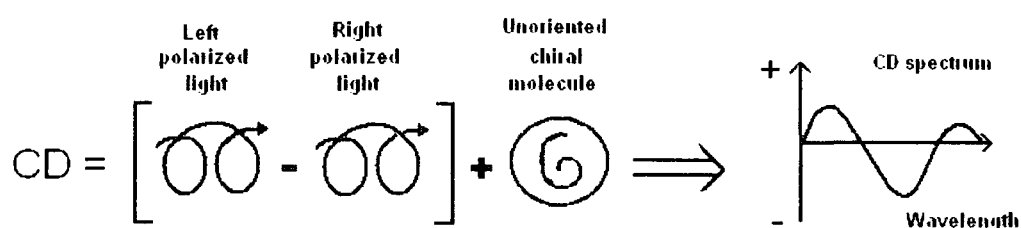
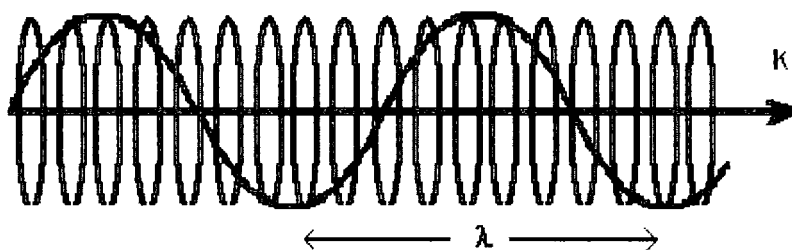


Figure II.2.1. Diagram showing the generation of a CD spectrum.



Light, as electromagnetic radiation has two components, an electric and a magnetic field that oscillate at right angles to each other and to the direction of propagation of the radiation. When a beam of light is circularly polarized, the electric field component traces out a helix along the axis of propagation of the beam.



*Figure II.2.2. Circularly polarized light, where K is the propagation direction.*

Chiral molecules are asymmetrical, they have no reflection plane and their elections will adopt a helical motion in circularly polarized light, interacting to different extents with the left and right-handed photons of the circularly polarized light. The helical motions of the electrons in a chiral molecule can be related through this difference in absorption, which produces the CD signal, to the arrangement within the molecule of atoms and bonds in space.<sup>31</sup>

All common proteinogenic amino acids are chiral molecules; they show the same handedness (L configuration), with the exception of glycine. The amino acid building blocks transmit this handedness to the protein structure along the protein backbone, giving chirality to the whole protein. The CD spectrum of a protein or peptide is thus directly related to its secondary structure, which has enabled considerable structural information to be obtained using a quite straight forward technique.

The CD signal is produced in units of ellipticity,  $\theta$ , in millidegrees, versus wavelength (nm)  $\lambda$ , rather than difference in absorption, ( $\Delta A$  versus  $\lambda$ ) and is expressed as the mean molar ellipticity.

$$\begin{aligned}\text{CD} &= \Delta A = (A_l - A_r) \\ &= 4\pi \theta \text{ (degrees)} / 180 \ln 10 \\ &= \theta \text{ (millidegrees)} / 32,982\end{aligned}$$

### II.2.1.2. Evaluation of secondary structure content of a peptide

CD spectral data do not always lend themselves easily to interpretation and often distinguishing the extent to which one structural motif is present in a macromolecule over that of another can be quite daunting. Bands produced in the CD spectrum by certain structural motifs such as  $\beta$ -sheet and  $\beta$ -turn motifs tend to overlap, producing a more difficult or complex spectrum to interpret.<sup>41</sup>

A number of algorithms have been written to deconvolute CD spectra, which have been very useful for identifying and quantify the percentage of the major structural motifs present within the overall peptide or protein structure.<sup>32</sup> Secondary structural motifs from numerous peptides and proteins for which the structure has been determined by other reliable methods such as X-ray crystallographic and solution NMR techniques, have been well documented and are used as reference libraries to help interpret CD spectra.<sup>33,34,35,37</sup>

CD spectroscopy is mostly used in peptide research, as a means of monitoring changes in peptide conformation, as peptides are exposed to different environments, such as an aqueous media with a range of additives or lipidic and detergent micelles, both of which are thought to mimic membrane bilayers.

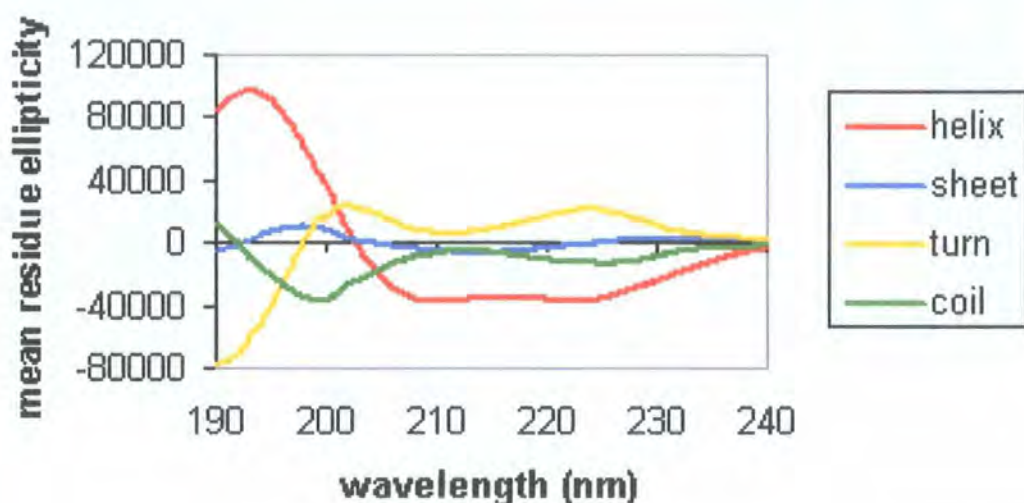


*Figure II.2.3 Diagram showing typical CD spectra for different types of protein secondary structure.<sup>31</sup>*

Often interpretation of spectra from a peptide, because of the limited sequence size (from a few residues to several tens of residues) can be achieved through comparison of the spectrum with reference spectra for the different typical structural motifs, as these are characteristic for each motif type.

The CD spectrum of a random coil or unordered structure shows a single strong minimum below 200 nm. The general characteristics of a  $\beta$ -sheet motif are those of a negative band between 210 and 215 nm as well as a positive band between 195 and 200 nm, whereas the  $\alpha$ -helix typically exhibits a large positive band near 200 nm and double minima of similar magnitude at 208 nm and 222 nm.

These typical spectra are then complicated by the particular structural content of a peptide in a given environment.

Peptides with high  $\beta$ -sheet content have been reported to show double minima, similar to an  $\alpha$ -helix except in the relative magnitude of the peaks, with a band

around 210 nm and another around 220 nm; however in peptides with moderate  $\beta$ -sheet content the second band at about 220 nm is reduced relative to the band around 210 nm.<sup>37,34</sup>

A number of other factors can also affect the CD spectrum of a peptide, adding further to the level of difficulty of structural determination: aggregation of peptide monomers is thought to produce a marked reduction in ellipticity of spectral data; twists in the  $\beta$ -strand have been observed to induce a red-shift in the CD spectra and the relative number of aromatic side-chains in a peptide is also thought to affect the strength of any negative bands around 200 nm.<sup>35,36</sup>

Aromatic side chains produce a CD signal in the near UV region of the spectra the intensity of this signal is very much dependent on the immediate environment of the aromatic residues and therefore the signal will also be affected by a change in solvent and other solutes.

#### **II.2.1.3. The dependence of the peptide structure on its environment.**

A number of solvents are known to have stabilizing effects on the secondary structure for which the peptide has a propensity. The fluorinated alcohols, trifluoroethanol, TFE and hexafluoroisopropanol, HFIP have the strongest structure promoting effect, though other solvents such as methanol, ethanol and acetonitrile are also thought to have weaker structure stabilizing effects.<sup>37,38,39,40</sup>

The stabilizing effect mediated by fluorinated alcohols like TFE and HFIP is thought to be an entropically driven process that arises from interaction between the hydrophobic portion of the alcohol with the hydrophobic groups present in the peptide and the consequent displacement of the shell of water molecules from around the peptide.<sup>37</sup>

Linear peptides like cecropins and magainins, which are unordered in aqueous media, are reported to adopt a helical structure in the presence of both HFIP and TFE.<sup>41,42</sup>

The structure adopted by a peptide in one environment may be different from that assumed in another; some peptides, which have helical structures in presence of stabilizing solvents and under aqueous conditions, adopt a  $\beta$ -sheet conformation

in presence of lipid vesicles or detergent micelles.<sup>37</sup> Detergents, like Sodium Dodecyl Sulphate, SDS are used, below their critical micellar concentration to mimic the hydrophobic core of membranes and lipid vesicles are commonly used as substitute models for biological membranes.<sup>40,43,44</sup>

#### **II.2.1.4. Circular dichroism study of amphiphilic synthetic peptides.**

Circular dichroism, CD was used to investigate the secondary structure adopted by the synthetic amphiphilic peptides under different environmental conditions and over a range of peptide concentrations. The peptides were designed to contain a basic structure for pore forming  $\beta$ -barrel peptides and therefore to have a propensity for  $\beta$ -sheet type structures in membranes.

The question then arises as to whether the peptide would have an ordered structure in aqueous media or would only adopt a stable structured conformation in a lipidic environment.

### II.2.1.5. Conformation of the template amphiphilic peptide in aqueous solution.

The structure of the template amphiphilic peptide were first monitored in a 4 % TFE/water solution over a range of peptide concentrations from 30 to 50  $\mu\text{M}$ .

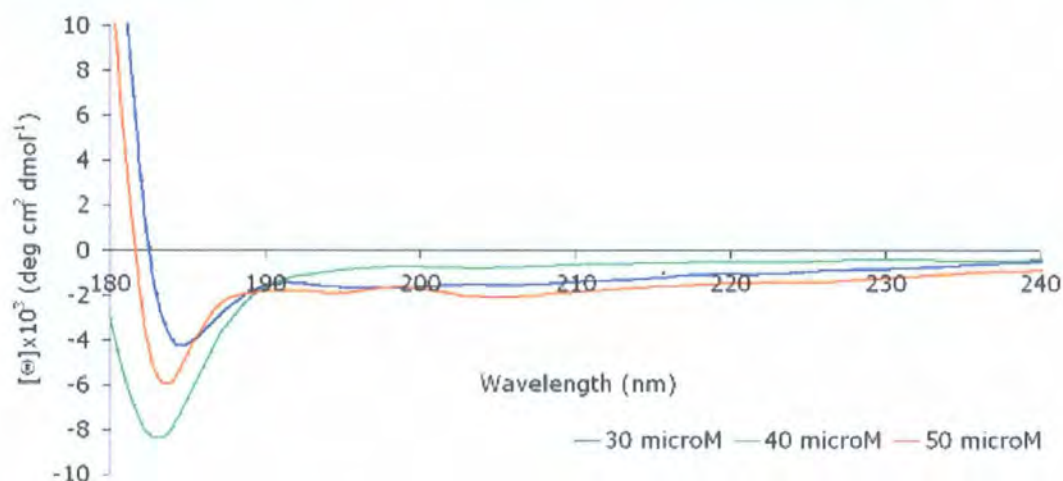


*Figure II.2.4. CD spectra of the template peptide 6Y01 in a 4 % TFE solution of pure water.*

The CD spectra clearly showed the peptide to have an unstructured conformation in the 4 % TFE pure water solution over the range of peptide concentrations studied. This result isn't surprising considering the highly hydrophobic nature of the peptides and the fact that peptides with  $\beta$ -sheet type structure assume less readily native conformations than their more hydrophilic counterparts which have a predisposition towards  $\alpha$ -helical structures.



### II.2.1.6. Conformation of the template amphiphilic peptide in a buffer-salt solution.

The peptide conformation was then study over a range of concentrations in a 10 mM Tris-150 mM NaCl buffer containing 4 % TFE (at pH 7.4); the resulting spectra were no longer indicative of typical unordered structures but showed the emergence of maxima between 200 nm and 215 nm.

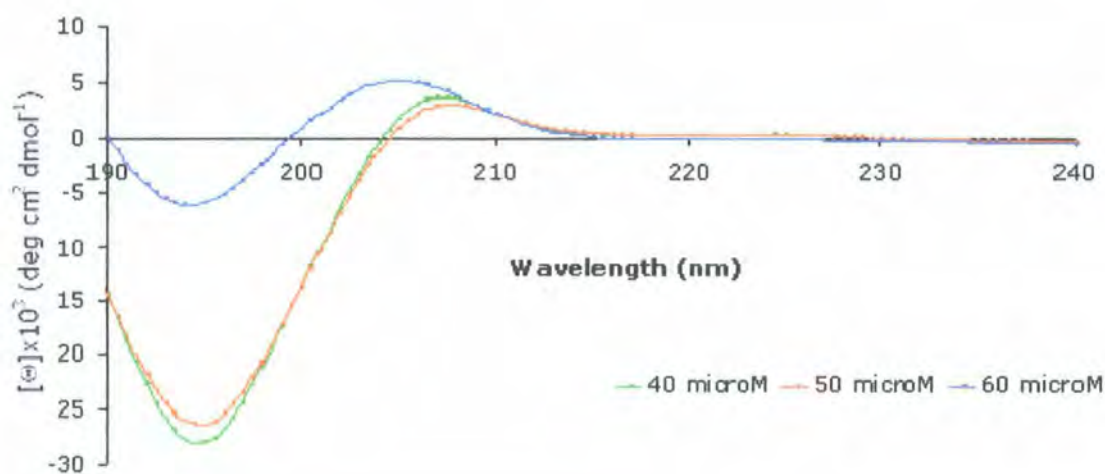


*Figure II.2.5. CD spectra of the peptide 6Y01 measured over arrange of concentrations from 40 to 60  $\mu$ M in a 10 mM Tris-150 mM NaCl solution with 4 % TFE at pH 7.4.*

Following an increase in peptide concentration from 40 to 60  $\mu$ M, a net reduction in the intensity of the negative band arising at 195 to 200 nm and an increase in the positive band above 200 nm, were measured in the CD spectra. These changes are indicative of a concentration dependence effect on peptide conformation. The sharp change in ellipticity for the peptides at 60  $\mu$ M is strongly indicative of the occurrence of peptide self assembly, which may further complicate determination of the peptide conformation.<sup>45</sup>

After monitoring the peptide behaviour for indication of aggregation over a range of peptide concentrations from 10 to 80  $\mu\text{M}$ , the circular dichroism study was further pursued using a peptide concentration of 50  $\mu\text{M}$  that gave both a strong signal and did not appear to show signs of peptide aggregation.

#### **II.2.1.7. Conformation of the template amphiphilic peptide in a TFE buffer solution.**

Various amounts of TFE, from 15 % to 75 % (v/v) of the total sample solution, are reported to induce ordered secondary structure in peptides; the effect of TFE, in promoting a structured conformation in the amphiphilic peptide, was investigated by increasing the initial volume of 4 % to 15 % (v/v) TFE.

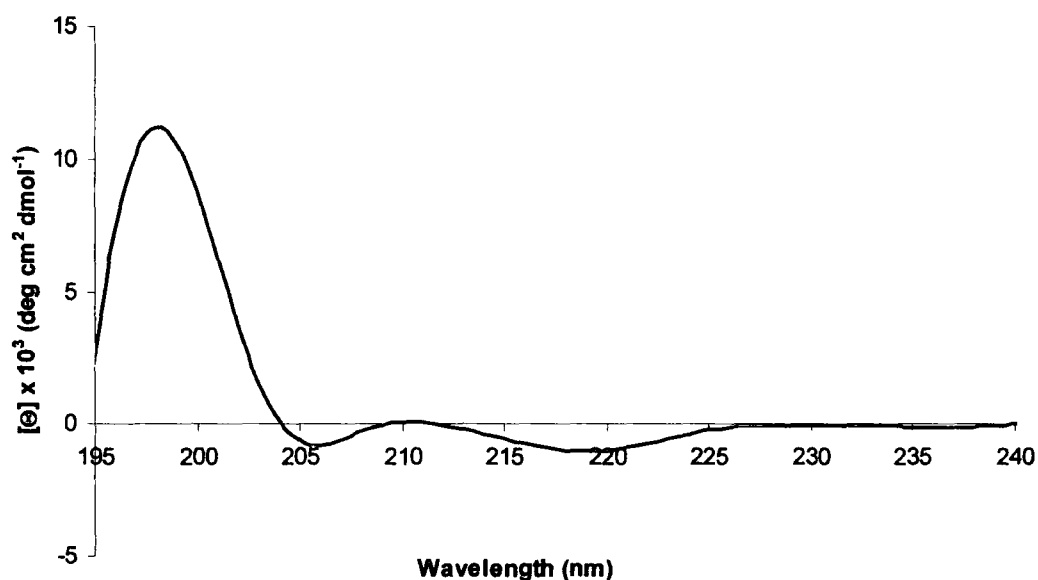


*Figure II.2.6. CD spectra of peptide 6Y01 at a concentration of 50  $\mu\text{M}$  in 10 mM Tris-150 mM NaCl buffer with 15 % TFE (v/v) at pH 7.4.*



The CD spectra for the peptide changed considerably on addition of 15 % TFE to the sample buffer, which strongly suggests that TFE in relatively low concentrations can induce the amphiphilic peptide to adopt a conformation comparable to that of an antiparallel  $\beta$ -sheet with a maximum centred on 200 nm and two minima of lower magnitude around 208 and 220 nm.<sup>47</sup>

An increase in the TFE concentration from 15 % to 30 % (v/v) appears to further stabilize an antiparallel  $\beta$ -sheet conformation in the amphiphilic peptide, suggesting that it has a strong propensity for this conformation (Fig.II.2.7).

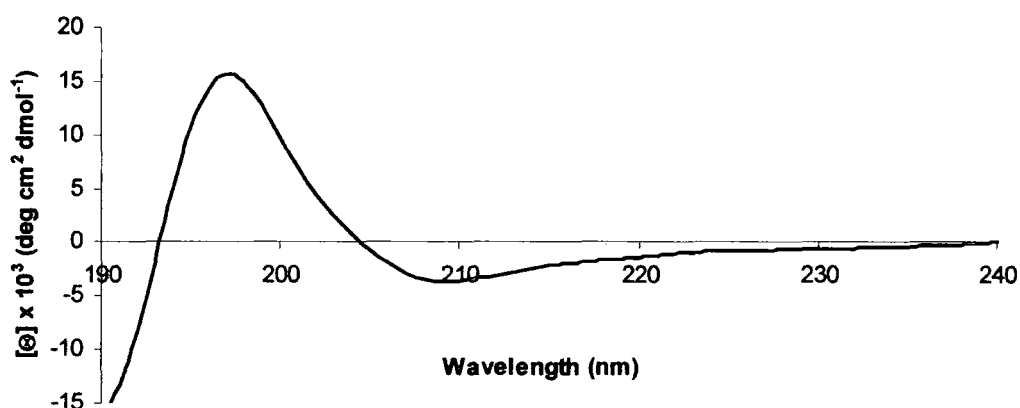


*Figure II.2.7 CD spectrum of the peptide 6Y01 at 50  $\mu$ M concentration in a 10 mM Tris-150 mM NaCl buffer with 30 % TFE (v/v) at pH 7.4.*

The concentration of TFE was further increased to 50 % (v/v) which did not show any significant change in the peptide structure.

### II.2.1.8. Conformation of the amphiphilic peptides in unilamellar lipid vesicles.

In order to determine the conformation that the peptides would adopt in a lipid membrane the structure of the amphiphilic peptides was monitored in the presence of a 1 mM concentration of unilamellar vesicles (100 nm in diameter) composed of egg phosphatidyl choline, EPC, a mixture of phospholipids commonly used as models for biological membranes.

The CD spectra of the amphiphilic peptides were recorded, over a range of concentrations from 30  $\mu\text{M}$  to 50  $\mu\text{M}$ , in an EPC lipid-buffer solution with 4 % TFE.

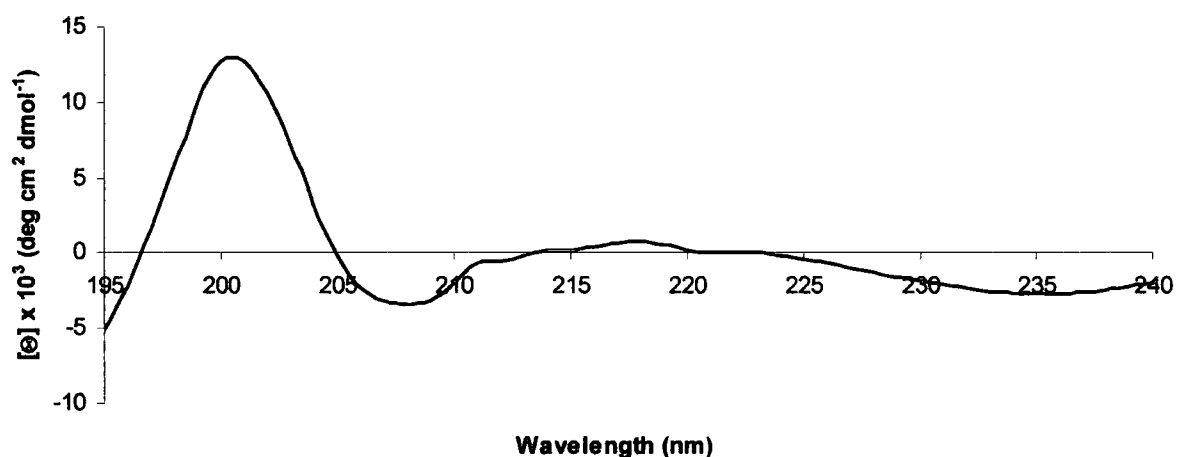


*Figure II.2.8. CD spectrum of the peptide 6Y01 at 50  $\mu\text{M}$  in EPC (1 mM) and Tris (10 mM)-NaCl (150 mM).*

The CD spectrum of the 6Y01 peptides in EPC solution exhibited a typical  $\beta$ -sheet pattern with a maximum at 200 nm and a minimum between 205 and 210 nm. The second minimum from 225 to 240 nm may be attributed to the aromatic side chains of the peptide tyrosine residues.<sup>46,47</sup>

The conformation of the analogous peptides 2W4Y02 and 2K4Y03, in which two of the original tyrosine residues had been replaced by two tryptophan and two lysine residues respectively, was also analysed by circular dichroism in an EPC lipid vesicle and buffer solution.

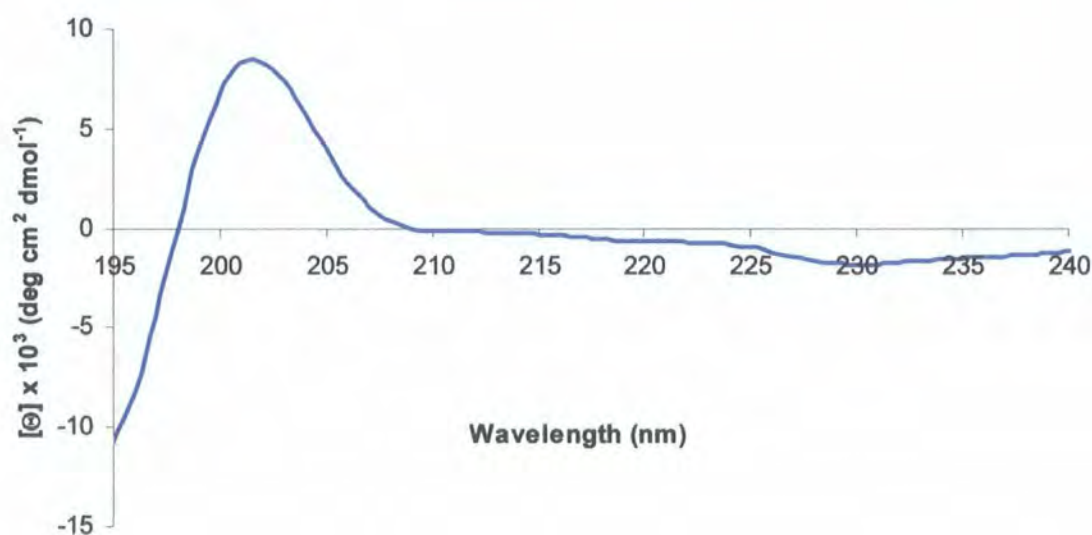


*Figure II.2.9. CD spectrum of the peptide 2W4Y02 at 50  $\mu$ M in EPC (1 mM) and Tris (10 mM)-NaCl (150 mM) with 4 % TFE.*

The CD spectrum of the 2W4Y02 peptide in lipid environment exhibited a  $\beta$ -sheet pattern with a maximum at 200 nm and a shallow minimum from 215 nm to 220 nm, which then extended into another stronger minimum from 225 nm to 240 nm. This second minimum may as in the case of the 6Y01 cyclic peptide be attributed to the aromatic tryptophan and tyrosine side chains of the peptide.<sup>46,47</sup>

The 2K4Y03 peptide produced a CD spectrum in EPC lipid bilayers that was again characteristic of a  $\beta$ -sheet structure with a maximum just below 200 nm and a minimum from 205 nm to 210 nm. The second minimum from 225 nm to 240 nm, which was quite significant in the spectra of both the 6Y01 and 2W4Y02 peptides, had only a weak presence in the CD spectrum of the 2K4Y03 peptide; the decrease in ellipticity of the second minima could be due to a reduction in the number of aromatic side chains in this peptide.

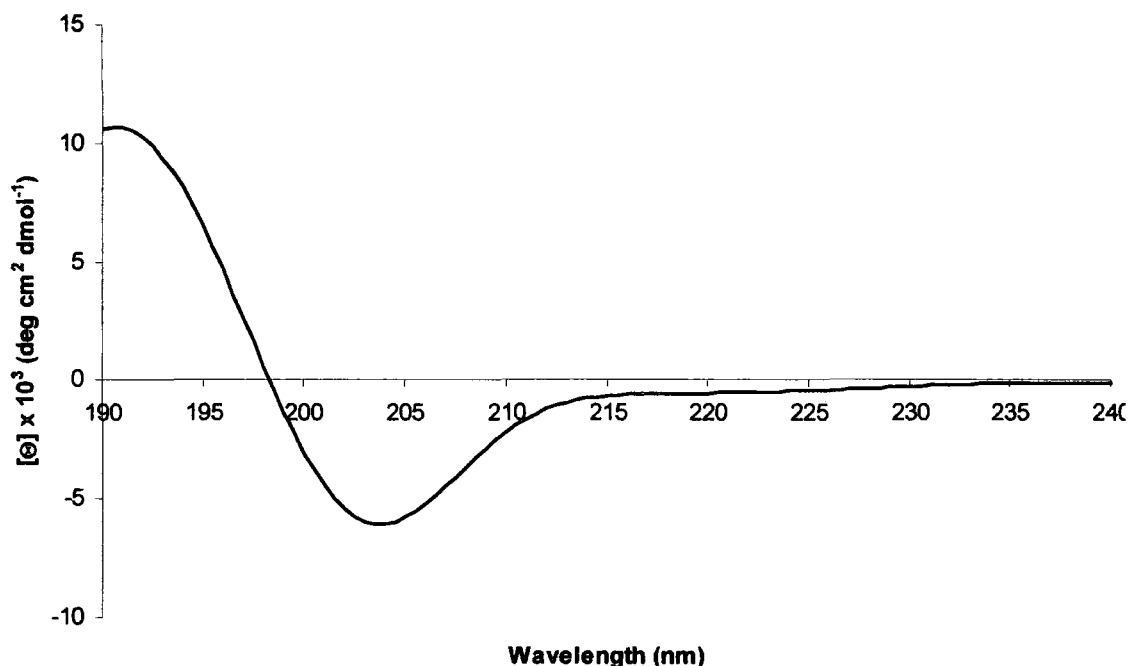


*Figure II.2.10. CD spectrum of the peptide 2K4Y03 at 50  $\mu$ M in EPC (1 mM) and Tris (10 mM)-NaCl (150 mM) with 4 % TFE.*

Circular dichroism is the most common technique for monitoring conformational changes in both peptides and proteins, as a consequence of a change brought about to the environment of the macromolecule, such as the addition of solutes or a change in pH of the solution. The present study was conducted in order to establish whether the amphiphilic peptides have a propensity to adopt  $\beta$ -sheet structures, by studying their conformation in a range of environments; in aqueous solutions, in the structure stabilizing solvent TFE and in an EPC lipid vesicle solution, which is commonly used to mimic a membrane environment.

The template amphiphilic peptide 6Y01 was shown to adopt an unordered conformation in a solution of 4 % TFE (v/v) and pure water, but was clearly no longer completely unordered when its CD spectrum was monitored in a 10 mM Tris-150 mM NaCl buffer again with 4 % (v/v) TFE, which suggests that the peptide had adopted some intermediate non random state in this solution.<sup>45</sup>

The concentration of TFE was increased to a level which has been shown to provoke conformational changes by inducing the peptide to adopt a preferred or most stable conformation in presence of the fluorinated alcohol. The amphiphilic peptide clearly revealed a propensity for a  $\beta$ -sheet type structure over the range of TFE concentrations used in this study.

In phosphatidylcholine membranes, all the peptides examined, displayed a characteristic  $\beta$ -sheet type structure, which strongly indicates that the main driving force behind  $\beta$ -sheet formation could be the interaction with a hydrophobic environment and therefore that these analogous amphiphilic peptides are predominantly membrane bound.

A range of synthetic cyclic and linear transmembrane peptides, designed to investigate the mechanism of  $\beta$ -sheet formation in lipid membranes, have been shown by circular dichroism to successfully adopt  $\beta$ -sheet structures in a membrane environment.

A systematic investigation was carried out on a synthetic hydrophobic hexapeptide (acetyl-WLLLLL) to explore contributions from side chain-side chain and side chain-membrane interactions, as well as interstrand hydrogen bonds on  $\beta$ -sheet formation in phospholipid membranes. The primary structure of the hexapeptide was modified by replacing the central leucine residue with one of a range of more polar or hydrophobic residues or with residues such as glycine, which would give conformational flexibility or proline, which would display structure breaking properties in the peptide. These peptides all adopted random coil structures in aqueous media and oligomeric antiparallel  $\beta$ -sheets in phospholipid membranes, when the central leucine residue was replaced by a hydrophobic residue of any size or character. This study demonstrates the essential function that the hydrophobicity of the peptide sequence has on  $\beta$ -sheet formation in membranes.<sup>46</sup>

A series of cyclic peptide analogues of the antimicrobial peptide gramicidin S (GS), which is known to adopt a stable  $\beta$ -hairpin structure with 2  $\beta$ -turns in membranes, were designed with distinct structural and functional characteristics in order to assess the effect of varying the hydrophobicity and amphipathicity of the peptides on  $\beta$ -sheet formation in membranes.

The more hydrophobic and amphipathic peptides displayed the strongest affinity for phospholipid membranes as well as a tendency to self aggregate.<sup>36</sup>

A dodecyl cyclic peptide {Cyclo-(LLLD)<sub>3</sub>}, where D is a L-diaminopropionic acid, which is thought to play a role in conductance of peptide channels} was designed to adopt an amphiphilic planar ring structure in membranes with hydrophobic side chains oriented towards the lipidic media and polar residues towards the centre of the ring structure to form a hydrophilic channel. Circular dichroism demonstrated that the synthetic peptide could form a stable  $\beta$ -sheet structure in the absence of a hydrophobic environment and that the peptide could adopt a  $\beta$ -sheet structure in both aqueous media as well as in membrane mimicking environments such as octanol-methanol.<sup>48</sup>

A high level of ring structure stability has been shown to have a major influence on  $\beta$ -sheet formation. Hydrophobic peptides, which possess ring structures stabilized by several disulphide bonds such as the 18 residue cyclic defensin peptide RTD-1, which has 3 intramolecular disulphide bonds, can adopt a  $\beta$ -sheet conformation in both aqueous solution and in lipidic environments.<sup>49</sup>

## II.2.2. Linear dichroism

### II.2.2.1 Introduction to the technique

Linear dichroism, the sister technique to circular dichroism, has been optimized by A. Rodger *et al*, 2002,<sup>50</sup> to provide useful information on the interactions between molecules and the orientation of the molecules relative to one another. This technique has revealed itself to be particularly valuable for determining the orientation of amphiphilic peptides on interaction with lipid membranes and was used in this work to give a measure of the orientation of the template peptide 6Y01 following interaction with a phospholipid bilayer.

Linear dichroism, LD is the difference in absorption of light polarized parallel and perpendicular to an oriented direction or axis,  $LD = A_{\parallel} - A_{\perp}$

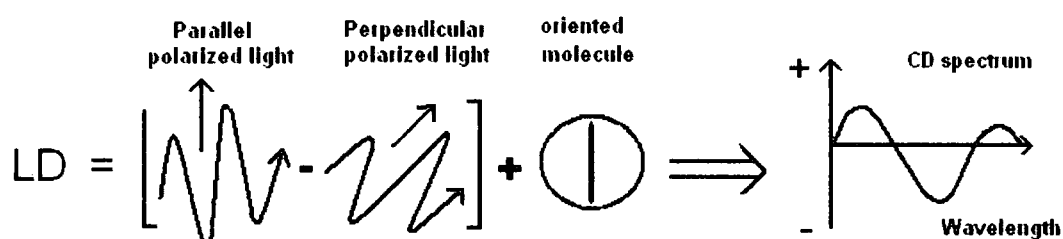


Figure II.2.11. Diagram showing the generation of a LD spectrum.

A number of conditions need to be met in order for a molecule or a system, such as peptide interacting with a lipid bilayer, to give a LD signal; molecules must have a significant absorption in the visible and near UV regions of the spectrum as well as the ability to be physically aligned parallel to one of the polarization directions of the light. The electronic transitions of the molecules, which interact with the incident light, are aligned to ensure that they conserve maximum interaction with the polarized or oriented light.

The sample molecules can be aligned if they have an intrinsic property such as a charge dipole, a naturally elongated shape or the capacity to be deformed during the experiment.

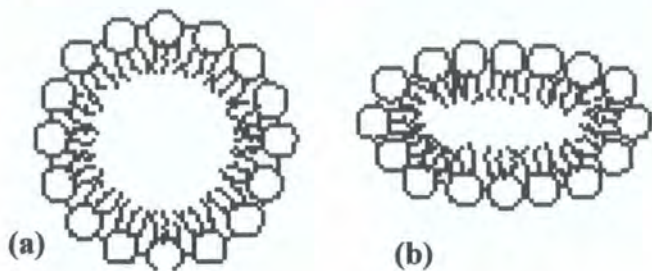


Figure II.2.12. Diagrams of (a) a liposome and (b) a shear deformed liposome.

In peptide-lipid systems, the liposomes are the component that is oriented as they can be physically elongated by sheer deformation in a spinning flow Couette cell.

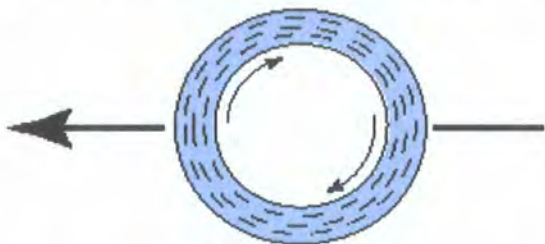


Figure II.2.13. Diagram showing the alignment of molecules in solution by sheer flow gradient in a Couette cell, which is basically a spinning cylinder within a concentric sleeve.<sup>51</sup>

The orientation direction in the peptide-lipid system is defined as the orientation of the peptide transition moments relative to the normal of liposome bilayer.

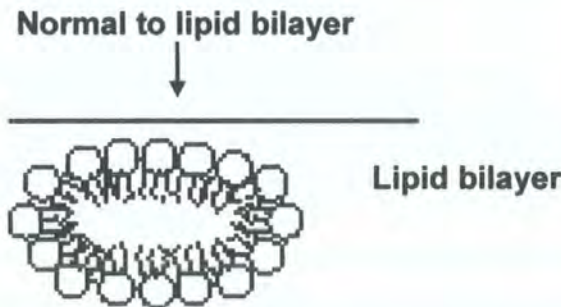


Figure II.2.14. Showing the orientation direction in the peptide-lipid system.



The deformed liposome system was modelled as a cylinder by Ardhammer *et al.*<sup>52,53,54</sup> with the LD signal of the system given by:

$$LD \approx 3 S / 4 (1 - 3 \cos^2 \alpha_i)$$

Where  $S$  is the proportion of liposomes that have oriented parallel to the flow direction, and is assumed to be equal to 1 and  $\alpha_i$  is the angle made by the transition moment of the peptide relative to the normal of the lipid bilayer.

#### II.2.2.2. The peptide transition moments need to be determined for interpretation of the template peptide-lipid LD signal.

Typical absorbance for proteins and peptides in the UV region are from 180 nm to 240 nm and for residues with aromatic side chains from 250 nm to 280 nm<sup>55</sup>. The  $n$  to  $\pi^*$  transition for which no simplistic modelling can be devised gives a series of perpendicular and parallel bands from 210 nm to 230 nm with the perpendicular bands appearing at lower energy than the parallel band. The  $\pi$  to  $\pi^*$  polarization is located along the C=O bond axis with net polarization perpendicular to the peptide backbone run at about 190 nm to 200 nm and the transition moment for the tyrosine residues gives a signal from 260 nm to 300 nm.<sup>51</sup>

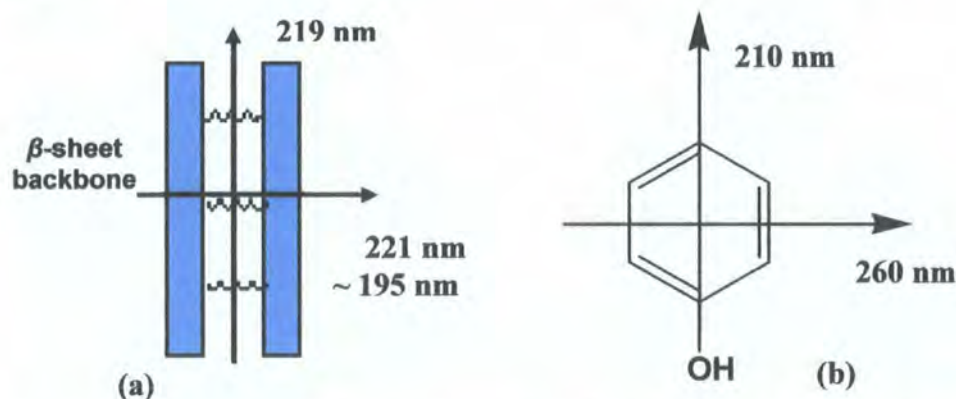
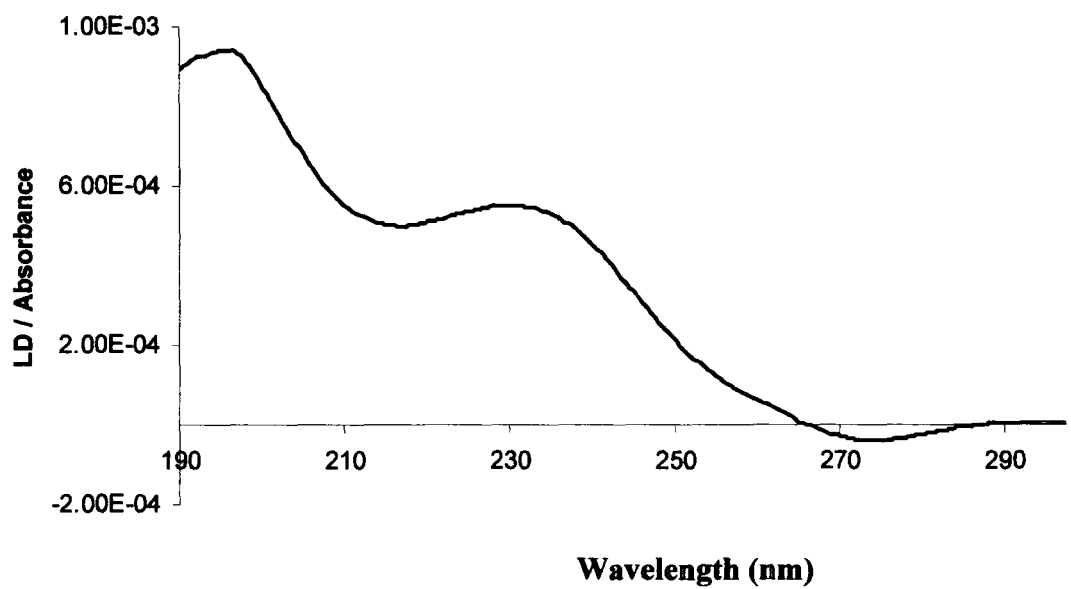


Figure II.2.15. Showing (a) the orientation of the  $\beta$ -sheet transition moments polarizations relative to the peptide backbone and (b) the tyrosine transition moment polarizations.

The interaction of the template peptide 6Y01 with egg phosphatidyl choline, EPC liposomes was analysed by linear dichroism using a rotating Couette flow cell to orient the EPC, liposomes in the sample mixture.



*Figure II.2.16. Linear dichroism spectrum (averaged over 64 scans) of amphiphilic cyclic peptide, 6Y01 (0.4 mg mL<sup>-1</sup> in 1 mg mL<sup>-1</sup> lipid in H<sub>2</sub>O) in EPC liposomes.*



The LD spectra shows two positive peaks at 200 nm and at 230 nm corresponding to transition polarizations perpendicular to the peptide backbone and hence perpendicular to the normal of the lipid bilayer and parallel to the bilayer itself. This result shows strong support for the template peptide insertion into the lipid bilayer of the EPC liposome with the peptide backbone oriented in a more parallel than perpendicular direction relative to the normal of the lipid bilayer.

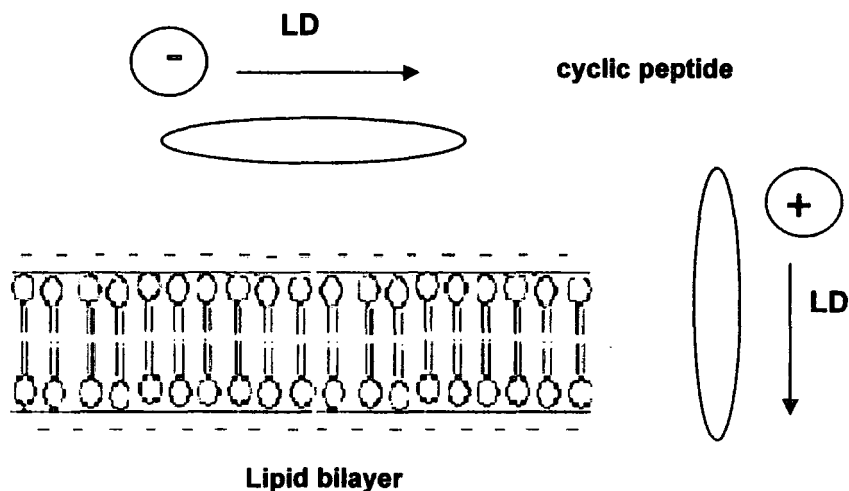


*Figure II.2.17. Diagram showing the peptide backbone orientation relative to the lipid bilayer for negative and positive LD signals.*

The absence of a peak at 208 nm which is typical of  $\alpha$ -helical structures and the strong positive peak at 200 nm confirm the peptide to have adopted a  $\beta$ -sheet type conformation. The tyrosine residues give a negative peak from about 270 to 280 nm and show the aromatic rings to have oriented more in the plane of the normal to the lipid bilayer and hence in the same plane as the lipid monomers in the bilayer.

The Linear dichroism study of the cyclic amphiphilic template peptide-EPC system has not only provided support for previous evidence from CD, that the peptide adopts a  $\beta$ -sheet type conformation in presence of phosphatidyl choline bilayers, but also strongly suggests that the peptide inserts in the lipid bilayer with the peptide backbone oriented parallel to the normal of the lipid bilayer.

Another technique for detecting the orientation of peptides embedded in lipid layers is by means of a conventional circular dichroism spectrometer on oriented samples (OCD). The cyclic antimicrobial  $\beta$ -sheet peptide rhesus theta defensin, RTD-1 was mixed with phosphatidylcholine and phosphatidylglycerol lipids in a solution of chloroform and TFE, before being spread onto quartz plates. As the solvent evaporated the sample self-assembled into multilayers aligned parallel to the substrate surface. The orientation of the peptide in the lipid membrane was shown by OCD to change as a function of sample hydration, as the relative degree of humidity of the sample was increased up to 100 %. In fully hydrated samples the ring of the peptide backbone appeared to adopt an orientation parallel to the plane of the bilayer, which would indicate that the peptide could form channels in membranes through stacking of the peptide backbone ring structure to form a tubular structure with the hydrophilic residues oriented towards the inside of the ring.<sup>49</sup>

The synthetic amphiphilic cyclic peptide 6Y01 on the other hand was shown (by linear dichroism) to orient with its backbone perpendicular to the plane of the phospholipid bilayer and could therefore possibly form a  $\beta$ -barrel type structure in phospholipid membrane similarly to those formed by prokaryotic outer membrane proteins.

### II.2.3. Differential scanning calorimetry (DSC).

#### II.2.3.1. Introduction to the technique.

Differential scanning calorimetry is the study of thermodynamic parameters associated with thermally induced phase transitions and has proven to be an extremely useful tool for the study of the thermotropic phase behaviour of lipids in biological and model systems.<sup>56</sup>

Phospholipids spontaneously form concentric multilayered bilayers vesicles separated by layers of water, on hydration with aqueous media.

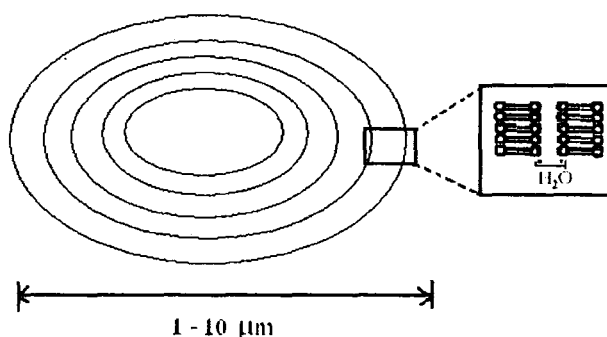


*Figure II.2.18. Multilamellar liposome.*

The lipid bilayer undergoes a fully reversible phase transition from an ordered solid-gel like state to a fluid liquid crystalline state as the temperature of the hydrated lipid is increased to above the transition temperature ( $T_m$ ) of the lipid.

Phospholipids show a pre-transition,  $T_p$  which is associated with a small enthalpy change and a main transition,  $T_m$  associated a much larger enthalpy change (Fig. II.2.19).

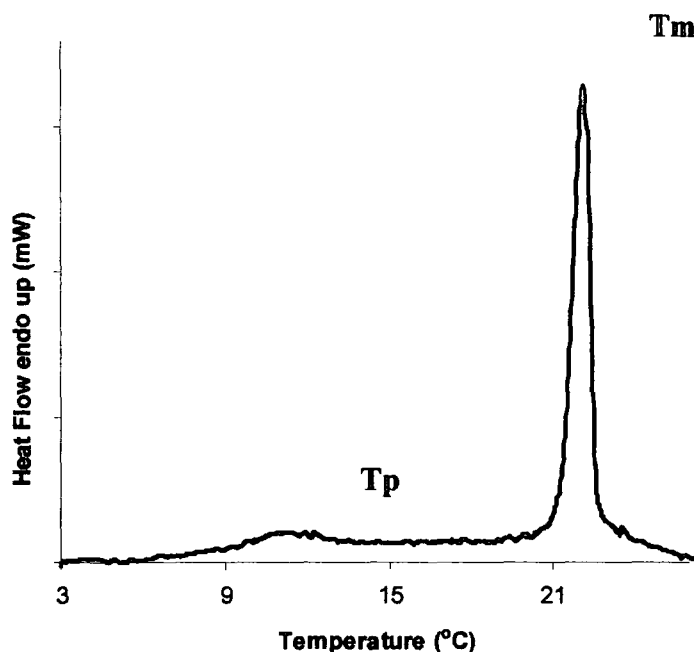


*Figure II.2.19. DSC thermogram of fully hydrated dimyristoyl phosphatidyl choline, DMPC, showing the lipid pre-transition,  $T_p$  centred on 12 °C and the main transition,  $T_m$  on 23 °C.*

The phospholipid bilayers adopt, below the lipid pre-transition temperature, a structured arrangement in which the lipid monomers are tilted to as much as 58° relative to the plane of the bilayer; this arrangement is thought to maximise lipid chain interactions by filling space created by the bulky choline lipid headgroups in the gel phase.<sup>58</sup>

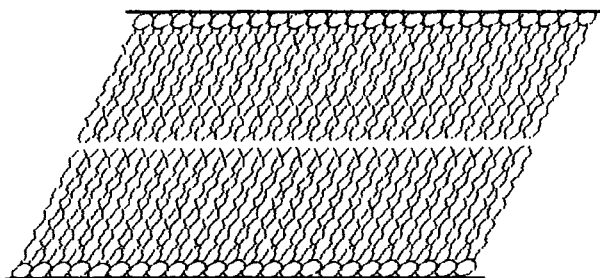


*Figure II.2.20. Showing the tilted lipid monomers in the gel phase, below the pre-transition temperature.*

The lipid monomers undergo a change in orientation during the pre-transition, from a tilted to a more perpendicular orientation relative to the plane of the bilayer. The pre-transition can be used as a sensitive indicator of the presence of even minor amounts of impurities in the lipid bilayer and consequently will be absent from the DSC trace of a disturbed bilayer.<sup>56,57</sup>

As the temperature is further increased past the pre-transition and up to the main transition, the bilayer appears to adopt a rippled structure; above the main transition temperature the lipids become more disordered and fluid like as the degree of freedom of the lipid monomers increases with temperature.

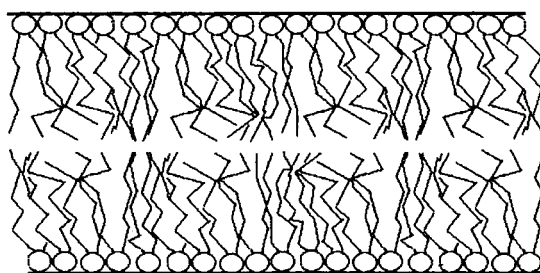


*Figure II.2.21. Showing the disordered lipids in the fluid phase, above the main transition temperature of the lipids.*

The actual conformation of the lamellar bilayer is not affected by the phase change, although the bilayer undergoes a lateral expansion as well as a decrease in thickness as it reaches the fluid state.

#### **II.2.3.2. Differential Scanning Calorimetric analysis of peptide-lipid systems.**

This calorimetric technique was used to examine the effect of the template peptide 6Y01 on the temperatures and enthalpies of the pre-transition,  $T_p$  and the main transition,  $T_m$  of phospholipid bilayers.

### II.2.3.3. Peptide-DMPC systems.

The fully hydrated pure DMPC sample gave two peaks in the DSC thermogram, a weak broad peak centred at 12 °C corresponding to the phospholipid pre-transition and a strong narrow main transition peak at 23 °C in agreement with the literature values.<sup>58,59</sup> The effect of the amphiphilic peptide 6Y01 on the phase transition temperature and the enthalpy change of DMPC was investigated over a range of peptide to lipid molar ratios.

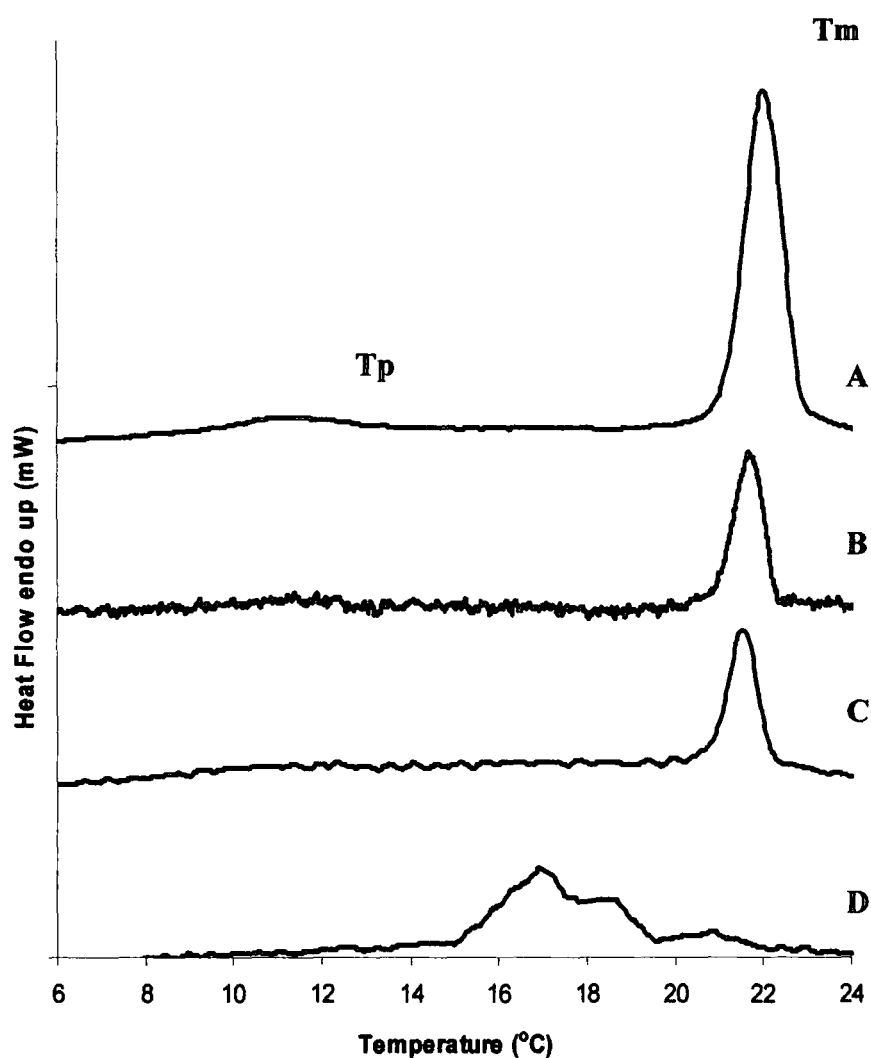


*Figure II.2.22. DSC thermograms of fully hydrated DMPC-6Y01 peptide mixtures (20-30 wt % suspension) with a range of molar ratios of peptide to lipid: 0 (A), 0.02 (B), 0.08 (C) and 0.2 (D). The samples were submitted to a minimum of 6 heating and cooling cycles from 6 to 26 °C, at a rate of 2 °C min<sup>-1</sup>.*



The peptide 6Y01 at peptide to lipid molar ratios as low as 0.02 had a significant effect on the integrity of the lipid bilayer; causing the disappearance of the pre-transition, a reduction by half of the enthalpy change as well as a slight decrease in the temperature of the main transition. At the higher molar ratio of 0.2, the effect was greater still with a considerable broadening of the main transition and a shift of around 4 °C to a lower temperature.

These results indicate that at the highest peptide to lipid ratio of 0.2, the 6Y01 peptide produced a significant overall destabilisation of the gel state DMPC bilayers.

#### II.2.3.4. Peptide-DPPC systems.

Another saturated phospholipid with a longer chain length and a higher transition temperature was again studied over a range of peptide to lipid ratios in order to analyze the effect of the peptide on a lipid with a less fluid and much more rigid conformation.

The DSC thermogram of fully hydrated multilamellar vesicles of the dipalmitoyl phospholipid, DPPC in pure water showed a broad and weak pre-transition centred at 36 °C and a strong sharp main transition at 41 °C (Fig. II.2.23).<sup>60</sup>

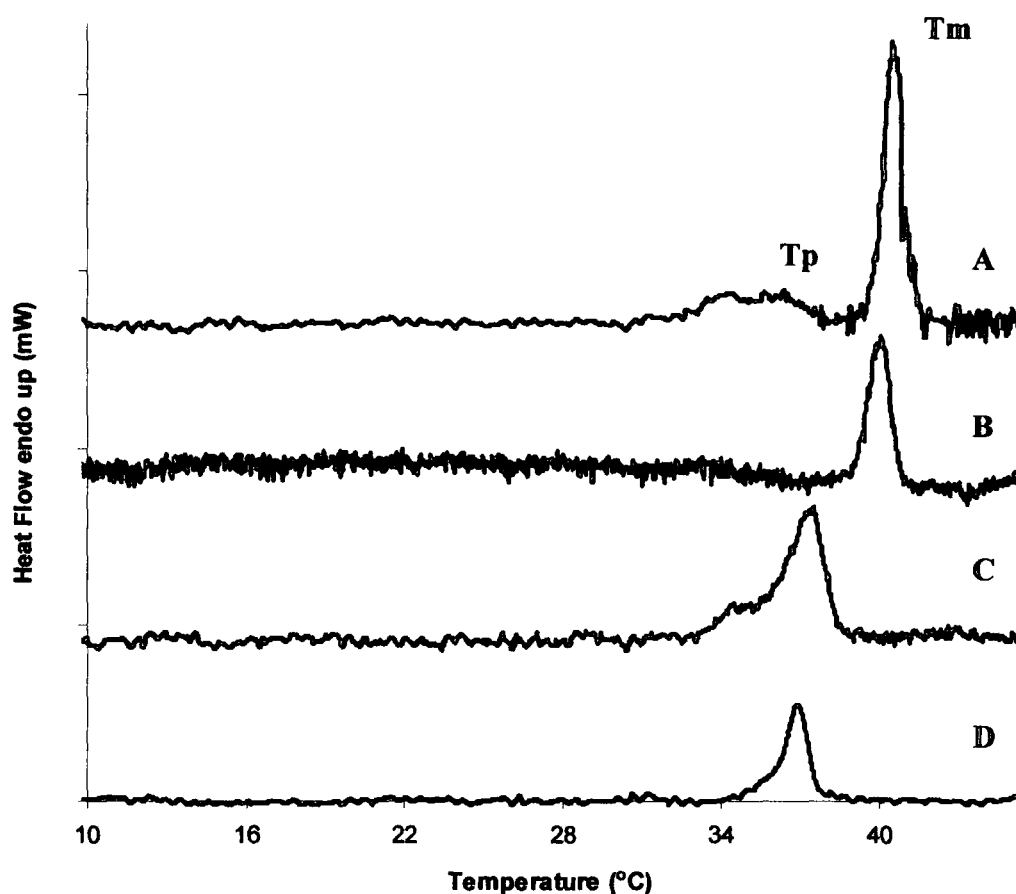


*Figure II.2.23. DSC thermograms of hydrated DPPC-6Y01 peptide with peptide to lipid molar ratios of: 0 (A), 0.05 (B), 0.1 (C) and 0.2 (D). (6 heating and cooling cycles were ran for each sample, from 6 to 48 °C at a rate of 2 °C min<sup>-1</sup>).*

The pre-transition was abolished at the lowest peptide to lipid ratio, 0.05 and the enthalpy change for the main transition was reduced by about a third of its original value. As the molar ratio was increased by two fold, the temperature of the main transition was reduced by about 3 °C and at the highest ratio studied, 0.2 the enthalpy change for the main transition was further reduced to about a third of the measured value for pure DPPC bilayers.

DSC experiments carried out on another cyclic  $\beta$ -sheet forming peptide gramicidin S (GS) with phospholipid DMPC multilamellar vesicles, showed that this peptide had a comparable affect to the 6Y01 peptide at similar peptide to lipid ratios, on both the temperature and the enthalpy change of the main phase transition of the lipid.<sup>59,61</sup>

A study showing the effect of the linear helical peptide gramicidin A on DMPC bilayers indicated that the peptide, in equivalent peptide to lipid ratios, appeared to have a much more disruptive effect on the gel state bilayers than both cyclic  $\beta$ -sheet forming peptides GS and 6Y01. The phase transition of the bilayer was completely abolished at peptide to lipid ratios of 0.08, whereas for both the GS and 6Y01 peptides the enthalpy change for the transition still retained at least a third of its original value at this ratio.<sup>62</sup>

## II.2.4. Transmission Electron Microscopy.

The synthetic amphiphilic peptides were imaged by electron microscopy in order to gain some understanding of the behaviour of the peptides in terms of the structures formed and their degree of aggregation in a buffer solution with the fluorinated alcohol HFIP. The behaviour of the peptides in solution strongly influences their suitability for 2D crystallisation in that solution. The appearance of the peptide 2K4Y03 was monitored by depositing, on to a carbon coated copper grid, a drop (2  $\mu\text{L}$ ) of peptide solution ( $0.5 \text{ mg ml}^{-1}$ ) from a 30 % HFIP solution and negatively staining the sample with a 2 % (w/v) uranyl acetate solution.

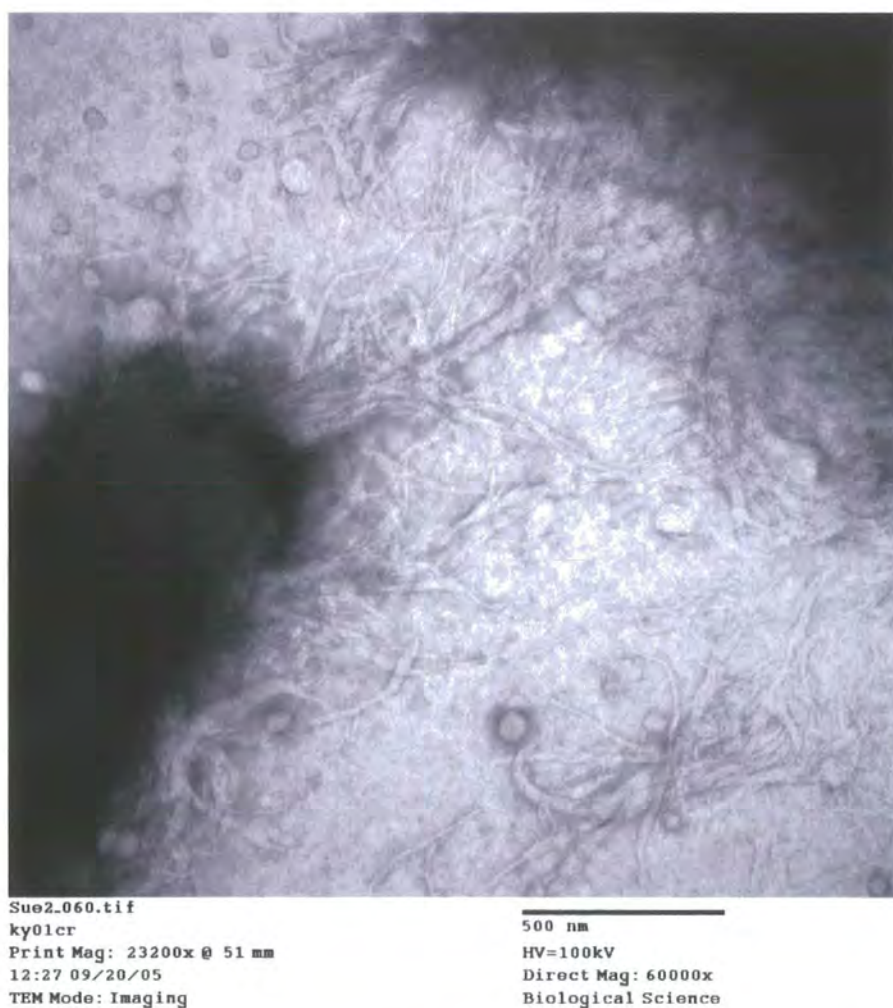


*Figure II.2.24. TEM image of the negatively stained 2K4Y03 peptides showing filamentous structures.*

The peptides formed fibrous structures when precipitated from HFIP on to the carbon coated TEM grids, over the range of concentrations studied.

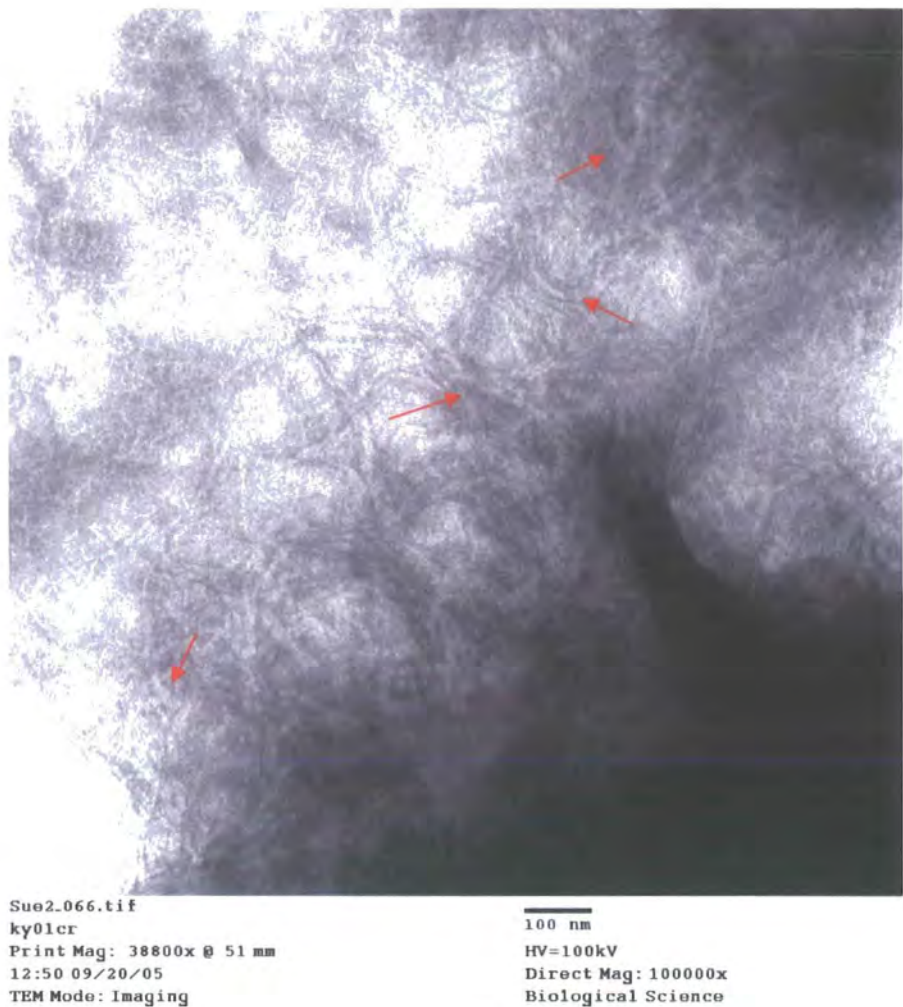


*Figure II.2.25. TEM image of the negatively stained 2K4Y03 peptides showing large areas of fibrous structures with a range of thicknesses.*

The individual fibres appeared to have aggregated into bundles of various widths, some of which showed twisted structures.

The thickness of the fibres and bundles of fibres were measured using Image J software.<sup>63</sup>



The individual fibres had an average width of  $13 \text{ nm} \pm 0.8 \text{ nm}$  and the bundles ranged in thickness from  $\sim 26 \text{ nm}$ ,  $39 \text{ nm}$ ,  $52 \text{ nm}$ ,  $65 \text{ nm}$ ,  $78 \text{ nm}$  and  $91 \text{ nm}$ , corresponding respectively to 2, 3, 4, 5, 6 and 7 fibres in thickness.

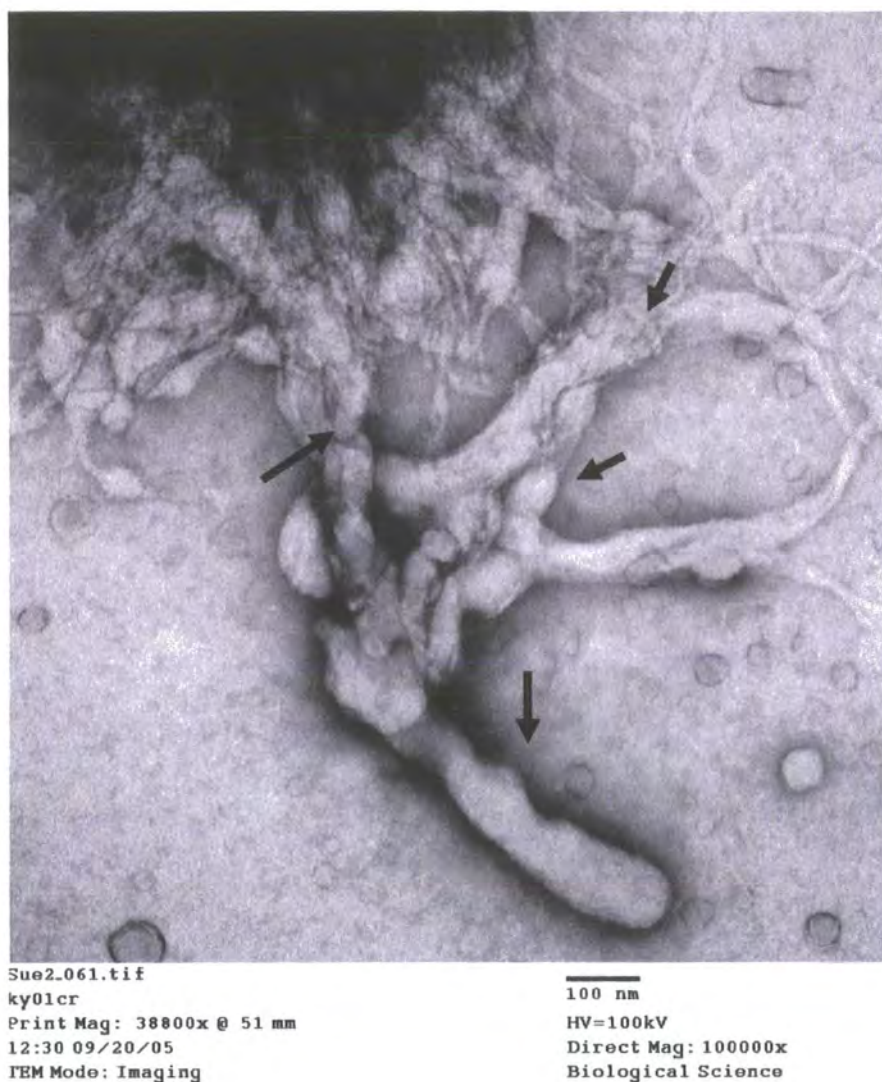


*Figure II.2.26. TEM image of the negatively stained 2K4Y03 peptides showing individual, bundles and twisted strands of fibre like structures. (The arrows are indicating the twisted bundles of fibres).*

The fibres and bundles of twisted fibres, which were observed by TEM in samples of the amphiphilic cyclic 2K4Y peptide deposited from a 30 % HFIP-buffer solution on to the carbon coated copper TEM grids, resembled both in size and in morphology the polypeptide assemblies of amyloid fibres formed by the prion protein (PrP).<sup>64</sup>

Amyloids are intracellular deposits of polypeptides that have assembled through formation of intermolecular  $\beta$ -sheets and are an essential feature of prion diseases such as Gerstmann-sträussler-scheinker disease (GSS) and variant Creutzfeldt-jakob disease. They are also present in numerous other diseases including Alzheimer's, Parkinson's and Huntington's diseases. Amyloids are thought to be formed quite readily by any polypeptide that displays a propensity for  $\beta$ -sheets, especially if the peptide has a tendency to aggregate and does not fold rapidly to form a stable  $\beta$ -sheet structure, but could coexist in equilibrium with partially folded and unfolded forms.<sup>65,66</sup>

## II.2.5. Chapter summary.

A series of amphiphilic cyclic peptides, designed to form  $\beta$ -sheet structures in lipid bilayers, were successfully synthesized using solid phase Fmoc chemistry with *in situ* cyclisation in a fully automated peptide synthesizer. The peptides were purified using RP-HPLC and analysed by MALDI mass spectrometry following optimization of the solvent systems.

The cyclic amphiphilic peptides were examined using a wide range of analytical techniques in order to establish whether the cyclic amphiphilic peptides had a propensity to adopt  $\beta$ -sheet structures in phospholipid bilayers and to gain some understanding of their behaviour under different environments, aqueous and lipidic.

**Circular Dichroism**, which was used to examine the amphiphilic cyclic peptide structure in a range of environments, showed the template peptide 6Y01 to undergo a conformational change on addition of increasing concentrations of TFE to the peptide solution and in presence of phospholipid bilayers. The CD spectra clearly revealed that the cyclic amphiphilic peptide had a propensity to adopt  $\beta$ -sheet structures in buffer-salt solutions containing over 30 % TFE and in EPC/buffer-salt solutions. The structural change from random coil to  $\beta$ -sheet is also confirmation of the cyclic amphiphilic peptide affinity for lipid media and of its ability to form a polymeric structure in membranes.

**Linear Dichroism**, which was carried out on the template cyclic 6Y01 peptide with EPC unilamellar vesicles, confirmed the predisposition of the cyclic amphiphilic peptide for a  $\beta$ -sheet type structure and also provided strong evidence of peptide insertion in to phospholipid membranes, together with the direction of insertion of the peptide backbone relative to the normal of the lipid membrane. The cyclic peptide was shown to interact with phospholipid membranes by inserting into the bilayer with the peptide backbone in a perpendicular orientation to the plane of the membrane. This orientation suggests that the peptide would not form channels by stacking of the cyclic peptide



backbone ring structure to form a tubular structure, as proposed for the cyclic antimicrobial  $\beta$ -sheet peptide rhesus theta defensin RTD-1, but could form a  $\beta$ -barrel type structure in phospholipid membranes similarly to those formed by prokaryotic outer membrane proteins.

**Differential Scanning Calorimetry** performed on the cyclic amphiphilic peptides with phospholipid multilamellar bilayers explored the effect of the amphiphilic peptides on the cooperativity of the phospholipid phase transition. The template cyclic peptide 6Y01, in peptide to lipid ratios as low as 0.02 abolished the pre-transition and decreased the temperature and the enthalpy change of the main transition of both DMPC and DPPC lipid bilayers. At peptide to lipid ratios of 0.2 the enthalpy change of the phospholipid was significantly reduced by at least a half of its initial value for DMPC and a third for DPPC bilayers and the temperature of the main transition decreased by about 4 °C for DMPC and 3 °C for DPPC bilayers. The DSC study provided strong support for the insertion of the cyclic amphiphilic peptide into phospholipid membranes and gave comparable results to DSC investigations carried out on another cyclic  $\beta$ -sheet peptides, gramicidin S with DMPC membranes.

**Transmission Electron Microscopy** revealed that the cyclic amphiphilic peptide 2K4Y03 appeared to form amyloid type fibres on precipitation from a 30 % solution of the fluorinated alcohol, HFIP in water. The fibres and bundles of twisted fibres, which were similar in size and morphology to those, observed in prion diseases, are thought to be readily formed by  $\beta$ -sheet proteins that have a tendency to aggregate and do not fold rapidly to adopt their stable conformation.

## II.3.1. Materials and Methods.

### II.3.1.1. Materials.

Trifluoroethanol (TFE) and hexafluoroisopropanol (HFIP) were obtained from Apollo and biological grade trifluoroacetic acid (TFA), piperidine, diisopropylethylamine (DIPEA), 1-Hydroxybenzotriazole (HOBt), 1,2-ethanedithiol (EDT), sodium diethyldithiocarbonate, acetic acid ( $\text{CH}_3\text{CO}_2\text{H}$ ), *N*-methylmorpholine (NMM) and triisopropylsilane (TIS) were all from Lancaster.

The Fmoc protected amino acid residues, Fmoc-Asp(OAll)-OH, Fmoc-Gly-OH, Fmoc-Val-OH, Fmoc-Cys(tBu)-OH, Fmoc-Ser(tBu)-OH, Fmoc-Asn-OH, Fmoc-Lys(Boc)-OH and the Fmoc Protected pseudoproline dipeptides, Fmoc-Tyr(tBu)-Ser( $\psi^{\text{Me,Me}}\text{Pro}$ )-OH, Fmoc-Val-Ser( $\psi^{\text{Me,Me}}\text{Pro}$ )-OH, Fmoc-Trp(Boc)-Ser( $\psi^{\text{Me,Me}}\text{Pro}$ )-OH and Fmoc-Leu-Ser( $\psi^{\text{Me,Me}}\text{Pro}$ )-OH were all purchased from Novabiochem, EMD Biosciences, Inc. The resin (Novasyn TGR) and benzotriazol-1-yl-oxy-tris-pyrrolidinophosphonium, Hexafluorophosphate salt (PyBOP) were obtained from Merck biosciences, Inc.

The dimethylformamide (DMF), water, acetonitrile ( $\text{CH}_3\text{CN}$ ), unstabilised dichloromethane (DCM), chloroform ( $\text{CH}_3\text{Cl}$ ) and methanol ( $\text{CH}_3\text{OH}$ ) were all HPLC grade solvents from Fisher chemicals.

Dipalmitoyl phosphatidyl choline (DPPC) and dimyristoyl phosphatidyl choline (DMPC) were purchased from Avanti polar lipids and egg phosphatidyl choline (EPC) was obtained as a solution ( $100\text{ mg ml}^{-1}$ ) in chloroform from Sigma.

## II.3.2. Methods.

### II.3.2.1. Peptide synthesis.

Peptide synthesis was performed in a fully automated programmable Advanced Chemtech peptide synthesiser, model 348  $\Omega$  MPS. The software used was Act 348  $\Omega$  provided by Advanced Chemtech.

**1<sup>st</sup> step: loading of solid support.** A suspension of the resin (Novasyn TGR, 0.10 g, 0.03 mmol) in DMF (2 ml) was mechanically agitated for 15 min (at 400 rpm).

**2<sup>nd</sup> step: coupling of the first amino acid (aspartic acid) to the solid support.** Following the addition of Fmoc-Asp (OAll) (0.060 g, 0.15 mmol, 5 eq), PyBOP (0.075 g, 0.14 mmol, 5 eq), DIPEA (0.026 g, 0.15 mmol, 5 eq) and HOBt (0.023 g, 0.15 mmol, 5 eq) in DMF (2.5 ml), the mixture was agitated (400 rpm) under a N<sub>2</sub> atmosphere for 60 min at room temperature. Following filtration, the resin was suspended in DMF (2 ml) and the above coupling process was repeated once again.

The resin was then filtered and washed 3 times by each time mechanically shaking the resin (at 400 rpm) for 1 min in DMF (2 ml) and then filtering.

**Fmoc deprotection.** Removal of the Fmoc protection from the Asp (OAll) amino acid was achieved by mechanically agitating the resin (at 400 rpm) for 10 min in a 20 % (v/v) piperidine/DMF solution (2.5 ml) and filtering. This process was repeated twice before washing the resin 4 times in DMF as described above.

The synthesis of all the amphiphilic cyclic peptides follows on from the steps described above (section II.3.2.1.).

**(1). Synthesis of cyclo-Asn-Gly-Asn-Val-Ser-Leu-Ser-Val-Ser-Tyr-Ser-Tyr-Ser-Val-Ser-Tyr-Ser-Asn-Gly-Asn-Val-Ser-Leu-Ser-Val-Ser-Tyr-Ser-Tyr-Ser-Val-Ser-Tyr-Ser (6Y01)**

**3<sup>rd</sup> step: coupling of Fmoc protected glycine.** Following the addition of Fmoc-Gly-OH (0.044 g, 0.15 mmol, 5 eq), PyBOP (0.078 g, 0.15 mmol, 5 eq), DIPEA (0.026 g, 0.15 mmol, 5 eq) and HOBt (0.023 g, 0.15 mmol, 5 eq) in DMF (2.5 ml), the mixture was agitated (400 rpm) under a N<sub>2</sub> atmosphere for 90 min at room temperature.

The resin was then filtered and washed 3 times, by each time mechanically shaking the resin (at 400 rpm) for 1 min in DMF (2 ml) and filtering. Fmoc deprotection and subsequent washing were then carried out as described above.

**4<sup>th</sup> step: coupling of Fmoc protected asparagine.** Following the addition of Fmoc-Asn-OH (0.089 g, 0.15 mmol, 5 eq), PyBOP (0.078 g, 0.15 mmol, 5 eq), DIPEA (0.026 g, 0.15 mmol, 5 eq) and HOBt (0.023 g, 0.15 mmol, 5 eq) in DMF (2.5 ml), the mixture was agitated (400 rpm) under a N<sub>2</sub> atmosphere for 90 min at room temperature.

The resin was then filtered and washed 3 times, by each time mechanically shaking the resin (at 400 rpm) for 1 min in DMF (2 ml) and filtering. Fmoc deprotection and subsequent washing were then carried out.

**5<sup>th</sup> step: coupling of the Fmoc protected pseudo proline dipeptide tyrosine-serine.** Following the addition of Fmoc-Tyr(tBu)-Ser( $\psi^{Me,Me}Pro$ )-OH (0.088 g, 0.15 mmol, 5 eq), PyBOP (0.078 g, 0.15 mmol, 5 eq), DIPEA (0.026 g, 0.15 mmol, 5 eq) and HOBt (0.023 g, 0.15 mmol, 5 eq) in DMF (2.5 ml), the mixture was agitated (400 rpm) under a N<sub>2</sub> atmosphere for 90 min at room temperature.

The resin was then filtered and washed 3 times by each time mechanically shaking the resin (at 400 rpm) for 1 min in DMF (2 ml) and filtering. Fmoc deprotection and subsequent washing were then carried out.

**6<sup>th</sup> step: coupling of the Fmoc protected pseudo proline dipeptide valine-serine.** Following the addition of Fmoc-Val-Ser( $\psi^{Me,Me}Pro$ )-OH (0.070 g, 0.15 mmol, 5 eq), PyBOP (0.078 g, 0.15 mmol, 5 eq), DIPEA (0.026 g, 0.15 mmol, 5 eq) and HOBt (0.023 g, 0.15 mmol, 5 eq) in DMF (2.5 ml), the mixture was agitated (400 rpm) under a N<sub>2</sub> atmosphere for 90 min at room temperature.

The resin was then filtered and washed 3 times by each time mechanically shaking the resin (at 400 rpm) for 1 min in DMF (2 ml) and filtering. Fmoc deprotection and subsequent washing were then carried out.

**7<sup>th</sup> step: coupling of the Fmoc protected pseudo proline dipeptide tyrosine-serine.** As described above in step 5.

**8<sup>th</sup> step: coupling of the Fmoc protected pseudo proline dipeptide tyrosine-serine.** As described above in step 5.

**9<sup>th</sup> step: coupling of the Fmoc protected pseudo proline dipeptide valine-serine.** As described above in step 6.

**10<sup>th</sup> step: coupling of the Fmoc protected pseudo proline dipeptide leucine-serine.** Following the addition of Fmoc-Leu-Ser( $\psi^{\text{Me,Me}}$ Pro)-OH (0.072 g, 0.15 mmol, 5 eq), PyBOP (0.078 g, 0.15 mmol, 5 eq), DIPEA (0.026 g, 0.15 mmol, 5 eq) and HOBt (0.023 g, 0.15 mmol, 5 eq) in DMF (2.5 ml), the mixture was agitated (400 rpm) under a N<sub>2</sub> atmosphere for 90 min at room temperature.

The resin was then filtered and washed 3 times by each time mechanically shaking the resin (at 400 rpm) for 1 min in DMF (2 ml) and filtering. Fmoc deprotection and subsequent washing were then carried out.

**11<sup>th</sup> step: coupling of the Fmoc protected pseudo proline dipeptide valine-serine.** As described in step 6.

**12<sup>th</sup> step: coupling of Fmoc protected asparagine.** As described in step 4.

**13<sup>th</sup> step: coupling of Fmoc protected glycine.** As described in step 3.

**14<sup>th</sup> step: coupling of Fmoc protected asparagine.** As described in step 4.

**15<sup>th</sup> step: coupling of the Fmoc protected pseudo proline dipeptide tyrosine-serine.** As described in step 5.

**16<sup>th</sup> step: coupling of the Fmoc protected pseudo proline dipeptide valine-serine.** As described in step 6.

**17<sup>th</sup> step: coupling of the Fmoc protected pseudo proline dipeptide tyrosine-serine.** As described in step 5.

**18<sup>th</sup> step: coupling of the Fmoc protected pseudo proline dipeptide tyrosine-serine.** As described in step 5.

**19<sup>th</sup> step: coupling of the Fmoc protected pseudo proline dipeptide valine-serine.** As described in step 6.

**20<sup>th</sup> step: coupling of the Fmoc protected pseudo proline dipeptide leucine-serine.** As described in step 10.

**21<sup>st</sup> step: coupling of the Fmoc protected pseudo proline dipeptide valine-serine.** As described in step 6.

**(2) Synthesis of cyclo-Asn-Gly-Asn-Val-Ser-Leu-Ser-Val-Ser-Tyr-Ser-Tyr-Ser-Val-Ser-Trp-Ser-Asn-Gly-Asn-Val-Ser-Leu-Ser-Val-Ser-Tyr-Ser-Tyr-Ser-Val-Ser-Trp-Ser (2W4Y02).**

The synthesis of peptide (2) 2W4Y02 followed all the steps described above for the synthesis of peptide (1) 6Y01, except steps 5 and 15, which are as follows:

**5<sup>th</sup> step: coupling of the Fmoc protected pseudo proline dipeptide tryptophan-serine.** Following the addition of Fmoc-Trp(Boc)-Ser( $\psi^{\text{Mc,Mc}}\text{Pro}$ )-OH (0.098 g, 0.15 mmol, 5 eq), PyBOP (0.078 g, 0.15 mmol, 5 eq), DIPEA (0.026 g, 0.15 mmol, 5 eq) and HOBt (0.023 g, 0.15 mmol, 5 eq) in DMF (2.5 ml), the mixture was agitated (400 rpm) under a N<sub>2</sub> atmosphere for 90 min at room temperature.

The resin was then filtered and washed 3 times by each time mechanically shaking the resin (at 400 rpm) for 1 min in DMF (2 ml) and filtering. Fmoc deprotection and subsequent washing were then carried out.

**15<sup>th</sup> step: coupling of the Fmoc protected pseudo proline dipeptide tryptophan--serine.** As described above in step 5(2).

**(3) Synthesis of cyclo-Asn-Gly-Asn-Val-Ser-Leu-Ser-Val-Ser-Tyr-Ser-Tyr-Ser-Val-Ser-Lys-Ser-Asn-Gly-Asn-Val-Ser-Leu-Ser-Val-Ser-Tyr-Ser-Tyr-Ser-Val-Ser-Lys-Ser (2K4Y03)**

The synthesis of peptide (3) 2K4Y03 followed all the steps described above for the synthesis of peptide (1) 6Y01, except steps 5 and 15, which are as follows:

**5<sup>th</sup> step: coupling of the Fmoc protected pseudo proline dipeptide lysine-serine.** Following the addition of Fmoc-Lys(Boc)-OH (0.089 g, 0.15 mmol, 5 eq), PyBOP (0.078 g, 0.15 mmol, 5 eq), DIPEA (0.026 g, 0.15 mmol, 5 eq) and HOBt (0.023 g, 0.15 mmol, 5 eq) in DMF (2.5 ml), the mixture was agitated (400 rpm) under a N<sub>2</sub> atmosphere for 90 min at room temperature.

The resin was then filtered and washed 3 times by each time mechanically shaking the resin (at 400 rpm) for 1 min in DMF (2 ml) and filtering. Fmoc deprotection and subsequent washing were then carried out.

**15<sup>th</sup> step: coupling of the Fmoc protected pseudo proline dipeptide lysine-serine.** As described above in step 5(3).

**(4) Synthesis of cyclo-Asn-Gly-Asn-Val-Ser-Leu-Ser-Val-Ser-Cys-Ser-Tyr-Ser-Val-Ser-Tyr-Ser-Asn-Gly-Asn-Val-Ser-Leu-Ser-Val-Ser-Cys-Ser-Tyr-Ser-Val-Ser-Tyr-Ser (2C4Y04)**

The synthesis of peptide (4) 2C4Y04 followed all the steps described above for the synthesis of peptide (1) 6Y01, except steps 8 and 18, which are as follows:

**8<sup>th</sup> step (a): coupling of the Fmoc protected cysteine.** Following the addition of Fmoc-Cys(tBu)-OH (0.088 g, 0.15 mmol, 5 eq), PyBOP (0.078 g, 0.15 mmol, 5 eq), DIPEA (0.026 g, 0.15 mmol, 5 eq) and HOBt (0.023 g, 0.15 mmol, 5 eq) in DMF (2.5 ml), the mixture was agitated (400 rpm) under a N<sub>2</sub> atmosphere for 90 min at room temperature.

The resin was then filtered and washed 3 times by each time mechanically shaking the resin (at 400 rpm) for 1 min in DMF (2 ml) and filtering. Fmoc deprotection and subsequent washing were then carried out.

**8<sup>th</sup> step (b): coupling of the Fmoc protected serine.** Following the addition of Fmoc-Ser(tBu)-OH (0.057 g, 0.15 mmol, 5 eq), PyBOP (0.078 g, 0.15 mmol, 5 eq), DIPEA (0.026 g, 0.15 mmol, 5 eq) and HOBt (0.023 g, 0.15 mmol, 5 eq) in DMF (2.5 ml), the mixture was agitated (400 rpm) under a N<sub>2</sub> atmosphere for 90 min at room temperature.

The resin was then filtered and washed 3 times by each time mechanically shaking the resin (at 400 rpm) for 1 min in DMF (2 ml) and filtering. Fmoc deprotection and subsequent washing were then carried out.

**18<sup>th</sup> step (a): coupling of the Fmoc protected cysteine.** As described in step 8(a)(4).

**18<sup>th</sup> step (b): coupling of the Fmoc protected serine.** As described in step 8(b)(4).

### II.3.2.2. Allyl ester deprotection and cyclisation.

Following peptide synthesis (1-4), deprotection was carried out on the allyl ester protected aspartic acid residue and then all peptides were cyclised *in situ*.

**Allyl ester deprotection.** The resin was washed 3 times in DCM (2 ml) by each time mechanically shaking the resin (at 400 rpm) for 2 min and filtering. A solution of Tetrakis(triphenylphosphine) Palladium(0) catalyst (0.051 g, 0.044 mmol) dissolved in a chloroform (1.38 ml), acetic acid (0.075 ml), *N*-methylmorpholine (0.037 ml) solution was added to the resin with DCM (2 ml) and was mechanically shaken (at 400 rpm) for 2 hours under a nitrogen atmosphere. The resin then was filtered and a solution DIPEA (0.026 g, 0.15 mmol) in DMF (3.3 ml) was added to the resin and mechanically shaken (at 400 rpm) for 5 min before filtering the resin again. A solution of sodium diethyldithiocarbonate (0.013 g, 0.058 mmol) in DMF (2.5 ml) was then added to the resin, which was mechanically shaken (at 400 rpm) for 15 min under a nitrogen atmosphere. The resin was then filtered and washed twice by each time mechanically shaking the resin (at 400 rpm) for 2 min in DMF (3 ml) and filtering.

**Cyclisation.** A solution of DIPEA (0.026 g, 0.15 mmol), HOBt (0.023 g, 0.15 mmol) and PyBOP (0.078 g, 0.15 mmol) in DMF (3 ml) were added to the resin and mechanically shaken (at 400 rpm) for 5 hours at room temperature under a nitrogen atmosphere. The resin was then filtered and washed 14 times, 4 times in DMF (1.5 ml), 5 times in methanol (2 ml) and 5 times in DCM (2 ml) by each time adding the required amount of solvent and mechanically shaking the resin (at 400 rpm) for 1 min before filtering. The resin was then allowed to dry for 30 min under a nitrogen atmosphere, before being carefully removed from the automated peptide synthesiser and weighed out into clearway extraction units for peptide cleavage. The amount of crude peptide (with attached resin) obtained was 194 mg for peptide 6Y01, 182 mg for peptide 2W4Y02, 195 mg for the peptide 2K4Y03 and 180 mg for peptide 2C4Y04.



#### **II.3.2.3. Peptide cleavage from the resin and side chain deprotection.**

Cleavage and final deprotection were carried out on aliquots of 50 mg (peptide with resin) at a time. A solution of TFA (0.95 ml), H<sub>2</sub>O (0.025 ml), EDT (0.025 ml) and Tis (0.01 ml) was added to each aliquot of peptide with resin (50 mg) in a clearway extraction unit and gently shaken (in a table top shaker) for 4 hours. The solution was then filtered under reduced pressure and the filter was washed a further 3 times with TFA (0.5 ml) to remove any residual peptide from the resin. The filtrate containing the peptide was collected in a centrifuge tube and the peptide was precipitated out of solution by drop wise addition of a 10 fold volume of diethyl ether cooled over ice. The peptide solution was then centrifuged (in a table top centrifuge, 14,000 x g for 10 min). The supernatant was slowly decanted off and discarded. The pellet was dried to a constant weight under vacuum before being dissolved in HFIP (0.5 mg ml<sup>-1</sup>) and filtered to remove any insoluble material from the solution.

#### **II.3.2.4. Purification.**

The peptide in HFIP (0.5 mg ml<sup>-1</sup>) was injected by aliquots of 100 µl per run, into an analytical C8 Supelco column of dimensions, 250 x 4.6 mm, 5 µm with C8 silica packing and a pore size of 100-300 Å.

The HPLC unit was composed of a Perkin Elmer series 200 pump with Gilson sample injection and dilutor with programmable keypad (231XL). The UV detector was a Waters<sup>TM</sup> 486, Tunable Absorption Detector.

The HPLC conditions, the solvent gradient and flow rate are detailed below (Table II.2.1). The optimised separation method used a multi solvent system with solvents: (A) 10 % HFIP/TFE; (B) 0.1 % TFA/acetonitrile and (C) 0.1 % TFA/water. The temperature of the column was maintained at 30 °C throughout the run and the UV detector was tuned to a wavelength of 274 nm.

Step	Time (minutes)	Flow rate (ml / minutes)	Solvent system			Gradient
			A %	B %	C %	
0	0.5	0.7	90	0	10	none
1	6	1.0	80	10	10	linear
2	5	1.0	10	80	10	linear
3	3	1.0	0	100	0	none
4	6	1.0	90	0	10	linear
5	0.5	1.0	90	0	10	none

*Table II.3.1. Optimised RP-HPLC conditions for the synthetic cyclic peptides.*

Fractions corresponding to the area under each distinct peak were collected and the solvent was removed using a rotary evaporator. The dried samples were then redissolved in TFE, which produces less interference than HFIP with the UV absorbance spectra of the peptide.

#### **II.3.2.5. Determination of peptide concentration.**

UV spectra were obtained on a UNICAM 2 UV-Vis dual beam spectrophotometer in quartz UV cells with a path length of 1 cm. A reference cell containing the background solution (TFE) was run in parallel to the sample cell and then automatically subtracted (UNICAM /vision software) from the sample spectrum. Samples were scanned over a wavelength range of 190 to 300 nm.

Peptide concentration was determined from the UV absorbance of the peptide at 280 nm using the Beer Lambert law. The residue extinction coefficients at 280 nm, for the tyrosine, tryptophan and cystine residues, used in the calculation, were 1280, 5690 and 120 Moles<sup>-1</sup> cm<sup>-1</sup> respectively.<sup>67</sup> The number of tyrosine, tryptophan and cystine residues in the peptide sequence were counted, multiplied by the appropriate extinction coefficient for each type of residue and then summed to give the extinction coefficient ( $\epsilon_{280\text{ nm}}$ ) for the whole peptide:

Peptide	N° of residues in the sequence multiplied by $\epsilon_{280\text{ nm}}$ for the residue:			Overall $\epsilon_{280\text{ nm}}$ for the peptide
	Tyr	Trp	Cys-Cys	
<b>6Y01</b>	6*1280 = 7680	0	0	7680 Moles <sup>-1</sup> cm <sup>-1</sup>
<b>2W4Y02</b>	4*1280 = 5120	2*5690 = 11380	0	16500 Moles <sup>-1</sup> cm <sup>-1</sup>
<b>2K4Y03</b>	4*1280 = 5120	0	0	5120 Moles <sup>-1</sup> cm <sup>-1</sup>
<b>2C4Y04</b>	4*1280 = 5120	0	2*120 = 240	5360 Moles <sup>-1</sup> cm <sup>-1</sup>

*Table II.3.2. Calculation of the extinction coefficient for the analogous cyclic peptides for UV absorption at a wavelength 280 nm.*

**II.3.2.6. Analysis by mass spectrometry.** The Electrospray Mass Spectrometry was carried out on a Micromass LCT and Matrix Assisted Laser Desorption Ionisation Mass Spectroscopy was performed on a MALDI Voyager mass spectrometer.

**II.3.2.7. Positive electrospray ionisation.** ESI<sup>+</sup> MS was performed on the purified cyclic amphiphilic peptide(6Y01) dissolved in TFE. A series of multi charged ions of the correct mass for the peptide. Mr: 3590 g mol<sup>-1</sup> were produced.

**ESI<sup>+</sup> MS:** 740 m/z [(M + 5Na<sup>+</sup>)/5] 15 %; 620 m/z [(M + 6Na<sup>+</sup>)/6] 20 %; 535 m/z [(M + 7Na<sup>+</sup>)/7] 12 %; 471 [(M + 8Na<sup>+</sup>)/8] 10 %; 421 m/z [(M + 9Na<sup>+</sup>)/9] 22 %.

**II.3.2.8. MALDI MS.** The matrix, which was either HABA or sinapinic acid was dissolved at a concentration of 10 mg ml<sup>-1</sup> in HFIP with 0.1 % TFA and vortexed. The supernatant was premixed with the peptide also dissolved in HFIP (~1 mg ml<sup>-1</sup>) in molar ratios ranging from 1:140 to 1:14,000. A 1 µl drop of this solution was then spotted on to a stainless steel, 100 well sample plate to dry. The sample tended to spread quite extensively over the plate and had to be concentrated by carefully spotting again on top of the dry sample.

**II.3.2.9. Preparation of Tetrakis(triphenylphosphine) Palladium(0).** Palladium dichloride (0.44 mg, 2.5 mmol) and triphenylphosphine (3.27 g, 12 mmol) were added to 30 ml of dimethyl sulfoxide and stirred in a flask equipped with a condenser. The mixture was heated in an oil bath to above 140 °C under nitrogen, until completely dissolved. The bath was then removed and the solution was further stirred for 15 minutes. Hydrazine hydrate (0.5 g, 10 mmol) was rapidly added by syringe and the resulting dark mixture was left to cool to room temperature under nitrogen.

The reaction mixture was then filtered and the solid obtained was washed with 2 x 2 ml aliquots of ethanol and again with diethyl ether; then dried under nitrogen before being stored in a freezer under argon.

The yellow crystalline product weighed 2.57 g (68 % yield).

Calculated elemental composition for  $C_{72}H_{60}PdP_4$ : C: 75.88; H: 5.25; P: 10.75.

Found: C: 75.62; H: 5.54; P: 10.68.

#### **II.3.2.10. Preparation of the quaternary ammonium ion,**

##### **[2-(acetylamino)ethyl]trimethylammonium iodide for peptide derivation.**

##### **II.3.2.10.1. Preparation of trimethylamine anhydride.**

A saturated solution of Sodium hydroxide (10.2 g, 0.26 mol) in  $H_2O$  was added to trimethylamine hydrochloride (25 g) and stirred over a hot ( $50\text{ }^{\circ}C$ ) bath. A cold trap ( $CO_2$ /Acetone) and drying guard, filled with  $K_2CO_3$ , were connected by a condenser to the reaction flask.

Trimethylamine (bp.  $3-4\text{ }^{\circ}C$ ) was collected (6.2 g) in the trap and stored in a freezer over  $K_2CO_3$ .

##### **II.3.2.10.2. Preparation of N-trimethyl-1,2-diaminoethane.**

Trimethylamine (4.22 g, 0.072 mol) was added slowly to a solution of 2-Bromoethylamine hydrobromide (5 g, 0.024 mol) in a methanol (6 ml) and stirred for 30 mins over an ice bath.

The mixture was centrifuged; the solid by product, trimethylamine bromo hydrate was separated from the solution and discarded. The solvent was removed from the supernatant on a rotary evaporator, leaving behind an oily product which was then mixed with a 50 % methanol: 50 % isopropanol solution and then neutralised (monitored by pH paper) with hydriodic acid. After removing the solvent under reduced pressure, a cream coloured solid, N-trimethyl-1,2-diaminoethane (1.9 g, 21 % yield) was obtained.

$^1H$ -NMR (300 MHz): 4.67 (s,  $D_2O$ ); 3.52 (t, 2H); 3.41 (t, 2H) and 3.08 (s, 9H).

#### II.3.2.10.3. Preparation of [2-(acetylamino)ethyl]trimethylammonium iodide.

Two methods were used to prepare [2-(acetylamino)ethyl]trimethylammonium iodide.

**Method 1.:** A solution of sodium hydroxide (0.089 g; 2.28 mmol) in ethanol (1.5 ml) was added to a stirred solution of N-trimethyl-1, 2-diaminoethane (0.3 g; 1.14 mmol) in 20 mL of ethanol. Iodoacetyl chloride (0.46 g; 2.28 mmol) was added to the mixture over an ice bath and the mixture was stirred for 30 mins. The solvent was evaporated under reduced pressure and the solid obtained was recrystallised from ethanol. The creamy-white crystals (0.47 g, 57 % yield) were washed in methanol.

**Method 2.:** N-trimethyl-1,2-diaminoethane (0.3 g) was suspended in DMF (20 mL) and trimethylamine (0.23 g, 3.9 mM) was slowly added under a flow of nitrogen over an ice bath. Iodoacetyl chloride (0.46 g; 2.28 mmol) was slowly added to the mixture and stirred for 30 mins. A precipitate formed on addition of diethyl ether to the solution and was filtered before drying under reduced pressure; a creamy white solid (0.42 g, 42 % yield) was produced.

The mass spectrum data strongly suggested the presence of both chloride products and

[2-(acetylamino)ethyl]trimethylammonium iodide.

**ESI<sup>+</sup> MS:** 271 m/z  $[(\text{CH}_3)_3\text{N}^+(\text{CH}_2)_2 \text{NCOCH}_2\text{I}]$  (92%); 179 m/z  $[(\text{CH}_3)_3\text{N}^+(\text{CH}_2)_2 \text{NCOCH}_2\text{Cl}]$  (100%).

Separation was readily achieved by addition of the crude product (0.24 g, 1.5 mmol) to a solution of DMF (5 ml) and sodium iodide (0.22 g, 1.5 mmol) stirring for 30 mins and then filtered to remove the resulting sodium chloride by-product. The solvent was evaporated under reduced pressure to give the pure iodide form of the compound.

**ESI<sup>+</sup> MS:** 271 m/z  $[\text{M}^+]$  100 % and 212 m/z  $[\text{M}^+ - (\text{CH}_3)_3\text{N}]$  58 %.

**<sup>1</sup>H NMR (300 MHz):** 4.67 (s, D<sub>2</sub>O); 3.64 (s, 2H, CH<sub>3</sub>-CO); 3.58 (t, *J*=5.8, 2H); 3.39 (t, *J*=5.8, 2H) and 3.04 (s, 9H, N(CH<sub>3</sub>)<sub>3</sub>).

**Melting point:** 176 °C (Literature Mp: 176-177 °C).

**II.3.2.10.4. Derivatization of peptides.** The peptide (6Y01) (2 mg,  $5.6 \times 10^{-7}$  mol) was added to 12 equivalents of [2-(acetylamino)ethyl]trimethylammonium iodide (1.8 mg,  $6.72 \times 10^{-6}$  mol) and 12 equivalents of Et<sub>3</sub>N (0.7 mg,  $6.72 \times 10^{-6}$ ) in 0.6 ml of a 1:3 solution of TFE and water. The mixture was heated to 30 °C and stirred for an hour. The solution was then filtered and the solvent removed from the filtrate under reduced pressure. The reaction vessel was kept covered to prevent exposure to light.

### **II.3.3. Analytical methods.**

#### **II.3.3.1. Unilamellar vesicles of phospholipids.**

ULVs were prepared by evaporating a lipid solution from CHCl<sub>3</sub> (1 mg ml<sup>-1</sup>) to dryness under vacuum to form a thin film and hydrating the film with pure water or a 10 mM Tris-150 mM NaCl buffer (adjusted to pH 7.4). The mixture was vortexed until complete lipid dispersal had been achieved and was then submitted to 5 cycles of freeze-thawing between -195 and 30 °C. Following this treatment the lipid suspension was extruded 10 times through a polycarbonate membrane (Whatman) with a pore size of 100 nm in diameter using a thermobarrel extruder (Lipex Biomembranes) at 30 °C.

#### **II.3.3.2. Circular dichroism (CD).**

The data was collected at a scan speed of 50 nm min<sup>-1</sup> on a Jasco J-810 spectropolarimeter and averaged over 6 runs. A background spectrum was run before collecting the data for a sample, using the same cell in a same orientation and with the same solvent composition as that in which the peptide sample was collected. The background also averaged over 6 runs was subtracted from the sample spectrum, which was then corrected for baseline.

The resulting data was converted to mean residue ellipticity units:

$$[\Theta] = \Theta / (10 * C_p * n * l)$$

*where  $\Theta$  is the ellipticity;  $C_p$  is the molar concentration;  $n$  is the number of residues in the peptide and  $l$  is the cell path length.*

All data processing was performed using the Jasco software. The quartz cell used for the CD measurements of the peptide in water and in buffer-TFE solutions had a 1 cm path length and for peptide-EPC mixtures, the cell path length was 1 mm.

#### **II.3.3.3. Linear Dichroism.**

The peptide 6Y01 was added to a final concentration of 0.4 mg mL<sup>-1</sup> to a 1 mg mL<sup>-1</sup> solution of EPC vesicles (100 nm in diameter) extruded in pure HPLC grade water. The solution was mixed by vortexing and was then refrigerated for at least an hour before collecting the linear dichroism spectra.

The instrument used was a Jasco J-715 circular dichroism spectropolarimeter, which was adapted for flow LD measurements. The rotation speed used in the experiment was ~ 1000 rpm, chosen as to avoid bubble formation in the 50  $\mu$ L CaF<sub>2</sub> Couette cell.<sup>68</sup> The data was collected and averaged over 64 runs. The LD base line was measured on the same sample again over 64 runs but without cell rotation and was then subtracted from the sample spectra. All data processing was performed using the Jasco software.

#### **II.3.3.4. Differential Scanning Calorimetry.**

The template peptide 6Y01 dissolved at a concentration of 15  $\mu$ M in TFE (1 ml), was added in predetermined volumes of 100  $\mu$ L, 40  $\mu$ L and 10  $\mu$ L to aliquots of lipid (5 mg) dissolved in chloroform (200  $\mu$ L); the solvent was removed on a rotary evaporator with the dried peptide-lipid mixtures forming a thin film around the inside of the flask and then further dried under reduced pressure for 3 hours. The peptide-lipid samples were then hydrated with 100  $\mu$ L of pure water



by constant agitation using a vortex-mixer until all the sample film had desorbed before being submitted to at least 5 cycles of freeze-thawing to anneal the peptide-lipid solutions.

The sample solution was pipetted into tared pans and weighed before the pans were sealed for DSC analysis. Each sample was scanned a minimum of 6 times to allow for equilibration on a Perkin Elmer Pyris1 DSC. The peptide-DMPC and peptide-DPPC samples were scanned from 6 to 26 °C and 6 to 48 °C respectively, at a rate of 2 °C min<sup>-1</sup>. Data processing was performed using the software Origin (OriginLab, Aston scientific, version 7.5)

#### **II.3.3.5. Transmission Electron Microscope.**

The peptide dissolved (0.5 mg ml<sup>-1</sup>), in a 30 % HFIP-10 mM tris-150 mM NaCl buffer (pH 7.4) solution, was spotted (2 µL of peptide solution) onto a carbon coated copper grid (Agar scientific) and left in air; after 30 seconds, excess solution was withdrawn with blotting paper from the edge of the grid and a 2 % (v/v) solution of uranyl acetate (Agar scientific) was spotted onto the grid, which was again left for about 30 seconds before withdrawing the excess as before.

The sample grid was then analysed in a H-7200 Hitachi TEM and imaged at 100 KV using x 60 K to x 100 K magnifications.

## II.4. References.

- 
- 1 Ciba Foundation Symposium 186, *Antimicrobial peptides*, p.5, 1994, Wiley and sons, Chichester.
  - 2 J. M. Sanderson and S. Yazdani, *Chem. Commun.*, 2002, 1154.
  - 3 R. B. Merrifield, *J. Amer. Chem. Soc.*, **85**, 1963, 2149.
  - 4 J. Jones, *Amino acid and peptide synthesis*, 2<sup>nd</sup> edition., 2002, Oxford University Press.
  - 5 J. M. Stewart, J. D. Young, *Solid phase peptide synthesis*, 2<sup>nd</sup> edition., 1984, Pierce Chemical Co., Rockford, Illinois.
  - 6 E. Atherton, R. C. Sheppard, *Solid phase peptide synthesis: a practical approach*, 1989, IRL Press at Oxford University Press.
  - 7 W. Bammworth, *Tetrahedron Lett.*, **33**, 1992, 4557.
  - 8 F. Albericio, *Tetrahedron Lett.*, **34**, 1993, 1549.
  - 9 *Protein Purification Techniques, a practical approach*, 2nd edition, 2001, Eds. S. Roe, Oxford University Press.
  - 10 J. Schaller, *Analysis of hydrophobic proteins and peptides by mass spectrometry, Methods in Molecular Biology*, Eds. J. R. Chapman, Humana Press Inc., Totowa, NJ., **146**, 2000, 425-437.
  - 11 P. A. Schindler, A. Van Dorsselaer and A. M. Falick, *Anal. Biochem.*, **213**, 1993, 256-263.

- 
- 12 D. R. Barnidge, E. A. Dratz, A.J. Jesaitis and J. Sunner, *Anal. Biochem.*, **269**, 1999, 1-9.
- 13 J. B. Fenn, M. Mann, C. K. Meng, S. F. Wong and C. M. Whitehouse, *Science*, **246**, 1989, 64-71.
- 14 K. B. Green-Church and P. A. Limbach, *Anal. Chem.*, **70**, 1998, 5322-5325.
- 15 A. Lespagnol, E. Cuingnet and M. Debaert, *Bull. de la societe de Chemie de France*, **2**, 1960, 383- 389.
- 16 B. O. Keller and L. Li, *Anal. Chem.*, **73**, 2001, 2929-2936.
- 17 Y. J. Kim, A. Freas and C. Fenselau, *Anal. Chem.*, **73**, 2001, 1544-1548.
- 18 M. Cadene and B. T. Chait, *Anal. Chem.*, **72**, 2000, 5655-5658.
- 19 F. Gharahdaghi, M. Kirchneer, J. Fernandez and S. M. Mische, *Anal. Biochem.*, **233**, 1996, 94-99.
- 20 G. A. Breaux, K. B. Green-church, A. France and P. A. Limbach, *Anal. Chem.*, **72**, 2000, 1169-1174.
- 21 O. Vorm, P. Roepstorff and M. Mann, *Anal. Chem.*, **66**, 1994, 3281-3287.
- 22 K. Gevaert, H. De Mol, M. Puype, T. Houthaeye, S. De Boeck, and J. Vanderkerckhove, *J. Protein Chem.*, **17**, 1998, 560.
- 23 M. Karas and F. Hillenkamp, *Anal. Chem.*, **60**, 1988, 2301-2303.
- 24 J. B. Ghaim, P. H. Tsatsos, A. Katsonouri, D. M. Mitchell, R. Salcedo-Hernandez and R. B. Gennis, *Biochim. Biophys. Acta*, **1330**, 1997, 113-120.

- 
- 25 K. L. Schey, *Proteins and Peptide Analysis by Mass spectrometry, Methods in Molecular Biology*, Eds. J. R. Chapman, Humana Press Inc., Totowa, NJ., **61**, 1996, 227-230.
- 26 J. Angelici, *Inorganic synthesis*, **28**, 1990, 107-108.
- 27 T. Yan-Chun and D. Charles, *Biopolymers*, **76**, 2004, 110-8.
- 28 H. Hsiang-Ming; C. Wen-Yih; R. Ruoh, *Journal of colloid and interface science*, **263**, 2003, 23-8.
- 29 I. Ernest, J. Kalvoda, C. Sigel, G. Rihs, H. Fritz, M. Blommers, F. Raschdorf, E. Francotte and M. Mutter, *Helv. Chim. Acta*, **76**, 1993, 1539-1563.
- 30 G. H. Bird, A. R. Lajmi and J. A. Shin, *Anal. Chem.*, **74**, 2002, 219-225.
- 31 A. Rodger and B. Norden, *Circular dichroism and linear dichroism*, 1997, Oxford University Press.
- 32 W. Curtis Johnson, *Proteins: Structures, Function and Genetics*, **35**, 1999, 307-312.
- 33 A. C. Gibbs, T. C. Bjorndahl, R. S. Hodges and D. S. Wishart, *J. Amer. Chem. Soc.*, **124**, 2002, 1203-1213.
- 34 S. E. Radford, E. D. Laue, R. N. Perham, S. R. Martin and E. Appella, *J. Biol. Chem.*, **264**, 1989, 767-775.
- 35 D. J. Gordon, R. Tappe and S. C. Meredith, *J. Peptide Res.*, **60**, 2002, 37-55.
- 36 M. Jelokhani-Niaraki, E. J. Prenner, C. M. Kay, R. N. McEllaney, R. S. Hodges, *J. Peptide Res.*, **60**, 2002, 23-36.

- 
- 37 L. H. Kondejewski, D. L. Lee, M. Jelokhani-Niaraki, S. W. Farmer, R. E. W. Hancock and R. S. Hodges, *J. Biol. Chem.*, **277**, 2002, 67-74.
- 38 M. Wu and R. E. W. Hancock, *J. Biol. Chem.*, **274**, 1999, 29-35.
- 39 S. Takahashi, *Biochemistry*, **29**, 1990, 6257-6264.
- 40 A. Jasanoff, A. R. Fersht, *Biochemistry*, **33**, 1994, 2129-2135.
- 41 H.-D. Arndt, A. Vescovi, A. Schrey, J. R. Pfeiffer and U. Koert, *Tetrahedron*, **58**, 2002, 2789-2801.
- 42 N. Sitaram, R. Nagaraj, *Biochim. Biophys. Acta*, **1462**, 1999, 29-54.
- 43 S.E. Blondelle, K. Lohner, M. Aguilar, *Biochim. Biophys. Acta*, **1462**, 1999, 89-108.
- 44 G. Choi, J. Landin and X. Q. Xie, *J. Peptide Res.*, **60**, 2002, 169-177.
- 45 D. L. Luisi, W.-J. Wu and D. P. Raleigh, *J. Mol. Biol.*, **287**, 1999, 395-407.
- 46 C. M. Bishop, W. F. Walkenhorst and W. C. Wimley, *J. Biol. Chem.*, **309**, 2001, 975-988.
- 47 W. C. Wimley, K. Hristova, A. S. Landokhin, L. Silvestro, P. H. Axelsen and S. H. White, *J. Biol. Chem.*, **277**, 1998, 1091-1110.
- 48 D. Wang, L. Guo, J. Zhang, L. R. Jones, Z. Chen, C. Pritchard and R. W. Roeske, *J. Peptide Res.*, **57**, 2001, 302-306.
- 49 T. M. Weiss, L. Yang, L. Ding, A. J. Waring, R. I. Lehrer and H. W. Huang, *Biochemistry*, **41**, 2002, 10070-10076.

- 
- 50 R. Marrington, T. R. Dafforn, D. J. Halsall and A. Rodger, *Biophys. J.*, **87**, 2004, 2002-2012.
- 51 T. R. Dafforn and A. Rodger, *Curr. Opin. Struct. Biol.*, **14**, 2004, 541-546.
- 52 M. Ardhammer, P. Lincoln and B. Norden, *J. Phys. Chem. B*, **105**, 2001, 11363-11368.
- 53 A. Rodger, J. Rajendra, R. Marrington, M. Ardhammer, B. Norden, J. Hirst, A. T. B. Gilbert, T. R. Dafforn, D. J. Halsall, C. A. Woolhead, C. Robinson, T. J. T. Pinheiro, J. Kazlauskaitė, M. Seymour, N. Perez and M. Hannon, *Phys. Chem. Chem. Phys.*, **4**, 2002, 4051-4057.
- 54 M. Ardhammer N. Mikati and B. Norden, *J. Amer. Chem. Soc.*, **120**, 1998, 9957-9958.
- 55 M. Bloemendal, *Chem. Soc. Rev.*, 1994, 265-273.
- 56 R. N. McElhaney, *Biochim. Biophys. Acta*, **864**, 1986, 361-421.
- 57 M. Polikandritou Lambros, E. Sheu, J. S. Lin, H. A. Pereira, *Biochim. Biophys. Acta*, **1329**, 1997, 285-290.
- 58 R. R. C. New (Edt), *Liposomes, a practical approach*, Oxford University Press, New York, 1989, p. 5-32.
- 59 E. J. Prenner, R. N. A. H. Lewis and R. N. McElhaney, *Biochim. Biophys. Acta*, **1462**, 1999, 201-221.
- 60 E. J. M. Van Kan, D. N. Ganchev, M. M. E. Snel, V. Chupin, A. Van der Bent and B. de Kruijff, *Biochemistry*, **42**, 2003, 11366-11372.
- 61 K. Lohner and E. J. Prenner, *Biochim. Biophys. Acta*, **1462**, 1999, 141-156.

---

62 Y. Kobayashi and K. Fukada, *Biochim. Biophys. Acta*, **1371**, 1998, 363-370.

63 Software package downloaded free from <http://rsb.info.nih.gov/ij/>

64 M. Salmons, M. Morbin, T. Massignan, L. Colombo, G. Mazzoleni, R. Capobianco, L. Diomedea, F. Thaler, L. Molleca, G. Musco, J. J. Kourie, O. Bugiani, D. Sharma, H. Inouye, D. A. Kirschner, G. Forloni and F. Tagliavini, *J. Biol. Chem.*, **48**, 2003, 48146-48153.

65 A. Shukla, M. Raje and P. Guptasarma, *Protein Eng.*, **16**, 2003, 875-879.

66 D. J. Gordon, R. Tappe and S. G. Meredith, *J. Peptide Res.*, **60**, 2002, 37-55.

67 Gill and Von Hippel, *Anal. Biochem.*, **182**, 1989, 319-326)

68 T. R. Dafforn, J. Rajendra, D. j. Halsall, L. C. Serpell and A. Rodger, *Biophys. J.*, **86**, 2004, 404-410.

## Chapter III

### III.1. Two dimensional (2D) crystallisation of membrane proteins.

The series of synthetic amphiphilic peptides were designed to adopt  $\beta$ -sheet structures and potentially self assemble in lipid bilayers by forming pores with a  $\beta$ -barrel conformation. A previous study using fluorescence marker release experiments, in which a marker was encapsulated into a liposome, showed that on addition of these peptides, liposome integrity was effectively disrupted and the marker released; this was a clear indication that these peptides could form pore structures in lipid bilayers.<sup>1</sup> A popular method for investigating protein assemblies in membranes is 2D crystallisation, which can lead to densely packed highly ordered assemblies in lipid vesicles. A microscopy study of membrane proteins in crystalline arrays would enable the position of proteins relative to each other; their orientation in the membrane, as well as protein-protein and protein-lipid interactions to be determined whilst the protein is in its functional or biologically active state.

The  $\beta$ -barrel channel forming moiety of an autotransporter protein was overexpressed for use in 2D crystal trials in order to both provide comparison of a natural  $\beta$ -barrel system and to investigate the crystallisation process before attempting 2D trials on the synthetic amphiphilic peptides.

The number of membrane proteins that have been characterized to atomic resolution is very small and although genomic studies show that over a quarter of the proteins in any living cell are membrane proteins, the three dimensional (3D) structures of around 100 membrane proteins only have been determined by X-ray diffraction compared to several thousands of soluble proteins.<sup>2</sup>

This large discrepancy is due to difficulties associated with the expression, purification and stability of membrane proteins (Fig.III.1.1) in sufficient quantities for crystallisation as their amphiphilic nature can be a considerable



handicap and in addition most membrane proteins form oligomeric complexes with high molecular weights, which can put them outside the range of current NMR structural studies, although progress is being made in this area on both protein solutions and 2D crystal arrays.<sup>3,4,5</sup>

A powerful alternative approach is to investigate and solve membrane protein structures by electron diffraction which relies on the reconstitution of membrane proteins in presence of a lipid bilayer to form well ordered protein arrays, 2D lattices.

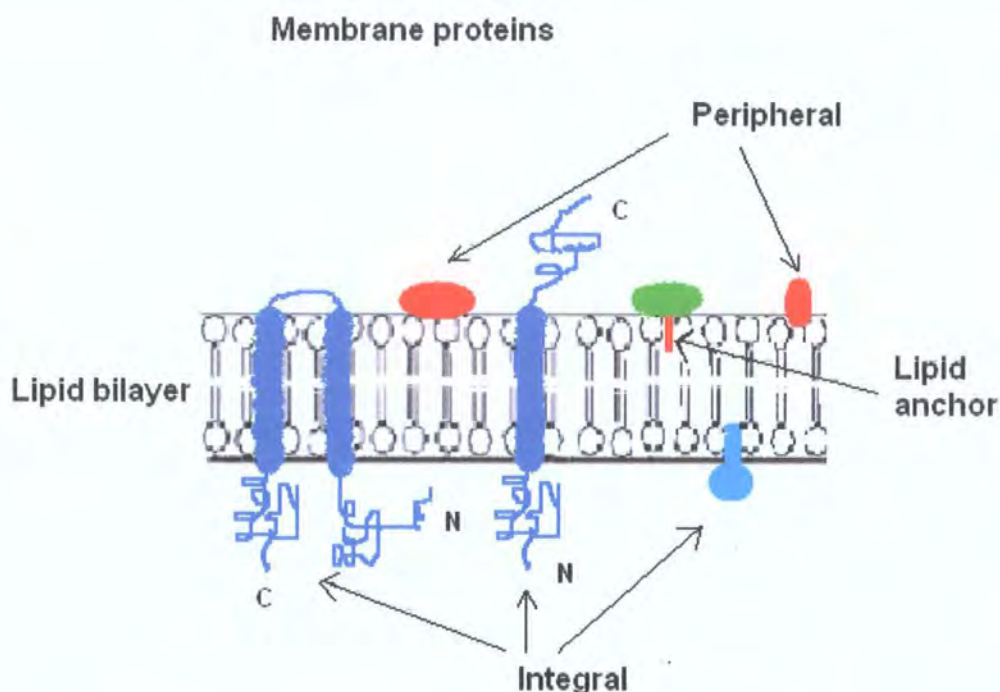


Figure III.1.1. Schema of membrane proteins in a lipid bilayer.

High resolution information is obtained from the position of the protein molecules in the unit cells of these 2D crystal structures and may be precisely determined by the crystal lattice vectors with the aid of computer programs such as *ALLSPACE*.<sup>6</sup>

2D crystal formation is largely due to hydrophobic interactions whereas 3D crystal growth is predominantly governed by hydrophilic interactions.

Detergents are heavily involved in solubilisation and purification of membrane proteins (Fig.III.1.2) and to different extents in both 3D and 2D crystallisation processes. 3D crystals are grown from isotropic detergent solutions in which

each protein molecule is incorporated into a detergent micelle, the detergent molecules mask the hydrophobic regions of the protein which are normally hidden in the membrane. This leads to formation of crystals with a high content of detergent, whose size and structure depend on the physical properties and size of the detergent molecules used in the process. For example, detergents which form small micelles often cause more disruption than detergents that form larger micelles, but can fit better into a crystal lattice as they allow closer contact between the proteins.

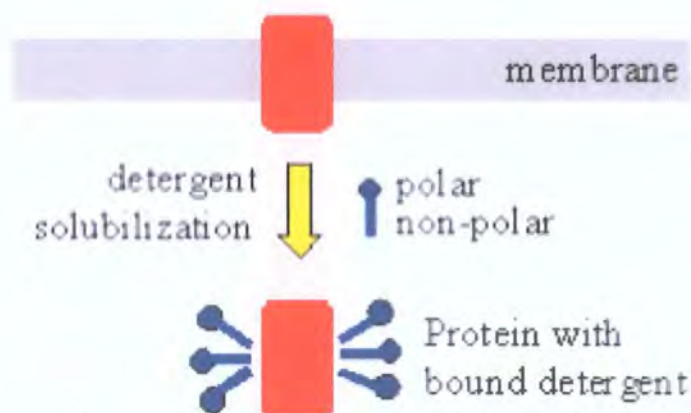


*Figure III.1.2. Representation of membrane protein solubilisation by detergent molecules.*

During 2D crystallization, the protein is only exposed to high levels of detergent for a limited period of time, which favours the formation of more stable protein structures as the crystal contacts are predominantly hydrophobic in 2D crystals, especially for the smaller membrane proteins. The ease with which some membrane proteins adopt well ordered crystalline arrays depends very much on the properties of the membrane protein itself. A high degree of intrinsic molecular symmetry and a tendency to form only heterogeneous oligomers are factors that are more likely to favour crystalline growth.<sup>7</sup>

The proteins that are found in bacterial, mitochondrial or chloroplast membranes pack tightly together and tend to form 2D crystals more readily, as the electrostatic repulsion and steric hindrance constraints are lower in these systems.

Furthermore electrostatic interactions caused by polar groups such as lysine side chains and N termini can be reduced by reaction of the free amine group with reagents such as *N*-hydroxy succinimides, isothiocyanates and acetic anhydride.<sup>7</sup>

### **III.1.1. Properties of membrane proteins.**

Progress in determining high-resolution structures of membrane proteins has not yet gained a steady pace; this is essentially due to the difficulties associated with their manipulation and in particular crystallization, resulting from properties such as solubility, purity, refolding, final concentration, aggregation and stability.<sup>8</sup>

#### **III.1.1.1. Quantities.**

A major handicap is to overexpress and purify the membrane proteins in sufficient quantities for structural analysis: In 2D crystal assays, protein concentrations from 1 to 5 mg ml<sup>-1</sup> are sufficient for successful trials but considerably higher concentrations of pure protein are required for 3D crystal growth.

#### **III.1.1.2. Purity.**

The purity of the protein is of prime importance in a crystallisation process because as the protein crystallises, the concentrations of impurities in the solution increases and will then interfere with crystal lattice formation. For large 2D crystals of a sufficient quality for electron diffraction studies, the purity of the starting material is just as important as in 3D crystallizations.



### III.1.1.3. Aggregation.

Membrane proteins especially those that favour  $\beta$ -sheet structures have a higher tendency to aggregate than other types of proteins.<sup>9</sup> The production of soluble active proteins from expression in prokaryotes such as *E. coli* is difficult, as overexpression favours the formation of aggregates of misfolded, non functional protein, such as inclusion bodies.<sup>10</sup>

### III.1.2. The purification process.

Although the protein from an inclusion body is fairly easy to purify, its solubilisation requires strongly denaturing conditions such as high concentrations of urea or guanidine which are not compatible with a subsequent refolding process.<sup>11</sup> Purification of the protein is commonly carried out by chromatographic separation methods. A high degree of purity may be reached by adding a short chain of polyhistidine residues, a His-tag, to the protein through gene modification techniques; the protein will then specifically bind a nickel-chelated nitroacetic acid ( $\text{Ni}^{2+}$ -NTA) resin *via* the His-tag (Fig.III.1.3).<sup>12,13</sup>

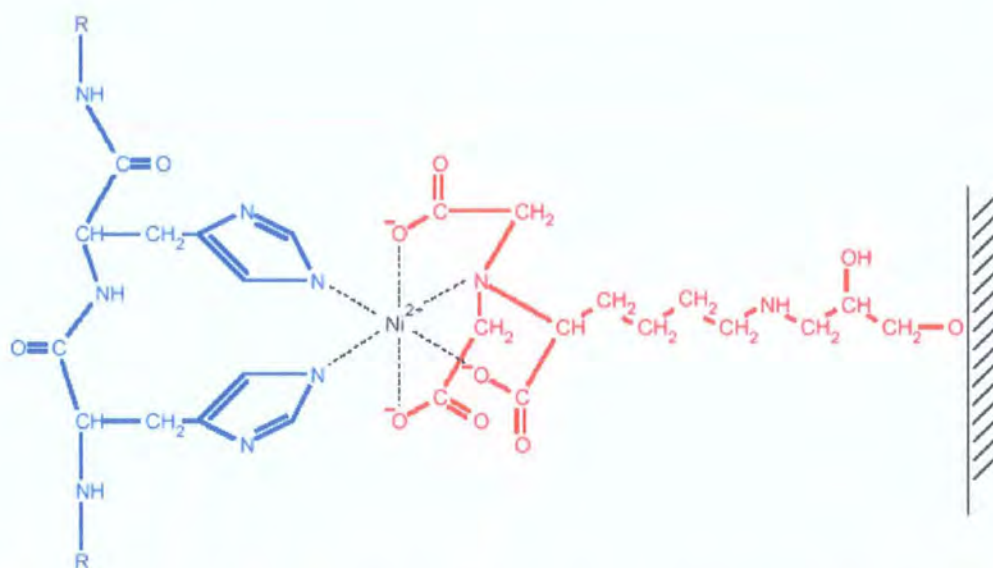
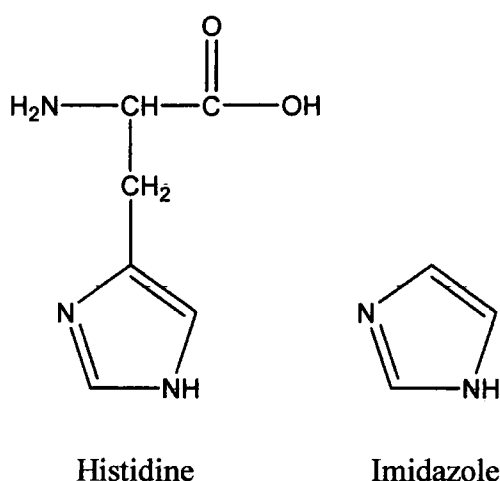


Figure III.1.3. Diagram of the interaction between the histidine residues on a tagged protein with a  $\text{Ni}^{2+}$  ion on a Ni-NTA column.

The histidine structure contains an imidazole ring (Fig.III.1.4) that chelates through its less sterically hindered nitrogen atom to nickel ions on the Ni-NTA resin.



*Figure III.1.4. Diagram showing the structure of histidine with its imidazole ring*

Imidazole in high enough concentration (100-250 mM) acts as a competitor for the binding sites on the nickel affinity column and displaces the histidine tag as its concentration is increased in the buffer. The His-tagged protein should then elute with a high degree of purity from the column. There is some speculation as to whether the His-tag could interfere to some degree with the formation of well ordered 2D crystals.<sup>10</sup>

Purification can also be carried out on an ion exchange column if the protein has a suitable isoelectric point (IP) and is solubilised in high concentrations of urea; the bound protein is eluted from the column by increasing the ionic strength of the mobile phase.

After purification the protein may be refolded, either by slowly dialysing out the denaturant with an appropriate buffer, which may contain mild detergents, or by refolding *in situ* whilst still bound to the chromatographic column.<sup>10</sup>

The folding conditions such as the protein concentration, the rate of denaturant removal, the temperature profile and the addition of detergents, salts and reducing agents like DTT, which breaks disulphide bridges, must be controlled in order to both minimize aggregation and to optimize refolding.

Aggregation is less likely to occur if the denaturant concentration is lowered quite rapidly in the presence of a mild detergent such as Triton X-100 at low temperatures (4°C). This enables the protein to be dispersed and refolded before aggregation can occur to any great extent. The presence of any residual denatured protein as well as aggregates can greatly disrupt the formation of coherent crystalline patches.

The yeast mitochondrial outer membrane protein Tom40 was refolded by dilution and incorporation into liposomes.<sup>14</sup> The refolding process of the light harvesting complex II from pea was performed whilst the protein was bound to a Ni-NTA column *via* a His-tag because the dilution method did not produce the functional form of the protein.<sup>15</sup>

### **III.1.3. 2D crystallisation.**

The most common method for growing 2D crystals is by detergent dialysis in presence of lipid.<sup>7,16</sup> The purified protein is premixed with detergent and then added to a suspension of detergent-lipid micelles. This solution is then generally incubated at low temperature for a few hours to allow the lipid to equilibrate with the detergent-protein micelles before removal of the detergent.

In addition to the purity and concentration of the protein, there are a range of other parameters that need to be considered when setting up a crystallisation: for instance the physical characteristics and concentration of the detergents, the protein-lipid ratio, the nature of the lipids, the pH and ionic strength of the solutions, the temperature profile and the length of time for crystallisation. All of these need to be optimized specifically for each protein. The best initial conditions are generally found by trial and error; therefore ready access to an electron microscope for routine scanning of the dialysis solution to monitor

crystal growth is essential. These initial conditions are then used as the starting point for further optimization.

Typical 2D crystal growth resulting from the dialysis of detergent solubilised membrane proteins produces an array (Fig.III.1.5) in which the protein molecules are oriented at  $180^\circ$  to each around a 2-fold axis in the plane of the membrane.<sup>17</sup>

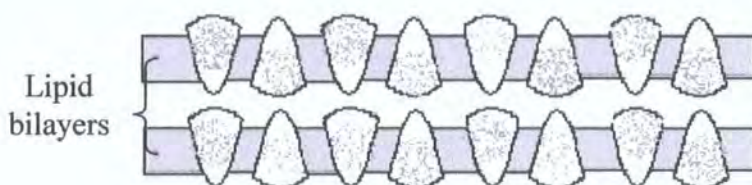


*Figure III.1.5. Schematic diagram of membrane protein crystals in cross section.*

Depending on the size of the protein molecules, the thickness of the crystals can range from 5 to 20 nm with crystalline patches generally growing up to a few microns in diameter. These are often composed of two superimposed crystal lattices one from each of the two layers of the bilayer.

#### **III.1.3.1. Lipids used in reconstituted membrane environments.**

The 2D crystallisation process relies on the insertion of protein into a lipid matrix that should ideally mimic the original membrane environment and the subsequent rearrangement of these protein-lipid arrays into highly ordered structures. The choice of lipid therefore, may be determined by the properties of the natural membrane lipids.<sup>18</sup>

Unsaturated lipids with long chain lengths may be required for successful 2D crystal growth of eukaryotic membrane proteins, as the native lipid mixtures from eukaryotic cells contain a high proportion of fluid lipids, whereas proteins from prokaryotic membranes which are rich in saturated lipids, perform well in crystal trials with synthetic saturated lipids like DMPC (Fig.III.1.6).<sup>19</sup>

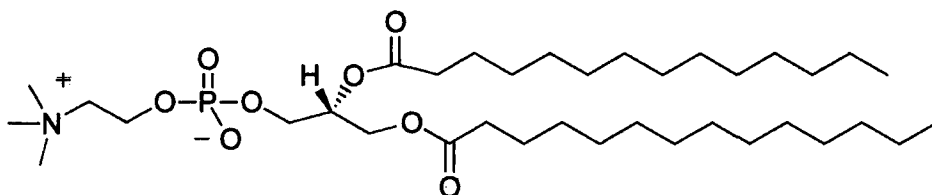


*Figure III.1. 6. Typical structure of a phosphatidylcholine lipid, dimyristoyl phosphatidylcholine (DMPC).*

The fluidity of the lipid membrane is governed by physical factors such as the length of the hydrocarbon chains, their degree of saturation and the size and charge of the lipid head groups. The most common lipids, used in a vast number of crystallisation processes, have been the saturated and unsaturated zwitterionic phospholipids;<sup>20</sup> DMPC; *E. coli* phospholipid; Soybean PC; Egg PC and DOPC.<sup>21</sup> These lipids preferentially form vesicular-bilayer structures in aqueous media that range from a few nanometers to several microns in size.

Successful crystal trials have shown that 2D crystals start to form at temperatures above the gel to liquid crystalline phase, when the lipid is in a fluid state, giving the protein a greater degree of freedom to move and rearrange into ordered arrays in the lipid membrane. Protein-lipid ratios are difficult to predict as they depend both on nature and size of the protein and on the packing density of the crystals. 2D crystals of porins, water filled channels spanning the outer membrane of Gram-negative bacteria have been formed at low lipid-protein ratios.<sup>22</sup> Larger membrane proteins like CaATPases can accommodate a greater number of lipid molecules and will form crystal arrays at significantly higher lipid to protein ratios.



Excess lipid can be removed by treatment of the dialysis solution with phospholipase A<sub>2</sub>, which may improve the crystallinity of the protein arrays.<sup>23</sup> The sample is incubated at 38°C for about 4 h to convert excess phospholipids to lysophospholipids, which are then removed by dialysis.

The lipid to protein ratio is thought to have an effect on the size and shape of the crystal patches; for example a tendency to form vesicles rather than flat sheets has been reported in samples with high lipid content.<sup>7</sup>

### **III.1.3.2. Role and choice of detergent.**

Protein 2D crystallisation relies on detergents for both solubilisation of the protein and lipid molecules and for the reconstitution of the protein in a lipid bilayer through controlled removal of the detergent.<sup>24</sup>

There is a wide choice of detergents with a broad range of physical properties readily available for biomolecular work (see appendix for detergent property table) therefore selection of a detergent that is appropriate for a particular application and is compatible with the other reagent molecules involved in the process can be quite difficult.<sup>25</sup>

Detergents are generally classed in 3 groups, ionic, zwitterionic (Fig.III.1.7) and non ionic. Ionic detergents which tend to affect protein structure more severely than the other types, may cause the protein to become denatured. Non ionic detergents which are milder than their zwitterionic counterparts can also affect protein stability to a degree so the choice of detergent also has to take in to consideration the sensitivity of a protein towards a particular detergent.

A simple rule is that detergents with longer acyl chains and bulkier head groups tend to be less denaturing than detergents with shorter chains and smaller head groups.

Detergent molecules cover the hydrophobic surfaces of the protein and mask parts of the protein that would normally come into contact with the lipid head groups.<sup>26</sup>

A choice has to be made between the use of a milder detergent with a bulky head group and a harsher detergent with a smaller head group but increased protein contact, unless the physical properties of different detergents can be combined by using a mixture of detergents in the crystallisation solution.<sup>56</sup>

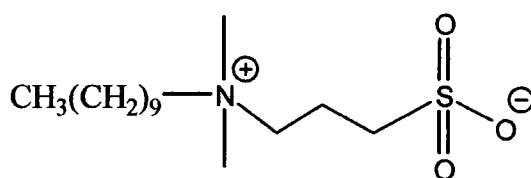


*Figure III.1.7. Structure of zwittergent 3-12, n-decyl-N,N-dimethyl-3-ammonio-1-propanesulfonate, a zwitterionic detergent with a CMC of 2-4 mM.*

Above a certain concentration, the critical micelle concentration (CMC), the detergent molecules associate in aqueous media to form micelles, with segregation of the hydrophobic chains and polar head groups. An equilibrium is established between the concentration of the monomers, which is independent of the overall detergent concentration and the micelles in solution (Fig.III.1.8).

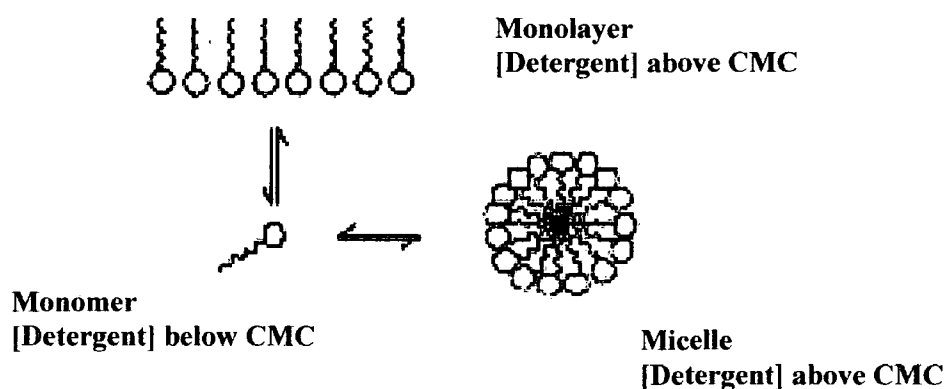


*Figure III.1.8. Diagram showing monomer – micelle equilibrium in aqueous solution.*

The initial detergent concentration needs to be higher than the critical micelle concentration as detergent monomers can pass through the dialysis membrane quite freely and only the micelles will be retained within.

Another important factor is the value of the critical micelle concentration itself, as this determines the rate of dialysis and by consequence the rate of crystal formation.<sup>27</sup>

Dialysis of detergents with low CMCs is much slower and easier to control than those with higher CMCs, as they may take several hours to reach dialysis equilibrium. A very gradual elimination of detergent from the dialysate is thought to promote 2D crystal formation by reducing the number of protein nucleation sites and favouring the growth of larger crystalline patches.

A general trend is that detergents with bulky head groups tend to have higher CMC values than detergents with smaller head groups and for a given head group size, CMC values tend to decrease with chain length, but in the case of ionic detergents, this depends also on the counter ion and salt concentration of the dialysis solution.

The most common detergents for biological applications are the milder non denaturing zwitterionic and non ionic detergents with either a sugar base or a polyoxyethylene head group (Fig.III.1.9).<sup>28,29,30,31</sup>

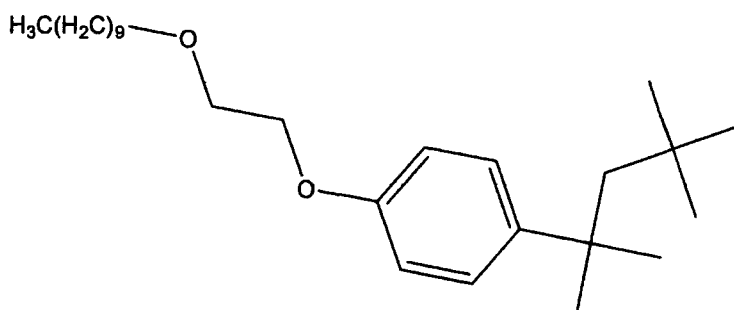


*Figure III.1.9. Structure of Triton X-100, a non ionic polyoxyethylene detergent with a relatively low CMC of 0.2 mM*

In particular the sugar based detergents (Fig.III.1.10) are among the most popular type of detergent used with membrane proteins.<sup>32,33</sup> The crystallisation of the pore-forming  $\alpha$ -Toxin protein, *Staphylococcus aureus* was performed using the sugar based non ionic detergent, octylglucoside.<sup>17</sup>

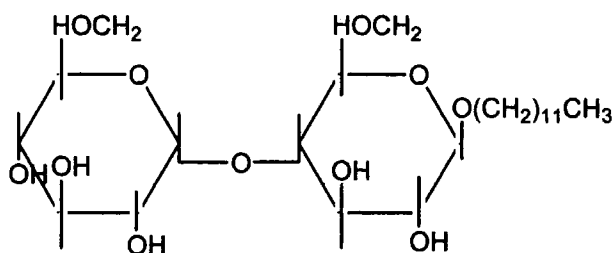


*Figure III.1.10. Structure of DDM, n-dodecyl- $\beta$ -D-maltoside, a non ionic sugar based detergent with a low CMC of 0.15 mM.*

Once a detergent has been selected, the conditions under which the dialysis is carried out require careful consideration and optimization, as their affect can be large enough to promote or even interfere with the crystallisation process.

The most important parameters to set are the ionic strength and pH of the solutions, the temperature profile and the duration of the dialysis.

### III.1.3.3. The ionic strength and pH of buffer solutions.

Bound water molecules at the surface of a protein interfere with close protein-protein and protein-lipid contacts and by consequence with the crystal growth process. Small molecules and ions perturb the specific arrangement of water molecules, the solvation forces around the proteins and even the protein conformation itself by inducing contact between protein molecules at specific sites with a lock and key type adhesion that induces directional growth in protein arrays.

The presence of divalent cations are well known to promote the formation of filaments in proteins such as actin and tubulin, they act by defining a growth direction in 2D assemblies, where lock and key sites are thought to develop in

two directional assemblies of subunits. Enhanced protein-protein contact leads to a much greater degree of order in protein arrays and to the formation of highly crystalline patches.<sup>56</sup>

Addition of ions to the dialysis buffer also has a significant affect on the crystallisation of proteins that have large extra-membranous domains, by effectively screening any charged amino acids on the protein surface.

Many proteins also require the presence of different additives in order to remain soluble, which may include metal cofactors, salts and co solvents such as glycerol, glucose and sucrose. Amphiphiles, like taurine are also used to help promote 2D crystal formation.<sup>34</sup>

Successful crystallisation of membrane proteins has been carried out at low ionic strengths and a neutral pH, as the risk of protein aggregation tends to increase at high ionic strength and at pH values above the isoelectric point of the protein.<sup>35,36</sup>

#### **III.1.3.4. The temperature profile and the duration of dialysis.**

2D Crystallization protocols follow characteristic temperature profiles, often with an incubation period of up to a few hours at 4°C to allow for equilibration before the actual dialysis, which may start at room temperature for a period of several hours and then move to temperatures above 37°C for a day and more.

As mentioned previously, temperatures above the main transition from gel to fluid state of the lipid are required for 2D crystal formation. This is centered at 23°C for the fully saturated phospholipid, DMPC.

The increase in temperature is thought to enhance the rate of 2D crystal formation by favouring both protein diffusion in the bilayer and hydrophobic interactions between the protein molecules. For the PhoE porin, increasing the temperature induced the formation of large 2D crystal sheets from smaller mosaic lattices.<sup>37</sup>

Temperature is also a significant factor for controlling interactions between detergent micelles. Those of the polyoxyethylene detergent, Triton X-100 interact more strongly as the temperature is raised but micelles of sugar based detergents like octylglucoside merge as the temperature is lowered. These

different tendencies could be exploited by using a mixture of detergents in the protein crystallisation process.

The average size of most 2D crystals lies in the range of 0.5 to 5 microns in diameter, as crystalline patches above this limit tend to break up due to thermal vibrations or fold up into rolls because of the inherent mechanical instability associated with large unsupported 2D structures. Once formed 2D crystals generally remain stable enough to be stored at 4°C for several weeks.

#### **III.1.3.5. The mechanism of crystal formation from detergent solution.**

The detergent dialysis method for 2D crystal formation relies on mutual interactions between the protein, lipid and detergent molecules as well as significant contributions from buffers, salts and additives and any influence from parameters such as temperature and dialysis time. The crystallisation process is thought to involve several consecutive steps before well ordered protein-lipid arrays are formed.

The lipid and protein molecules are premixed in appropriate ratios with detergent; this solubilises the molecules by forming mixed micellar structures in which the hydrophobic regions are shielded from the aqueous media. The detergent is then gradually removed by dialysis either into detergent free buffers or into a buffer with a lower concentration of detergent. A common way of doing this is to reduce the concentration of detergent in the buffer by halving it every few hours or by dilution with a peristaltic pump. The membrane protein should then integrate into the lipid membrane to form stable assemblies or arrays of protein and lipid. Formation of the lipid bilayers from lipid-detergent micelles may take place either before protein insertion or as the protein-lipid micelles merge on dilution of the detergent.

The final step involves rearrangement of the protein-lipid arrays into well ordered 2D lattices through specific interactions with close protein-protein and protein-lipid contacts.

The insertion of membrane proteins into lipid bilayers is an energetically favourable process due to the tendency of the protein to adopt conformations that allow hydrophilic regions to remain in contact with the aqueous media on either side of the bilayer and hydrophobic regions to be hidden within the lipid interior. This whole process is entropically driven, with a net gain in entropy on segregation of protein and lipid hydrophobic areas from the surrounding aqueous media through formation of large vesicular or sheet like structures, since any exposed hydrophobic domains would force the aqueous molecules to adopt a non-random arrangement and thereby decreasing the overall entropy of the system.<sup>38</sup>

Aggregation of the protein molecules, especially those with large protruding hydrophilic domains, can interfere and disrupt crystallisation, but this problem can be minimised if the protein-lipid and detergent ratios are adjusted correctly and appropriate dialysis conditions selected.

The first 2D crystallisations to be carried out using the detergent dialysis method were on the membrane protein Cytochrome reductase from mitochondria of *Neurospora crassa*.<sup>39</sup> A wide variety of 2D crystal growth trials have since been attempted on a number of membrane proteins in order to obtain crystal lattices of sufficient quality for structure determination by electron microscopy and even atomic force microscopy.

No one set of crystallisation conditions will be successful for all proteins, which means that trials to establish the best conditions need to be carried out for each protein.

Highly ordered 2D crystals of purified lactose “red” permease, membrane transporter protein were reconstituted in the presence of a mixture of saturated and unsaturated phospholipids solubilised in octyl- $\beta$ ,D-glucopyranoside (OG) and decyl- $\beta$ ,D-maltopyranoside (DM) detergents with sodium and magnesium chloride salts in the dialysis solution and produced.<sup>11</sup>

The best crystallisation conditions for the bacterial outer membrane protein, OmpF were achieved using a 1:1 protein to lipid ratio of DMPC and a 1 % (w/v) solution of octyl-polyoxyethylene (C<sub>8</sub>POE), a detergent with a high CMC and which is consequently easily dialysed.

Highly ordered 2D arrays of PhoE were produced following incubation with DMPC with a 4 fold excess of protein and 0.6 % (w/v) SDS under controlled dialysis conditions.<sup>40,41,42</sup>

Whereas the best result for the Cytochrome *b<sub>6</sub>f* complex from spinach purified protein was obtained by reconstitution with EPC and a phosphoglycerol lipid, DOPG solubilised in Hecameg, a non ionic detergent with a CMC value some 78 times that of Triton X-100.<sup>43</sup>

The detergent dialysis method is the most common and reproducible 2D crystallisation process although it is not by far the only or always the most appropriate method available.

A range of other processes have been explored and some successfully developed in order to enhance the growth, stability, size and reproducibility of the crystal arrays.<sup>44</sup>

#### **III.1.3.6. Other methods for 2D crystallization.**

One method that has produced good results and which is gaining more and more scope is the use of solid supports to grow 2D crystal arrays in situ (Fig.III.1.11).<sup>45</sup>

Several techniques are currently employed to meet a variety of conditions: proteins can be engineered for anchorage to a film of functionalised or natural lipids spread at the air-water interface. Binding the proteins in this way forces the protein monomers to adopt a preferred orientation relative to the interface and will also induces high local protein concentration both of which are an advantage in 2D crystallisation trials. Proteins are frequently tagged with short sequences of histidine residues to aid in purification on a nickel affinity column however the His tag can also be used to crystallize membrane proteins on lipids derivatised with a Ni<sup>2+</sup>-chelating nitrilotriacetate (Ni-NTA) group.<sup>46, 47</sup> This method is not without problems as the detergents used to solubilise the protein disrupt and also solubilise the lipid film therefore a detergent with a low CMC or a lipid with resistance to detergent solubilisation is required for successful crystallization.



A solution was developed by designing partially fluorinated lipids that show resistance to detergent solubilisation when spread at the air-water interface; this arises because alkane and perfluoroalkane mixtures are not miscible.

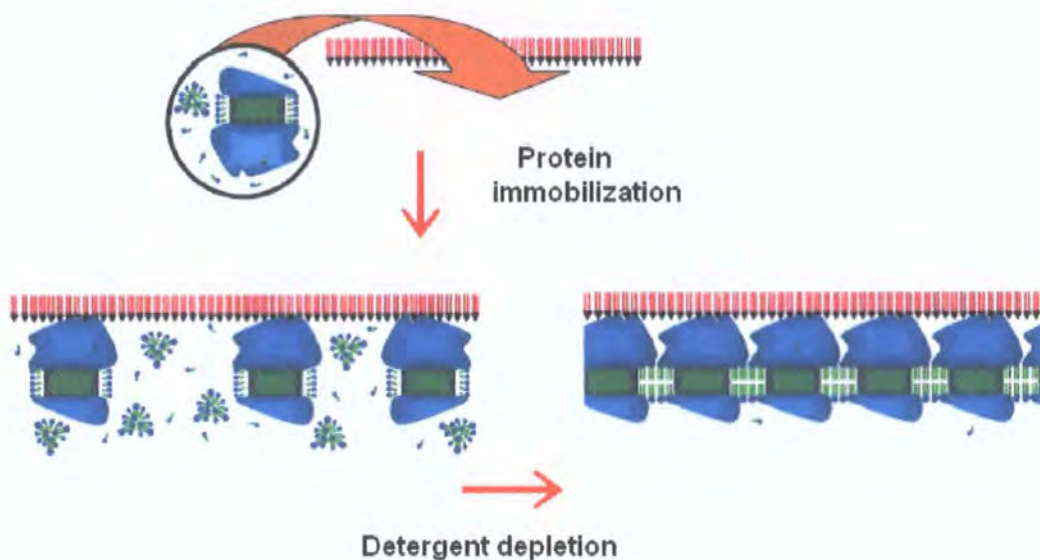


*Figure III.1.11. 2D crystallisation of membrane proteins anchored to functionalised fluorinated lipid spread at the air-water interface.<sup>48</sup>*

2D crystalline arrays of a membrane protein, proton ATPase from plant plasma membranes, were successfully grown on functionalised fluorinated lipids spread at the air-water interface.<sup>48</sup>

Another strategy for minimizing detergent solubilisation of the lipid film is to spread a layer of lipid in slight excess to that required for monolayer coverage over a detergent free buffer and to inject the protein detergent solution into the sub-phase. In this way the lipid film is stable enough for crystallization to proceed.<sup>47</sup>

Detergents with low CMCs can be especially difficult to eliminate by the dialysis method and can require quite lengthy dialysis times. Adsorption of the detergent with polystyrene Bio-Beads, which are neutral, macroporous polymeric beads

with high surface areas, provides a much quicker solution although this process also has its shortcomings in that the rate of detergent removal may be too rapid for crystal growth and lipid and protein molecules may also adsorb to the beads.<sup>49</sup>

This method is becoming more popular as crystal trials have successfully employed Bio-Beads for the formation of highly ordered protein arrays of sarcoplasmic reticulum  $\text{Ca}^{2+}$  ATPase, melibiose permease from *E. coli* and Cytochrome *b*<sub>6</sub>f from *C. reinhardtii*.<sup>50</sup>

### **III.1.4. Electron microscopy analysis.**

The choice of a 2D Crystallisation method and optimisation of the conditions is not straightforward or easily predictable as there are too many factors influencing the process. Therefore the crystallisation solutions will require routine scanning to establish the right conditions and adjust these to produce well ordered protein arrays.

The best method for monitoring 2D crystal growth is by electron microscopy as sample preparation is both relatively simple and the quality of any protein-lipid arrays can be rapidly assessed.<sup>51</sup>

The two most commonly used electron microscopy techniques are scanning electron microscopy (SEM) and transmission electron microscopy (TEM).

#### **III.1.4.1. Scanning electron microscopy.**

Electron optics are very similar in design and use to light optics; electron microscopy (Fig.III.1.12) uses a beam of accelerated electrons instead of visible light. Rapidly moving electrons take on a wave like behaviour with wavelengths that are much shorter than those of visible light, by at least four orders of magnitude (typically 0.012 nm for electrons accelerated to 10 KeV), which means that samples can be resolved down to distances of less than a nanometre.

Because electrons are charged species they will be deflected by electromagnetic fields; this property is exploited in an electron microscope to focus and move the beam back and forth, thus effectively scanning the sample.

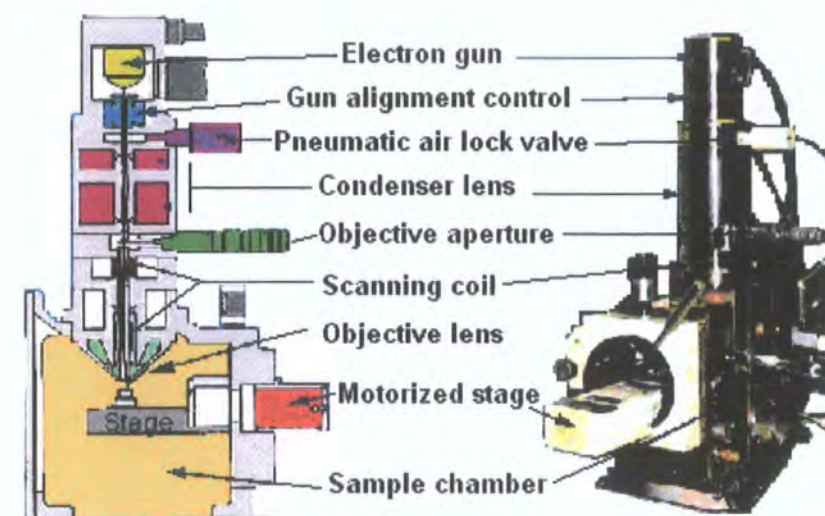


*Figure III.1.12. Diagram showing the main parts of a scanning electron microscope.*

The electrons that strike the sample surface emit signals that are simultaneously detected and then converted to give a topographical image or detailed information about the sample composition depending on the type of detector used (Fig.III.1.13). Electrons are very much more strongly scattered by gases than light and therefore all the optical paths must be evacuated to pressures lower than  $10^{-2}$  Pa.



The most widely used signal in SEM is from the secondary electrons which are detected by a scintillator (phosphor screen) photomultiplier system.

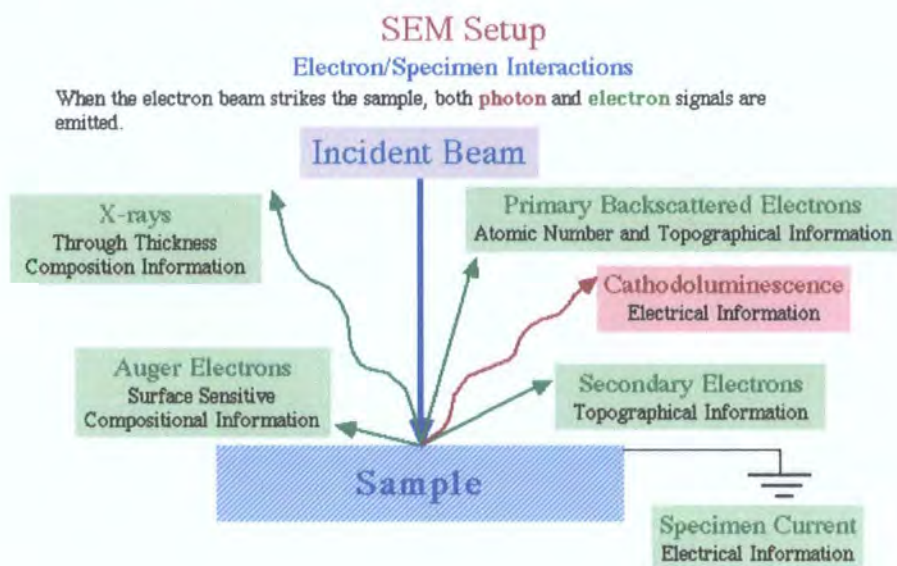


*Figure III.1.13. Diagram showing the different signals and information that can be obtained in a scanning electron microscope.*

Briefly an electron strikes the scintillator and light is emitted, the light is then transmitted through a fibre optic cable and into a photomultiplier which converts photons into pulses of electrons. These are amplified and used to modulate the intensity of a cathode ray tube (CRT).

#### **III.1.4.2. Transmission electron microscopy.**

The electrons in this technique are transmitted through the sample and detected by a phosphor screen (a scintillator) which then relays the signal following the same process as in scanning electron microscopy.

Transmission electron microscopy routinely reaches very high magnifications which can resolve fine details of the internal structures in a sample and may even in some cases resolve features on a near atomic scale.

The images obtained by TEM are 2D sections of the material studied, but it is also possible to carry out 3D reconstructions from data obtained by TEM.

#### **III.1.4.3. Sample preparation for electron microscopy.**

The most common method for preparing samples for screening is by negative staining with for example a solution of 1-2% uranyl acetate, phosphotungstic acid or ammonium molybdate.<sup>52</sup> The high contrast of the protein against the heavy metals contained in the stains allows the 2D crystal lattice structures to be clearly visible by electron microscopy and if the protein contains small extra membranous domains that are not exposed beyond the lipid surface then a low concentration of detergent can be added for deeper stain penetration into the membranes providing a better contrast to any lattice structures.<sup>53,54</sup>

Negative staining does have a few disadvantages, amongst which are the risk of staining artefacts such as stain crystallisation and precipitation that can compromise and make interpretation of the sample quite difficult. There is a limit to the resolution that can be obtained with negatively stained specimens; samples prepared with an ionic negative stain or by metal shadowing have a resolution that will be limited by the grain size of the heavy metal ions outlining the structures. The limit is about 1.6 nm for uranyl acetate though this can be reduced to 1 nm when the stain is combined with glucose.<sup>55</sup>

It is therefore advantageous to also prepare unstained samples for comparison. Specimens can be fixed by cryo-EM, which consists of rapid freezing of pre-treated samples and also offers some protection against the high vacuum conditions present in electron microscopy. Samples may be washed with a tannin solution and then frozen in liquid nitrogen or ethane before the sample is completely dry. Problems associated with this method are due to the low contrast between crystals and the surrounding buffer, the high radiation sensitivity of the samples prepared in this way and also beam induced movements.

The resolution of any features is limited by high background scattering from layers of vitrified buffer as well as some charging from the sample.

Another technique is to freeze fracture the sample followed by heavy metal and carbon shadowing, but this is not a routine procedure and would not be convenient for screening.<sup>54</sup>

The state of the sample supports also needs to be considered; these generally consist of freshly carbon coated copper grids which tend to remain hydrophilic for a few days to a week before becoming more and more hydrophobic. In order to maintain affinity with the samples they can then be treated by a glow discharge process, which will reactivate the carbon.

#### **III.1.4.4. Electron diffraction.**

Electron diffraction patterns are relatively simple to record and can give a rapid assessment of the degree of order of the crystalline arrays.<sup>56</sup>

Large crystalline areas, from about 0.5 to 2  $\mu\text{m}$  in diameter with tens of thousands of unit cells, depending on the lattice size and crystal packing density, are required for good diffraction patterns as the signal to noise ratio of the diffraction peaks increases with the square root of the number of unit cells.

The structures of highly ordered protein-lipid arrays can be determined by electron crystallography from the unit cell dimensions and crystallographic symmetry. The images are also processed with a variety of imaging techniques such as Fourier transformation, which will average peak amplitudes and phases to generate a projection map from which information about crystal size, shape and symmetry can be obtained.<sup>57,58</sup>

A more complete picture of the structure can be attained by processing extensive series of 2D images recorded with a gradual variation in sample tilt angles and focus.<sup>59</sup>

### III.1.5. Other techniques used for crystallographic studies.

#### III.1.5.1. Atomic Force Microscopy.

Atomic Force Microscopy, AFM is a surface sensitive technique which can enable high resolution topographical images of biological structures to be observed under near physiological conditions using a solution cell.<sup>60,61</sup>

This microscopy technique allows a sample to be imaged through interaction of a probing tip with the sample surface. The tip, which is attached to a cantilever, exerts a force on the surface of the sample through the atoms at the apex of the tip.

In contact mode AFM, the deflections of the cantilever tip as it scans the surface of a sample are recorded by a detector. These deflections are recorded as a function of position and build up an image of the surface on the atomic scale.

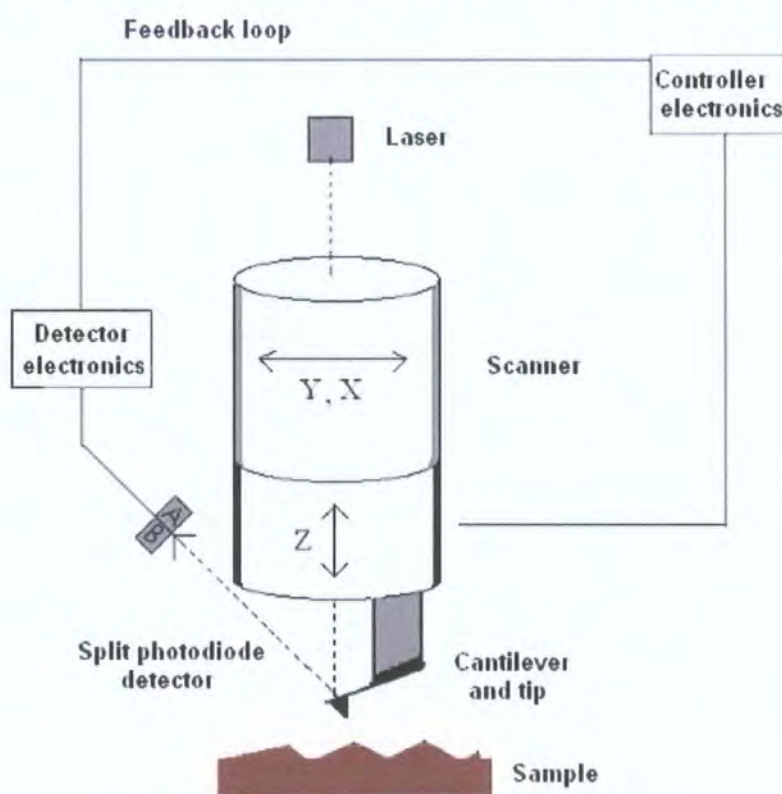


Figure III.1.14. Diagram showing the main features of contact mode AFM.

Cantilever deflection is kept constant using a feedback loop, which adjusts the probe at each displacement or position to ensure that the force between the tip and the surface remains constant.

The force is calculated from Hooke's law:  $F = -kx$

*Where  $F$  is force;  $k$  is the spring constant and  $x$  is the cantilever deflection.*

### **III.1.5.2 Imaging conditions.**

Samples must be firmly attached to a solid support as scanning produces strong lateral movements, which could easily displace the sample and solutions from within the sample cell area.<sup>62,63,64</sup> A Sample support is typically a freshly cleaved mica disc glued to a steel stub, which is held magnetically in place, on the AFM stage. Another problem associated with contact mode AFM, is the ease with which soft biological samples can be damaged by the tip ploughing through the sample surface.

Tip-sample interactions also have to be enhanced in order to gain high resolution images; the double layer repulsion that exists between the tip-sample and the tip-support can strongly affect the spatial resolution of the AFM. The electric double layer results from interactions at the solid-liquid interface and is composed of a firmly bound layer of ions at the surface of the solid, the Helmholtz layer and a diffuse ion cloud.<sup>65,66</sup> This double layer repulsion can be minimized by adjusting the electrolyte concentration in the sample solution.<sup>67</sup> The solution salt concentration is important for both firm adhesion of the sample to the support as well as close contact between the AFM tip and the sample surface; optimum sample adsorption to the support, require solutions with much higher salt concentrations (~300 mM for monovalent cations) than those required for high resolution sample imaging (~150 mM). AFM is not a suitable technique for routine monitoring of 2D crystal formation, but on samples with tightly packed and highly ordered protein arrays of 2D crystals, nano to subnanoscale structural details can be imaged under optimum conditions.<sup>68,69,70</sup>



### **III.1.5.3. X-ray diffraction.**

X-ray diffraction can be used to investigate the degree of order in 2D crystal and is an excellent method for determining accurate measurements of unit cell dimensions, but the amount of sample required needs to be quite concentrated (e.g. a few mgs of crystalline material). Samples are prepared by either pelleting the 2D crystal solutions by centrifugation or by drying layer after layer of sample on to a flat compatible surface.<sup>7</sup>

## **III.2. Natural $\beta$ -barrel pore forming models for structural analysis: the *Bordetella pertussis* autotransporter BrKA C-terminal protein.**

### **III.2.1. Introduction.**

A key factor for the survival of bacterial is the ability to secrete proteinaceous materials, such as virulence factors, adhesins or toxins, into host cells.

Virulent proteins produced by Gram-negative bacteria face quite a challenge in order to leave the bacterial cell, as they must cross both an inner and outer membrane, as well as the periplasmic space and the peptidoglycan layer, in order to reach the cell surface.<sup>71,72</sup>

Several different mechanisms for protein transportation have been described in Gram-negative bacteria and depending on the type of protein, these may follow either a two step process with secretion systems for the inner membrane and other mechanisms for the outer membrane or a one step transportation *via* a complex oligomeric structure spanning both membranes. The latter process, which may require activation on substrate binding, could enable protein injection directly into host cells may.<sup>73</sup>

Autotransporters are a family of secreted proteins, which contain within their own polypeptide sequence the basic units, required for translocation of part of the protein to the cell surface. The virulence factors of significant human pathogens, such as the IgA1 protease from *Neisseria gonorrhoeae*, *Neisseria meningitides* and *Haemophilus influenzae* are known members of the autotransporter family.<sup>12</sup>

The autotransporter protein BrKA from *Bordetella pertussis*, a highly efficient bacterial pathogen responsible for causing whooping cough and mediating resistance to antibody dependent killing in humans, was selected as a model for a natural pore forming protein because of strong evidence suggesting that it adopts a  $\beta$ -barrel structure in the bacterial outer membrane.<sup>74</sup>

Members of the autotransporter family have a generic or modular primary structure, which is composed (Fig. III.2.1) of 3 domains with very distinct roles; an N-terminal signal sequence of about 30 to 40 amino acids in length, a passenger domain ( $\alpha$ -domain), which can exhibit sequences of over a 100 KDa (IgA1 protease), and a C terminus called the  $\beta$ -domain, which has a short  $\alpha$ -helical linker region of 21-39 amino acids and a multistranded  $\beta$ -barrel domain typically of 250-300 amino acids. The  $\beta$ -barrel domain, which forms a channel in the outer membrane through which the passenger proteins are exported to the cell surface, was found in general to consist of 14 antiparallel  $\beta$ -stands of 9 to 12 residues each.<sup>75,76</sup>

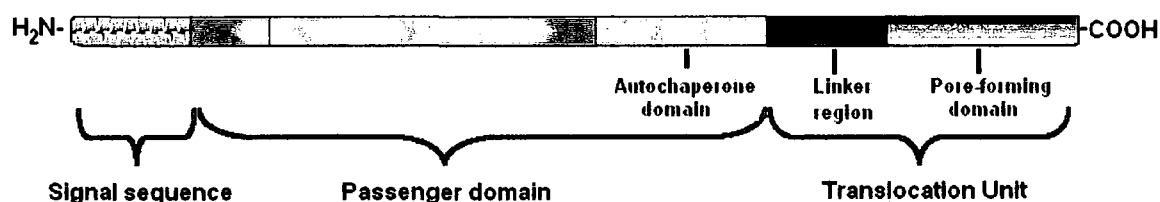


*Figure III.2.1. Diagram of the primary structure of an autotransporter.*

The role of the N-terminal signal sequence is to direct the autotransporter complex across the inner membrane, after which it is cleaved to the periplasm. The C-terminal domain is then thought to fold spontaneously in a thermodynamically favourable process, as it comes into contact with the lipidic non polar environment of the outer membrane, to form an aqueous  $\beta$ -barrel channel (Fig.III.2.2).

The sequence of the C-terminal domain is highly conserved in all known autotransporters and has even been referred to as a structural hallmark for classifying this family of protein complexes.<sup>77</sup>

An  $\alpha$ -helical linker region associated with the  $\beta$ -domain is thought to adopt a hairpin conformation on folding into the aqueous channel, as in the case of the autotransporter IgA and is believed to play a role in directing the passenger secretion through the channel onto the cell surface.<sup>78</sup>

The passenger domain part of the autotransporter complex is the active agent or effector molecule that must be exported to the cell surface in order for it to carry

out its function, which could be that of an adhesin, toxin or an enzyme such as a protease, a peptidase, a lipase or an esterase.

Once exported to the outer membrane surface the active passengers may be cleaved and released into the extracellular media or, as proposed in the BrKA autotransporter system remain anchored to the membrane surface possibly through the linker region of the C-terminal domain.

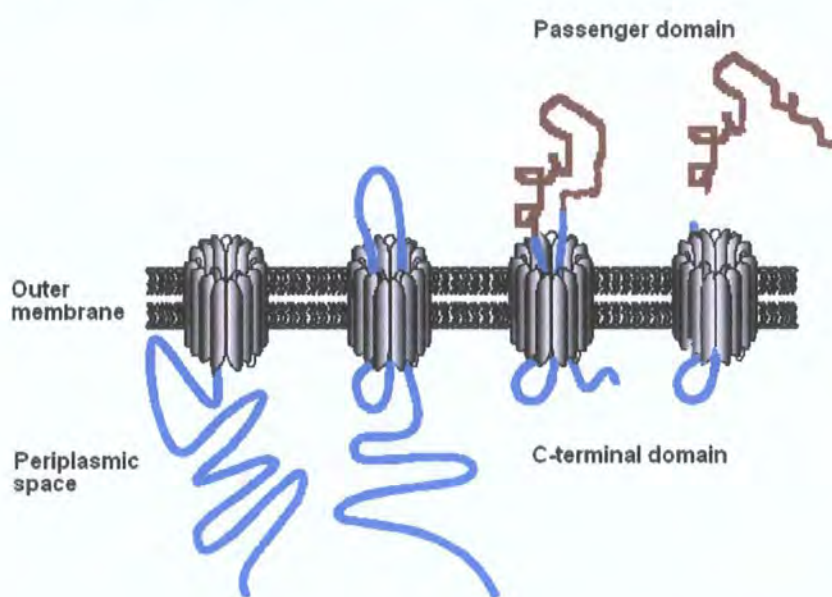


Figure III.2.2. Diagram showing insertion of outer membrane protein C-terminal domain into outer membrane.<sup>79</sup>

The dimensions of an autotransporter channel have been investigated using a polyhistidine tagged version of the C-terminal domain of the IgA protease from *Neisseria gonorrhoeae*.<sup>12</sup> Electron microscopy carried out on the negatively stained samples showed evidence of pore like structures with an inner diameter of about 2 nm and an outer diameter of about 9 nm. These channels would then be at least two and a half to five times smaller than those of other protein translocation systems and clearly indicate that large or bulky folded proteins would be very unlikely to fit through a channel of this size. This suggests that a passenger domain would have to adopt a non folded competent conformation appropriate for translocation through the channel and would then be subsequently refolded on the outer membrane surface.

As the unfolded passenger domain emerges from the outer membrane up to the bacterial surface, it begins to fold in a directional process from the C terminus to the N-terminus while using the junction region as a scaffold.

The refolding process which leads to the active conformation is thought to be carried out with the help of an intramolecular chaperone contained within the polypeptide sequence itself adjacent to the beta domain.<sup>80</sup> The barrel conformation of the channel affords a sufficiently stable structure to resist degradation and thus to remain in the outer membrane after translocation; this could lead to an accumulation of pores in the outer membrane and eventually to cell death.

### **III.2.2. The outer membrane C-terminal domain of BrKA.**

Analytical and structural studies often require a large amount of pure protein, which can simply not be obtained by isolation of naturally expressed protein alone; substantial quantities of functionally expressed channel forming or outer membrane recombinant protein in the membrane would be very toxic to the cell itself and result in cell lysis.

Consequently other methods such as overexpression of protein as inclusion bodies in the cytoplasm are often the only solution for producing the high yields required.<sup>81</sup>

Outer membrane proteins (OMP) when overexpressed without an N-terminal signal sequence are predominately produced in the form of inclusion bodies (Fig. III.2.3), since it is the signal sequence that directs the protein through the inner membrane into the periplasmic space, where the native protein can then fold and insert into the outer membrane following cleavage of the signal sequence.

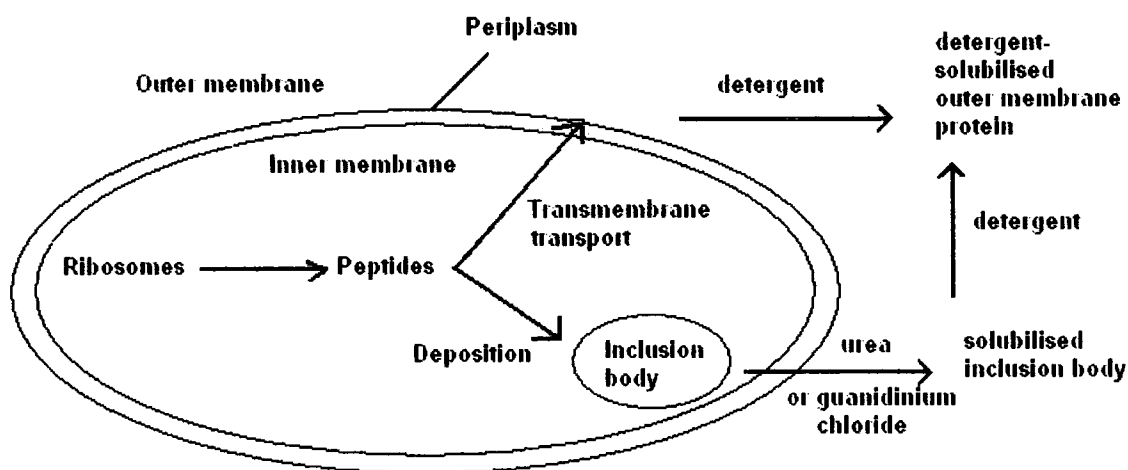


Figure III.2.3. Expression of prokaryotic outer membrane proteins.<sup>81</sup>

### III.2.2.1. The BrKA C-terminal protein.

A construct of the C-terminal domain of BrKA in a pET (11 a) expression vector (driven by a T7-promoter system) was kindly donated to us by Dr Blackburn from Glasgow University.

The DNA was sequenced by the Biological and Biomedical departmental DNA sequencing service at the University of Durham and a similarity search was carried out through the electronic-mail server BLAST (at the NCBI). The sequence was found to be an exact match for the C-terminal domain of BrKA which represents amino acids 715 to 1011 of the protein.<sup>82</sup> A database search, carried out for homologs of BrKA using BLAST, revealed that the closest match was the *Bordetella* outer membrane protein pertactin, which is a hundred amino acids shorter than the BrKA protein.

The two proteins showed a 54.4 % match over their last 300 amino acids with the best fit situated in the C-terminal region, where the proteins were found to share a C terminal outer membrane motif.<sup>82</sup>

The most common method for overexpression of recombinant proteins into inclusion bodies is using the phage T7-promoter system and the *E. coli* BL21 (DE3) strain as the expression host. This strain contains a source of T7 RNA polymerase under control of the *lac* promoter. Gene expression can then be induced by addition of IPTG which enables the polymerase to transcribe the target gene in the expression vector.<sup>83,84</sup> In addition, genes that confer antibiotic resistance are built into the vector. They encode enzymes or transmembrane pumps to degrade or remove antibiotics and consequently when antibiotics are incorporated into the growth media only the target cells that contain the plasmid vector encoding antibiotic resistance will grow. The cultivation temperature was typically set at 37 °C for an optimum expression yield and the growth media selected was generally a standard Luria broth (LB) media.

Following protein expression, the cultures were passed through a French press cell to rupture the cells, before they were harvested by centrifugation. The resulting protein pellet was dissolved in a 6 M urea-phosphate buffer (pH 8), as high concentrations of urea are strongly denaturing and therefore allow the protein to be isolated from inclusion bodies and completely solubilised.

The disadvantage of using strong denaturing conditions is mainly due to incompatibility of the solutions with any subsequent refolding processes.<sup>14,85</sup>

The BrKA  $\beta$ -domain was found to express very poorly or not at all on a large scale and in order to obtain a good yield, cultures had to be grown in 10 ml bottles. A possible explanation for this behaviour is that the protein expresses better when exposed to the reduced volume of oxygen contained in the 10 ml bottles as opposed to the more extensive oxygenation afforded by the larger 250 ml or 500 ml flasks.

An SDS-Polyacrylamide gel was used to estimate the amount of target protein in the different fractions and expression controls.

SDS-Page (Sodium dodecyl sulfate-Polyacrylamide electrophoresis gel) is an extremely useful and straight forward method of separating proteins according to their size.

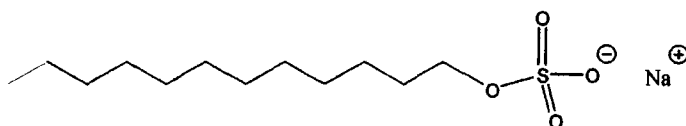


*Figure III.2.4. Structure of Sodium dodecyl sulfate (SDS).*

The protein is first reduced and denatured by incubation at 100 °C with  $\beta$ -mercapto ethanol and sodium dodecyl sulfate, SDS (Fig.III.2.4) and is then injected along with a range of molecular weight markers (SDS7) into the wells in the gel. On application of an electric current, the proteins migrate down the gel at a rate, which is dependant on molecular size.



The resulting protein bands are then stained to reveal their position in the gel, before being compared to the standard protein markers of known molecular weights (Fig. III.2.5).

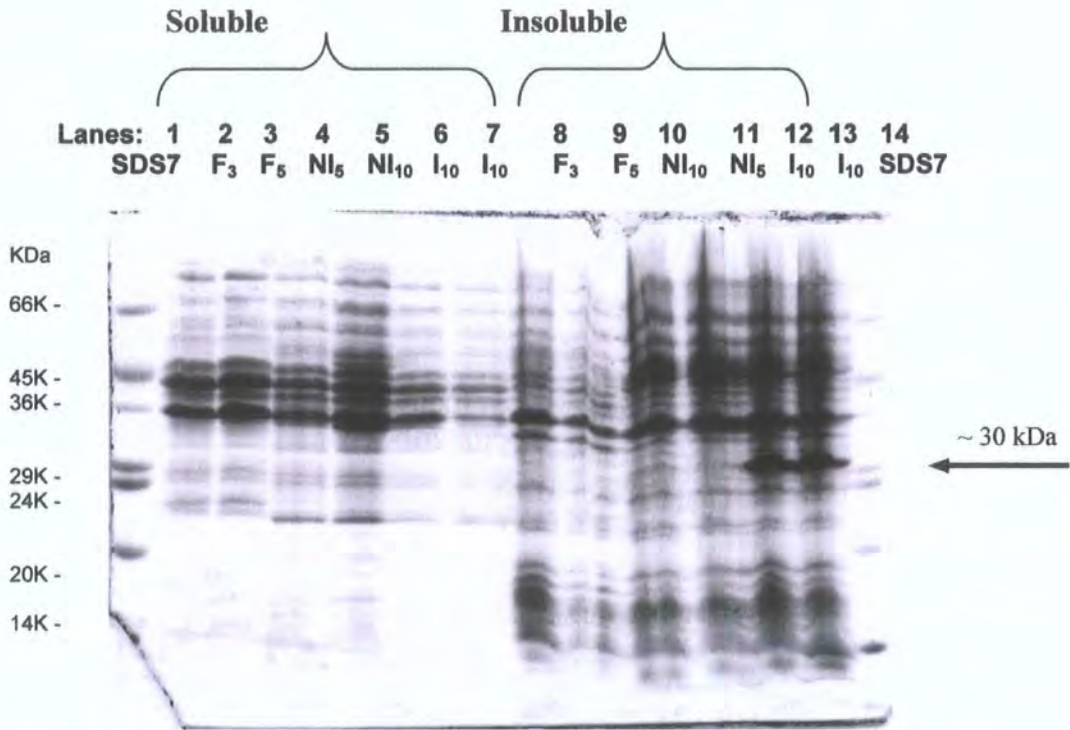


*Figure III.2.5. SDS-page showing the change in protein production following a range of different expression conditions: F<sub>3</sub>: induced / 300 ml culture; F<sub>5</sub>: induced / 50 ml culture; NI<sub>5</sub> non induced / 50 ml culture; NI<sub>10</sub> non induced / 10 ml culture; I<sub>10</sub> induced / 10 ml culture.*

After determining the best expression conditions for the protein, the next step was to select an efficient purification method.

Using a protein calculator program, the BrKA  $\beta$ -domain protein was predicted to have a high content of hydrophilic sites and a high isoelectric point of 9.8.<sup>86</sup> This result suggested that an ion exchange column with negative packing: (Sulphopropyl(s) sepharose fast flow column) could be used for the protein purification.

The protein-urea solution was centrifuged and the supernatant loaded on to the column. The protein was then eluted from the column with a linear gradient of 500 mM sodium chloride in a phosphate-urea buffer against the same buffer but without NaCl. The eluate was analysed by SDS-15 % Polyacrylamide gel electrophoresis along with a sample from the flowthrough (FT) and the pellet, remaining after urea extraction, in order to establish if any protein had remained in these fractions. The gel indicated that although the pellet still contained a high proportion of the target protein, a weak band at around 30 kDa did show, that extracted protein had eluted from the column, with a high degree of purity.

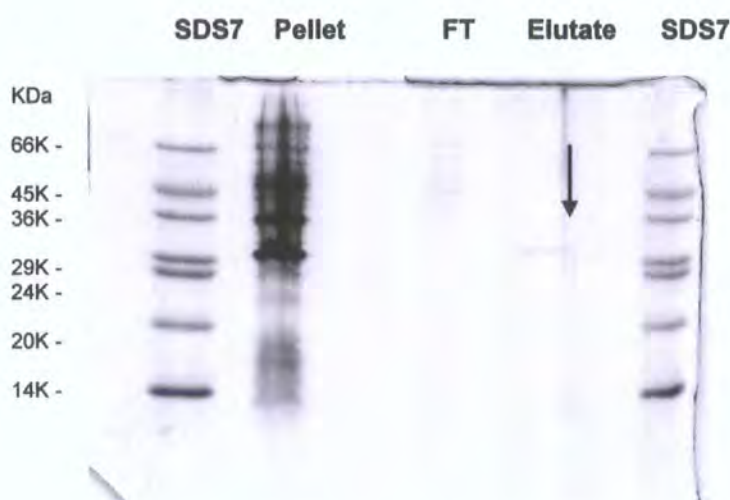


*Figure III.2.6. SDS Page showing the concentration of protein present in the different fractions: pellet, flow through (FT) and eluted pure protein.*

The solubility of the protein was tested in a range of solutions and it was found to be only mildly soluble in all of the solutions tried including 6 M Guanidine HCl and a range of detergents including n-octyl- $\beta$ -D-glucopyranoside, OG and n-decyl- $\beta$ -D-maltopyranoside, DM in Tris-HCl buffer.

The typical concentration of protein expressed and purified for this system was estimated by SDS-page at around 10  $\mu$ g for 200  $\mu$ l of eluted pure protein solution (acetone precipitated and dissolved in 1 x sample buffer) by comparison with the standard SDS7 marker band, which contains approximately 3.3  $\mu$ g per band in a 10  $\mu$ l loading.



This lead to an estimation of only 0.05 mg ml<sup>-1</sup> eluted from the ion exchange column, for the protein expressed in 100 ml of culture media (Fig. III.2.7) and which would decrease even further after refolding the denatured protein

The typical quantities of pure renatured protein, considered sufficient for growing 2D crystalline arrays, are estimated at about 1 to 2 mg ml<sup>-1</sup> which leads to the problem of increasing significantly the yield of expressed protein.

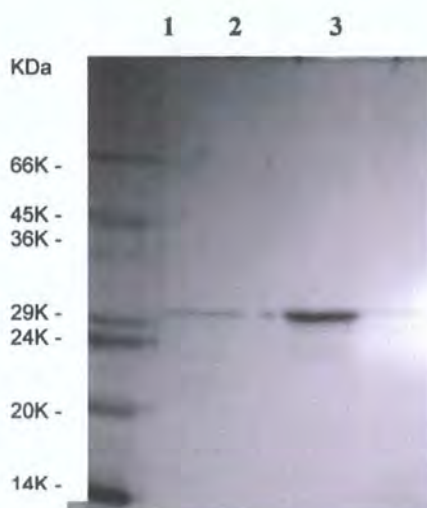


*Figure III.2.7. SDS Page showing the reference markers SDS7(1) and the pure fractions of eluted protein (2 and 3).*

#### **III.2.2.2. Generation of a His-tagged BrKA C-terminal protein.**

As the most common strategy for increasing the yield of pure and subsequently refolded protein is by addition of an affinity tag to the protein sequence, a gene construct was generated to encode for a functional polyhistidine tagged version of the BrKA C-terminal protein. The target DNA was ligated in to an appropriate vector pET-19b (Fig. III.2.8). This vector contains a sequence encoding for a 10 histidine tag as well as a short 10 amino acid sequence up-stream (N-terminal) from the target protein insertion site, which lead to an increase in molecular weight of the BrKA C-terminal protein to around 33 kDa. After transformation into *E. coli* BL21 (DE3) cells, the constructs were grown overnight at 37 °C on a LB agar plate containing ampicillin antibiotic, from which singles colonies were

lifted and inoculated into LB culture media with antibiotic. The cells were grown until it was assumed that a high cell density had been reached.

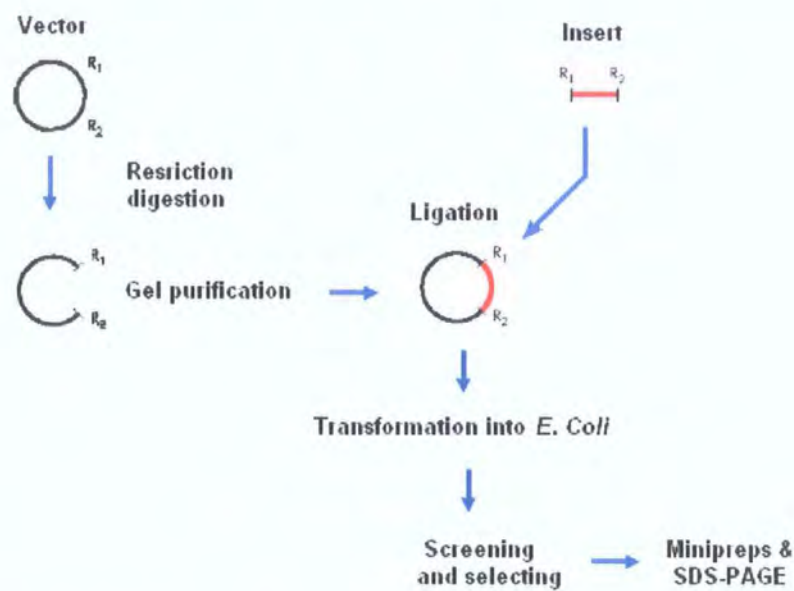


Figure III.2.8. Diagram outlining the steps in a generic ligation process.

The best protein expression conditions were selected by carrying out a series of control tests with a range of culture volumes and temperatures (Fig. III.2.9), as well as performing trials for induced and non induced protein expression.

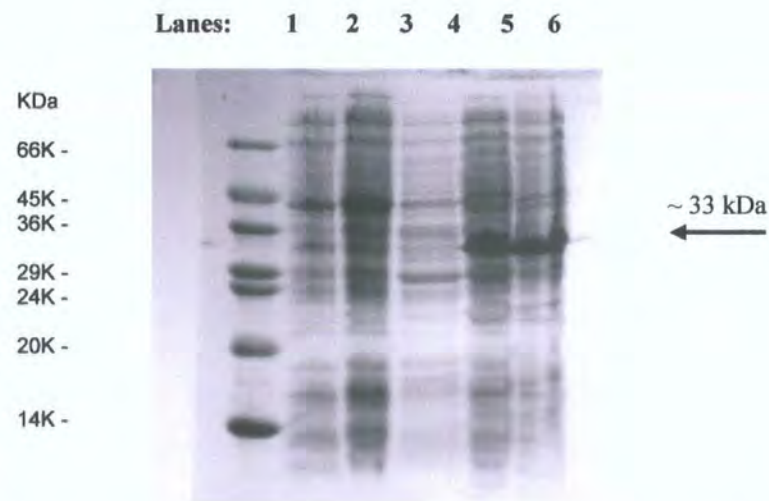
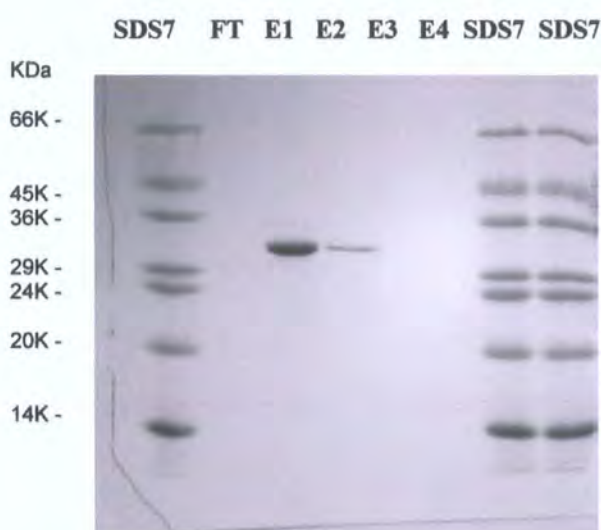


Figure III.2.9. SDS-page showing total cell protein expression levels at different temperatures: 1. SDS 7, 2. 20 °C; 3. 25 °C; 4. 30 °C; 5. and 6. 37 °C.



SDS-page revealed that expression of the His-tagged version of the BrKA  $\beta$ -domain was just as difficult to scale up as the non His-tagged protein and that over the range of temperatures tested, the protein expressed better at the highest temperature tested of 37 °C. The protein also appeared to express equally well in the non induced cultures which is a phenomenon that has been observed in some systems and could be due to mutation around the T7 promoter location in the host vector following ligation.

After harvesting and preparing the cells in a similar process to that described for the non His-tagged BrKA C-terminal domain, the expressed protein was resuspended in a phosphate (50 mM)-urea (8 M) and sodium chloride (0.5 M) buffer (pH 7.8) and purified on a nickel affinity ( $\text{Ni}^{2+}$ -NTA) column. The eluate was then analysed by SDS-page (Fig. III.2.10), which clearly showed that the target protein (~33 kDa) had bound efficiently to the column and had eluted with a high degree of purity.



*Figure III.2.10. SDS-page showing the high level of purity of the eluted protein fraction: E1 – E4: Eluted fractions; FT: flowthrough.*

The eluted fractions of pure protein were pooled and their concentration estimated at around 0.5 mg ml<sup>-1</sup>, giving at least a 5 fold increase in yield when compared to the non His-tagged version of the BrKA C-terminal protein.

**III.2.2.3. Protein folding.**

The protein was renatured following the method used by Shannon and Fernandez and other groups for refolding membrane proteins, after extraction from inclusion bodies.<sup>22,75,87,101,88</sup> Shannon and Fernandez showed that the BrKA C-terminal domain protein renatured following their procedure had the capacity to form channels in membranes as assessed by black lipid bilayer experiments.<sup>75</sup> The pure eluted protein fractions were pooled and then dialysed against a phosphate-sodium chloride buffer (PSB) to slowly remove the urea at a rate of 0.2 % dilution min<sup>-1</sup> whilst maintaining the temperature at 4 °C. Once all the urea had been eliminated from the system the protein was again slowly dialysed with a Tris-salt buffer (pH 7.4) with 0.1 % of the non ionic polyoxyethylene detergent, Triton x-100 to help keep the protein in solution and to prevent aggregation. The protein solution was then centrifuged (10 mins at 17000 x g) and both the resulting supernatant and the pellet were analysed by SDS-page (Fig.III.2.11). In order to concentrate and increase the sample visibility in the gel, a 300 µl aliquot of the supernatant was acetone precipitated and resuspended in 20 µl of 1 x SDS sample buffer before being loaded on to the gel.

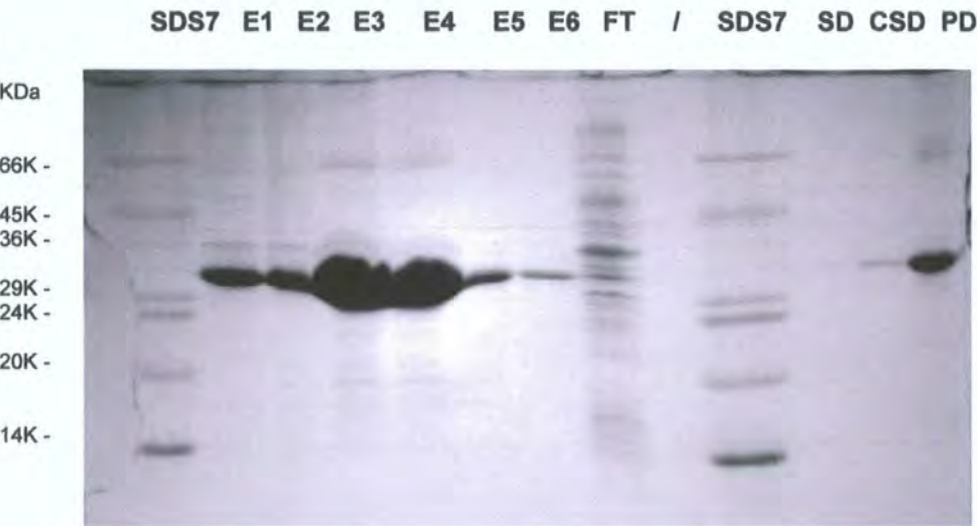


*Figure III.2.11. SDS-page showing the pure (denatured) fractions, from E1 to E6 and the flowthrough, FT from the BrKA C-terminal protein after elution from a Ni<sup>2+</sup> affinity column and again following dialysis to remove urea with the supernatant (SD); concentrated supernatant (CSD) and pellet (PD).*



The concentration of the soluble fraction of the protein (supernatant), which was considered to have adopted a native conformation, was estimated at less than 20 % of the total protein content, revealing that the large majority of the protein had remained in the insoluble and denatured form. The same dialysis method was used but with other detergents such as n-octyl- $\beta$ -D-glucopyranoside, OG and n-decyl- $\beta$ -D-maltopyranoside, DM with concentrations above the CMC of each detergent but these were no more successful than Triton X-100.

#### III.2.2.4. Concentration determination.

In order to carry out structural studies on the protein, a more accurate concentration for the BrKA C-terminal domain was determined by using the Beer Lambert law:

$$\text{Molar Concentration} = \text{Abs}_{280\text{nm}} / \epsilon_{280\text{ nm}} * \text{dilution factor (i)}$$

UV titrations were carried out to measure the protein absorbance in the aromatic region of the spectrum; the extinction coefficient ( $\epsilon_{280\text{ nm}}$ ) for the protein, 69840  $\text{M}^{-1} \text{ cm}^{-1}$ , was calculated by taking in to consideration the spectral contributions at 280 nm of all the tyrosine, tryptophan and cysteine residues in the protein sequence.<sup>89</sup>

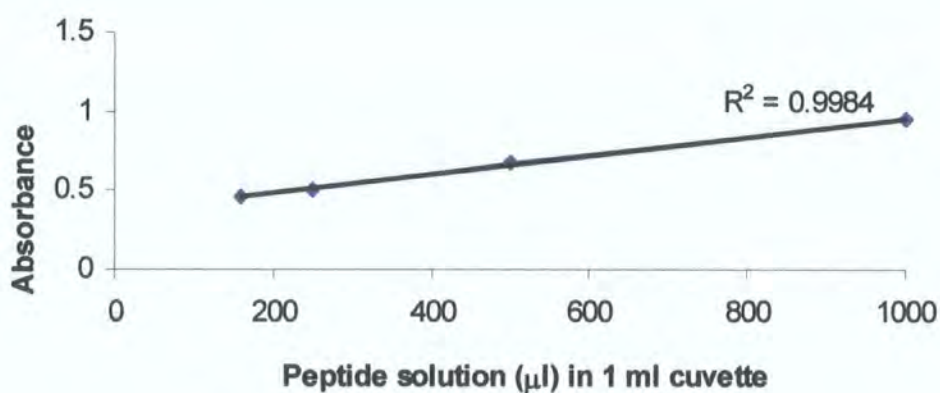


*Figure III.2.12. Plot of protein absorbance against change in concentration (dilution) of the protein.*

### III.2.2.5. Structural analysis.

The secondary structure of the purified and dialysed BrKA C-terminal protein, in a Tris- detergent buffer, was investigated by circular dichroism, CD in an attempt to establish whether the protein had efficiently refolded to its active conformation and had not misfolded to a partially native state after the renaturation (Fig. III.2.13).

The native conformation for an autotransporter is thought to be very similar to that of an outer membrane protein, OMP which adopts multistranded  $\beta$ -barrel structures in the membrane.<sup>79</sup>

Therefore a spectrum with a high  $\beta$ -sheet content would be a very favourable indication that the BrKA C-terminal protein had successfully refolded.<sup>79</sup>

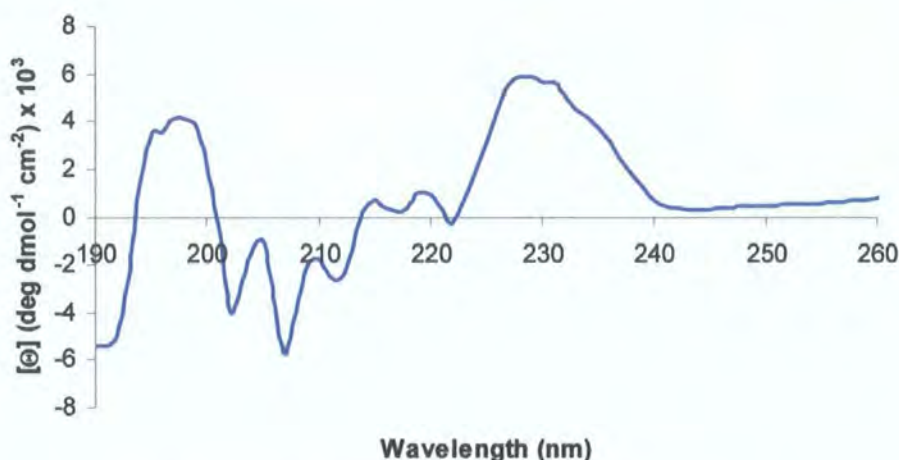


*Figure III.2.13. CD spectrum of purified and dialysed BrKA C-terminal protein (0.1 mg ml<sup>-1</sup>) was measured in 0.1 % Triton X-100–10 mM Tris at pH 8.0.*

*A minimum of 6 spectra were accumulated and contributions from the detergent-buffer solution were subtracted.*

The CD spectrum was analysed using the CDsstr program (at <http://www.alpha.als.orst.edu>) originally developed by Hennessey and Jonhson in 1981 and which has since been considerably optimised.<sup>90,91</sup> This program uses a singular value decomposition, SVD algorithm to analyse the CD spectra of a series of proteins whose structures have been accurately determined by X-ray crystallography.



The spectra are deconvoluted into orthogonal basis curves which are correlated to known combinations of  $\alpha$ -helix, antiparallel and parallel  $\beta$ -sheets,  $\beta$ -turns and random coil conformations. The extracted curves are then used as reference standards against which unknown protein spectra are compared and then assigned to certain structural conformations with determination of the percentage for each different type.<sup>92</sup>

The conformation of the dialysed BrKA C-terminal protein in detergent-Tris buffer could not be assigned unambiguously to any particular type of structure and consequently the  $\beta$ -sheet content of the protein could not be evaluated.<sup>93</sup>

Extraction of protein from inclusion bodies involves complete denaturation with reagents like urea, guanidine or detergents and therefore efficient refolding methods are required that may need optimising for each protein. Some membrane proteins will only refold correctly from urea and not from guanidine which is used at a higher ionic strength and could inhibit specific interactions necessary for protein folding. The spontaneous refolding *in vitro* of the denatured archaeobacterial protein, Bacteriorhodopsin, as well as the *E. coli* outer membrane proteins, OmpA, OmpF and OMPLA, has demonstrated that this can be carried out successfully.<sup>94,95,96</sup>

Membrane proteins adopt their stable native conformations on interaction with appropriate lipid bilayers therefore it seems reasonable to assume that a better understanding of the interactions and the properties of lipids with proteins could be used to develop a more efficient or tailored method of protein folding as well as to an increase in structural stability.<sup>97,98</sup>

The folding process of proteins solubilised in detergent, is thought to go through an intermediate state, before the proteins undergo structural rearrangement to adopt a stable fully functional conformation, on interaction with a lipid bilayer.

Mixed lipid-detergent systems can provide the appropriate conditions for correct folding, as the protein structure is more stable in a membrane than in detergent alone on account of the specific protein-lipid interactions that stabilise the protein structure.

The detergent will facilitate protein insertion into the membrane by reducing the curvature or the elastic energy of the lipid bilayer and therefore fine tuning of the protein tertiary structure will depend on selecting the best detergent-lipid

combinations to allow the protein to rearrange, extend and pack into a fully functional conformation.<sup>31</sup>

#### **III.2.2.6. Optimisation of folding process.**

The folding method used for BrKA C-terminal protein was modified to include a mixed lipid-detergent system with addition to the folding solution of the fully saturated DMPC phospholipid, dimyristoyl phosphatidyl choline, in a 5:1 molar ratio of lipid to protein and a 0.1 % (v/v) of polyoxyethylene detergent, Triton X-100.

In order to assess the affect of both the lipid and the detergent on the folding process, the denatured protein was incubated with a solution containing either lipid or detergent or both lipid and detergent. The mixed protein, lipid and detergent solutions were then dialysed against a phosphate-salt buffer (PSB) with 0.1 % (v/v) Triton X-100 at 4 °C and then again with a Tris-salt buffer containing 0.1 % (v/v) Triton X-100 detergent. Following dialysis the protein solutions were centrifuged (20 min at 19000 x g) and an aliquot (300 µl) of the supernatant from each of the folding solutions was acetone precipitated and analysed (Fig. III.2.14) by SDS page.

The protein was visibly more soluble, when both lipid and detergent were used in the folding solution.

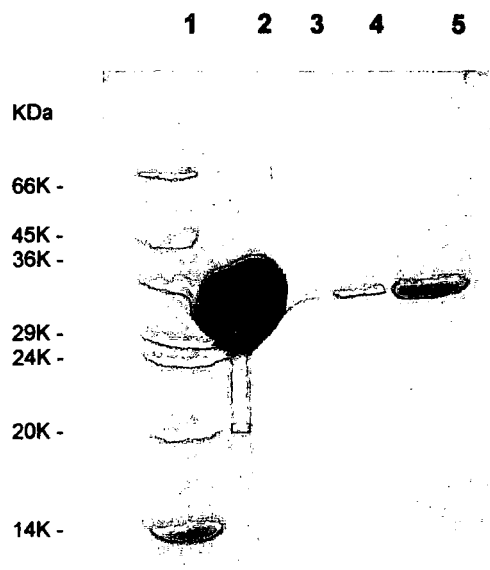


*Figure III.2.14. SDS-page of the folding solutions: 1. SDS 7 protein standard; 2. mixed protein-lipid-detergent; 3. protein only; 4. protein-lipid and 5. protein-detergent.*

### **III.2.2.7. Structural analysis after optimisation of folding conditions.**

The secondary structure of the renatured BrKA C-terminal protein was again investigated by circular dichroism, CD in order to analyse the  $\beta$ -sheet content of the protein and to determine as far as possible if the protein had successfully refolded.

The CD spectrum revealed a classical antiparallel  $\beta$ -sheet structure with typical maximum at 200 nm and minimum at 215 nm as well as a second minimum at about 230 nm which has been proposed to be strongly indicative of absorbance due to specific interactions or arrangement of the tryptophan residues within the  $\beta$ -sheet structure.<sup>99,100,96</sup>

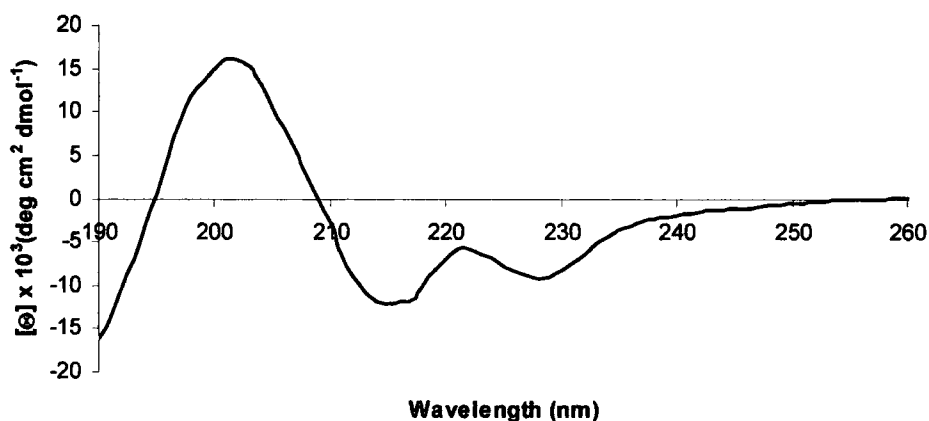


*Figure III.2.15. CD spectrum of refolded BrKA C-terminal protein (0.1 mg ml<sup>-1</sup>) measured in a 0.1 % Triton X-100–10 mM Tris at pH 7.4. A minimum of 6 spectra were accumulated and contribution from the detergent-buffer solution was subtracted.*

The structural components derived from this spectrum were analysed using the CDsstr program which showed the protein to contain 44 %  $\beta$ -sheet and 15 % turns. This is compatible with a  $\beta$ -barrel system with more than 15 strands of  $\beta$ -sheet and may also be taken as confirmation that the protein is very likely to have adopted its fully functional native conformation.<sup>12,101</sup>

Other folding methods were considered in an attempt to eliminate urea from the system altogether, by extracting the protein from inclusion bodies with high concentrations of a zwitterionic detergent, zwittergent 3-14, which is used to solubilise membrane proteins, but this procedure proved to be only mildly successful as most of the protein remained insoluble.

### **III.2.3.1. Two-dimensional (2D) trials of BrKA C-terminal domain.**

Following the development of a promising folding method, the protein was used in a range of two-dimensional (2D) crystal trials, in an attempt to obtain structural information on the BrKA C-terminal domain.

A wide range of conditions had to be established and optimised before the crystallisation process could be carried out. These included the choice of method, the lipids and detergents, the lipid-protein ratio, the temperature and the duration of the process as well as any buffers and additives required.

Dialysis was selected as the method of choice in the present study, as it is the most common and straight forward process and has been used successfully in a number of 2D crystallisations.<sup>7</sup> Two phospholipids, the fully saturated DMPC and the monounsaturated DOPC lipids were either used separately or in a 1:1 ratio (w/w) with two different lipid-protein ratios of either 1:1 or 1:2 (w/w).

A mixture of detergents, one with a high CMC, octyl- $\beta$ -D-glucopyranoside, OG and another with a low CMC, n-decyl- $\beta$ -D-maltopyranoside, DM were considered to offer the best probability of success, as they had worked well in 2D crystal trials of outer membrane proteins.<sup>102,103</sup>

The temperature profile, the duration of the trials, as well as the buffer systems were developed after considering a range of similar processes in the literature.<sup>19,104</sup>

### **III.2.3.2. Preparation and imaging.**

Protein and lipid solutions, premixed with the detergents, Triton X-100 and OG were incubated at 4 °C for up to an hour, to allow for equilibration of the system. The crystallisation solution was then typically dialysed in a 10 mM Tris-0.1 % (v/v) Triton X-100 buffer in presence of both monovalent, Na<sup>+</sup> and divalent, Mg<sup>2+</sup> cations, at 4 °C. The detergent was slowly removed by pumping (peristaltic pump) a detergent free Tris-salt buffer into the dialysis flask, before submitting the dialysis solution to several further buffer exchanges and to a temperature

profile, which included warming the solution to room temperature for a defined period (4-6 hours) and then heating to physiological temperatures (37 °C) from 48 hours to a week. A final dialysis was performed with salt free Tris buffer, before samples were removed for imaging by transmission electron microscopy or scanning electron microscopy. Sample preparation for EM analysis consisted of the sample solutions being either used directly or centrifuged and the supernatant spotted on to the carbon coated copper support grids. The dried sample was then negatively stained with a 1 to 2 % uranyl acetate solution.

### III.2.3.3. Lipid sheets.

Transmission electron microscopy, TEM images, of the first crystallisation trials, showed that the solutions contain large lipid sheets and vesicles packed with non ordered arrays (Fig. III.2.16). These structures were thought to be composed of either protein or of a mixture of protein and detergent molecules.

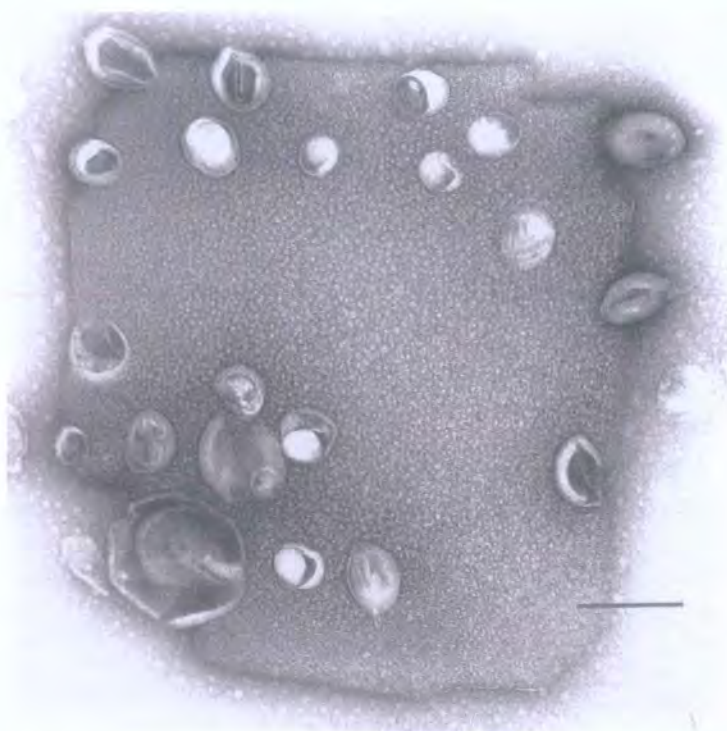


*Figure III.2.16. TEM image of a DMPC lipid sheet packed with protein arrays formed following dialysis of protein and lipid in a 1:1 ratio from a solution containing Triton X-100 and OG. (scale bar 0.1  $\mu$ m).*

The possibility that the arrays could be either uranyl acetate crystals or precipitates was also considered but thought unlikely as the stain does not normally precipitate under these conditions and this was further supported by tests carried out on the solution in the absence of sample in which no such depositions were observed.

In an attempt to induce the growth of crystalline protein arrays, the dialysis solution was incubated (at 38 °C for about 4 h) with phospholipase A<sub>2</sub>, which eliminate excess lipid by hydrolysing the lipid headgroups and therefore converts the phospholipids to lysophospholipids, which can then be removed by dialysis.<sup>23</sup> Analysis by electron microscopy unfortunately did not show any improvement in the crystallinity of the sample, following this treatment and by consequence a systematic modification of the dialysis conditions was under taken.

The detergent content of the sample was the first modification to be considered, with the addition of a mixture of OG and DM, at concentrations just above their respective CMC values (see appendix 1), to both the protein and the lipid solution. Samples were then dialysed using the method previously outlined and then imaged by TEM.



#### III.2.3.4. Striated domains.

A considerable proportion of the sample grid was covered with what can be described as “worm” like features that appeared to be in the process of arranging into large ordered areas (Fig. III.2.17). The structures themselves were measured using the software Image J, which gave a value of  $3.4 \pm 0.7$  nm for the width and  $3.4 \pm 0.6$  nm for the length.<sup>105</sup>



*Figure III.2.17. TEM image showing “worm” like features after varying the dialysis conditions.*

The effect of the detergent was assessed by carrying out the dialysis under the same conditions on lipid-detergent solutions without protein.



The sample was analysed by TEM, but no such structures were observed on any of the grids prepared, whereas the samples that contained the BrKA C-terminal protein all revealed “worm” like features and ordered areas or domains (Fig. III.2.18a).

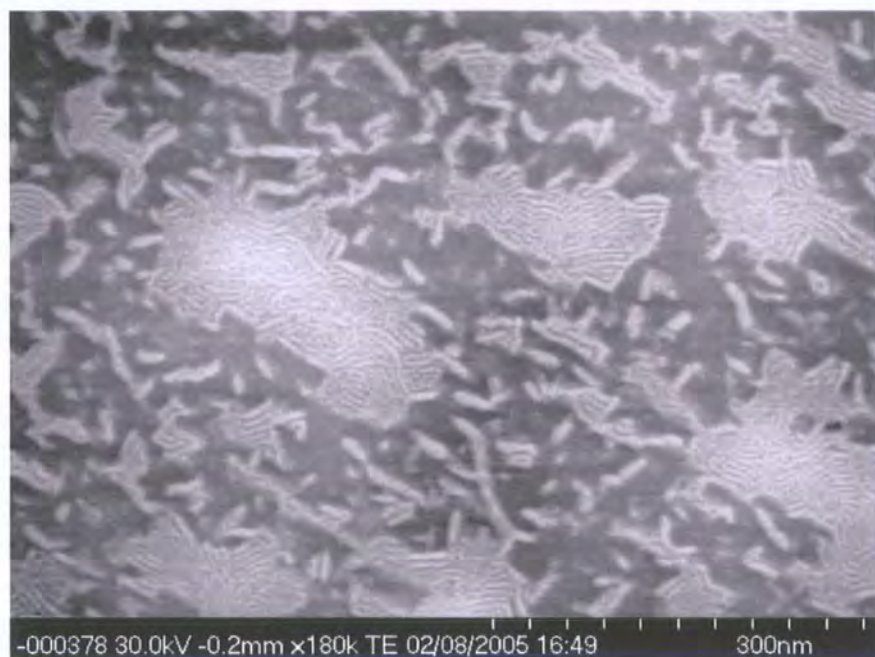


*Figure III.2.18a. TEM image of ordered striated areas following addition of a mixture of detergents, DM and OG to both the protein and DMPC before carrying out dialysis.*

Similar patterns of striated domains from about 10 to 100 nm in size have been observed by atomic force microscopy, AFM on phospholipids preparations with amphiphilic peptides at 1 to 5 mol % peptide.<sup>106,107</sup>

These ordered regions, which are described as consisting of low (dark) and high (light) lines have a regular repeat distance of  $6.8 \pm 0.5$  nm in the case of BrKA C-terminal protein and are produced at 2 mol % protein which is consistent with the concentrations used in the AFM studies on the striated domains formed with amphiphilic peptides.

Domains are well known in biological membranes; lipid bilayers that have been heated to above their transition temperature, as is the case in dialysis preparations, will on cooling order within different areas of the bilayer and within each area the acyl chains of the lipids will be tilted in a same direction, slightly different from that of the neighbouring areas. This leads to the creation of lipid areas defined by a difference in tilt orientation of the lipid acyl chains within each domain.

Proteins are also well known to affect the state of neighbouring lipids and may induce a change from gel phase to liquid crystalline phase in a lipid membrane. The striated pattern of the domains is thought to reflect the arrangement of the amphiphilic peptides in the lipid bilayer.<sup>106</sup> This idea could also be extended to the present study on the BrKA C-terminal protein, which would integrate into the lipid bilayer as it forms a  $\beta$ -barrel channel in the membrane. In addition, the BrKA C-terminal domain has a sequence composed of around 10 % aromatic residues, tyrosine and tryptophan; these are believed to locate preferentially at the interface between lipid headgroups and acyl chains and therefore keep the protein below the lipid surface.

The striated patterns are thought to arise when the protein forms oligomeric arrays within the lipid bilayer inducing, on one hand, a change in the surrounding lipids to a more fluid state, which produces the dark low lines or depressions and on the other hand, forcing the lipids from different domains (area of lipid with a different tilt or orientation) to pack in a more constrained gel state, thus giving the higher light or elevated lines (Fig. III.2.18b).

These striated patterns are therefore thought to arise from the general geometrical factors of both the lipids and the proteins as well as the properties of the bilayer itself.

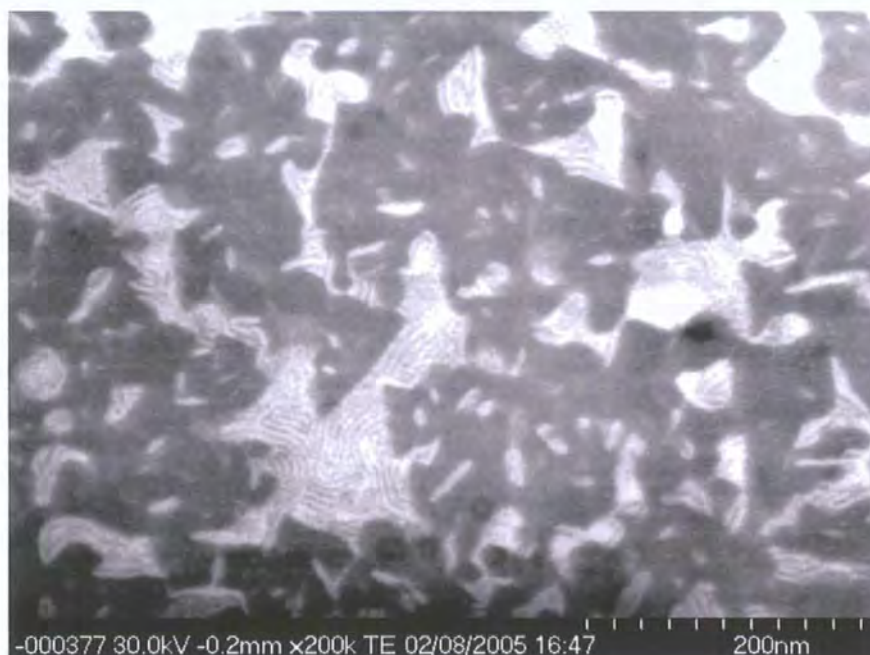


*Figure III.2.18b. TEM image of distinct patches of striated domains.*

These characteristic areas could reveal an intermediate state in the arrangement of the protein structures in the bilayer, but do not as yet show evidence of well ordered crystalline structures.

### **III.2.3.5. Stacks.**

The rate of detergent removal was the next key parameter to be considered in the 2D crystal trials of the BrKA C-terminal protein, as this was considered to strongly influence the morphology and the size of crystalline arrays. The dialysis rate was increased to twice the previous value and several further complete buffer exchanges were carried out, in order to ensure complete detergent removal. Electron microscopy images of the negatively stained samples showed the formation of planar disk like structures stacked in layers (Fig. III.2.19).



These disk structures were determined to have an average width of  $3.4 \pm 0.6$  nm and an average diameter of  $33 \pm 3.5$  nm per disk.



*Figure III.2.19. TEM images of stacked planar structures obtained after a two fold increase in the dialysis rate.*

The number of stacked structures varied considerably from as few as five or six to over a hundred all stacked in register (Fig. III.2.20) and therefore creating what appeared to be long screw like features on the TEM grid.

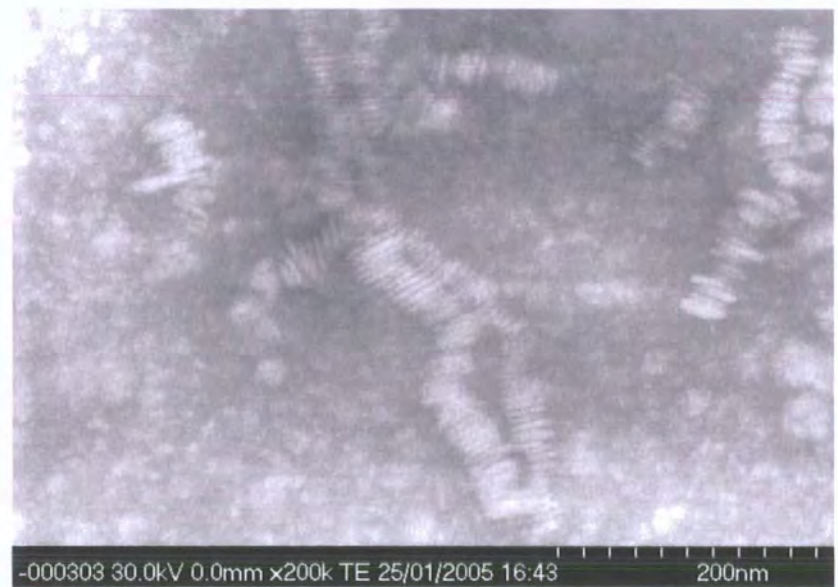


*Figure III.2. 20. TEM images showing the extensive stacking of disk like structures.*

The multilayer stacking of planar protein-lipid structures (Fig. III.2.21) is thought to occur as detergent is gradually removed from the dialysis system and appears to be sensitive to both the lipid to protein ratios as well as to the rate of detergent removal.<sup>108</sup>



*Figure III.2.21. TEM images of disk like structures stacked with different orientations.*

The stacking process is believed to involve interactions between the detergent molecules and the exposed hydrophilic headgroups of the protein molecules. As detergent molecules are eliminated from the protein-lipid-detergent micellar solution, a series of micelle-micelle interactions are induced, which results in the formation of the large disk like mixed micelles.

These structure will still contain detergent molecules, which locate towards the micellar edges and could induce the large micelles to merge into bilayers after further detergent removal.



The rate of detergent removal is a critical factor in the formation and the stacking of the disk like structures; at too rapid rate of detergent removal could impede the protein-lipid interactions, since the detergent molecules appear to be directly involved in the formation and packing of the protein molecules into these arrays.

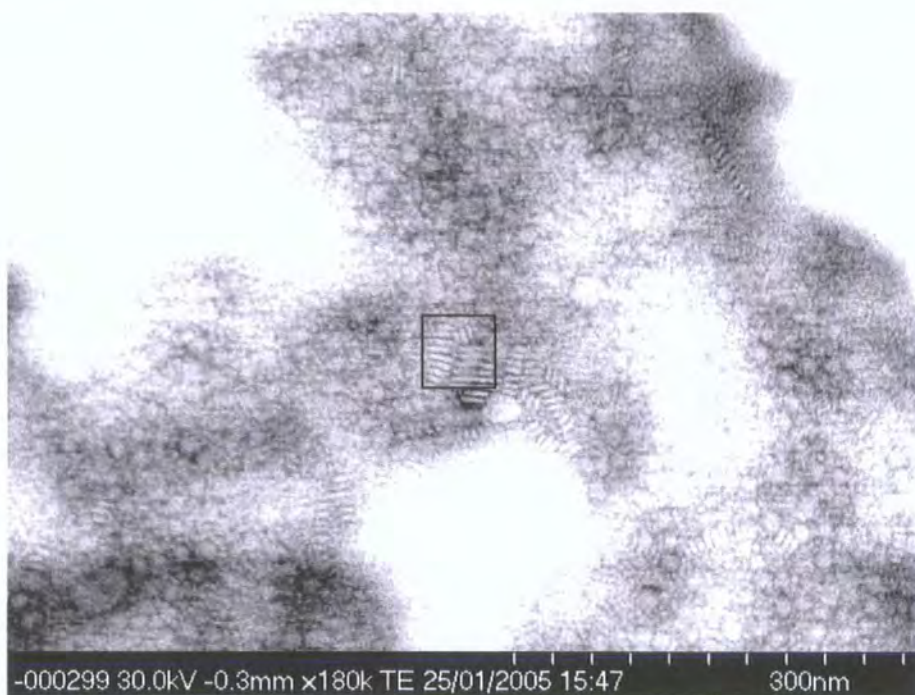


*Figure III.2.22. TEM images of non stacked disk like structures along side groups of stacked structures.*

#### **III.2.3.6. Fourier transform processing of digital images**

The boxed area in figure III.2.22 was processed to reveal any specific patterns in the protein-lipid structures. Inverse Fourier Transform performed on the filtered Fourier Transform image showed a high degree of ordering in the stacked structures (Fig. III.2.23).<sup>105</sup>

In order to determine the degree of ordering or the special frequency within the imaged structure, the digital image processing algorithm, Fourier Transform (FT) was used to transform the electron microscope images into frequency domains, which were then displayed as a power spectrum.

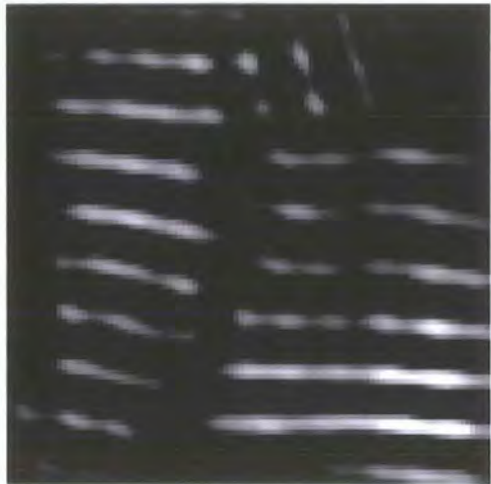


*Figure III.2.23. Inverse Fourier Transform of a filtered Fourier Transformed image of stacked structures*

Once the image has been transformed and described as a series of space frequencies, a range of filtering algorithms can be applied (to the power spectrum) to eliminate either noise or spatial frequency information, that may reveal specific well ordered patterns or periodicity within the image, hence within the sample structure itself. Retransformation is then performed to process the image back into the spacial domain. The processed image, depending on the type of filtering performed, would be a specifically enhanced version of the original image.



The digital processing as described above was applied to a number of EM images recorded on the protein-lipid samples and to specific areas within these images (Fig. III.2.24) that were considered to contain features of interest

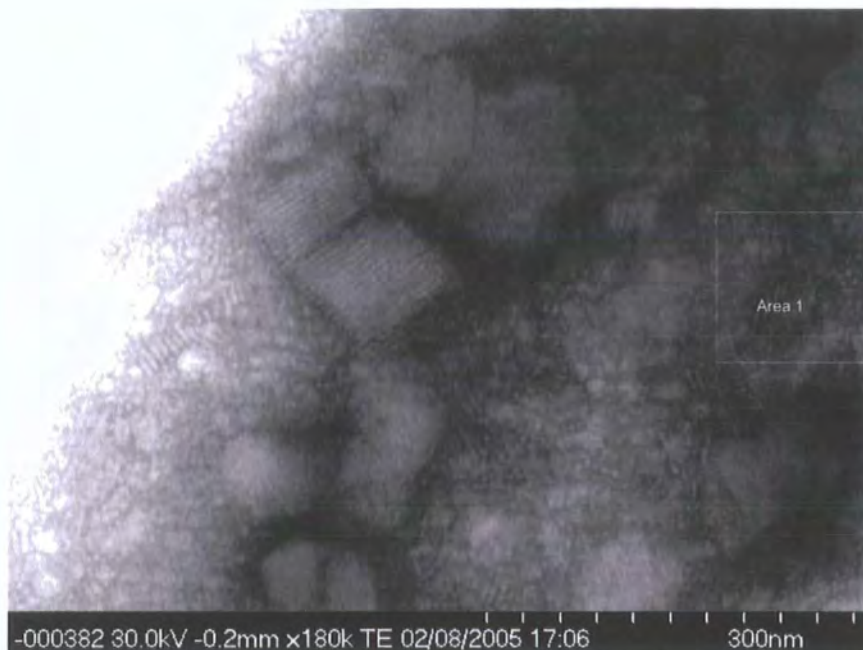


*Figure III.2. 24. Image of a large area of protein-lipid structures with a variety of clearly defined domains*

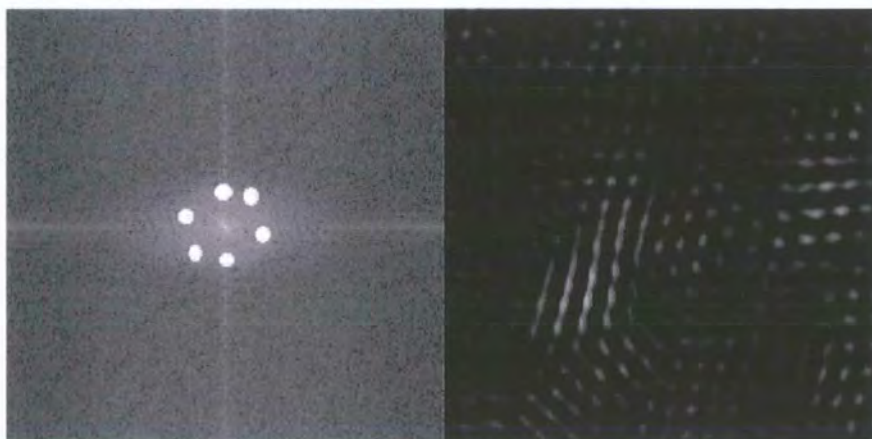


*Figure III.2.25. Power spectrum of the boxed area in figure III.2.24 showing the effect of filters and inverse Fourier Transform of filtered Fourier Transform image.*



The protein-lipid samples appeared to have adopted a variety of structures under the range of crystallisation conditions used with different degrees of ordering from well ordered striated domains to stacked disk like structures (Fig. III.2.25). Further optimisation of the 2D crystallisation process was considered and the rate of detergent removal was again increased. The rate of buffer exchange with detergent free buffer was increased to  $0.6\% \text{ min}^{-1}$ , while following the same temperature profile and dialysis duration as previously.

Examination by electron microscopy of the crystallisation solution (Fig. III.2.26), revealed that the disk like structures were still apparent and that although no stacking could be detected, the disks appeared to be involved in the formation of larger sheet like structure.

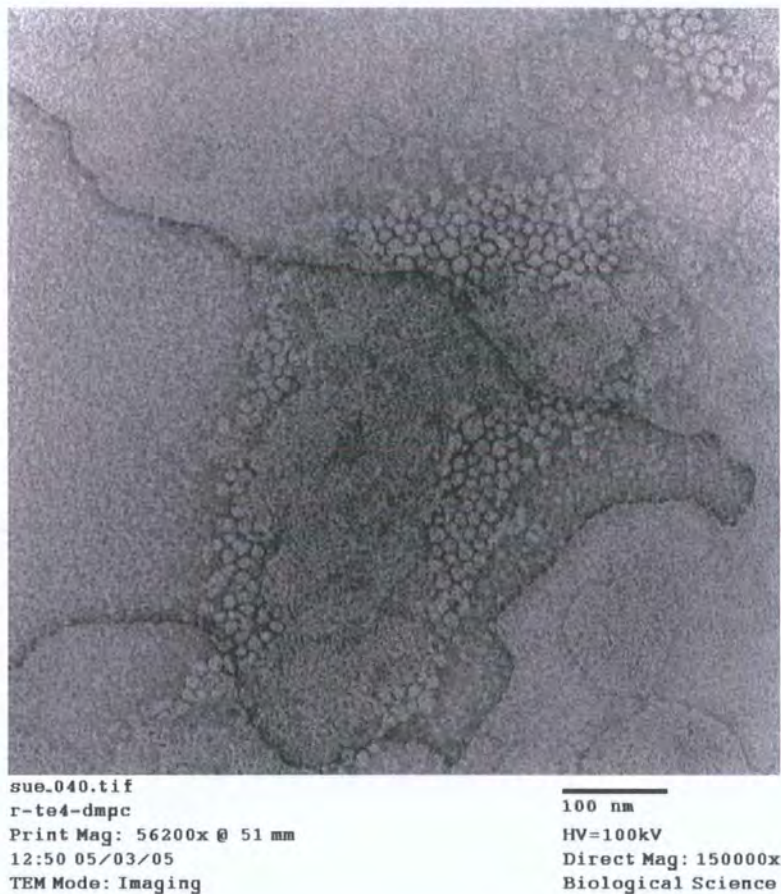


*Figure III.2.26. TEM images of non stacked disk structures merging into a sheet like layer following a further increase in the rate of dialysis.*

### III.2.3.7. Pore structures.

The lipid composition was changed to a 1:1 (w/w) mixed saturated and unsaturated phospholipid, DOPC-DMPC system with a range of lipid to protein ratios.<sup>108</sup> Electron microscope images of the dialysis solution with a 1:1 (w/w) lipid to protein ratio, revealed pore like structures that appeared at different focal planes on the sample grid (Fig.III.2.27).<sup>12</sup> The pore structures from several grids and different sample batches were analysed using the pre-calibrated particle analysing and measuring functions on the imaging software, Image J.<sup>108</sup>

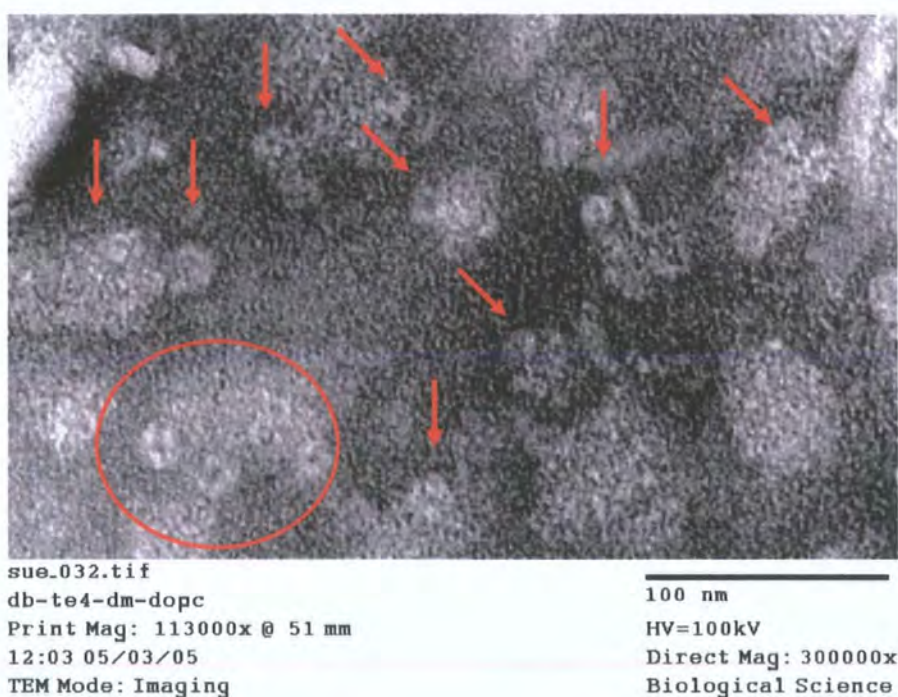


*Figure III.2.27. TEM image of pore like structures, which became apparent after a change to a mixed saturated and unsaturated phospholipid system. The arrows indicate pore structures visible on different focal planes and the circle pore structures, which are in focus*

The structures in the mixed phospholipid systems, all displayed a similar pore like appearance with an outer diameter of  $10.2 \pm 0.6$  nm and an inner diameter of  $3.1 \pm 0.5$  nm. These dimensions are in agreement with those of pores structures

imaged by electron microscopy for another His tagged autotransporter protein, C-IgAP from *Neisseria gonorrhoeae*, which was shown to form hydrophilic pores with an average outer diameter of about 9 nm and an inner diameter of about 2 nm. The pores formed were thought to be large enough to tolerate the passage of a range of secondary structural elements or small proteins in a partially folded state.<sup>85</sup> The CD spectrum of the protein C-IgAP from *Neisseria gonorrhoeae* indicated the presence of a 30 %  $\beta$ -sheet content, compatible with a 15 strand  $\beta$ -barrel structure similar to the core structure common to many integral outer membrane proteins of Gram-negative bacteria, which is thought to have been conserved throughout evolution<sup>109</sup>

The *E. Coli lactose permease* (with His tag) reconstructed in presence of phospholipids, showed trimeric particles with a similar sized diameter of  $10.4 \pm 2$  nm and porins of the trimeric membrane protein, PhoE were shown to be composed of 16 stranded monomers with short turns on the peri-side of the membrane and long loops on the cell surface.<sup>110</sup> The pore structures imaged for BrKA C-terminal protein therefore appear to be in good agreement with those of other autotransporter and integral outer membrane proteins.

#### **III.2.3.8. Extended regions of ordered protein-lipid arrays.**

The amount of detergent in the dialysis solution was reduced and dialysis time was increased to ensure the complete removal of detergent from the system, especially Triton X-100 and DM, which have low CMC values and are therefore more difficult to eliminate completely.

The initial concentration of Triton X-100 was decreased to half of its original value and the duration of the dialysis was extended by 4 to 5 days.



A simple technique, “the drop spreading method”, was employed to test for residual detergent in the sample solution and consisted of depositing a drop of protein crystallisation solution onto parafilm and estimating the degree of spreading of the drop by comparison with a drop of pure water of equal volume (Fig. III.2.28). Drops of sample solution, occupying the same surface diameter on the parafilm as a drop of pure water, and were therefore considered not to have spread, were estimated to be detergent free.



*Figure III.2.28. Diagram of “the drop spreading method” for detecting residual detergent.*

Detergent free samples with a 1:1 (w/w) protein to lipid ratio, analysed by Transmission electron microscopy (Fig. III.2.29), revealed that the dominant features present in these samples were of lipid sheets folded into several layers in places, with striated domains or arrays covering the entire sheet surface. Two sets of domains with different periodicities were apparent with one set running over and at a right angle to the other.

The periodicity in the first domain was determined at  $16.4 \pm 0.7$  nm and that of the second domain at  $6.6 \pm 0.5$  nm using the software image J.<sup>105</sup> The periodicity of the smaller domains was within the estimated size range for arrays of the BrKA C-terminal protein and provides strong evidence that the protein has adopted a regular arrangement in the membrane.

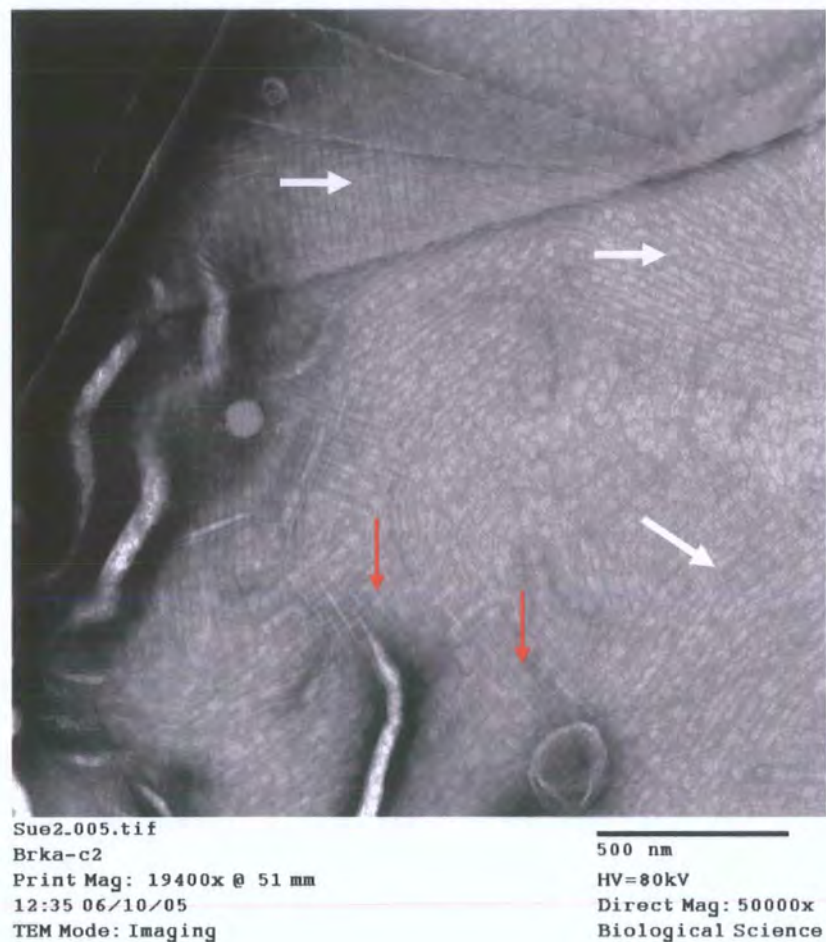


*Figure III.2.29. TEM image showing lipid sheets with different periodicities perpendicular to each other. Thick white arrows indicate the thicker domains and thin red arrows indicate the thinner domains.*

This TEM study puts forward a strong case for the formation of arrays of the BrKA C-terminal domain in saturated phospholipid bilayers (Fig. III.2.30), with closely packed structures that appear to have adopted a well ordered arrangement.



These results provide a encouraging indication, that arrays of the BrKA C-terminal domain of sufficient quality for structure determination by electron diffraction, could be grown under favourable crystallisation conditions.

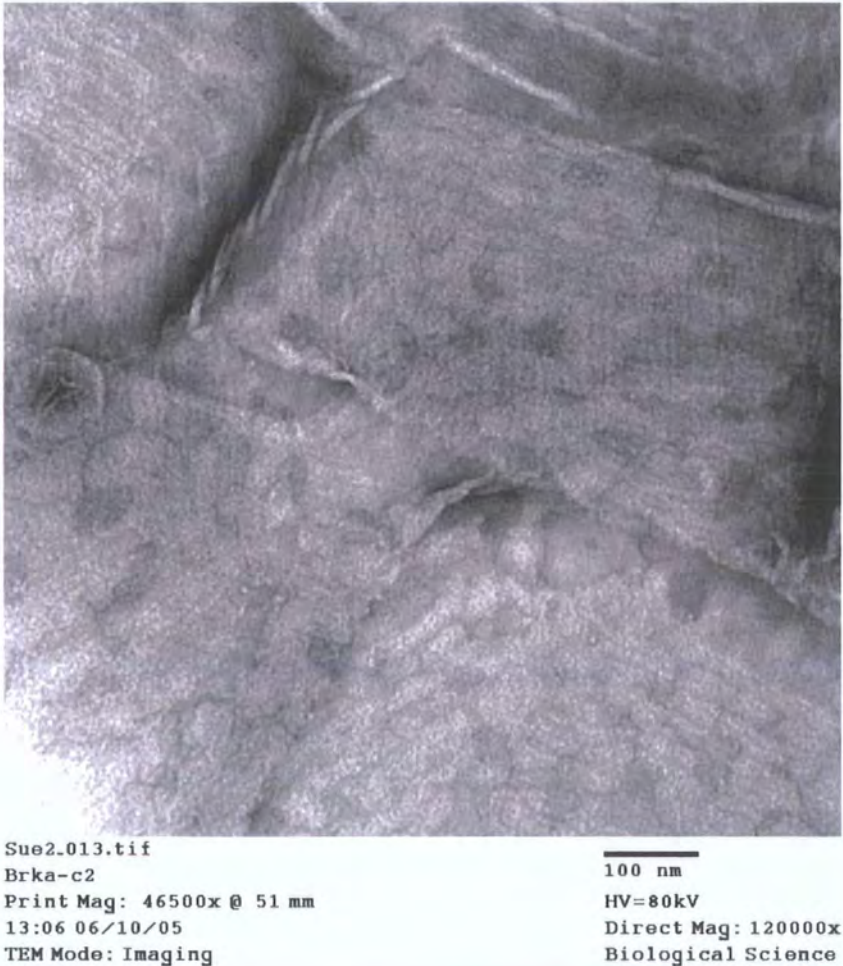


*Figure III.2.30. TEM image showing juxtaposed lipid sheets covered with arrays, which clearly show a high degree of ordering following an increase in the dialysis time and a decrease in the concentration of Triton X-100.*

### **III.2.3.9. Other systems for 2D crystal trials.**

2D crystal trials were carried out on the M protein from the respiratory syncytial virus using methods developed in the BrKA C-terminal protein trials

The respiratory syncytial virus is a member of the paramyxovirus family, which are negative-stranded, non-segmented RNA viruses. They initiate infection by attaching to cell surface receptors and allowing fusion of the viral membrane with the host cell membranes.

The virus resembles an enveloped particle whose membrane contains transmembrane proteins and a Matrix or M protein, which localises at the inner surface of the plasma membrane.<sup>111,112</sup> The M protein is thought to play a central role in viral assembly and budding, as well as being responsible for inhibition of the host gene expression.

### **III.2.4.1. The M protein.**

The fusion protein, M from the A2 strain of the respiratory syncytial virus, which had been inserted into a pET 16b vector, expressed in the *E. coli* BL21 strain and purified by Ni-affinity chromatography, was donated by Dr R. P. Yeo of the University of Durham, Biomedical and Biological sciences department.

The protein is of a similar size to the BrKA C-terminal protein with a sequence comprising of 281 residues and a molecular weight of 31.5 kDa.

### III.2.4.2. 2D crystallisation.

The M protein was dialysed with either DMPC or a 1:1 mixture of DMPC-DOPC in a Tris-NaCl buffer with both OG and DM detergents.<sup>113</sup>

Samples of the M protein crystallisation solution analysed by TEM, clearly showed the presence of well ordered areas of protein 2D arrays on large lipid sheets of several microns in size.



*Figure III.2.31. TEM image showing crystalline arrays of the M protein in sheets of the saturated lipid, DMPC*



Crystalline arrays of the M protein were produced, by reconstituted in presence of the saturated DMPC phospholipid, but not with mixed DMPC-DOPC systems (Fig. III.2.31). The M protein was obtained from a strain of the respiratory syncytial virus, which is active in the lung, where there is a predominance of saturated phospholipids. It is therefore not a surprising result that the M protein has demonstrated more affinity for the saturated phospholipid over the unsaturated phospholipid systems.

The arrays although crystalline were not of high enough quality for high resolution structure determination, but they clearly showed interaction of the M protein with the saturated phospholipid DMPC membrane (Fig. III.2.32) and have provided strong evidence of M protein binding with the lipid membrane.



*Figure III.2.32. TEM image showing a long vesicular structure packed with crystalline arrays of the M protein.*

EM analysis of the 2D crystallisation solution has also provided some evidence that the M protein could adopt ordered arrays with different morphologies, when produced from large lipid sheets or from small tubular lipid patches (Fig. III.2.33). The pattern of ordered protein arrays in each of the different crystal patches were shown to have the same periodicity of  $3.5 \pm 0.2$  nm, after analysis and reveals the extreme regularity of these structures.<sup>105</sup>



*Figure III.2.33. TEM image of larger lipid sheets again packed with clearly crystalline arrays of the M protein*

The crystallisation conditions were modified with respect to the initial detergent concentration, especially to that of Triton X-100 and to the dialysis time, but these modifications did not appear to increase the quality of the crystalline arrays. Further optimisation trials are therefore required in order to obtain highly ordered arrays for structure determination.

### **III.2.5. 2D trials on synthetic amphiphilic peptides.**

2D crystallisation trials were carried out on one of the synthetic amphiphilic peptides discussed in chapter II of this thesis, the 2K4Y03 peptide; sufficient quantities of this peptide had been produced, purified and analysed, to allow for a range of 2D trials.

Purified 2K4Y03 peptide in HFIP was mixed, in 1:1 and 1:2 peptide to lipid ratios, with either pure DMPC or a mixed DMPC-DOPC system, in Tris buffer (pH 7.4) containing both NaCl and MgCl<sub>2</sub> salts as well as a mixture of OG and DM. The dialysis conditions were the same as those used in the M protein 2D trials. EM examination, of the synthetic peptide crystallisation solutions, did not show evidence of the formation of any structures or arrays with a degree of ordering. Peptides and proteins, which adopt  $\beta$ -sheets conformations, have a tendency to aggregate and to precipitate out of solution; they will not readily form ordered structures and therefore can be very difficult to crystallise.

A much more extensive range of crystallisation conditions would need to be examined, such as the crystallisation method; peptide and lipid ratios; the lipids; the ionic strength, the additives and the pH of the buffer; the detergents used and the temperature profile, before reaching the conclusion that this peptide would not lend itself to crystallisation. To this end batch methods could be designed to accelerate the trial process, such as those already employed by a number of well know research groups in this field.<sup>124</sup>



### III.2.6. Examination of protein-lipid arrays by AFM.

Samples from the most successful 2D trials of both BrKA and the M protein, which contained the more ordered protein-lipid arrays, were examined by AFM, as the samples could be imaged under solution without further preparation and it was hoped, at much higher resolutions.<sup>61,113,114</sup>

#### III.2.6.1. Supported lipid bilayers.

In order to assess effects or features induced in the lipid membrane by any of the species present in the crystallisation solution; samples prepared in the absence of protein with the saturated DMPC or monounsaturated DOPC phospholipids were incubated on an atomically flat mica support and imaged by contact mode AFM in a 10 mM Tris-150 mM NaCl buffer (pH 7.4) at 20 °C.<sup>115</sup>

The monounsaturated DOPC supported bilayer, which adopts a fluid-liquid crystalline state above -20 °C, appeared by AFM as a featureless-carpet like surface showing very few defects.

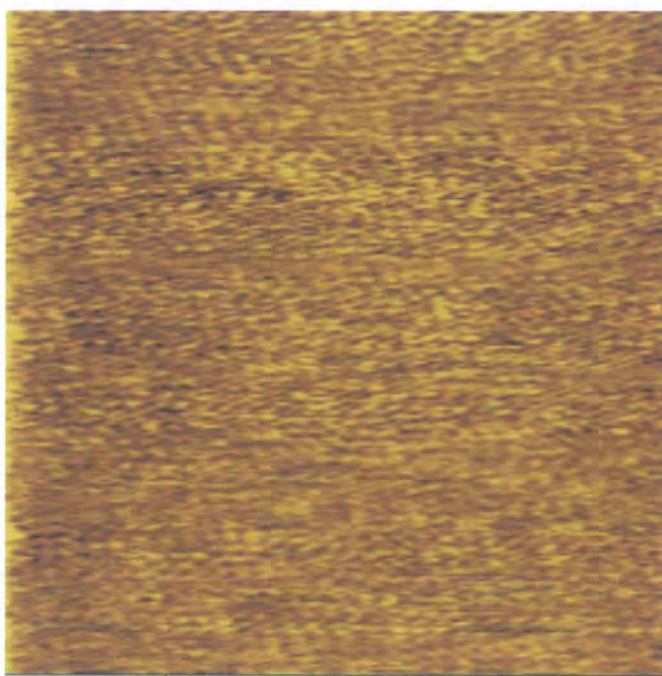


*Figure III.2.34. AFM image of a supported DOPC bilayer (300 nm x 300 nm frame).*

The supported bilayer, formed with the saturated DMPC lipid, appeared to offer a much less uniform coverage by comparison with the DOPC bilayer; large defects were clearly visible on the bilayer surface.

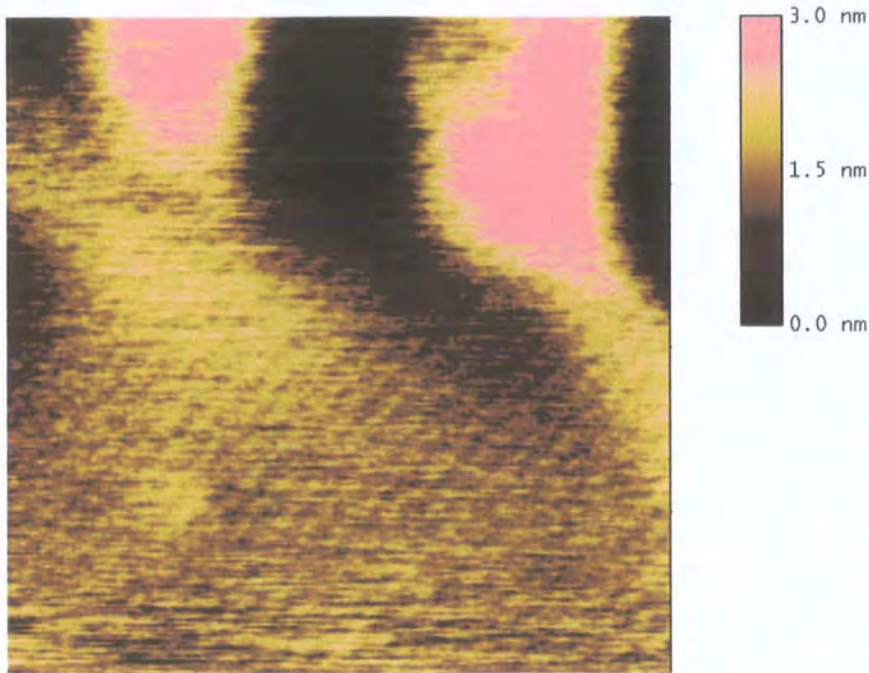


Figure III.2.35. AFM image of a supported DMPC bilayer (300 nm x 300 nm).

The thickness of the DMPC bilayer was estimated by measuring the depth of the holes in the supported lipid surface; these defects showed the bilayer had a thickness of 6–7 nm, which is within literature values for single bilayers of saturated phospholipids.<sup>106</sup>

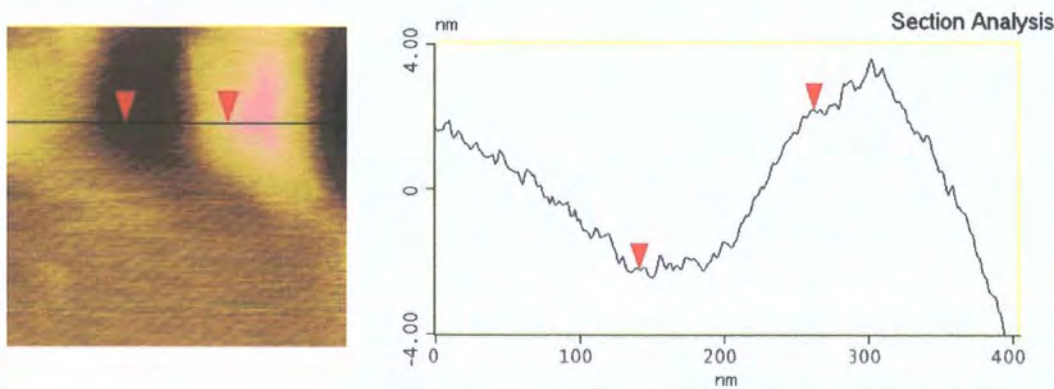


Figure III.2.36. Cross section of the line drawn on the DMPC bilayer surface.



### III.2.6.2. Electrostatic repulsion.

The resolution of the AFM image is dictated by reliable and close contact between the probe tip and the sample surface; regulating the ionic strength or salt concentration of the buffer solution used in the AFM fluid cell, helps reduce double layer electrostatic repulsion during imaging, and should be adjusted to around 150 mM for monovalent cations, such as NaCl or KCl in Tris buffer.<sup>116,117, 118,119</sup> A particular problem associated, with contact mode AFM, is the ease with which a soft biological sample can be displaced or damaged by the tip ploughing through the sample surface; consequently the force exerted by the tip on the sample, must be kept as low as possible, whilst still maintaining contact with the sample.<sup>68,107,120</sup>

Force-distance plots can be recorded for a sample, at a given set of conditions, to monitor the contact or electrostatic repulsion between the tip and the sample surface.<sup>121</sup>

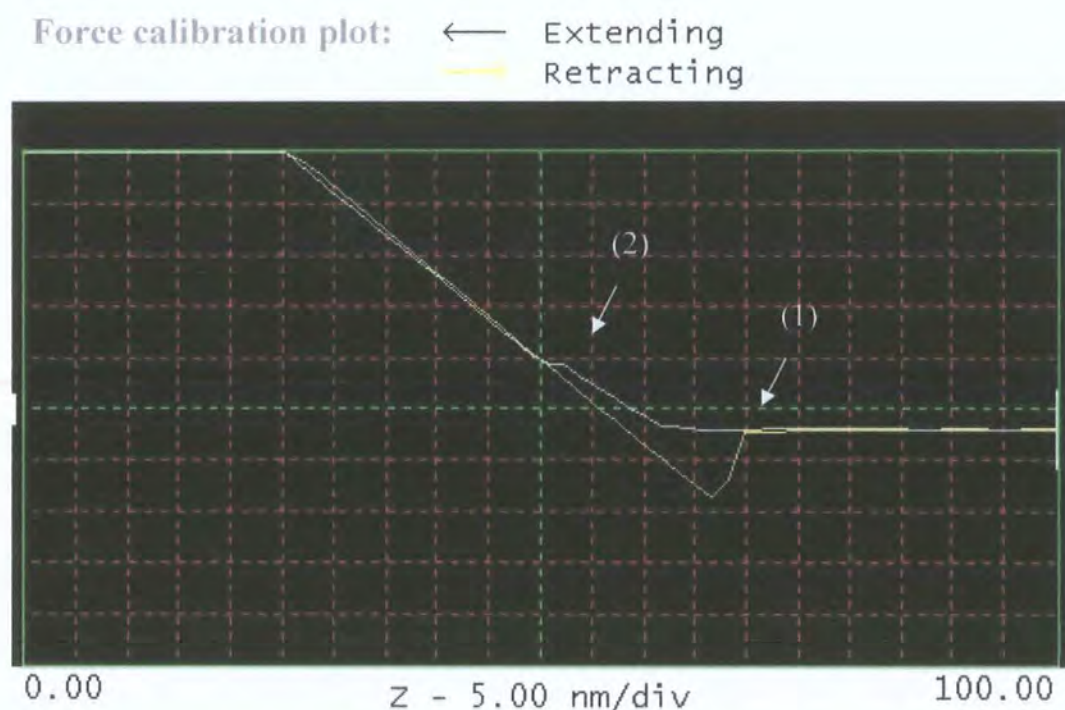


*Figure III.2.37. Force curves were recorded for all samples in 10 mM Tris-150 mM NaCl buffer (pH 7.4) at a scan frequency of 1.97 Hz and scan range of 50 nm. Arrow (1) marks the onset of measurable electrostatic repulsion and arrow (2) indicates the point of contact between the tip and sample.*

Force-distance plots enable the imaging conditions, such as cantilever deflection, scan rate and ionic strength of the solution, to be adjusted to ensure close contact between the tip and sample without disruption to the sample surface. A small electrostatic repulsion between 0.1 and 0.3 nN, appeared sufficient to provide reliable scanning of the sample surface in both directions.

### III.2.6.3. AFM imaging performed on BrKA-DMPC samples.

The BrKA-DMPC samples were incubated on an atomically flat mica support in a 10 mM Tris-150 mM NaCl Buffer (pH 7.4). Images were recorded in the sample buffer at least 30 minutes after the AFM cell and probe tip had been positioned over the sample, in order to allow the system to thermally equilibrate.

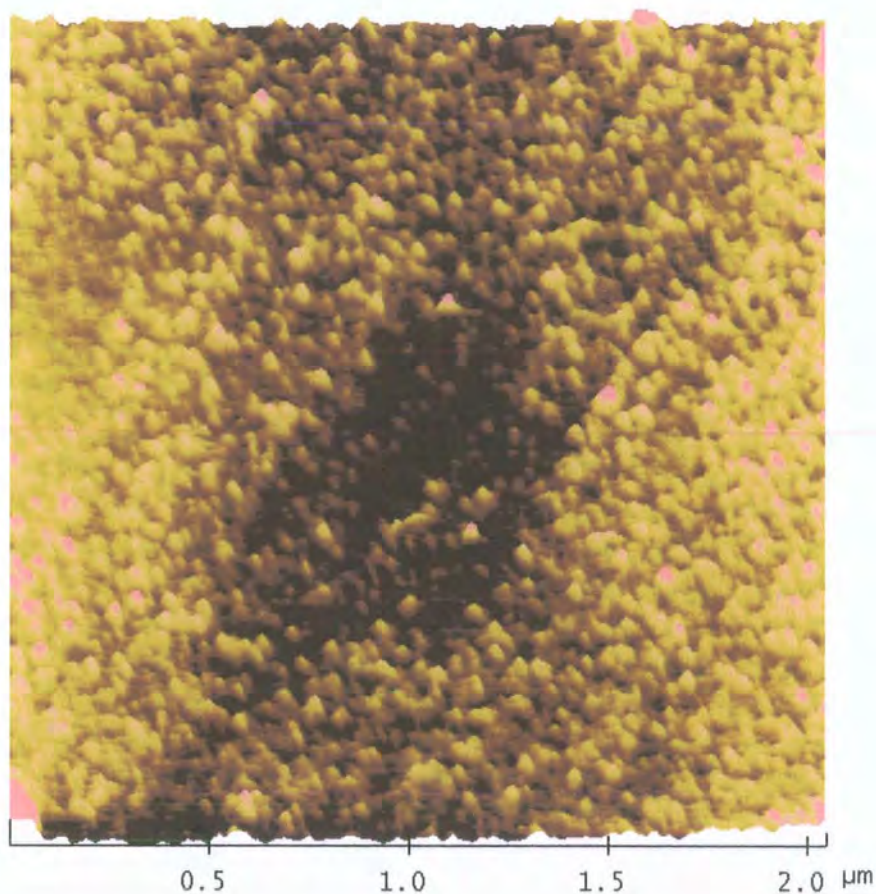


*Figure III.2.38. AFM performed on a BrKA-DMPC sample incubated at 4 °C overnight on a freshly cleaved mica support.*



The sample appeared quite densely packed in places, with distinct structures of similar size situated at different depths within the lipid membrane. The individual structures were measured at  $41 \pm 3$  nm in diameter.

Focusing on a less densely packed area of the sample and reducing the scan size, revealed each distinct structure to be in fact composed of a tetrameric unit. These oligomeric complexes are larger ( $\sim 3$  times) than those formed by other membrane proteins and characterised by AFM, which could be an indication that the imaging conditions, sharpness of the tips and force applied may be effecting the resolution.<sup>57,122</sup> These structures were observed reproducibly with a new tip under the same conditions.

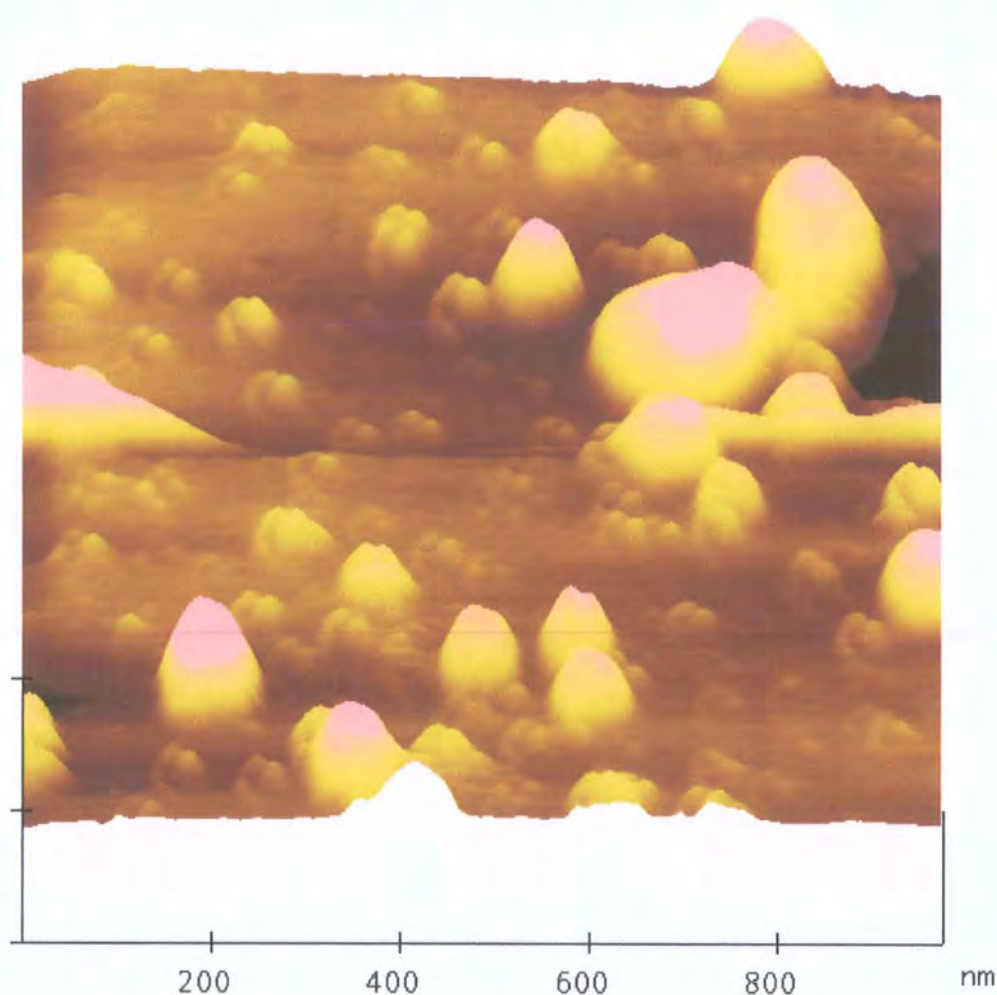


*Figure III.2.39. AFM image of BrKA C-terminal protein crystallisation samples showing features with a tetrameric appearance protruding from the lipid membrane.*



An area of the sample surface was removed by increasing the scan rate and the force applied to the sample surface. A depth profile measured over cross sections of the area, showed the oligomeric structures to have an average height of 5 nm.

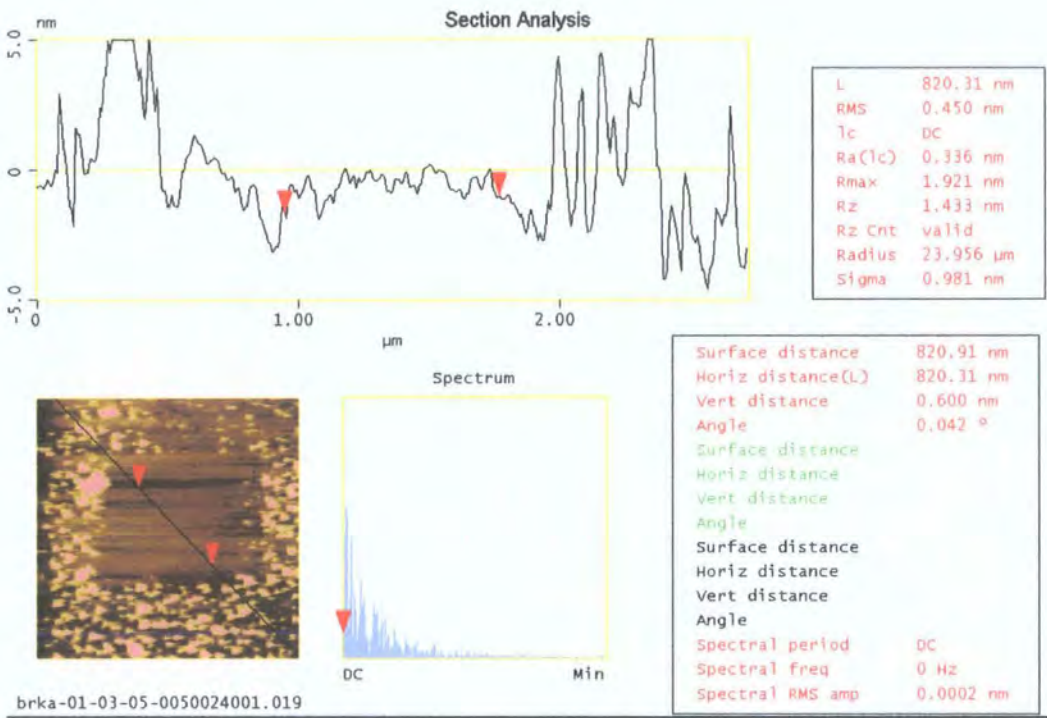
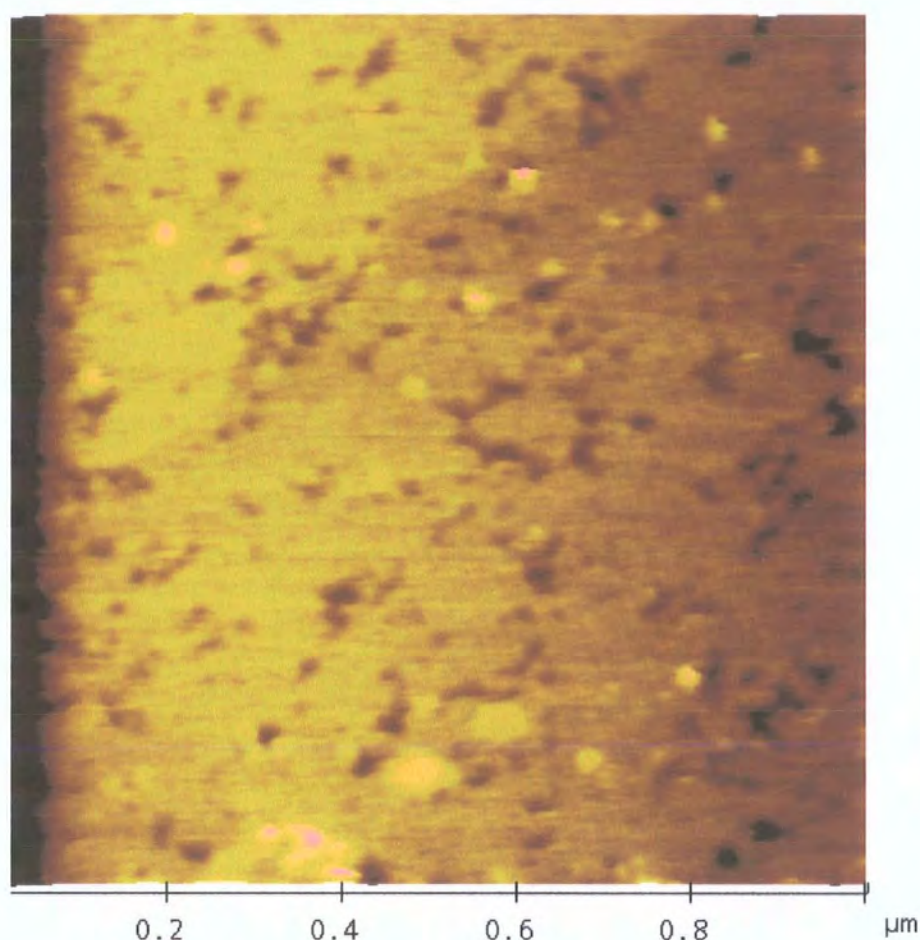


Figure III.2.40. Cross section analysis of a supported BrKA-DMPC sample, from which an area of the sample has been scrapped away with the probe tip.

The exposed underlying surface revealed spot like deep depressions in the supported lipid membrane, which do not appear to have been produced by the probe, as the strong scanning motion would create furrow type defects in supported membranes.

These localised depressions are believed to have been produced by the BrKA C-terminal protein, which forms channels in outer membranes.



*Figure III.2.41. Spot like depressions in a supported DMPC membrane visualised after removal of sample upper surface.*

Liquid cell AFM has provided support, along with the results obtained from the TEM analysis, towards the integration of the over expressed and renatured BrKA C-terminal protein, into saturated phospholipid membranes as well as for the formation of large oligomeric complexes.



#### III.2.6.4. AFM imaging performed on M protein-DMPC samples.

The M protein-DMPC crystallisation solution, absorbed onto mica and imaged in 10 mM Tris-150 mM NaCl, was shown by AFM to contain large striated areas with regular domains of  $3.4 \pm 0.7$  nm in width. The size and regularity of these structures suggest that they could be well ordered arrays of the M protein in DMPC membranes and would correspond to those observed by TEM.

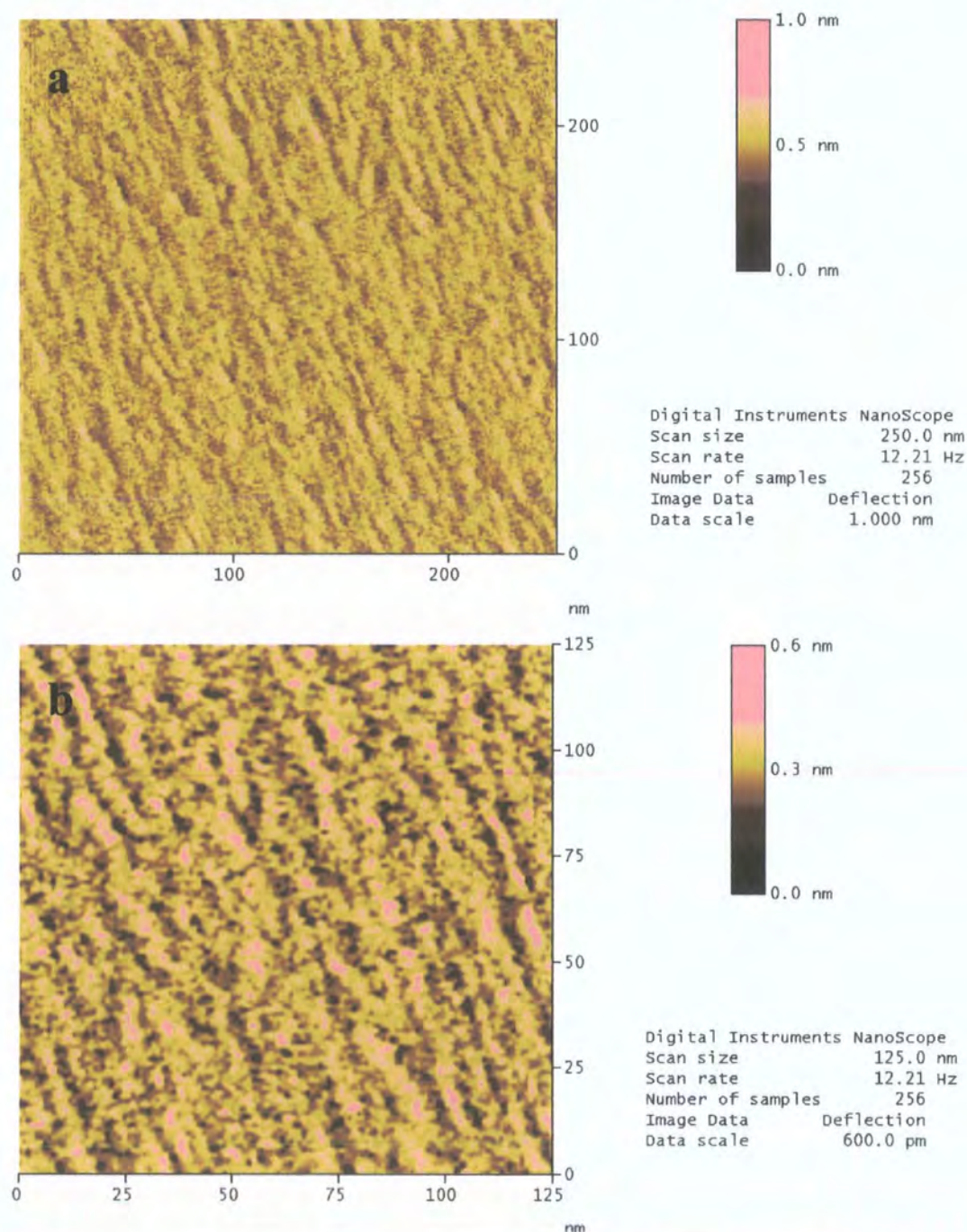


Figure III.2.42. Striated domains, **a** and **b** recorded on M protein-DMPC samples by AFM in 10 mM Tris-150 mM NaCl (pH 7.4)

AFM has help confirm the effects induced by both the BrKA C terminal domain protein and the M protein in lipid membranes under more natural physiological conditions and without interference or artifacts from preparative methods such as harsh drying and negative staining.

### **III.2.7. Further work.**

The aim of this study has been to gain further insight into the interactions between integral membrane proteins and lipid membranes, as well as to determine protein structures.

Although a better understanding of the behaviour of the BrKA C-terminal protein with phospholipid membranes has been achieved, there are still a considerable range of options to explore, especially in the 2D crystallisation process.

Further folding methods could also be considered, for example using other detergents such as SDS, which has been used successfully to extract protein from inclusion bodies; the dialysis rate could be optimised and attempting to refold the protein whilst attached to a column could also be tried. Highly ordered 2D crystal arrays may only be obtained if the protein has correctly refolded in the first place. Elimination of the His tag could also possibly help with both the refolding and crystallisation process.

Another option would be to examine the behaviour of the protein under different buffer-detergent conditions by electron microscopy and to determine the most appropriate conditions for future work.

The addition of a short protein sequence with a high proportional polar surface area could make the membrane protein easier to handle, as well as enhancing protein-lipid interactions and inducing 2D crystallisation.<sup>123</sup>

Considering a wider range of lipid to protein ratios should be an option, as some proteins crystallise only at low ratios, as for example in the case of Ca-ATPase of sarcoplasmic *reticulum* which formed highly ordered 2D arrays at protein-lipid ratios below 0.4 (w/w)<sup>108,124</sup>

Other methods of 2D crystallisation have demonstrated more efficient processes for certain protein-lipid systems; such as the use of Bio-beads SM2 for detergent removal combined with dialysis would allow a greater control over detergent removal and protein concentration could be increased by attaching the protein to a supported membrane.

Another approach, which has attracted much attention, is the exploitation of co-existing neighbouring cubic and lamellar phases within a bilayer (structures defined by Small Angle X-ray Scattering, SAXS) to promote the crystallisation of membrane proteins.<sup>125,126</sup>

### **III.3. Materials and Methods.**

#### **III.3.1. Materials.**

**Detergents:** Octyl- $\beta$ -D-glucopyranoside (OG) was obtained from Bachem Ltd. (UK); dodecyl- $\beta$ -D-maltopyranoside (DDM) and decyl- $\beta$ -D-maltopyranoside (DM) were from Anatrace (Switzerland); Triton X-100 and sodium dodecyl sulphate (SDS) was purchase from Lancaster Synthesis; Zwittergent 3-14 was from Calbiochem.

**Lipids:** Dimyristoyl phosphatidyl choline (DMPC) was obtained from Bachem Ltd. (UK) and dioleoyl phosphatidyl choline (DOPC) was purchased from Sigma. All phospholipids were used without further purification.

**Reagents:** Sodium Chloride, magnesium chloride, sodium azide, ethylenediamine tetraacetic acid (EDTA), tris(hydroxymethyl)aminomethane (Tris), sodium dihydrogen phosphate, urea, imidazole, trypticase (pancreatic digest of casein), yeast extract and agarose were all obtained from Lancaster Synthesis; 1,1,1,3,3,3-hexafluoroisopropanol (HFIP) was purchased from Apollo Scientific and further purified by distillation. HPLC grade water was from Fisher Scientific, and ultra pure water was purified using a Milli-Q purification system (Waters).

Isopropyl- $\beta$ -D-thiogalactopyranoside (IPTGs) was obtained from Gold biotechnology, inc, USA.

**Equipment.** All the eppendorf and falcon tubes and the pipette tips used in these preparations and processes were sterile.

### **III.3.2. Protein analysis.**

#### **III.3.2.1. Circular dichroism.**

Secondary structure determination was performed at a scan rate of 50 nm min<sup>-1</sup> on a Jasco J-810 Spectropolarimeter. The sample and background were analysed in quartz cell with a 1 cm path length and six scans were accumulated for each run. The background spectra were subtracted from the sample spectra and the resulting data converted to molecular ellipticity units.

#### **III.3.2.2. UV titrations.**

Determination of protein concentration was carried out on a Unicam 2 UV-Vis dual beam spectrophotometer in quartz UV cells with a path length of 1 cm. Samples were scanned over a wavelength range of 190 to 300 nm.

#### **III.3.2.3. Electron Microscopy.**

Samples were spotted on to carbon coated copper grids and after a period of 30 seconds, any excess solution was drawn off from the edge of the grid using blotting paper. A droplet of a 2 % (w/v) uranyl acetate solution was deposited on to the still wet grid, again any excess solution was drawn off after 30 seconds. **Transmission Electron Microscopy** was performed on a Hitachi H-7600 at an accelerating voltage of 100 kV and **Scanning Electron Microscopy** on a Hitachi S-5200 (FEG) operated at 30 kV. The carbon coated 400 mesh copper grids and the negative stain, uranyl acetate were both from Agar scientific.

#### **III.3.2.4. Atomic Force Microscopy.**

AFM images were obtained in contact mode using a liquid cell set up on a NanoScope IV AFM (Digital instruments). The probe tips used were of oxide sharpened Si<sub>3</sub>N<sub>4</sub> with a spring constant of 0.06 N/m (OMCL-RC800 PSA-1, Olympus). The tracking force was kept below 0.1 nN by manually adjusting the feedback gain and the scanning speed to compensate for the drift of the cantilever deflection during scanning. A range of scanning speeds were used but



these were mostly kept within the 3-8 Hz range and imaging was performed at room temperature.

The only treatment applied to the AFM images was flattening for images acquired in height mode (Nanoscope Reference Manual, 1996)

#### **III.3.2.5. Supported EPC, DMPC and DOPC bilayers**

were prepared by incubating 50  $\mu$ l of phospholipid unilamellar vesicle solution (prepared as below) onto a freshly cleaved mica disc (Agar scientific) at 4 °C overnight and then heating for 30 minutes to above 30 °C or to above the main transition of the lipid, which ever was highest. The sample surface was then washed carefully (x 10) by exchanging 50  $\mu$ l of 10 mM Tris-150 mM NaCl buffer (adjusted to pH 7.4), to remove excess lipid from the support whilst keeping the sample in solution, as exposing the lipid bilayer support to air would destroy its integrity.

#### **III.3.2.6. Protein-lipid sample preparation.**

The samples were prepared by incubating at 4 °C overnight a freshly cleaved mica disc with 50  $\mu$ l of the 2D trial protein-lipid preparation and then washing (x 10) the mica surface very gently by buffer exchange to remove any excess lipid from the support. The AFM fluid cell with rubber O-ring seal was then placed over the sample and clamped in place to produce a hermetical seal around the sample.

### **III.3.3. Methods.**

#### **III.3.3.1. Unilamellar vesicles of phospholipids.**

ULVs were prepared by evaporating a lipid solution from  $\text{CHCl}_3$  ( $1 \text{ mg ml}^{-1}$ ) to dryness under vacuum to form a thin film and hydrating the film with a 10 mM Tris-150 mM NaCl buffer (adjusted to pH 7.4). The solution was vortexed until complete lipid dispersal had been achieved and was then submitted to 5 cycles of freeze-thawing between  $-195$  and  $30^\circ\text{C}$ . Following this treatment the lipid suspension was extruded 10 times through a polycarbonate membrane (Whatman) with a pore size of 100 nm in diameter using a thermobarrel extruder (Lipex Biomembranes) at  $30^\circ\text{C}$ .

#### **III.3.3.2. Lipid preparation for 2D crystallisation trials.**

DMPC and DOPC were stored (at  $-20^\circ\text{C}$ ) as stock solutions in  $\text{CHCl}_3$  at a concentration of  $30 \text{ mg ml}^{-1}$ . Aliquots of  $167 \mu\text{l}$  of lipid solution ( $5 \text{ mg}$  of lipid) were dried to a thin film using a rotary evaporator and further dried under nitrogen for 2 hours.

The films were then hydrated with either buffer or a buffer-detergent solution and vortexed until all the lipid was dispersed in the solution. The suspension was then submitted to 5 cycles of freeze-thawing between  $-195$  and  $30^\circ\text{C}$  and sonicated for 20 minutes at  $30^\circ\text{C}$ . Lipid solutions were either used immediately or stored in the fridge for 2-3 days before use.

#### **III.3.3.3. Dialysis tube preparation.**

Dialysis cellulose tubing (Sigma-Aldrich) with a cut off size of 10,000 Da was cut into 10 cm sections and then boiled for 10 mins in 2 litres of distilled water with 1 mM ( $5.8 \text{ g}$ ) of EDTA and a small spatula end of sodium bicarbonate. The tubes were thoroughly washed with distilled water before use.

#### **III.3.3.4. Dialysis procedure.**

The sample solution was pipetted into dialysis tubes, which had been knotted at one end and then closed with a clip. The tubes were suspended into a buffer solution, from the neck of a 600 ml flask, which was fitted with an inlet tube for introduction of 800 ml of fresh buffer, at a rate of  $1 \text{ ml min}^{-1}$ , into the bottom of the flask using a peristaltic pump (Gilson). The buffer was continuously agitated with a magnetic stirrer bar and an outlet tube allowed removal of the buffer overflow from the dialysis flask.

#### **III.3.3.5. YT media.**

YT media was prepared in distilled water with  $8 \text{ g l}^{-1}$  of trypticase (pancreatic digest of casein),  $5 \text{ g l}^{-1}$  of yeast extract and  $5 \text{ g l}^{-1}$  of NaCl (all from Lancaster Synthesis). The media was thoroughly mixed, autoclaved and cooled to room temperature. Ampicillin ( $50 \text{ } \mu\text{g ml}^{-1}$  of YT media) was added to media before use.

#### **III.3.3.6. Agar plates.**

Agar plates were prepared by mixing  $10 \text{ g l}^{-1}$  trypticase,  $5 \text{ g l}^{-1}$  yeast extract,  $5 \text{ g l}^{-1}$  NaCl and 15 g of agar in distilled water. The media was thoroughly mixed and autoclaved. The mixture was heated to  $55 \text{ }^{\circ}\text{C}$  in a water bath until fluid and then ampicillin ( $50 \text{ } \mu\text{g ml}^{-1}$  of media) was added to the agar media, before it was poured carefully in to sterile Petri dishes and allowed to set in a sterile environment. Plates were then stored at  $4 \text{ }^{\circ}\text{C}$  until used.

#### **III.3.3.7. Standard 15 % SDS-Polyacrylamide gel.**

A resolving gel was prepared by mixing 7.5 ml of acrylamide, 1.9 ml of 3 M Tris-HCl (pH 8.8) buffer, 5 ml of pure water,  $150 \text{ } \mu\text{l}$  of a 10 % (v/v) SDS solution,  $560 \text{ } \mu\text{l}$  of a 2 % (v/v) ammonium persulphate solution and 7.5 of TEMED. The gel was gently mixed to avoid creating any air bubbles and was then poured in between two glass plates separated by a gasket seal and held together by clips. A shallow layer of water was carefully added on top of the gel, which occupied about  $2/3^{\text{rd}}$  of the space in between the plates.

The layer of water was removed with blotting paper, after the gel had set (~10 minutes) and a stacking gel was then prepared by gently mixing 1.25 ml of acrylamide, 2.5 ml of 0.5 M Tris-HCl (pH 6.8) buffer, 5.65 ml of pure water, 100  $\mu$ l of a 10 % (w/v) SDS, 500  $\mu$ l of a 2 % (v/v) ammonium persulphate solution and 7.5  $\mu$ l of TEMED. The stacking gel was poured on top of the resolving gel and a comb was pushed in to the opening at the top of the plates, with the comb teeth below the stacking gel surface. The gel was then left to set for approximately 30 minutes, before the comb was removed. The seal around the plates was then removed and the gel between the two glass plates inserted into the electrophoresis tank.

The purified protein and SDS-7 size markers (Dalton Mark VII-l, Sigma) were premixed with 10  $\mu$ l of 5 x sample buffer (0.2 M Tris, 20 % (v/v) glycerol, 5 % (w/v) SDS and 0.002 % BPB adjusted to pH 6.8) for 10  $\mu$ l of sample and boiled for 5 minutes with 1 % (v/v) of a reducing agent,  $\beta$ -mercapto-ethanol. After cooling to room temperature, the peptide solutions were pipetted into the wells, left by the comb teeth, in the gel. A 10 x reservoir buffer was prepared with 0.25 M Tris, 1.92 M glycine and 1 % (w/v) SDS (pH 8.3) and diluted 10 fold with distilled water to fill the tank. The terminals were attached to the tank and electric current was run through the tank to separate charged species within the gel.

**The gel stain** contained 0.05 % kenacid blue R ( $0.5 \text{ g l}^{-1}$ ) in a solution of 40 % methanol and 7 % glacial acetic acid in distilled water.

**The gel destain** was a solution of 40 % methanol and 7 % glacial acetic acid in distilled water.

#### **III.3.3.8. Agarose gel.**

Agarose (0.8 g) was dissolved in 90 ml of distilled water and heated 3 times, in a microwave for 2 minutes until the mixture started to boil. The solution was removed from the microwave periodically and gently swirled. Following this treatment, the agarose solution was cooled to 65 °C before adding 10 ml of 10 x reservoir buffer (0.25 M Tris, 1.9 M glycine and 1 % (v/v) SDS adjusted to pH 8.3) and 10  $\mu$ l of ethidium bromine. The solution was thoroughly mixed before pouring in to an agarose gel tray in which a comb had been inserted to create a

row of sample wells in the gel. The running buffer for a 600 ml tank contained 540 ml of distilled water, 60 ml of 10 x buffer and 60  $\mu$ l of ethidium bromide.

#### **III.3.3.9. BrKA C-terminal protein expression.**

Constructs of the C-terminal domain of BrKA (*Bordetella pertussis*) in a pET 11a expression vector (a kind donated from Dr Blackburn, Glasgow University) were transformed into BL21 (DE3) and spread on to an YT agar plate. The clones were left to grow at 37 °C overnight. Several cultures were then lifted from the culture plate and grown in 10 ml of YT media with ampicillin (50  $\mu$ g ml<sup>-1</sup>) overnight at 37 °C, with constant agitation of the growth media to ensure adequate aeration. These cultures were then further grown for 3 or 5 hours, following a 20 fold dilution into fresh YT media. After which it was assumed that a high cell density had been reached. Controls containing only *E. coli* BL21 (DE3) cells were also prepared and grown without antibiotic along side the BrKA-pET 11a clone.

#### **III.3.3.10. Protein expression.**

Protein expression was induced following addition of isopropyl- $\beta$ -D-thiogalactopyranoside (IPTGs) to a final concentration of 1 mM and cultures were incubated for 3 hours at 37 °C. It was found after further investigation that the protein would not express well on a large scale in shake flasks and had to be grown in 10 ml culture bottles.

#### **III.3.3.11. Cell harvesting.**

The cells were harvested by centrifugation (10 min at 3000 x g), put through a French press cell and centrifuged again for 25 minutes at 19000 x g. The supernatant was decanted and the pellet resuspended in a bacterial protein extraction reagent, B-PER<sup>TM</sup> (PIERCE, Biotechnology) and centrifuged before being frozen overnight, to further rupture the cells. The pellet was then suspended in a 50 mM Sodium dihydrogen phosphate and 8 M urea buffer at pH 8 and centrifuged for 25 minutes at 19000 x g. The concentration of the BrKA C-terminal protein was estimated by SDS-Page.

#### **III.3.3.12. Protein purification.**

The supernatant after urea extraction was purified on an ion exchange column with negative packing: Sulphopropyl(s) sepharose fast flow column, Amersham. The column was equilibrated for 10 minutes at a flow rate of 1 ml min<sup>-1</sup> with a 50 mM sodium dihydrogen phosphate-8 M urea buffer (pH 8), before loading the protein (in 5 ml of buffer per pellet spun down from a 10 ml culture) on to the column in the same buffer. The UV detector was set at a wavelength of 280 nm and at a flow rate of 1 ml min<sup>-1</sup>. Protein elution from the column was carried out using a linear gradient of a 50 mM sodium dihydrogen phosphate-8 M urea buffer (pH 8) against the same buffer but after addition of 0.5M NaCl (pH 8).

#### **III.3.3.13. Subcloning of BrKA C-terminal domain into a pET 19b Vector.**

BrKA-pET 11a clones transformed into BL21(DE3) (Novagen) were spread on an agar plate (containing ampicillin) and left to grow at 37 °C overnight. Several cultures from different areas of the agar plate were lifted into YT media and allowed to grow overnight at 37 °C. The suspension was centrifuged to give a cell pellet on which a miniprep was carried out to purify the DNA construct (plasmid DNA).

#### **III.3.3.14. Purification of constructs.**

Minipreps were performed using a Wizard SV kit (Promega); the pellet, resulting from 10 ml of culture, was completely resuspended in 250 µl of a 50 mM Tris-HCl buffer solution (pH 7.5) with 10 mM EDTA and 100 µg ml<sup>-1</sup> of RNase A (promega). Then 250 µl of a cell lysis solution, containing 0.2 M NaOH and 1 % (v/v) of SDS was added to the suspension and very gently mixed. This solution was incubated until it appeared clear (from 1-5 min), an alkaline protease solution (promega) was then added and the solution was incubated for 5 minutes at room temperature. Finally 350 µl of a neutralization solution containing 4.06 M guanidine hydrochloride, 0.76 M potassium acetate and 2.12 M glacial acetic acid adjusted to pH 4.2 was gently mixed with the solution, which was then centrifuged (at 14 000 x g) for 10 minutes. The supernatant containing the plasmid DNA was then filtered and washed 4 times with a 60 % ethanol, 60 mM potassium acetate, 8. mM Tris-HCl and 0.04 mM EDTA (pH 7.5) wash solution.

The DNA was eluted from the filter with Nuclease free water (promega) and then stored at -20 °C.

III.3.3.15. Subcloning.

Subcloning of the BrKA C-terminal domain DNA from a pET 11a to a pET 19b vector (Novagen), to incorporate an N-terminal His tag in the protein product, was carried out by digesting both the BrKA construct and the new vector with the restriction enzymes BamH1 and Nde1 which both have sites within their DNA sequence.

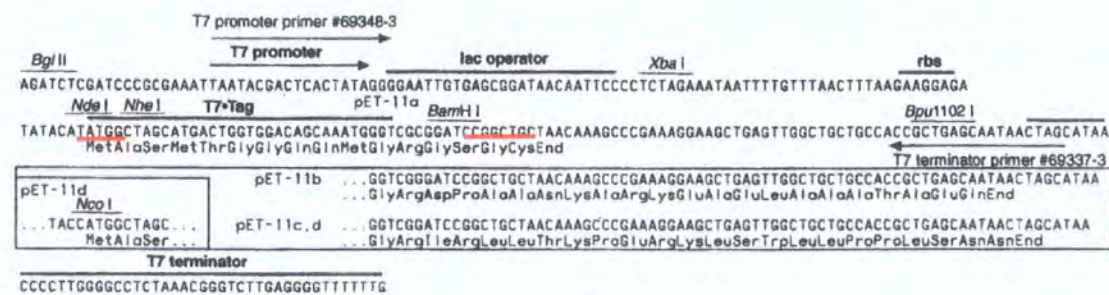


Figure III.3.1. Diagram depicting the pET 11a vector cloning and expression regions with NdeI and BamHI cloning sites underlined in red.

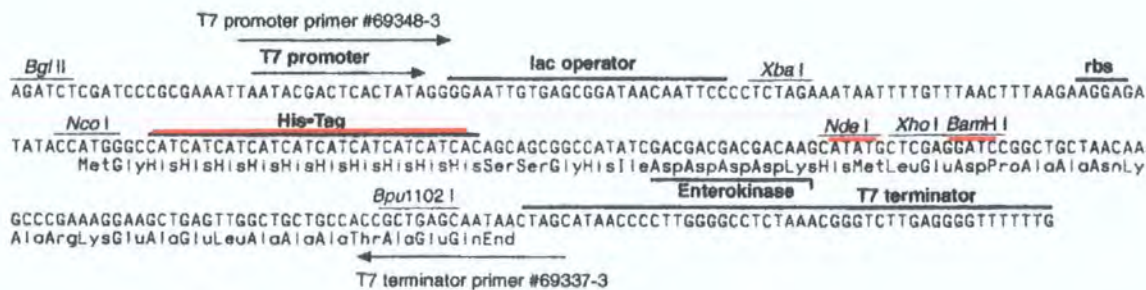


Figure III.3.2. Diagram depicting the pET 19b vector cloning and expression regions with NdeI and BamHI cloning sites and N-terminal His Tag sequence underlined in red.



Purified BrKA-pET 11a DNA from the miniprep was used and all other digestion components as listed below were purchased from Roche.

	pET 19b vector	BrKA-pET 11a
Vector/construct	1 µl	20 µl
NdeI	1 µl	1 µl
BamHI	1 µl	1 µl
Buffer B 10x (Roche)	3 µl	4 µl
H <sub>2</sub> O	24 µl	14 µl

*Table III.3.1. Digestion preparation of the BrKA construct and the pET 19b vector with the restriction enzymes BamHI and NdeI.*

The digestion preparations were mixed by pulse centrifugation and then incubated at 37 °C for 2 hours.

### **III.3.3.16. Separation of fragment by agarose gel electrophoresis.**

The digestion products were separated by agarose gel: dye was added to 30 µl of sample (1 part dye to 5 parts DNA) and run against the DNA standard, λ Eco 471 (2-5 µg). The vectors pET 11a and pET 19b have respectively 5,677 and 5,717 base pairs and the BrKA C-terminal domain has 856 base pairs. DNA gel bands corresponding to the pET 19b plasmid and to the BrKA C-terminal fragment were carefully cut out of the gel and inserted into dialysis tubes with 200 µl of running buffer for separation by electro elution.

### **III.3.3.17. Purification of target fragments.**

Following electro elution, the solution in the dialysis tubes was removed (avoiding any gel transfer) and submitted to a phenol-chloroform extraction process. The DNA buffer solutions (200 µl) were added to an equal part of phenol, vortexed and centrifuged for 3 minutes (in a table top centrifuge). The upper aqueous layers were removed and the phenol phases re-extracted with 100 µl of TE buffer containing 10 mM Tris-HCl and 1 mM EDTA (pH 8).

The two aqueous parts were pooled together and extracted twice (2 x 250 µl) with chloroform held at 4 °C, to give a final 300 µl aqueous phase, for each DNA extraction, to which were added: 12 µl of a 5 M ammonium acetate–MgCl<sub>2</sub> solution, 1 µl of glycogen and 630 µl of a 70 % ethanol solution (stored at -20 °C). These were then placed at -20 °C for at least 2 hours to precipitate the DNA. The solutions were centrifuged for 20 minutes at 4 °C and 19000 x g to give a pellet, which was then washed with 1 ml of a 70 % ethanol solution (stored at -20 °C) and centrifuged again for 10 minutes. The ethanol was decanted and the pellet dried in a desiccator for 5 minutes. The pellet was finally redissolved in 10 µl of sterile water.

#### **III.3.3.18. Ligation of recombinant pET 19b-BrKA C-terminal clone.**

The BrKA-C terminal fragment was ligated into the pET 19b vector using the following method: 4 µl of pET 19b plasmid DNA and 4 µl of BrKA C-terminal domain DNA were mixed with 1 µl of 10 x ligase buffer and 1 µl of ligase (T4 DNA) and then incubated at room temperature for 4 hours.

#### **III.3.3.19. Transformation into competent cells.**

The pET 19b-BrKA C-terminal construct was transferred to Top 10 competent cells: 2 µl from the ligation reaction were combined with 40 µl of Top 10 competent cells (Invitrogen™) and placed over ice for half an hour. This solution were then heat shocked (without agitation) for 30 seconds at 42 °C and transferred back to ice before adding 100 µl of SOC medium (Invitrogen™) and shaking the mixture for an hour at 37 °C. The transformed cells were then spread on a pre warmed agar plate (with ampicillin) and incubated overnight at 37 °C.

#### **III.3.3.20. Expression and cell harvesting.**

Several colonies from the plate were then grown in YT media (with ampicillin), expressed and harvested as described above in section III.3.3.11.

### III.3.3.21. Purification.

Purification was carried out on a  $\text{Ni}^{2+}$ -NTA affinity column equilibrated for 10 minutes with a buffer (a), containing 8 M Urea, 50 mM Sodium dihydrogen phosphate, 150 mM Sodium chloride and 5 mM Imidazole (adjusted to pH 7.4 with NaOH). The protein dissolved in the same buffer (a) was then loaded on to the column. The column was washed with buffer (a) containing a higher concentration of imidazole (20 mM Imidazole) and the protein was eluted then from the column again with buffer (a) with a 0.3 M concentration of imidazole. Protein elution was monitored at 280 nm at a flow rate of  $1 \text{ ml min}^{-1}$ .

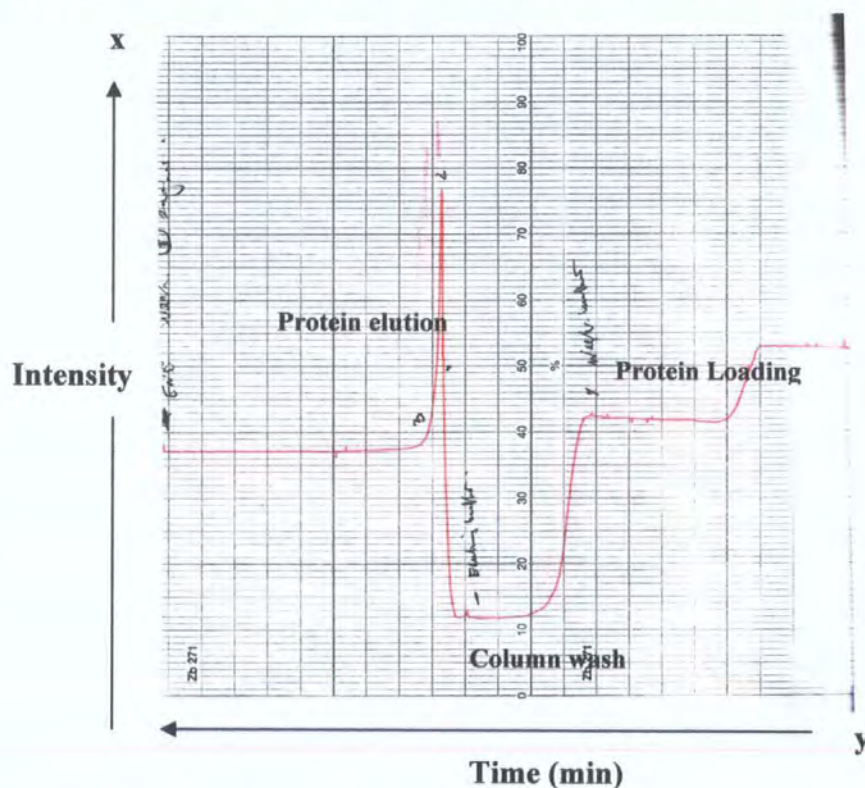


Figure III.3.3. Elution of BrKA C-terminal protein from the nickel affinity column.

### III.3.3.22. Protein refolding.

The protein ( $\sim 0.5 \text{ mg ml}^{-1}$ ) in elution buffer was either dialysed alone or after thoroughly mixing with either 0.05 mg of lipid (DMPC) or 0.1 % (v/v) Triton X-100, or with both 0.1 % (v/v) Triton X-100 and 0.05 mg of DMPC.

The mixtures were dialysed at a rate of 0.2 % min<sup>-1</sup> (at 4 °C) against a 20 mM sodium dihydrogen phosphate, 150 mM NaCl and 0.1 % (v/v) Triton X-100 buffer, adjusted to pH 7.4 with NaOH. A second dialysis was performed under the same conditions against a 10 mM Tris, 150 mM NaCl, 20 mM MgCl<sub>2</sub>, 3 mM NaN<sub>3</sub> and 0.1 % (v/v) Triton X-100 buffer (pH 7.4).

### III.3.3.23. Determination of protein concentration.

The protein concentration was determined by from the UV absorbance of the protein at 280 nm using the Beer Lambert law for which the protein extinction coefficient (at 280 nm) had to be calculated.

The residue extinction coefficients at 280 nm, for the tyrosine and tryptophan residues, used in the calculation, were 1280 and 5690 Moles<sup>-1</sup> cm<sup>-1</sup> respectively.<sup>89</sup>

The predicted number of tyrosine, tryptophan and cysteine residues in the recombinant protein sequence were counted, multiplied by the appropriate extinction coefficient for each type of residue and then summed to give the extinction coefficient ( $\epsilon_{280\text{ nm}}$ ) for the whole protein:

Residue	N <sup>o</sup> of residues in the sequence	N <sup>o</sup> of residues multiplied by $\epsilon_{280\text{ nm}}$ for each residue	$\epsilon_{280\text{ nm}}$ for the protein
Trp	8	8*5690 = 45520 (M <sup>-1</sup> cm <sup>-1</sup> )	69840 (M <sup>-1</sup> cm <sup>-1</sup> )
Tyr	19	19*1280 = 24320 (M <sup>-1</sup> cm <sup>-1</sup> )	
Cys-Cys	0	0	

*Table III.3.2. Calculation of the extinction coefficient ( $\epsilon_{280\text{ nm}}$ ) for the BrKA C-terminal domain.*

A plot of protein absorption at 280 nm against volume of peptide stock solution in the UV cuvette, gave a linear relationship, from the gradient of which, the protein concentration in a 1 ml cuvette with a path length of 1 cm, was calculated using the Beer Lambert law:  $\text{Abs} = \epsilon \cdot C \cdot l$  (1)

For which Absorption, Abs. was corrected for protein dilution and path length was equal to 1:

$$\text{Conc. (M)} = \text{Abs}_{280\text{nm}} / \epsilon_{280\text{nm}} * \text{vol. in cuvette} / \text{vol. of peptide. solution (2)}$$

and the gradient of Abs. against vol. of peptide solution was given by:

$$\text{Gradient} = (\epsilon_{280\text{nm}} * \text{Molar Conc.}) / \text{vol. in cuvette. (3)}$$

#### **III.3.3.24. 2D crystallisation procedures.**

The purified refolded protein (0.5 mg ml<sup>-1</sup>), in buffer (1) with 0.1 % Triton X-100 (v/v), was thoroughly mixed by vortexing, in a 1:1 (w/w) and 1:2 (w/w) protein to lipid ratio with DMPC, in buffer (1) with 1 % OG (w/v). The solution was then incubated in an eppendorf tube for one hour at 4 °C, before dialysis at a rate of 0.2 % min<sup>-1</sup> against detergent free buffer (1) using a peristaltic pump (Gilson), at 4 °C.

The solution was then dialysed from 4-6 hours, against fresh buffer (1), pre-equilibrated at 23 °C and following a third buffer change, the dialysis solution was placed at 37 °C for 48 hours. A final dialysis was then carried out for 2 hours, on samples prepared for EM but not AFM examination, with salt free 10 mM Tris-HCl buffer (pH 7.4) pre-equilibrated at 37 °C, before storing the samples at 4 °C. Samples were allowed to warm to room temperature for an hour before imaging either by EM or AFM.

**Buffer (1):** 10 mM Tris, 150 mM NaCl, 20 mM MgCl<sub>2</sub> and 3 mM NaN<sub>3</sub> buffer prepared in distilled water (adjusted to pH 7.4)

#### **III.3.3.25. Modified crystallisation procedures.**

The purified refolded protein (~0.5 mg ml<sup>-1</sup>) in a mixture of 1 % (w/v) OG and 0.1 % (w/v) DM in buffer (1) was mixed with either DMPC or a 1:1 (w/w) mixture of DMPC and DOPC, also in buffer (1) with a 1 % (w/v) OG and 0.1 % (w/v) DM mixture. Protein to lipid ratios of 1:1 and 1:2 (w/w) were used in all the 2D trials. Dialysis rates were increased two (0.4 % min<sup>-1</sup>) and four fold (0.6 % min<sup>-1</sup>) and dialysis at 37 °C was extended from 48 hours to a week.

#### **III.3.3.26. The M protein crystallisation procedures.**

The M protein was soluble in a (10 mM) Tris-(150 mM) NaCl buffer (pH 7.4) at concentrations below 1 mg ml<sup>-1</sup>. A 1:1 (w/w) mixture of the M protein with either DMPC or a 1:1(w/w) mixture of DMPC and DOPC, was pre-mixed with 1 % (w/w) OG and 0.1 % (w/w) DM in buffer (1). The solution was incubated at 4 °C for over an hour, to allow for equilibration of the system and then dialysis in buffer (1) with 0.1 % Triton X-100. Half the buffer was replaced by fresh detergent-free buffer following dialysis at room temperature (23 °C) for 4 hours. The dialysis flask was then transferred to a 37 °C environment and again half the buffer was replaced by 37 °C pre-equilibrated detergent-free buffer. After a 24 hour period, 3 complete buffer exchanges were carried out over 8 hours to ensure complete detergent elimination from the system. The solution was then allowed to cool to room temperature, before imaging by EM or AFM.

#### **III.3.3.27. The 2K4Y03 peptide crystallisation procedure.**

The purified 2K4Y03 peptide, in HFIP at a concentration of 0.5 mg ml<sup>-1</sup>, was mixed in a 1:1 and 1:2 peptide to lipid ratio, with either DMPC or a 1:1 mixture of DMPC-DOPC, in buffer (1) (pH 7.4) with 1 % (w/v) OG and 0.1 % (w/v) DM. The dialysis conditions were those used for the crystallisation trials of the M protein.

#### **III.3.3.28. Elimination of excess lipid.**

Excess lipid was eliminated by mixing the sample solution with 20 µg of phospholipase A<sub>2</sub> in buffer (1) and then dialysing the sample-phospholipase solution over night at 4 °C. After exchanging the dialysis buffer with fresh buffer (1), the sample was heated to 37 °C for 3 hours and then cooled to RT.

### III.4. Appendix 1.

#### Properties of detergents.<sup>127,128,129</sup>

##### Non-Ionic detergents.

Detergent Name	M.W. (monomer)	CMC(mM)	CMC Conditions
APO-10	218.3	4.6	50mM Na <sup>+</sup>
APO-12	246.4	0.568	50mM Na <sup>+</sup>
BRIJ-35(C <sub>12</sub> E <sub>23</sub> )	1200 (avg)	0.09	50mM Na <sup>+</sup>
C <sub>8</sub> E <sub>6</sub>	399.1	9.9	25°C
C <sub>10</sub> E <sub>6</sub>	427.1	0.9	50mM Na <sup>+</sup>
C <sub>12</sub> E <sub>6</sub>	451.1	0.087	50mM Na <sup>+</sup>
C <sub>12</sub> E <sub>10</sub> (atlas G2127)	539.1	0.11	50mM Na <sup>+</sup>
C <sub>12</sub> E <sub>9</sub>	583.1	0.08	50mM Na <sup>+</sup>
C <sub>16</sub> E <sub>12</sub>	771.1	0.0023	25°C
C <sub>16</sub> E <sub>21</sub>	1167.1	0.0039	25°C
Cyclohexyl-n-Ethyl-β-D-Maltoside	452.5	120	50mM Na <sup>+</sup>
Cyclohexyl-n-hexyl-β-D-Maltoside	508.6	0.56	50mM Na <sup>+</sup>
Cyclohexyl-n-methyl-β-D-Maltoside	438.5	340	50mM Na <sup>+</sup>
<i>n</i> -Decanoylsucrose	496.6	2.5	50mM Na <sup>+</sup>
<i>n</i> -Decyl-β-D-glucopyranoside	320.4	2.2	50mM Na <sup>+</sup>
<i>n</i> -Decyl-β-D-maltopyranoside	482.6	1.6	50mM Na <sup>+</sup>
<i>n</i> -Decyl-β-D-thiomaltoside	498.6	0.9	50mM Na <sup>+</sup>
<i>n</i> -Dodecanoyl	524.6	0.03	—



Non-Ionic detergents. (continued)

Detergent Name	M.W. (monomer)	CMC(mM)	CMC Conditions
Sucrose			50mM Na <sup>+</sup>
<i>n</i> -Dodecyl-β-D-glucopyranoside	348.5	0.13	50mM Na <sup>+</sup>
<i>n</i> -Dodecyl-β-D-maltoside	348.5	0.15	50mM Na <sup>+</sup>
HECAMEG	335.4	19.5	50mM Na <sup>+</sup>
Heptane-1,2,3-triol	148.2		
<i>n</i> -heptyl-β-D-glucopyranoside	278.3	79	50mM Na <sup>+</sup>
<i>n</i> -heptyl-β-D-thioglucopyranoside	294.3	30	50mM Na <sup>+</sup>
MEGA-8(Octanoyl-N-methylglucamide)	321.5	58	50mM Na <sup>+</sup>
<i>n</i> -nonyl-β-D-glucopyranoside	306.5	6.5	50mM Na <sup>+</sup>
<i>n</i> -Octanoyl-β-D-glucosylamine (NOGA)	305.4	80	50mM Na <sup>+</sup>
<i>n</i> -Octanoylsucrose	468.5	24.4	50mM Na <sup>+</sup>
<i>n</i> -Octyl-α-D-glucopyranoside	292.4	20	—
<i>n</i> -Octyl-β-D-glucopyranoside	292.4	25	50mM Na <sup>+</sup>
<i>n</i> -Octyl-β-D-maltopyranoside	454.5	23.4	50mM Na <sup>+</sup>
Triton X-100 (tert-C <sub>8</sub> -Ø-E <sub>9.6</sub> )	650(avg)	0.3	50mM Na <sup>+</sup>
Triton X-100 hydrogenated	631(avg)	0.25	50mM Na <sup>+</sup>
Triton X-114 (tert-C <sub>8</sub> -Ø-E <sub>7.8</sub> )	537(avg)	0.35	50mM Na <sup>+</sup>
Tween 80 (C <sub>18.1</sub> -Sorbitan-E <sub>20</sub> )	1310	0.012	50mM Na <sup>+</sup>

### Ionic Detergents.

Detergent Name	M.W. (monomer)	CMC(mM)	CMC Conditions
Cholic acid, Na <sup>+</sup> salt	430.6	4	50mM Na <sup>+</sup>
Decanesulfonic acid, Na <sup>+</sup> salt	244.3	32.6	–
Deoxycholic acid, Na <sup>+</sup> salt (DOC)	414.6	1.5	50mM Na <sup>+</sup>
Digitonin	1229	0.087	–
Lithium <i>n</i> -dodecyl sulfate	272.3	6-8	50mM Na <sup>+</sup>
Lysophosphatidyl-choline (16:0)	495.7	0.007	–
Sodium <i>n</i> -dodecyl sulfate (SDS)	288.5	2.30	50mM Na <sup>+</sup>
Taurocholic acid, Na <sup>+</sup> salt	537.7	3.3	20mM Na <sup>+</sup>
Taurodeoxycholic acid, Na <sup>+</sup> salt	521.7	2.7	50mM Na <sup>+</sup>
TOPPS	350.5	4.5	30°C

### Zwitterionic Detergents

Detergent Name	M.W. (monomer)	CMC(mM)	CMC Conditions
BigCHAP	878.1	3.4	50mM Na <sup>+</sup>
CHAPS	614.9	6-10	50mM Na <sup>+</sup>
CHAPSO	630.9	8	50mM Na <sup>+</sup>
EMPIGEN BB (N-Dodecyl-N,N, Dimethylglycine)	272.0	1.6-2.1	50mM Na <sup>+</sup>
ZWITTERGENT 3-08	279.6	330	50mM Na <sup>+</sup>
ZWITTERGENT 3-10	307.6	25-40	50mM Na <sup>+</sup>
ZWITTERGENT 3-14	363.6	0.1-0.4	50mM Na <sup>+</sup>

The values of CMC given are for the temperature range between 20 °C and 25 °C.

### III.5. References.

- 
- 1 J. M. Sanderson and S. Yazdani, *Chem. Commun.*, 2002, 1154.
  - 2 H. M. Berman, J. Westbrook, Z. Feng, G. Gilliland, T. N. Bhat, H. Weissig, I. N. Shindyalov and P. E. Bourne, *Nucleic Acids Res.*, **28**, 2000, 235.
  - 3 H. Saito, *Chem. Phys. lipids*, **123**, 2004, 101-112.
  - 4 J. Fiaux, E. B. Bertelsen, A. L. Horwich and K. Wuthrich, *Nature*, **418**, 2002, 207-211.
  - 5 R. Riek, J. Fiaux, E. B. Bertelsen, A. L. Horwich and K. Wuthrich, *J. Am. Chem. Soc.*, **124**, 2002, 12144-12153.
  - 6 M. Behlau, D. J. Mills, H. Quader, W. Kuhlbrandt and J. Vonck, *J Mol. Biol.*, **305**, 2001, 71-77.
  - 7 W. Kuhlbrandt, *Quarterly Reviews of Biophysics*, **25**, 1992, 1-49.
  - 8 E. Van den Brink-Van der Laan, V. Chupin, J. A. Killian and B. de Kruijff, *Biochemistry*, **43**, 2004, 4240-4250.
  - 9 M. Calamai, N. Taddei, M. Stefani, G. Ramponi and F. Chiti, *Biochemistry*, **42**, 2003, 15078-15083.
  - 10 M. Bannwarth and G. E. Schulz, *Biochim. Biophys. Acta*, **1610**, 2003, 37-45.
  - 11 J. Zhuang, G. G. Prive, G. E. Werner, P. Ringler, H. R. Kaback and A. Engel, *J. Struct. Biol.*, **125**, 1999, 63-75.
  - 12 E. Veiga, E. Sugawara, H. Nikaido, V. de Lorenzo and L. A. Fernandez, *EMBO J.*, **21**, 2002, 2122-2131.

- 
- 13 H. Rogl, K. Kosemund, W. Kuhlbrandt and I. Collinson, *FEBS Letters*, **432**, 1998, 21-26.
- 14 K. Hill, K. Model, M. T. Ryan, K. Dietmeier, F. Martin, R. Wagner, N. Pfanner, *Nature*, **395**, 1998, 516-521.
- 15 E. De Bernadez-Clark, E. Schwars and R. Rudolph, *Methods Enzymol.*, **309**, 1999, 217-236.
- 16 P. N. Tyminski, L. H. Latimer and D. F. O'Brien, *Biochemistry*, **27**, 2696-2705.
- 17 M. J. Ellis, H. Hebert and M. Thelestam, *J. Struct. Biol.*, **118**, 1997, 178-188.
- 18 A. Schouten, B. Agianian, J. Westerman, J. Kroon, K. W. A. Wirtz and P. Gros, *EMBO J.*, **21**, 2002, 2117-2121.
- 19 R. P. Goncalves, J. Busselez, D. Levy, J. Seguin and S. Scheuring, *J. Struct. Biol.*, **149**, 2005, 79-86.
- 20 N. Ruiz, S. Merino, M. Vinas, O. Domenech, M. T. Montero and J. Hernandez-Borrell, *Biophys. Chem.*, **111**, 2004, 1-7.
- 21 T. Walz and R. Ghosh, *J. Mol. Biol.*, **265**, 1997, 107-111.
- 22 B. Schmid, M. Kromer and G. E. Schulz, *FEBS Letters*, **381**, 1996, 111-114.
- 23 C. A. Mannella, *Science*, **224**, 1984, 165-166.
- 24 A. Davies, G. F. X. Schertler, B. E. Gowen and H. R. Saibil, *J. Struct. Biol.*, **117**, 1996, 36-44.

- 
- 25 T. Odahara, *Biochim. Biophys. Acta*, **1660**, 2004, 80-92.
- 26 H. J. Snijder, P. A. Timmins, K. H. Kalk and B. W. Dijkstra, *J. Struct. Biol.*, **141**, 2003, 122-131.
- 27 M. Dolder, A. Engel and M. Zulauf, *FEBS Letters*, **382**, 1996, 203-208.
- 28 C.-C. Yin, H. Han, R. Wei and F. A. Lai, *J. Struct. Biol.*, **149**, 2005, 219-224.
- 29 M. Behlau, D. J. Mills, H. Quader, W. Kuhlbrandt and J. Vonck, *J. Mol. Biol.*, **305**, 2001, 71-77.
- 30 T. Walz, B. L. Smith, M. L. Zeidel, A. Engel and P. Agre, *J. Biol. Chem.*, **269**, 1994, 1583-1586.
- 31 H. de Cock, S. Van Blokland and J. Tommassen, *J. Biol. Chem.*, **271**, 1996, 12885-12890.
- 32 D. A. Koppel, K. W. Kinnally, P. Masters, M. Forte, E. Blachly-Dyson and C. Mannella, *J. Biol. Chem.*, **273**, 1998, 13794-13800.
- 33 L. Hasler, J. B. Heymann, A. Engel, J. Kistler and T. Walz, *J. Struct. Biol.*, **121**, 1998, 162-171.
- 34 E. J. Boekema, *Electron Microsc. Rev.*, **3**, 1990, 87-96.
- 35 R. C. Ford, A. Hefti and A. Engel, *EMBO J.*, **9**, 1990, 3067-3075.
- 36 J. P. Dekker, S. D. Betts, C. F. Yocum and E. J. Boekema, *Biochemistry*, **29**, 1990, 3220-3225.
- 37 B. K. Jap, *J. Mol. Biol.*, **205**, 1989, 407-419.

- 
- 38 M. T. Paternostre, M. Roux and J. L. Rigaud, *Biochemistry*, **27**, 1988, 2668-2677.
- 39 P. Wingfield, T. Arad, K. Leonard and H. Weiss, *Nature*, **280**, 1970, 696-697
- 40 D. L. Dorset, A. Engel, M. Haner, A. Massalski and J. P. Rosenbusch, *J. Mol. Biol.*, **165**, 1983, 701-710.
- 41 A. Engel, A. Massalski, H. Schindler, D. L. Dorset and J. P. Rosenbusch, *Nature*, **317**, 1985, 643-645.
- 42 B. K. Jap, *J. Mol. Biol.*, **199**, 1988, 229-231.
- 43 J. Dietrich and W. Kuhlbrandt, *FEBS Letters*, **463**, 1999, 97-102.
- 44 J. L. Rigaud, B. Pitard and D. Levy, *Biochim. Biophys. Acta*, **1231**, 1995, 223-246.
- 45 I. Reviakine, W. Bergsma-Schutter, and A. Brisson, *J. Struct. Biol.*, **121**, 1998, 356-361.
- 46 D. Levy, G. Mosser, O. Lambert, G. S. Moeck, D. Bald and J. L. Rigaud, *J. Struct. Biol.*, **127**, 1999, 44-52.
- 47 D. Levy, M. Chami, J. L. Rigaud, *FEBS Letters*, **504**, 2001, 187-193.
- 48 L. Lebeau, F. Lach, C. Venien-Bryan, A. Renault, J. Dietrich, T. Jahn, M. G. Palmgren, W. Kuhlbrandt and C. Mioskowski, *J. Mol. Biol.*, **308**, 2001, 639-647.
- 49 J. L. Rigaud, M. T. Paternostre, and A. Bluzat, *Biochemistry*, **27**, 1988, 2677-2688.



- 
- 50 J. L. Rigaud, G. Mosser, J. J. Lacapere, A. Olofsson, D. Levy and J. L. Ranck, *J. Struct. Biol.*, **118**, 1997, 226-235.
- 51 P. J. L. Werten, H.-W. Remigy, B. L. de Groot, D. Fotiadis, A. Philippsen, H. Stahlberg, H. Grubmuller and A. Engel, *FEBS Letters*, **529**, 2002, 65-72.
- 52 L. Lebeau, S. Nuss, P. Schultz, P. Oudet, and C. Mioskowski, *Chem. Phys. Lipids*, **103**, 1999, 37-46.
- 53 R. H. Haschemeyer, R. J. Myers, *In Principals and Techniques of Electron Microscopy*, Eds. M. S. Hayat, New York: Van Nostrand Reinhold, pp.101-150. 1972.
- 54 P. J. Goodhew, J. Humphreys and R. Beauland, *Electron microscopy*, Eds. Taylor and Francis, CRC press, 2001.
- 55 J. M. Valpuesta, R. Henderson and T. G. Frey, *J. Mol. Biol.*, **214**, 1990, 237-251.
- 56 B. K. Jap, M. Zulauf, T. Scheybani, A. Hefti, W. Baumeister, U. Aepli and A. Engel, *Ultramicroscopy*, **46**, 1992, 45-85.
- 57 H. Stahlberg, D. Fotiadis, S. Scheuring, H. Remigy, T. Braun, K. Mitsuoka, Y. Fujiyoshi and A. Engel, *FEBS Letters*, **504**, 2001, 166-172.
- 58 W. O. Saxton, T. J. Pitt and M. Horner, *Ultramicroscopy*, **4**, 1979, 343-353.
- 59 L. A. Amos, R. Henderson and P. N. T. Unwin, *Prog. Biophys. Mol. Biol.*, **39**, 1982, 182-231.
- 60 J. Yang, J. Mou and Z. Shao, *FEBS Letters*, **338**, 1994, 89-92.
- 61 A. Engel and D. J. Muller, *Nature Struct. Biol.*, **7**, 2000, 715-718.

- 
- 62 J. Yang, J. Mou and Z. Shao, *FEBS Letters*, **338**, 1994, 89-92.
- 63 D. J. Muller, M. Amrein and A. Engel, *J. Struct. Biol.*, **119**, 1997, 172-188.
- 64 D. M. Czajkowsky, S. Sheng and Z. Shao, *J. Mol. Biol.*, **276**, 1998, 325-330.
- 65 D. J. Muller, D. Fotiadis, S. Scheuring, S. A. Muller and A. Engel, *Biophys. J.*, **76**, 1999, 1101-1111.
- 66 D. Sarid, *Scanning Force Microscopy*, 1991, Oxford University Press.
- 67 A. Engel and D. Muller, *Nature Struct. Biol.*, **7**, 2000, 715-717.
- 68 C. Moller, M. Allen, V. Elings, A. Engel and D. J. Muller, *Biophys. J.*, **77**, 1999, 1150-1156.
- 69 S. Scheuring, D. J. Muller, P. Ringler, J. B. Heymann and A. Engel, *J. Microsc.*, **193**, 1999, 28-35.
- 70 D. Fotiadis, D. J. Muller, G. Tsiotis, L. Hasler, P. Tittmann, T. Mini, P. Jenö, H. Gross and A. Engel, *J. Mol. Biol.*, **283**, 1998, 83-94.
- 71 A. D. Ferguson, W. Welte, E. Hofmann, B. Lindner, O. Holst, J. W. Coulton and K. Diederichs, *Structure*, **8**, 2000, 585-592.
- 72 K. Zeth, K. Diederichs, W. Welte and H. Engelhardt, *Structure*, **8**, 2000, 981-992.
- 73 I. R. Henderson, F. Navarro-Garcia and J. P. Nataro, *Trends Microbiol.*, **6**, 1998, 370-378.

- 
- 74 C. Locht, R. Antoine and F. Jacob-Dubuisson, *Curr. Opin. Microbiol.*, **4**, 2001, 82-89.
- 75 J.L. Shannon and R. C. Fernandez, *J. Bacteriology*, **181**, 1999, 5838-5842.
- 76 M. R. Yen, C. R. Peabody, S. M. Partovi, Y. Zhai, Y. H. Tseng and M. H. Saier, *Biochim. Biophys. Acta*, **1562**, 2002, 6-31.
- 77 C. Oliver, G. Huang and R. C. Fernandez, *J. Bacteriology*, **2**, 2003, 489-495.
- 78 D. Thanassi and S. J. Hultgren, *Curr. Opin. Cell Biol.*, **12**, 2000, 420-430.
- 79 M. Desvaux, N. J. Parham and I. R. Henderson, *Res. Microbiol.*, **155**, 2004, 53-60.
- 80 D. C. Oliver, G. Huang, E. Nodel, S. Pleasance and R. C. Fernandez, *Mol. Microbiol.*, **47**, 2003, 1367-1383.
- 81 D. Drew, L. Froderberg, L. baars and J.-W. L. de Gier, *Biochim. Biophys. Acta*, **1610**, 2003, 3-10.
- 82 R. C. Fernandez and A. A. Weiss, *Infect. Immun.* **62**, 1994, 4727-4738.
- 83 Molecular Biology, P. C. Turner, A. G. McLennan, A. D. Bates and M. R. H. White, pp 116-121, 2nd edition, Bios Scientific Ltd, 2000.
- 84 D. N. Wang, M. Scafferling, M. J. Lemieux, H. Griffith, Y. Chen and X.-D. Li, *Biochim. Biophys. Acta*, **1610**, 2003, 23-36.
- 85 J. Zhuang, G. G. Prive, G. E. Werner, P. Ringler, H. R. Kaback and A. Engel, *J. Struct. Biol.*, **125**, 1999, 63-75.

- 
- 86 Directory of Bioinformatics and Molecular Biology Software for Sequence analysis, Genomics and Proteomics at [http:// www.bioinformatics.vg](http://www.bioinformatics.vg).
- 87 K. Saxena, V. Drosou, E. Maier, R. Benz and B. Ludwig, *Biochemistry*, **38**, 1999, 2206-2212.
- 88 G. Zhou, G. Parthasarathy, T. Somasundaram, A. Ables, L. Roy, S. J. Strong, W. R. Ellington and M. S. Chapman, *Protein Sci.*, **6**, 1997, 444-449.
- 89 Gill and Von Hippel, *Anal. Biochemistry*, **182**, 1989, 319-326.
- 90 L. A. Compton and W. C. Johnson, *Anal. Chem.*, **155**, 1986, 155-167.
- 91 W. J. Johnson, *Proteins Struct. Funct. Genet.*, **35**, 1999, 307-312.
- 92 N. J. Greenfield, *Anal. Chem.*, **235**, 1996, 1-10.
- 93 J. P. Hennessey and W. C. Johnson, *Biochemistry*, **20**, 1981, 1085-1094.
- 94 P. J. Booth, *Biochem. Biophys. Acta*, **1610**, 2003, 51-56.
- 95 J. H. Kleinschmidt and L. K. Tamm, *Biochemistry*, **35**, 1996, 12993-13000.
- 96 N. Dekker, K. Merck, J. Tommassen and H. M. Verheij, *Eur. J. Biochemistry*, **232**, 1995, 214-219.
- 97 G. E. Schulz, *Curr. Opin. Struct. Biol.*, **10**, 2000, 445-447.
- 98 S. K. Buchanan, *Curr. Opin. Struct. Biol.*, **9**, 1999, 455-461.
- 99 W. C. Wimley, K. Hristova, A. S. Ladokhin, L. Silvestro, P. H. Axelsen and S. H. White, *J. Mol. Biol.*, **227**, 1998, 1091-1110.

- 
- 100 C. M. Bishop, W. F. Walkenhorst and W. C. Wimley, *J. Mol. Biol.*, **309**, 2001, 975-988.
- 101 B. Schmid, L. Maveyraud, M. Kromer and G. E. Schulz, *Protein Sci.*, **7**, 1998, 1603-1611.
- 102 A. Engel, A. Massalski, H. Schindler, D. L. Dorset and J. P. Rosenbusch, *Nature*, **317**, 1985, 643-645.
- 103 B. K. Jap, *J. Mol. Biol.*, **199**, 1988, 229-231.
- 104 B. K. Jap, M. Zulauf, T. Scheybani, A. Hefti, W. Baumeister, U. Aepli and A. Engel, *Ultramicroscopy*, **46**, 1992, 45-85.
- 105 The software Image J (1.34n) is available from the National Institute of Health, USA at <http://rsb.info.nih.gov/ij>
- 106 H. A. Rinia, R. A. Kik, R. A. Demel, M. M. E. Snel, J. A. Killian, J. P. J. M. Van der Eerden and B. de Kruijff, *Biochemistry*, **39**, 2000, 5852-5858.
- 107 J. Mou, D. M. Czajkowsky and Z. Shao, *Biochemistry*, **35**, 1996, 3222-3226.
- 108 J. J. Lacapere, D. L. Stokes, A. Olofsson, and J. L. Rigaud, *Biophys. J.*, **75**, 1998, 1319-1329.
- 109 T. Klauser, J. Kramer, K. Otzelberger, J. Pohlner and T. F. Meyer, *J. Struct. Biol.*, **234**, 1993, 579-593.
- 110 S.W. Cowan, at. Schirmer, G. Rummel, M. Steier, R. Ghosh, R. A. Jansonius and J. P. Rosenbusch, *Nature*, **358**, 1992, 727-733.

- 
- 111 T. G. Morrison, *Biochem. Biophys. Acta*, **1614**, 2003, 73-84.
- 112 S. G. Peisajovich and Y. Shai, *Biochem. Biophys. Acta*, **1614**, 2003, 122-129.
- 113 M. J. Conroy, S. J. Jamieson, D. Blakey, T. Kaufmann, A. Engel, D. Fotiadis, M. Merrick and P. Bullough, *EMBO reports*, **5**, 2004, 1153-1158.
- 114 Y. Fang, S. Cheley, H. Bayley and J. Yang, *Biochemistry*, **36**, 1997, 9518-9522.
- 115 N Ruiz, S. Merino, M. Vinas, O. Domenech, M. T. Montero and J. Hernandez-Borrell, *Biophys. Chem.*, **111**, 2004, 1-7.
- 116 J. Mou, J. Yang, Z. Shao, *Biochemistry*, **33**, 1994, 4439-4443.
- 117 H. Rinia, J. W. P. Boots, D. T. S. Rijkers, R. A. Kik, M. M. E. Snel, R. A. Demel, J. A. Killian, J. P. J. M. Van der Eerden and B. de Kruijff, *Biochemistry*, **41**, 2002, 2814-2824.
- 118 D. Muller, H. J. Sass, S. A. Muller, G. Buldt and A. Engel, *J. Mol. Biol.*, **285**, 1999, 1903-1909.
- 119 D. Muller, and A. Engel, *Biophys. J.*, **73**, 1997, 1633-1644.
- 120 D. Muller, and A. Engel, *J. Mol. Biol.*, **285**, 1999, 1347-1351.
- 121 P. Zammaretti, A. Fakler, F. Zaugg and U. E. Spichiger-Keller, *Anal. Chem.*, **72**, 2000, 3689-3695.
- 122 P. J. L. Werten, H.-W. Remigy, B. L. de Groot, D. Fotiadis, A. Philippsen, H. Stahlberg, H. Grubmuller and A. Engel, *FEBS Lett.*, **529**, 2002, 65-72.



- 
- 123 G. G. Prive, G. E. Verner, C. Weitzman, K. H. Zen, D. Eisenberg and H. R. Kevin, *Acta Cryst.*, **D50**, 1994, 375-379.
- 124 P. Quian, C. Neil Hunter and P. A. Bullough, *J. Mol. Biol.*, **349**, 2005, 948-960.
- 125 G. G. Shipley, *Curr. Opin. Struct. Biol.*, **10**, 2000, 471-473.
- 126 M. Caffrey, *Curr. Opin. Struct. Biol.*, **10**, 2000, 486-497.
- 127 Biochemistry LabFax, J. A.A Chambers and D. Rickwood, Eds., Bios Scientific Publishers, Oxford, Academic Press. 1993.
- 128 A guide to the properties and uses of detergents in biology and biochemistry, Calbiochem company handbook, 1987.
- 129 A. Helenuis, D. R. McCaslin, E. Fries and C. Tanford, *Methods Enzymol.*, **56**, 1979, 734-749.

## Chapter IV

### IV.1. Analytical studies of the interactions of the perfluorinated alcohol, hexafluoroisopropanol, with phospholipid membranes.

#### IV.1.1. Introduction.

Hexafluoroisopropanol, HFIP is a solvent commonly used, alongside trifluoroethanol,<sup>1</sup> in conformational and structural studies of peptides and proteins. This short chain, bulky alcohol with its six fluorine substituents is particularly efficient at solvating hydrophobic macromolecules such as the amphiphilic synthetic peptides described in chapter II.

Perfluorinated amphiphiles, such as HFIP, have unique properties due to their weak intermolecular interactions and higher conformational rigidity than their non fluorinated hydrocarbon and alcohol counterparts; the fluoroalkyl groups give a strong amphiphilic character to the alcohol molecule.<sup>2</sup> HFIP is miscible with water and has a high affinity for hydrophobic environments such as lipid membranes; its dual properties are attributed to the creation of a hydrophobic microenvironment in aqueous media.<sup>3</sup>

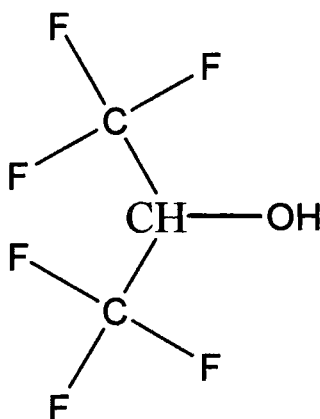


Figure IV.1.1. [1,1,1,3,3,3-hexafluoroisopropanol] (HFIP).

Before carrying out biophysical measurements on the interactions of the amphiphilic synthetic peptides with phospholipid membranes, using HFIP as the most efficient solvent for the amphiphilic peptides, a thorough understanding of the effects of HFIP on the phospholipid membranes was considered a crucial preliminary investigation in this analytical project.<sup>4,5</sup>

A study on the effect of a range of small alcohol molecules on the stability of phospholipid membranes, which had been carried out using Fluorescence Marker Release and  $^2\text{H}$  NMR experiments, revealed that of all the alcohols analysed, HFIP had the most potent effect on the phospholipid membranes.<sup>6</sup> This high affinity of HFIP for lipid membranes had also been observed during some preliminary work carried out on the analysis of liposomes by Raman spectroscopy.<sup>7</sup>

In the present study a wide range of analytical techniques:  $^{19}\text{F}$  NMR, Fluorescence Marker Release, Differential Scanning Calorimetry (DSC), Small Angle X-ray Scattering (SAXS), Pressure-Area Isotherms (Langmuir Blodgettry), Laser light scattering and Electron Microscopy were all explored in order to gain as comprehensive a view as possible of the interactions of HFIP with phospholipid membranes, without losing sight of the main research project.

#### IV.1.2. Investigation of the effects of HFIP on phospholipid membranes.

The affinity of HFIP for phospholipid membranes was first assessed by  $^{19}\text{F}$  NMR analysis by monitoring changes in the signal intensity of HFIP as a function of lipid concentration with reference to the fluoride ion, which was assumed not to partition into the lipid membranes.

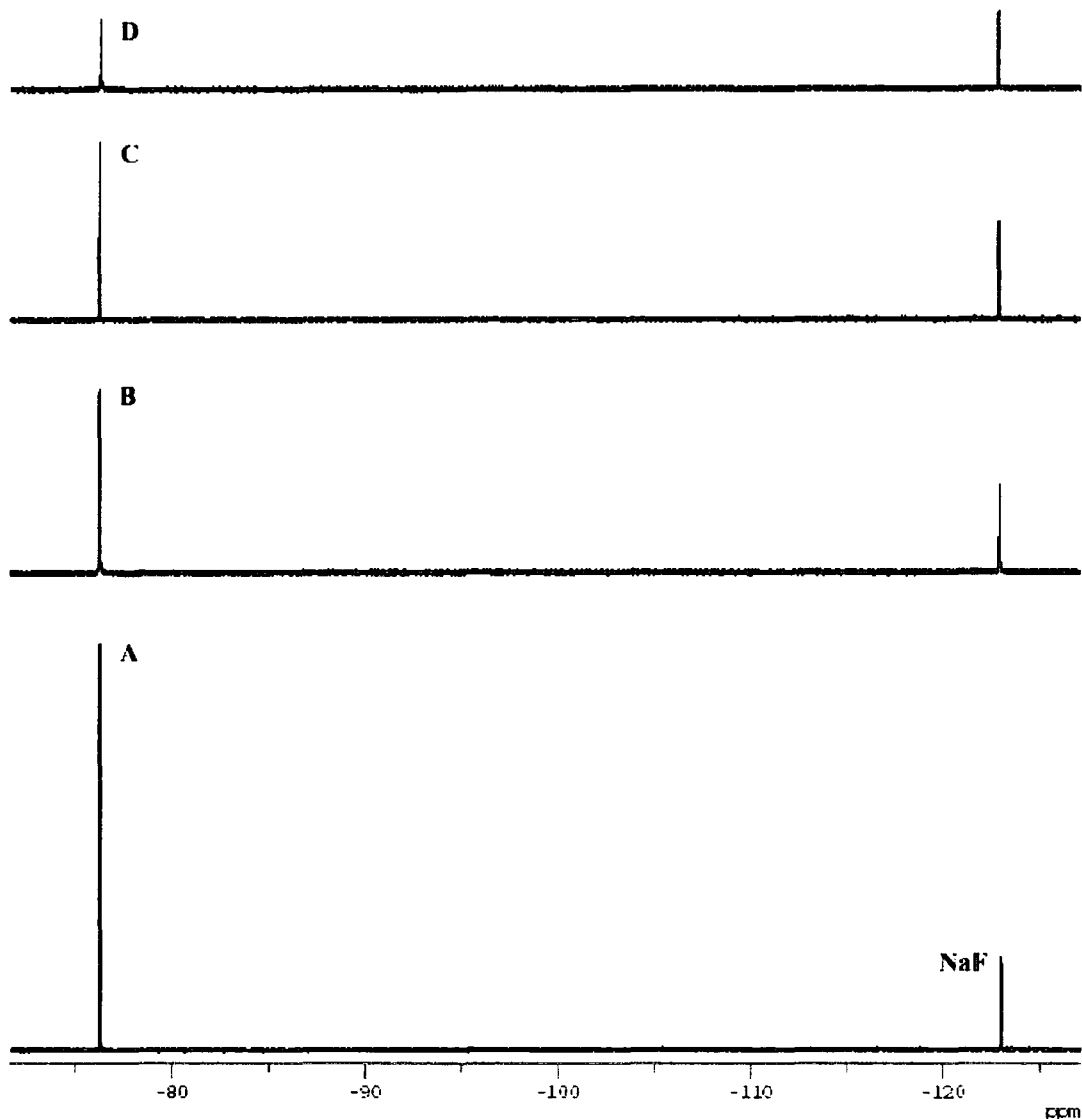


*Figure IV.1.2.  $^{19}\text{F}$  NMR spectra of HFIP-DMPC and HFIP-DOPC preparations performed in  $\text{D}_2\text{O}$  at 376 MHz: A, 1 % HFIP; B,  $[\text{HFIP}]/[\text{DOPC}] = 2:1$ ; C,  $[\text{HFIP}]/[\text{DMPC}] = 2:1$  and D,  $[\text{HFIP}]/[\text{DMPC}] = 1:1$ .*

Multilamellar vesicles of a fully saturated and a monounsaturated phospholipid, dimyristoyl phosphatidylcholine, DMPC and dioleoyl phosphatidylcholine, DOPC respectively, were used to investigate the effect of bilayer fluidity on the ability of HFIP to partition into phospholipid membranes. Multilamellar vesicles hydrated in deuterated water, D<sub>2</sub>O were added in a 1:1 and a 1:2 molar ratio relative to the concentration of HFIP, to a solution containing both HFIP and sodium fluoride, NaF. The volume of HFIP (1 % v/v) and the concentration of NaF (0.3 M) were kept constant throughout the experiment.

<sup>19</sup>F NMR spectroscopic analysis of the free HFIP molecules produced a sharp doublet at -76.23 ppm, which showed a clear decrease in intensity as the concentration of lipid in the sample was increased; a much boarder signal was produced as a function of HFIP partitioning in to the lipid, which was superimposed on the signal for the free HFIP (Figure IV.1.2.).

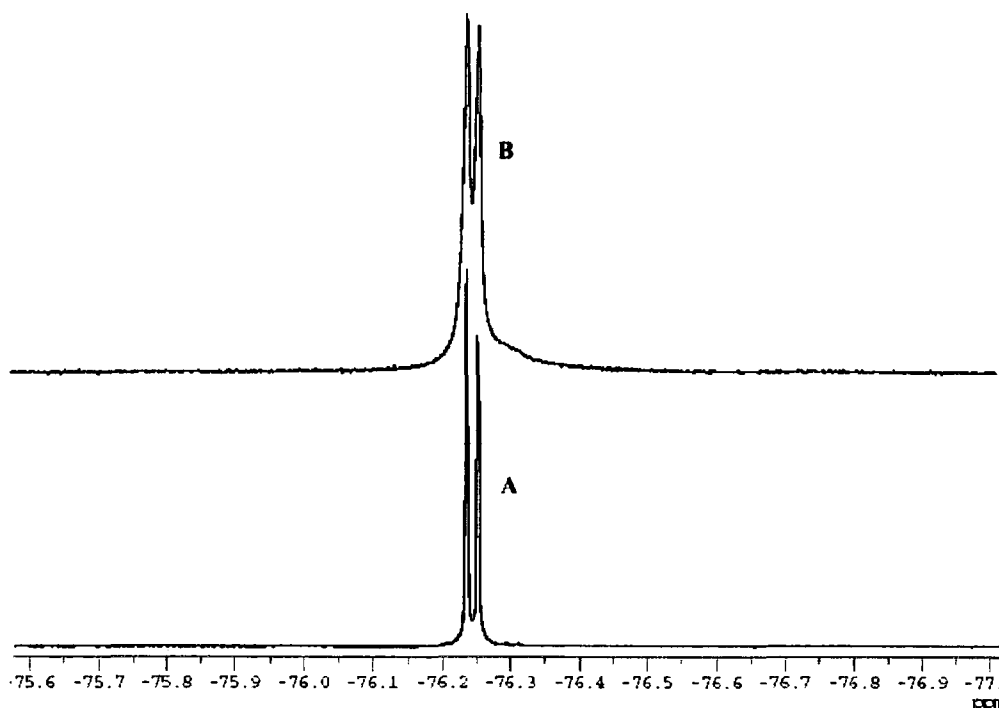


*Figure IV.1.3. Expanded section of <sup>19</sup>F NMR spectra recorded in D<sub>2</sub>O at 376 MHz of: A, a 1% solution of HFIP and B, a 1:1 molar ratio of HFIP/DMPC.*

A lipid-water partition coefficient,  $K_{LW}$  for HFIP was then estimated from the intensities of the free HFIP and lipid bound HFIP molecules according to:

$$K_{LW} = [W] I_L / [L]_T I_B$$

*Where  $[W]$  is the concentration of  $D_2O$ ,  $I_L$  is the signal intensity of the lipid bound HFIP,  $[L]_T$  is the concentration of lipid in the sample and  $I_B$  is the signal intensity of free HFIP in the aqueous phase.*

The partition coefficient,  $K_{LW}$  for HFIP partitioning into the saturated lipid, DMPC was estimated as 460 and for the monounsaturated, DOPC, as 660. These values are indicative of the very high affinity of the perfluorinated alcohol for phospholipid membranes, considering that the non fluorinated alcohol, isopropanol only has a  $K_{LW}$  value of 1.8 and that halothane has a coefficient of 200.<sup>8</sup> This  $^{19}F$  NMR study has also exposed a considerable difference in HFIP partition coefficients for the saturated and monounsaturated phospholipids, which reveals a far greater affinity of HFIP for the more fluid unsaturated membrane, DOPC.

The partitioning of HFIP into phospholipid bilayers was shown in a separate  $^{19}F$  NMR experiment to be fully reversible; following dialysis of the lipid-HFIP mixtures against deuterated water, the presence of HFIP appeared to have been completely eliminated from the samples.

#### **IV.1.3. (Fluorescence) Marker Release experiments.**

The extent of HFIP interaction with phospholipids membranes was probed through marker release experiments by encapsulating a fluorescent marker, carboxyfluorescein, CF into phospholipid liposomes and monitoring the fluorescence emission intensity immediately after HFIP addition to a solution of CF containing liposomes.



Carboxyfluorescein, CF was encapsulated into liposomes at concentrations above which the fluorescence marker was self quenching (>35 mM); significant increases in fluorescence intensity were observed once the integrity of the lipid bilayer was breached and the marker diluted in to the aqueous media surrounding the liposomes.

Aliquots of HFIP were added to a liposome suspension producing the release of short bursts of fluorescence marker, as indicated by an increase in fluorescence intensity, monitored at an emission wavelength of 518 nm following excitation at 491 nm; after an initial increase, fluorescence intensity remained stable between each new HFIP addition. Total CF release was assumed after addition of 1 % (v/v) of Triton X-100, a non-ionic detergent to the HFIP-CF-liposome mixture in the sample cell and the percentage release of CF was then calculated using the following equation:

$$\% \text{ release} = 100 * (F_s - F_o) / (F_m - F_o)$$

*Where  $F_s$  is the measured steady state emission signal at the start of the experiment;  $F_m$  is the emission following addition of Triton X-100 and  $F_o$  is the emission after addition of HFIP.*

Addition of aliquots of 0.03 % (v/v) of HFIP appeared to create a transient disruption to the liposomal membrane and enabled leakage of encapsulated CF for a short period after HFIP addition, following which no further increase in intensity was observed.

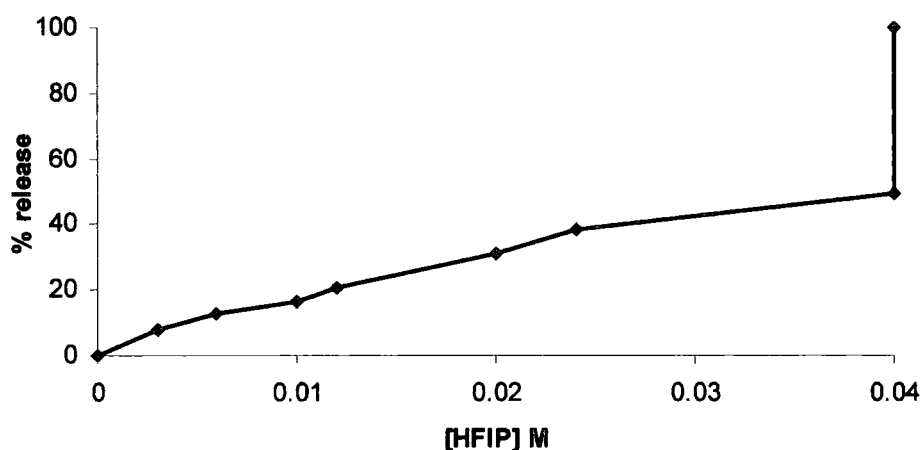


*Figure IV.1.4. Release of encapsulated CF (>35mM) from EPC liposomes, (0.05 mg ml<sup>-1</sup> in Tris (10mM)-NaCl (150mM) Buffer, pH 7.4) following addition of HFIP.*

The reverse process, which was carried out by addition of aliquots of CF encapsulated liposomes to a HFIP-buffer solution, gave very similar results, indicating that CF release was not due to inefficient HFIP-lipid mixing producing localized areas of high concentrations of HFIP.

The fluorinated alcohol induced disturbance in phospholipid membranes, as shown by the marker release experiments, was further examined by Differential Scanning Calorimetry (DSC) on HFIP-DMPC systems.

#### IV.1.4. Differential Scanning Calorimetry.

A Differential Scanning Calorimetric analysis of the effect of HFIP on multilamellar vesicles of DMPC, revealed that the fluorinated alcohol had a considerable impact on the DMPC bilayer system at low concentrations, ranging from 2 mM to 0.05 M and corresponding to HFIP/lipid molar ratios of 0.05 to 0.12 respectively.

Following addition of only 2 mM HFIP, the pre-transition,  $T_p$  could no longer be observed in the DSC thermogram and there was a marked decrease in both the temperature and enthalpy change of the main phase transition,  $T_m$  corresponding to the change from a gel to a liquid-crystalline state.<sup>9</sup>

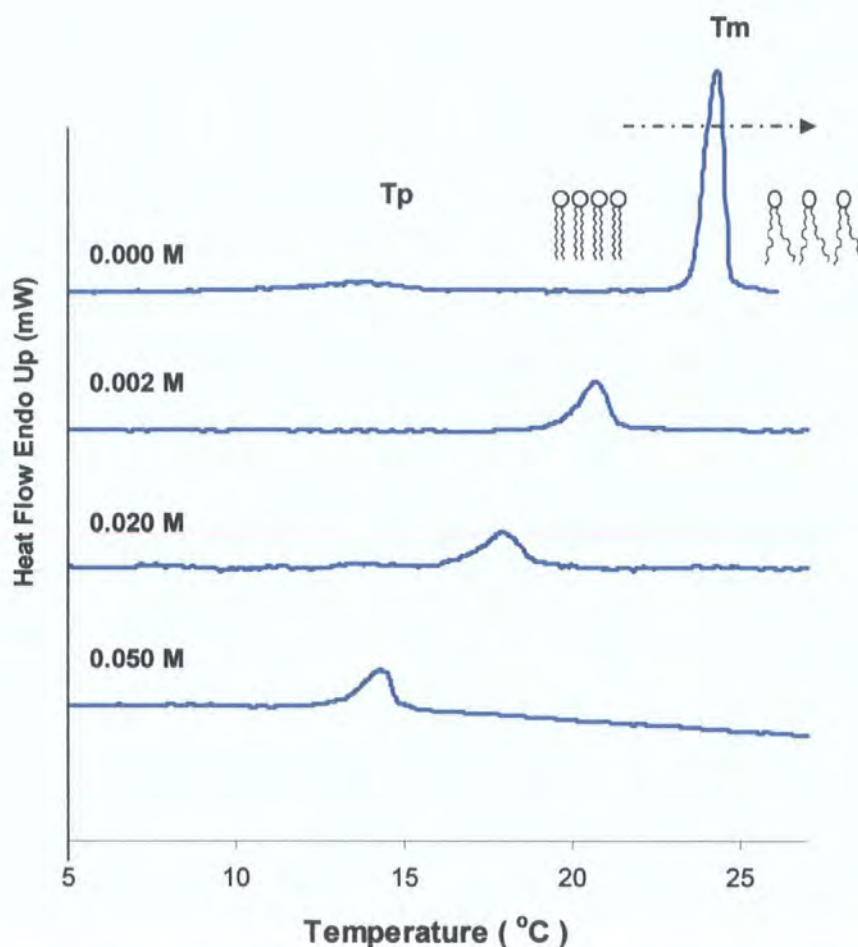
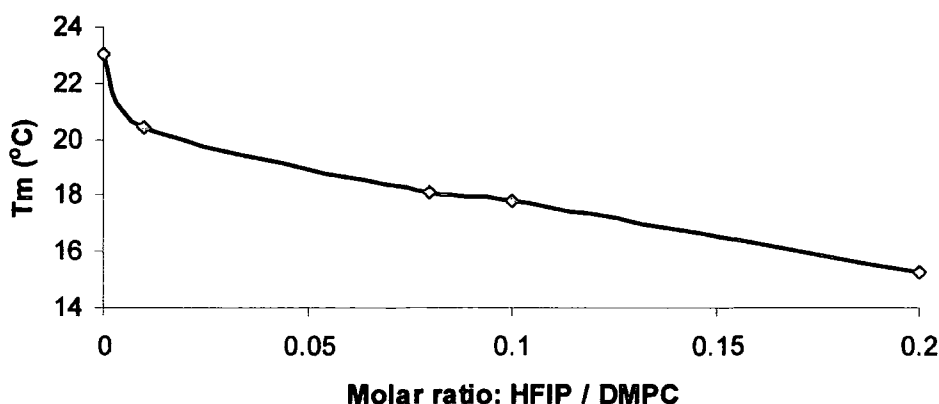


Figure IV.1.5. DSC thermograms showing the effect of HFIP, from 2 mM to 0.05 M on fully hydrated MLVs of DMPC; HFIP/DMPC molar ratios were 0.5 %, 5 % and 12 % respectively.

The enthalpy change for the main transition decreased by ~50 % of its original value on interaction of DMPC multilamellar vesicles at an initial HFIP concentration of 0.02 M (MR: 0.05), but then only decreased slightly further on addition of higher HFIP concentrations, up to 0.05 M (MR: 0.12). The effect of HFIP on the main transition temperature followed a concentration dependent trend, with a decrease of 3-4 °C at 0.02 M HFIP, which continued as the concentration of HFIP was further increased, to reach a reduction in temperature of 8-9 °C at the highest concentration examined of 0.05 M HFIP.



*Figure IV.1.6. The variation of phase transition temperature,  $T_m$  as a function of the increase in HFIP / DMPC molar ratios.*

This DSC study has clearly demonstrated that HFIP has a significant effect at low concentrations on the DMPC bilayer system, which is indicative of incorporation of the bulky fluorinated alcohol molecules into the phospholipid membrane; causing considerable disruption to the ordering and packing of the lipid monomers. This strongly suggests that once integrated in the lipid bilayer, HFIP could locate in the head group region of the bilayer, which would force the lipid chains further apart and substantially reduce their interactions; thereby increasing the fluidity of the bilayer resulting in the significant decrease in transition temperature observed in this study.

The lipid head group region is believed to be the preferred location for many other alcohol molecules including the fluorinated alcohol, TFE.<sup>6</sup>

Integration of the bulky fluorinated alcohol molecule, in to the glycerol part of the phospholipid head group region, would allow for hydrogen bonding between a HFIP hydroxyl group and an oxygen atom on the lipid phosphate group and could potentially accommodate at least two HFIP molecules.

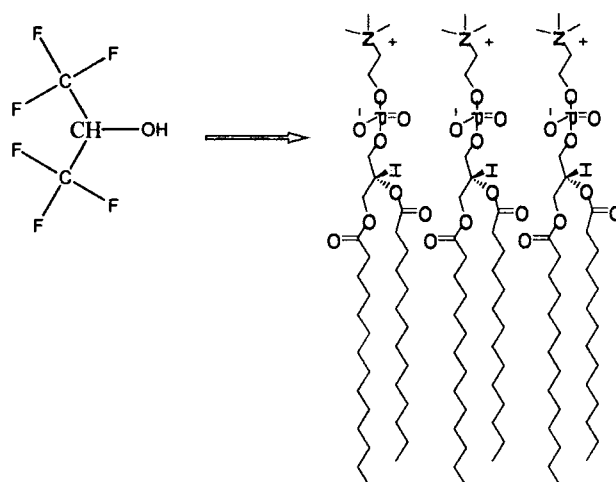


*Figure IV.1.7. Diagram showing suggested location of HFIP in phospholipid bilayers. The hydroxyl group of a HFIP molecule would form a hydrogen bond with an oxygen atom on the phosphate group.*

Perturbations created in saturated phospholipid bilayers by drugs and amphiphilic peptides at [introduced molecule] / [lipid] molar ratios of 10 % tend to affect the temperature of the main transition by only 1-2 °C. The smaller alcohol molecule, ethanol, which is also believed to integrate in the lipid head group region of saturated phospholipid bilayers, induces a shift in main transition temperature of around 2 °C, but this shift is produced at concentrations around 500 times those used in this study.<sup>10,11,12,13,14</sup>

### IV.1.5. Small Angle X-ray Scattering, SAXS.

Small Angle X-ray Scattering (SAXS) experiments were carried out over a similar range of HFIP/lipid molar ratios as those used in the DSC analysis, in order to explore further the interactions of HFIP with phospholipid membranes and to study their effect on the periodicity and the stability of the bilayer system.

A monounsaturated phospholipid, DOPC, with a main phase transition temperature of around  $-20^{\circ}\text{C}$  was used alongside the saturated phospholipid, DMPC ( $T_m \sim 23^{\circ}\text{C}$ ) to determine whether the effect of HFIP on the bilayer could be influenced by the phase of the bilayer.

#### IV.1.5.1. Description of the technique.

Small Angle X-ray Scattering, is a well established technique used for studying structural features of colloidal dimensions, from a few thousand to tens of Ångstroms (Å) in diameter. The periodicity of the lamellar structure, the contrast between the bilayers and the solution in a sample gives rise to small angle X-ray scattering on exposure to X-ray radiation.<sup>15,16,17,18,19</sup>

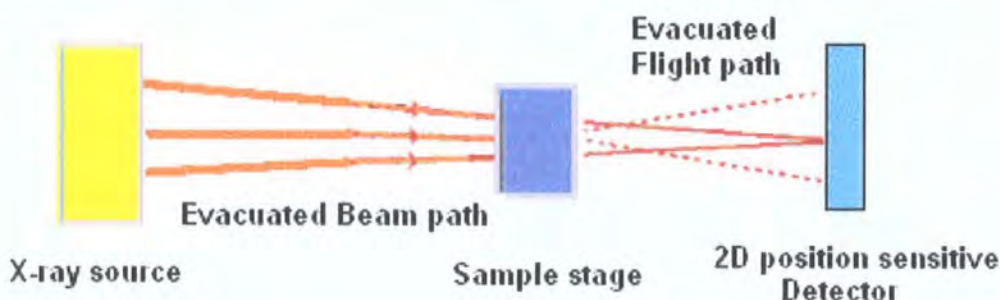


*Figure IV.1.8. Diagram of the basic components of an SAXS diffractometer.*

The X-rays are produced when an accelerated beam of electrons (by a high voltage ~40 000 volts) are directed toward a metal target and strike it with enough energy to ionize a few of the metal 1s electrons. An electron from a higher 2p or 3p shell will drop down to fill the 1s vacancy and release energy as X-rays in the process.

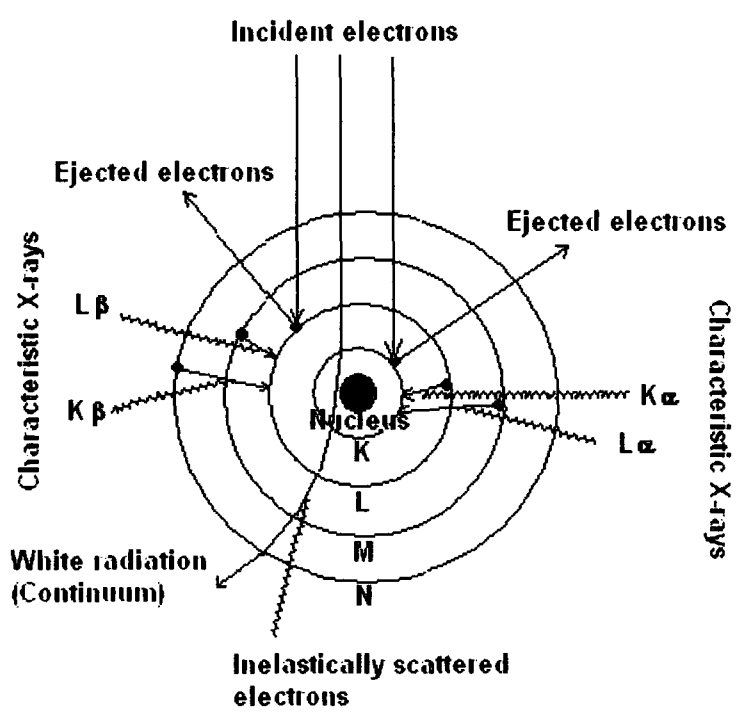


Figure IV.1.9. Diagram showing the production of X-rays.

When a low divergent beam of X-rays is focused on a sample, the electrons within the sample resonate at the frequency of the X-rays that are passing through and emit secondary waves that interfere with each other; the maximum scattering and hence the strongest signal is observed when all the waves are exactly in phase and in the direction of zero scattering angle. Coherent scattering arises from the inhomogeneous electron density within the sample and is produced at small angles for particles that are much larger than the X-ray wavelength (Cu K $\alpha$  -1.542 Å).



The angular range over which scattering is observed is quite small, typically from 0.1° to 5° (2 $\theta$ ). SAXS, like all other scattering processes, is governed by a reciprocal law that shows an inverse relationship between the sample particle size and the scattering angle.<sup>20</sup>

#### **IV.1.5.2. X-ray scattering data collection and processing.**

HFIP was added to fully hydrated multilamellar phospholipid vesicles (9 % w/v lipid content in pure water) over a small range of concentrations from 5.00 mM to 0.04 M corresponding to HFIP/lipid molar ratios of 0.03 to 0.25 respectively. The HFIP-lipid samples were injected into a quartz capillary placed in a sample holder in the path of the beam; the position of the sample was then adjusted by measuring the intensity of scattered transmission (by a glassy carbon) through the sample. Following collection, the sample and background scattering data were radially averaged and integrated; a transmission factor was calculated to correct sample data for background scattering and the intensity of the scattering data, measured in number of counts, was normalised to counts s<sup>-1</sup> against the collection time.

The transmission factor,  $\tau$ , for the sample was calculated from:

$$\tau_{\text{sample}} = I_{\text{sample}} - (\tau_{\text{GC}} * I_{\text{sample}}) / I_{\text{CG}} - (\tau_{\text{GC}} * I_{\text{Background}})$$

*where I is intensity and CG is the transmission through the glassy carbon.*

Correction for scattering was performed using:

$$I_{\text{normalised}} = I_{\text{sample}} - (\tau_{\text{sample}} * I_{\text{Background}})$$

The corrected scattering data was then shown as a plot of intensity against scattering vector,  $Q$ , from which information about bilayer repeat distance and bilayer thickness could be deduced.

The lamellar repeat distance,  $D$ , was calculated from the peak position of the diffracted X-rays using the Bragg equation:

$$2D \sin\theta = n\lambda$$

$$\text{and } Q = 4\pi \sin\theta / \lambda$$

$$\text{therefore } Q = 2\pi / D \text{ and } D = 2\pi / Q.$$

*Where  $n$  is an integer,  $\lambda$  is the monochromatic x-ray wavelength of 1.5418 Å and  $\sin\theta$  is the scattering angle.*

#### IV.1.5.3. SAXS from HFIP-DMPC systems.

The scattering data collected for HFIP-DMPC systems collected over a range of HFIP to lipid molar ratios, from 0.00 to 0.25 were characterized by a main reflection at 0.097 Q and a second order reflection at 0.194 Q. The shape, width and height of the subsidiary peak are more sensitive to small changes within the sample than those of the maximum peak.<sup>21</sup>

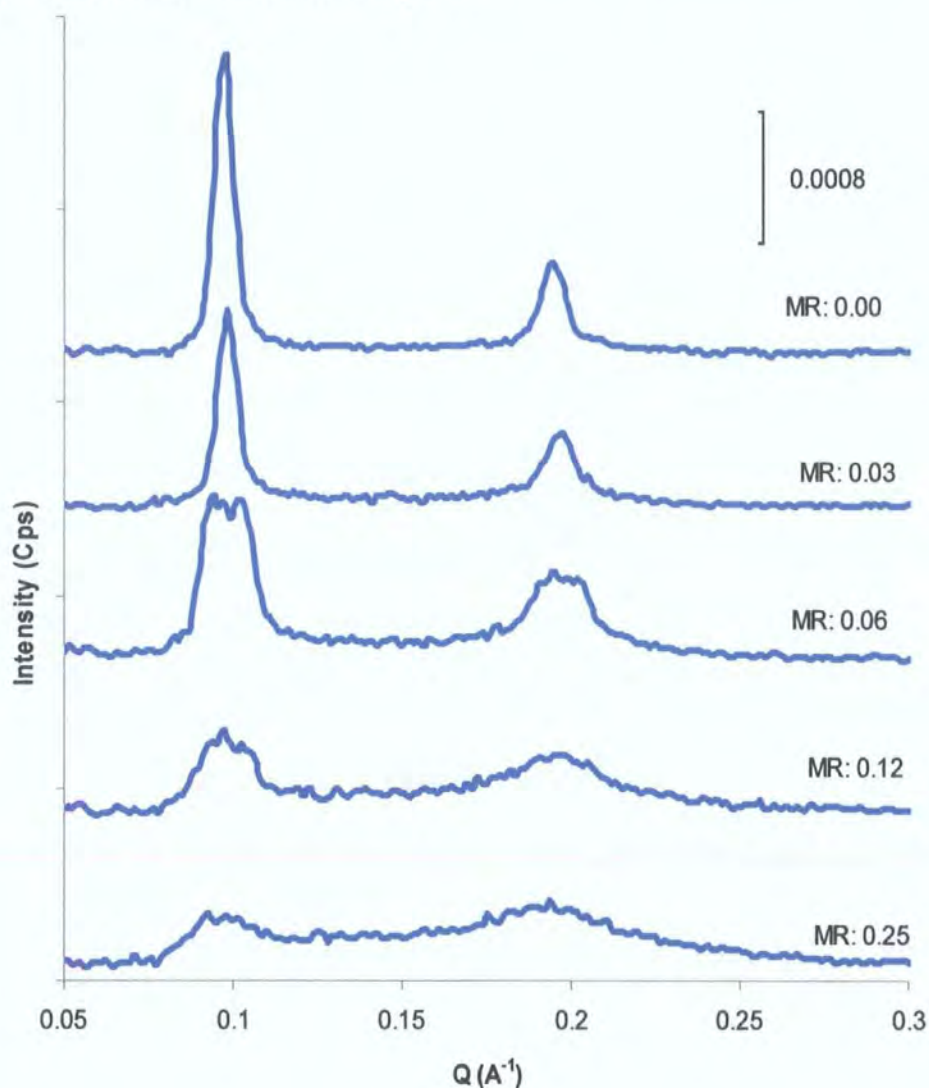


*Figure IV.1.10. The X-ray patterns for HFIP-DMPC systems were measured over a range of HFIP/DMPC molar ratios, MR from 0.03 to 0.25. [lipid]: 0.15 M and [HFIP] from: 0.005 M to 0.040 M. SAXS data were collected at 20 °C. The scale bar corresponds to the intensity in units of counts s<sup>-1</sup> (Cps).*

The intensity of both the main and the second order reflections for the fully hydrated saturated phospholipid changed considerably on addition of HFIP, over the range of HFIP to lipid molar ratios analysed.

The Small Angle X-ray Scattering data for HFIP to DMPC molar ratio of 0.03 showed a significant reduction in intensity for both the main and second order reflections as well as a slight decrease in the width of the second order reflection.

Increasing the HFIP concentration, to a HFIP to lipid molar ratio of 0.06, produced only a small reduction in the intensity, but quite a marked increase in the width of both reflections. A further increase to a molar ratio of 0.12 revealed a considerable decrease in the intensity accompanied by a significant broadening and loss of definition of both reflections. These effects continued at the highest molar ratio analysed of 0.25, revealing the considerable disruption produced by HFIP on saturated phospholipid bilayers.

Molar ratio of HFIP : DMPC	*	Area ( $\text{\AA}^{-1}$ )	Reflection (Peak) position ( $\text{\AA}^{-1}$ )	Width ( $\text{\AA}^{-1}$ )	Height ( $\text{\AA}^{-1}$ )
MR: 0.00	1.	$1.44 \times 10^{-5}$	0.097	0.007	0.002
	2.	$7.11 \times 10^{-6}$	0.194	0.009	$5.28 \times 10^{-4}$
MR: 0.03	1.	$1.25 \times 10^{-5}$	0.097	0.007	0.001
	2.	$9.06 \times 10^{-6}$	0.197	0.014	$4.45 \times 10^{-4}$
MR: 0.06	1.	$1.88 \times 10^{-5}$	0.094	0.018	$9.13 \times 10^{-4}$
	2.	$1.46 \times 10^{-5}$	0.195	0.024	$5.22 \times 10^{-4}$
MR: 0.12	1.	$1.21 \times 10^{-5}$	0.096	0.019	$4.99 \times 10^{-4}$
	2.	$1.78 \times 10^{-5}$	0.196	0.052	$3.76 \times 10^{-4}$
MR: 0.25	1.	$1.01 \times 10^{-5}$	0.093	0.034	$3.50 \times 10^{-4}$
	2.	$2.76 \times 10^{-5}$	0.193	0.074	$4.23 \times 10^{-4}$

\*1: Main reflection and 2: second-order reflection.

*Table IV.1.1. Table listing numerical values ( $\text{\AA}^{-1}$ ) calculated for the area under the first-order and second-order reflections, the position, width and height of the reflections for scattering data collected on HFIP-DMPC systems.*

*Data were processed using Origin software (Originlab, version 7.5).*

The decrease in peak intensity is clearly indicative of the creation of a large disruption to the periodicity of the bilayer, as HFIP integrates unevenly into the saturated bilayer, producing HFIP richer and poorer areas in the bilayer. The broadening of both reflections, at molar ratios above 0.03, strongly suggests that HFIP is having a destabilizing effect on the bilayer, which would be consistent with the bilayer becoming unstable under the strain of localized high concentrations of the fluorinated alcohol in the bilayer.

The lamellar repeat distance (thickness of the bilayer and water layer), which is calculated from the reflection positions in the HFIP-lipid systems, did not change significantly over the range of concentrations considered; a calculated value of  $6.43 \pm 0.02$  nm for these systems falls well within the reported range for DMPC bilayers.<sup>22</sup>

#### IV.1.5.4. SAXS from HFIP-DOPC systems.

Small Angle X-ray Scattering data were collected for DOPC-HFIP systems over the same range of concentrations considered in the HFIP-DMPC systems and under the same conditions.

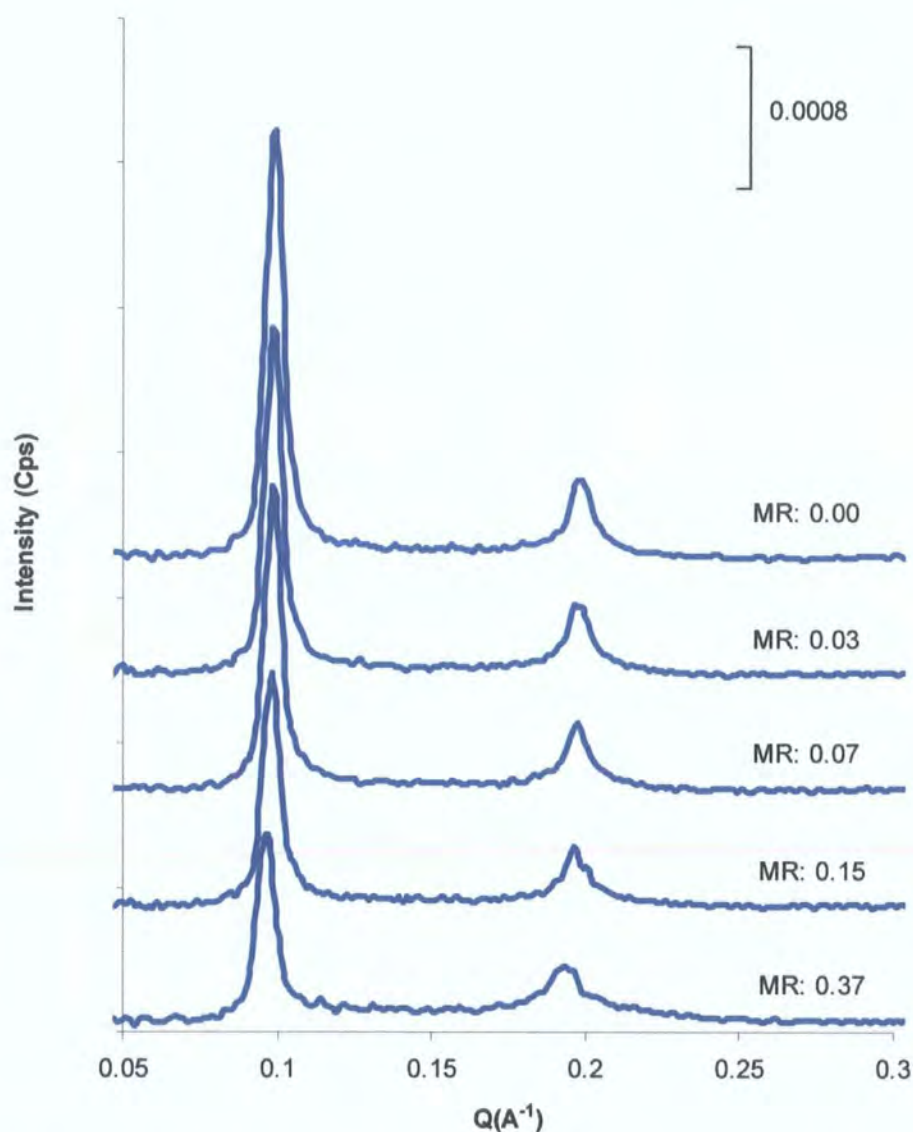


*Figure IV.1.11. SAXS data for the HFIP-DMPC systems was collected over a range of HFIP/DOPC molar ratios, MR from 0.03 to 0.25.*

*[lipid]: 0.15 M and [HFIP] from: 0.005 M to 0.040 M.*

*The scale bar corresponds to the intensity in units of counts s<sup>-1</sup> (Cps).*

The difference in the scattering data between the two HFIP-lipid systems is quite significant; the addition of HFIP over the same range of concentrations produced a much smaller effect on DOPC bilayers. A decrease in width as well as a much slighter and more gradual decrease in the intensity of both reflections is observed as the concentration of HFIP is increased in the DOPC systems.

The fluorinated alcohol noticeably produces a much smaller disturbance in DOPC bilayers; the greater fluidity of the monounsaturated bilayers and hence less densely packed lipids monomers, must clearly allow the bulky fluorinated molecule to integrate into the bilayer without perturbing lipid ordering to the extent it would, in the more tightly packed, saturated DMPC multilamellar systems.

#### **IV.1.6. HFIP-Phosphatidylcholine Monolayer experiments.**

The HFIP induced disturbances in the phospholipid systems were further investigated by lipid monolayer experiments over a range of HFIP-water subphases, in an attempt to gain deeper insight into the disordering and destabilizing effects observed in the previous experiments.

##### **IV.1.6.1. Monolayer technique.**

Lipids are amphiphilic molecules and when spread on the surface of an aqueous solution, they form insoluble monolayers (monomolecular films), with their hydrophilic headgroups oriented towards the aqueous solution, the subphase and their hydrophobic hydrocarbon chains towards the air.

The lipid dissolved in a suitably volatile solvent (usually chloroform) is spread drop wise onto an aqueous surface. Spontaneous spreading occurs, as the lipid peripheral molecules are pulled into the bulk solution and both the surface pressure of the monolayer and the equilibrium spreading pressure are equal.



The area occupied by the monolayer can be reduced by moving a barrier across the surface of the aqueous solution (using a Langmuir-Blodgett trough). Compression of the lipid film at a given subphase temperature leads to an increase in the surface pressure and as pressure is applied the lipids in the film are forced to become more and more ordered. The lipid acyl chains will undergo a phase change from a 2-D gas state with no noticeable ordering *via* an ordered liquid-expanded (LE) state to a more ordered and closer packed liquid-condensed (LC) state.<sup>23,24,25</sup>

Pressure-Area Isotherms are recorded for each monolayer as they are compressed over a range of HFIP-water subphases; they describe the compressional process of the monolayer, allowing quantitative information about the size and packing of the molecules in the film, to be obtained from the gradient of the phases the film goes through as it is compressed.

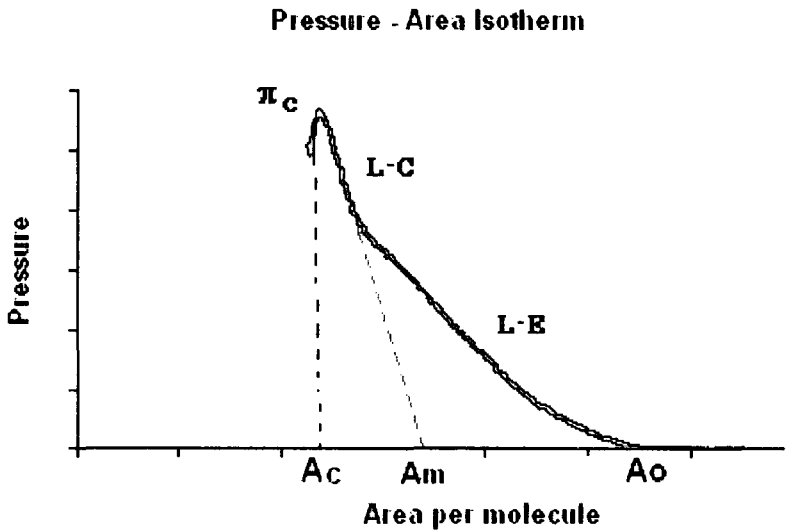


*Figure IV.1.12. Diagram of a pressure-area isotherm for DMPC over a pure H<sub>2</sub>O subphase.*

The collapse pressure ( $\pi_c$ ) (diagram IV.1.12) is the maximum pressure to which the monolayer film can be compressed before it begins to collapse into a 3-D folded structure and molecules are ejected from the film; the lift off area ( $A_o$ ) is the area at which the film starts to compress; the molecular area ( $A_m$ ) is the hypothetical area occupied by one molecule in the condensed state at zero pressure and is obtained by extrapolating to zero pressure from the gradient of the liquid condensed phase and the collapse area ( $A_c$ ) is the maximum area to which the film can be compressed extrapolated to zero pressure from the collapse pressure.

The most common method for measuring the surface pressure of the monolayer is with a Wilhelmy plate (sensitivity:  $10^{-3} \text{ mNm}^{-1}$ ). The surface pressure is taken as the difference between the surface tensions of pure water ( $\sim 72 \text{ mNm}^{-1}$ ) or a mixed subphase, such as HFIP- $\text{H}_2\text{O}$  and the subphase-monomolayer surface.

A Wilhelmy plate (Whatman filter paper) is suspended from a sensitive balance into the monolayer. The forces acting on the plate in a downwards direction are due to gravity and surface tension. Forces acting upwards are buoyancy due to displaced water.

The usual procedure is to measure the change in force acting on a thoroughly wetted stationary plate, where the change in force,  $\Delta F$  is related to the change in surface tension,  $\Delta\gamma$  by:

$$\Delta\gamma = \Delta F / 2w$$

*Where  $w$  is the width of plate in contact with the monolayer.*

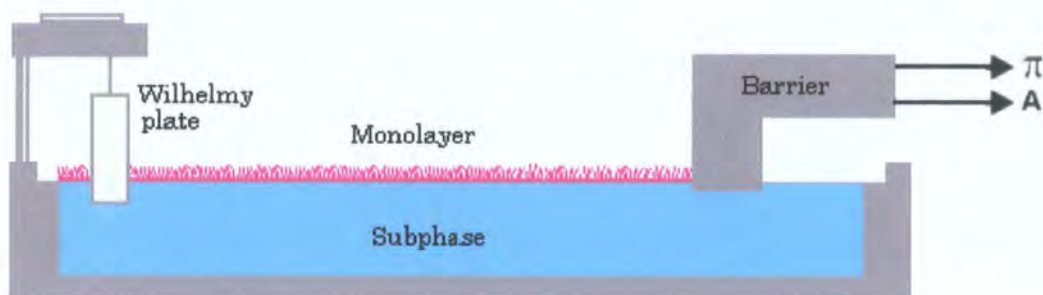


*Figure IV.1.13. diagram of a Langmuir-Blodgett trough.*

#### IV.1.6.2. Experimental procedure.

The lipids, dimyristoyl phosphatidylcholine, DMPC and oleoyl phosphatidylcholine, DOPC were dissolved in  $\text{CHCl}_3$  and spread drop wise, with a Hamilton micro-syringe, on the surface of the trough. The number of molecules spread on the surface was kept constant for all experiments and monolayers were left to evaporate for 10-15 min before initiating compression with a barrier speed of  $50 \text{ cm}^2 \text{ min}^{-1}$ .<sup>26,27,28</sup>

The pressure-area isotherms for the monolayers were recorded over a subphase maintained at  $20^\circ\text{C}$  (below  $T_m$  for DMPC and above  $T_m$  for DOPC) as the temperature of the subphase will affect the compressibility of the lipid and hence the packing of the acyl chains.<sup>29,30,31,32</sup>

The lipid monolayers were compressed to a point just below their collapse pressures and expanded several times (3-4 cycles) before finally being compressed to beyond the collapse area for the monolayer. This treatment was to ensure that the isotherms were reproducible and that no lipid material was being lost to the subphase.

The pressure-area isotherms for these lipids over pure water, were in agreement with literature values for both the area per molecule and the collapse pressure.<sup>33,34,35,36,37</sup>

#### IV.1.6.3. Monolayers of DMPC over HFIP-H<sub>2</sub>O subphases.

The lipid monolayers were compressed over a HFIP-pure water subphase with HFIP concentrations ranging from 0.00 M (0 %) to 0.38 M (4 % v/v).

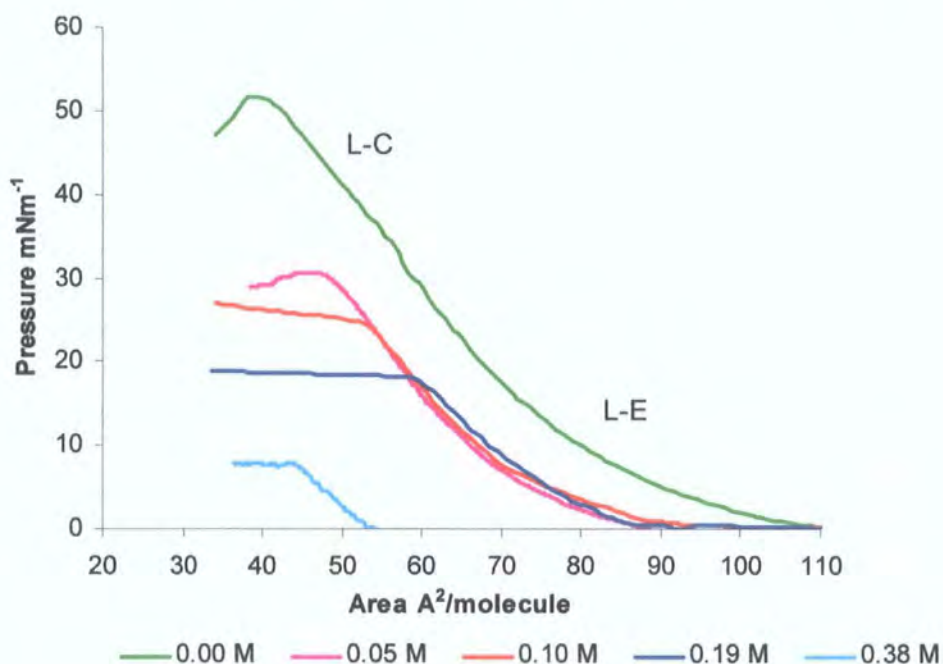
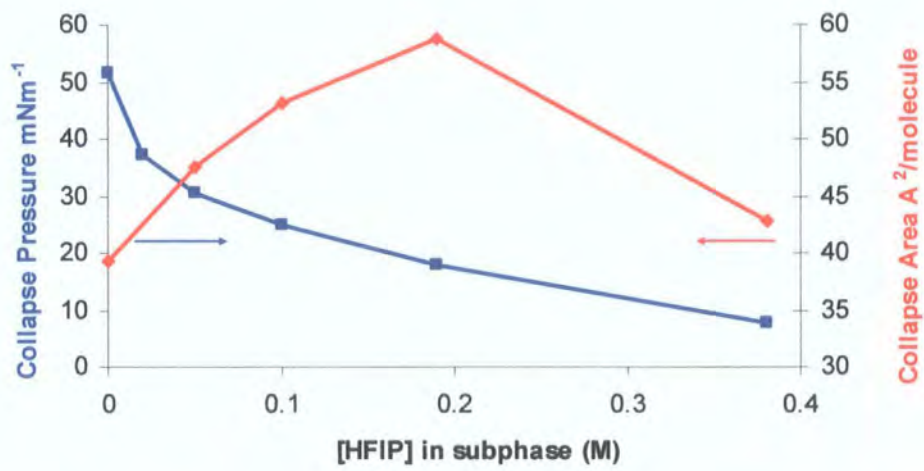


Figure IV.1.14. Pressure-area isotherm of DMPC over HFIP-H<sub>2</sub>O subphases. L-E is a liquid expanded state and L-C a liquid condensed state of the monolayer. HFIP concentrations are indicated in the legend above.

The collapse pressure ( $\pi_c$ ) of the DMPC monolayer decreased as the concentration of HFIP in the subphase increased. The collapse area (A) followed a different trend and increased for HFIP concentrations of up to 0.19 M, then decreased steadily at higher concentrations.

The plot of collapse pressure against subphase composition showed a clear correlation between the concentration of HFIP in the subphase and the pressure at which the monolayer collapsed.



*Figure IV.1.15. plot of collapse pressures and collapse areas against HFIP concentration in the subphase.*

The steady decrease in collapse pressure, over the range of HFIP concentrations studied is indicative of a decrease in the stability of the monolayer as a function of HFIP content in the subphase.

The lift off area ( $A_o$ ) decreased on addition of 0.05 M HFIP to the subphase, but then remained stable as the HFIP concentration was further increased up to 0.19 M and subsequently decreased again at higher concentrations. The decrease in monolayer lift off area is strongly indicative of an increase in fluidity of the lipid film, for subphase compositions of 0.05 M HFIP and again above 0.19 M HFIP.

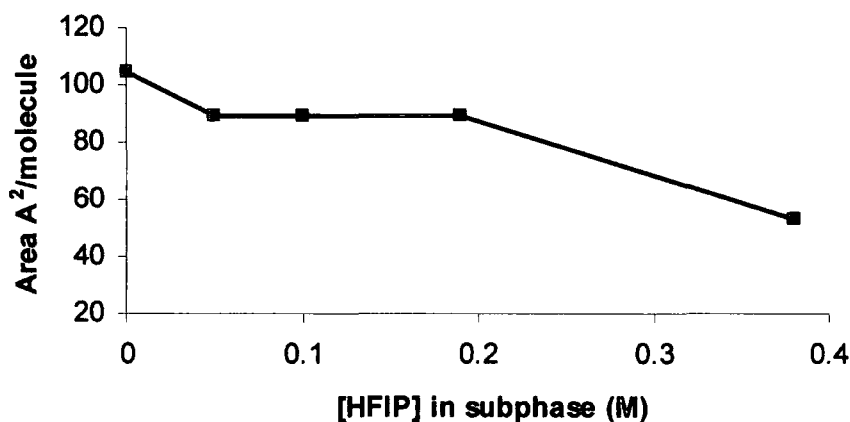


Figure IV.1.16. A plot of area,  $A_o$  against HFIP concentration in the subphase.

The area occupied by a lipid molecule is determined by an equilibrium of attractive (hydrophobic effect and van der Waals interactions) and repulsive forces (the electric charges of the lipid headgroups, hydration and steric repulsion) between the lipid molecules. An increase in packing of the lipid molecules implies a reduction in repulsive forces or an increase in attractive forces or both.

A measure of the compressibility of a monolayer, which gives a measure of the equilibrium elasticity of the monolayer film, can be calculated from the pressure-area isotherm, where the compressional modulus ( $\kappa$ ) in  $\text{mNm}^{-1}$  is the reciprocal of the compressibility:

$$\kappa = -A_m (\Delta\pi / \Delta A_m)_T$$

Where  $A_m$  is the molecular area in  $\text{\AA}^2$  and  $\pi$  is the lateral surface pressure in  $\text{mNm}^{-1}$ .



A DMPC lipid monolayer spread over pure water will go through two different states as it is compressed; a liquid expanded state (L-E) in which the lipid molecules are still quite wide apart and very compressible and a liquid condensed state (L-C) in which the molecules are more densely packed and much less compressible.<sup>24</sup>

The compressional modulus ( $\kappa$ ) calculated for the L-C state of DMPC monolayers, gave a value of 111.99 mNm<sup>-1</sup> over pure water in agreement with literature values,<sup>24</sup> and much lower values, ranging from 90.20 mNm<sup>-1</sup> to 44.90 mNm<sup>-1</sup>, over HFIP-water subphases with HFIP concentrations from 0.05 M to 0.38 M (Table IV.1.2). The compressional modulus ( $\kappa$ ) decreased quite significantly as the HFIP subphase concentration increased, which is a clear indication that the monolayer became less compact or more fluid as a function of HFIP concentration in the subphase.



#### IV.1.6.4. Monolayers of DOPC over HFIP-H<sub>2</sub>O subphases.

The pressure-area isotherm, recorded for a monolayer of the unsaturated DOPC phospholipid over pure water, had a collapse pressure and a compressional modulus in agreement with literature values for this lipid.<sup>38,39</sup>

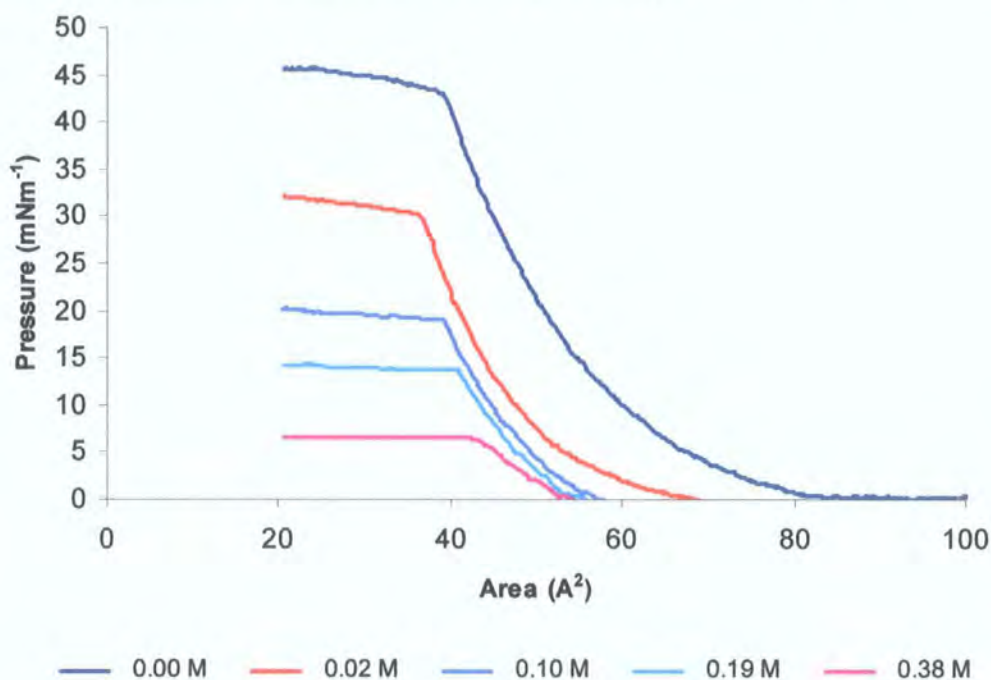


*Figure IV.1.17. Pressure-area isotherms of DOPC recorded over a range of HFIP-pure water subphases. HFIP concentrations are indicated in the legend above.*

The DOPC monolayer on compression showed a smooth transition from a liquid expanded (L-E) to a liquid condensed (L-C) state and had lower collapse pressures than the DMPC monolayers over both pure water and mixed HFIP-water subphases. The compressional modulus ( $\kappa$ ) calculated for the DOPC monolayer over pure water (Table IV.6.6) gave a value of 134.66 mNm<sup>-1</sup> and values ranging from 111.87 mNm<sup>-1</sup> to 36.20 mNm<sup>-1</sup> for subphase HFIP concentrations of 0.05 M to 0.38 M.

Compressional modulus ( $\kappa$ ) values for DOPC monolayers were much higher than those calculated for DMPC monolayers, over subphases with HFIP concentrations up to 0.19 M; but this trend was reversed at the highest HFIP concentration examined of 0.38 M, at which the saturated DMPC monolayer had a greater compressional modulus value than the DOPC monolayer.

Monounsaturated DOPC monolayers are naturally much more fluid than saturated DMPC monolayers and would therefore be expected to be more compressible without perturbations from HFIP.

[HFIP] (M) in subphase:	0	0.05	0.1	0.19	0.38
DMPC $\kappa$ (mNm <sup>-1</sup> ):	112.0	90.2	72.4	64.9	44.9
DOPC $\kappa$ (mNm <sup>-1</sup> ):	134.7	111.9	92.9	76.5	36.2

*Table IV.1.2. Showing data for the compressional modulus,  $\kappa$  of DMPC and DOPC monolayers over a range of HFIP-water subphases.*

The collapse pressures for DOPC monolayers, over the range of HFIP-water subphases investigated, decreased as the HFIP content in the subphase increased, but the molecular areas followed an opposite trend after an initial decrease on addition of 0.05 M HFIP and then increased for all further concentrations of HFIP in the subphase.

A plot of the collapse pressures of DOPC monolayers against HFIP-water subphase compositions showed that the stability of this monolayer was affected in a similar way to the fully saturated DMPC monolayer by the increase in HFIP subphase concentration.

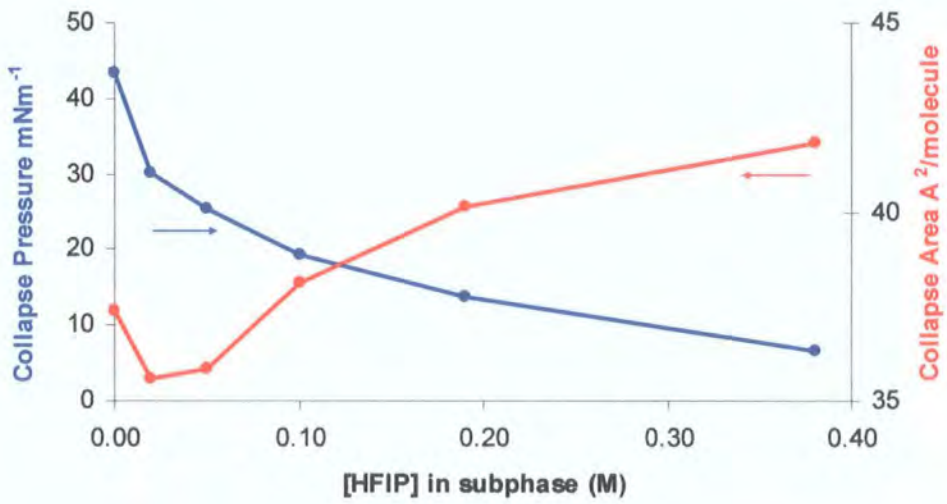
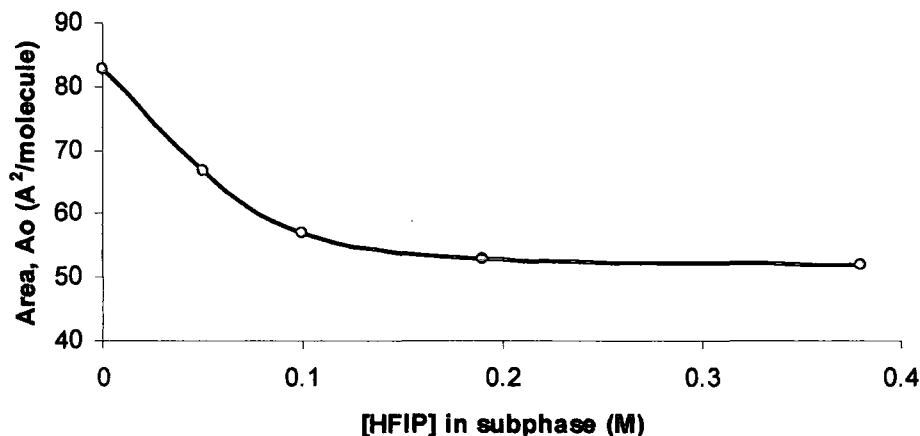


Figure IV.1.18. Plot of collapse pressures and areas against HFIP concentration in the subphase for DOPC monolayers recorded at 20 °C.

The collapse area ( $A_c$ ) extrapolated from the collapse pressure ( $\pi_c$ ) initially decreased on addition of HFIP to the subphase, but then expanded steadily as the concentration of HFIP increased (Figure IV.1.18). An expansion of the area occupied per molecule of lipid would be expected to occur on integration of the HFIP molecules from the subphase into the lipid monolayer.

The lift off area ( $A_o$ ) for DOPC monolayers initially decreased on addition of HFIP concentrations up to 0.1 M in the subphase and then remained steady for all further increases in HFIP concentration examined (Figure IV.1.19)



*Figure IV.1.19. Plot of lift off area,  $A_o$  against HFIP concentration in the subphase for DOPC monolayers recorded at 20 °C.*

The monolayer experiments on both the saturated and unsaturated phospholipids have demonstrated the dramatic effect of HFIP on these phospholipid films; increasing the concentration of HFIP significantly reduced the stability and increased the fluidity of both types of monolayers. A HFIP concentration of 0.19 M in the subphase appeared to be a critical concentration for the saturated lipid, as the molecular area increased up to this concentration and then decreased sharply above this value. The monolayer lift of area initially decreased on addition of HFIP, but then remained constant for HFIP subphase concentrations up to 0.19 M, above which there was a significant decreases in the lift off area. The unsaturated DOPC monolayers did not appear to be affected by a critical concentration and maintain a steady change over the 0.00 M to 0.38 M HFIP concentration range in the subphase.

An examination of the effects of HFIP on the size and morphology of both DMPC and DOPC unilamellar vesicles was performed in presence of HFIP. The techniques used, TEM and laser correlation spectroscopy, gave some very interesting results that have helped bring together our findings and draw up a general view of the effect of HFIP in these systems.

#### **IV.1.7. Light Scattering Analysis of the effects of HFIP on the size of DMPC and DOPC liposomes.**

The particle sizing technique used in our experiments only measures an average size for the bulk of particles in solution, but it can be used routinely as it is a quite straightforward analytical technique.

##### **IV.1.7.1. A brief description of the technique.**

Laser light shone through a suspension of particles is scattered by the particles and the intensity of the scattered light which fluctuates according to the movement or rate of diffusion of the particles in the solution (Brownian motion) is recorded as a series of photomultiplier bursts over a period of time. The fluctuation in intensity is related to the particle size and because the rate of diffusion of the particles is dependant on their size, smaller particles diffuse more rapidly than larger ones

A mathematical correlation can be performed on the signal to obtain an average size value for the particles in solution. The signal is multiplied with a copy of itself separated from the original by a given time delay (a corresponding set of channels). The product of which is then plotted for each time separation against the channel number corresponding to that separation; this produces a curve, which will decay exponentially to a mean value and at a rate that will depend on the rapidity of the signal fluctuations and hence on particle size.

#### IV.1.7.2. Particle sizing of DMPC-HFIP systems.

The effect of HFIP on the size of unilamellar vesicles (extruded through a polycarbonate membrane with pore diameters of 100 nm) was monitored by light scattering spectroscopy. The mean diameter of the fully saturated, DMPC liposomes in pure water was measured as 140 nm with a low polydispersity (0.19), typical of liposomes prepared by extrusion.

On addition of increasing concentrations of HFIP from 0.00 M to 0.3 M, to the liposome solution, the effective diameter of the DMPC liposomes increased significantly, from ~140 nm to ~208 nm, following a near linear trend. The intensity of the light scattering at 658 nm also decreased progressively as the HFIP concentration increased.

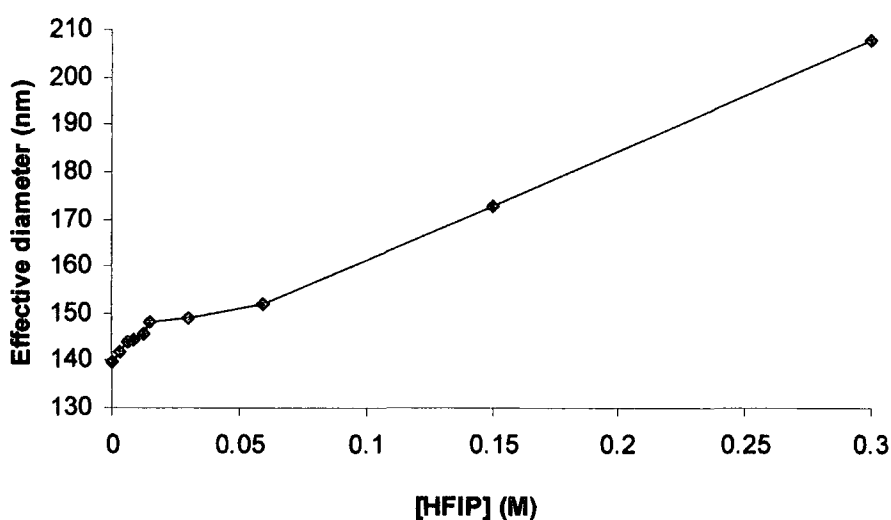


*Figure IV.1.20. Diameter of DMPC liposomes determined, as a function of HFIP concentration in the sample solution, by laser correlation spectroscopy.*

*DMPC concentration was 2 mM.*

The polydispersity of the DMPC liposome-HFIP samples increased slightly from 0.19 to 0.24 over the range of HFIP concentrations examined.

[HFIP] (M)	Effective diameter (nm)	Polydispersity
0	139.7	0.193
0.0032	141.7	0.218
0.0064	144.0	0.202
0.009	144.6	0.197
0.0127	145.5	0.213
0.015	148.2	0.182
0.03	149.1	0.207
0.06	152.1	0.212
0.15	172.6	0.24
0.3	207.8	0.235

*Table IV.1.3. Showing the effective diameter and the polydispersity of the DMPC liposome-HFIP samples over a range of HFIP concentrations.*

The linear increase in the effective diameter of the saturated liposomes, on addition of HFIP, is again indicative of HFIP integration into the DMPC bilayer with expansion of the bilayer area as a function of HFIP concentration. Light scattering experiments between ethanol and phospholipid liposomes have shown a similar increase in liposome diameter at equivalent concentrations.<sup>40</sup>



#### IV.1.7.3. Particle sizing of DOPC-HFIP systems.

Monounsaturated, DOPC unilamellar liposomes in pure water, also prepared by extrusion through a polycarbonate membrane (pore diameter of 100 nm), were analysed by Light Scattering to determine the effective diameter and polydispersity of the unsaturated phospholipid vesicles following addition of increasing concentrations of HFIP. The fluorinated alcohol, in accordance with results obtained from the wide range of experiments described in this chapter had a much more subdued effect on the DOPC liposomes; the effective diameter of the DOPC liposomes, which was ~143 nm in the absence of HFIP, decreased slightly by around 7 nm to 136 nm on addition of the smallest HFIP concentration of 3.2 mM (1 % v/v) and then increased from 6.4 mM (2 % v/v) to remain within 5 nm of the original effective diameter.

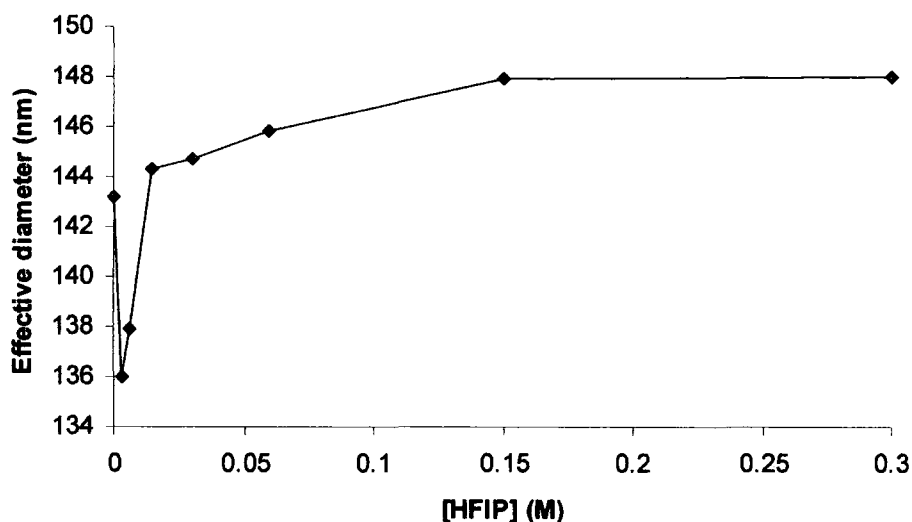


*Figure IV.1.21. Diameter of DOPC liposomes determined, as a function of HFIP concentration in the sample solution, by Light Scattering Spectroscopy.*

*DOPC concentration was 2 mM.*

The intensity of the scattered light or optical density of the samples did not change significantly throughout the experiments carried out on the DOPC liposomes, but the polydispersity of the sample was affected in a similar change to the DMPC systems over the range of HFIP concentrations examined.

Light scattering experiments on both the saturated and monounsaturated phospholipids confirm previous findings highlighting the much greater effect exerted by HFIP molecules on the saturated lipid systems.

#### **IV.1.8. Transmission Electron Microscopy, TEM.**

The change in diameter of the saturated DMPC liposomes, the decrease in stability and increase in fluidity of the lipid bilayers on interaction with HFIP molecules, are effects that might be detected as morphological changes in the liposomes by electron microscopy. Images showing the effects of HFIP would add to a general interpretation of the findings from the wide range of experiments conducted on the phospholipid-HFIP interactions.

Transmission electron microscopy was considered the instrument of choice due to the very high resolutions that this technique is capable of reaching routinely.

#### IV.1.8.1. TEM imaging of the effects of HFIP on DMPC liposomes.

Unilamellar vesicles of DMPC, prepared by extrusion (diameter of 100 nm) in pure water, were deposited on to a copper grid coated with a formvar film and then negatively stained (1-2 % uranyl acetate).<sup>41</sup> The DMPC liposomes were clearly visible at lipid concentrations of 0.6 mM; the liposomes observed had a mean diameter of  $123 \pm 35$  nm and showed no obvious deformations

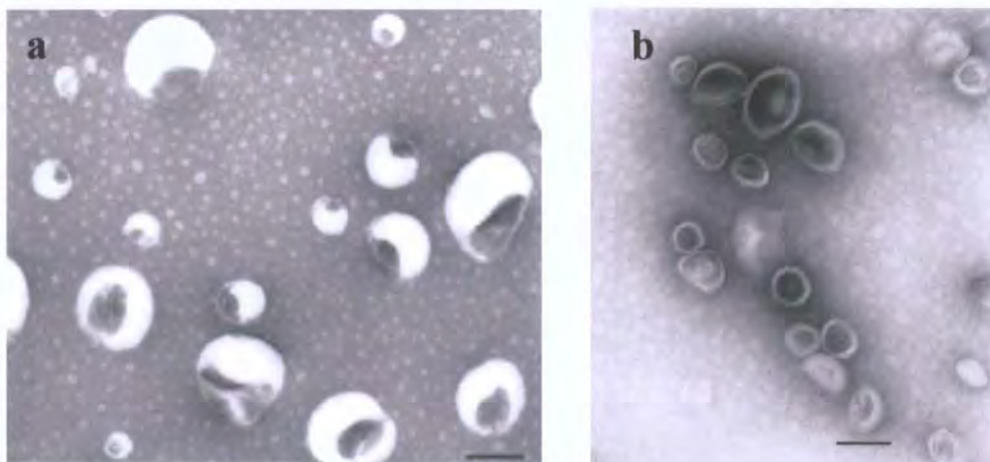


*Figure IV.1.22. TEM images of DMPC liposomes in pure water at magnifications of: a, x 100 000 and b, x 80 000.*

*The scale bars represent 100 nm.*

The DMPC liposomes in pure water were then thoroughly mixed with HFIP over a range of concentrations from 0.05 M to 0.38 M and imaged immediately.

On addition of the smallest concentration of HFIP, smooth particulate structures, with a mean diameter of  $60 \pm 17$  nm, were clearly visible along side and attached to the liposomes.

The mean diameter of the DMPC liposomes, in a 0.05 M HFIP-water solution, was  $105 \pm 26$  nm, which is around 20 nm smaller than liposomes in the absence of HFIP.

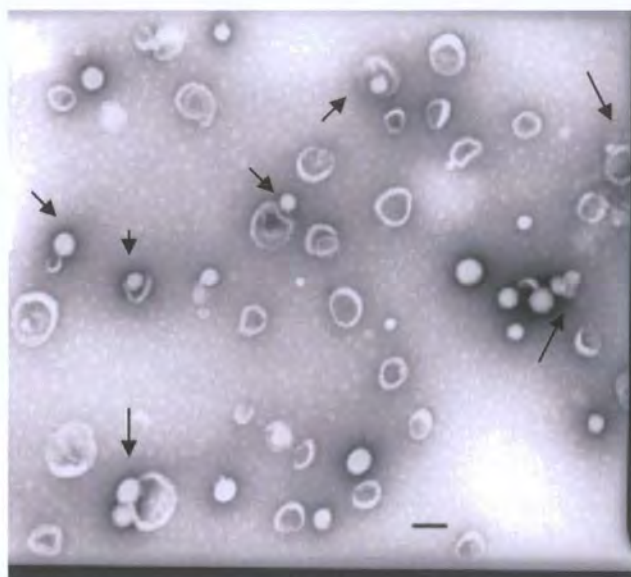


*Figure IV.1.23. DMPC liposomes in a 0.05 M HFIP- pure water solution imaged by TEM at magnifications of  $\times 46\,000$ . The arrows indicate the location of the smooth particulate structures. The scale bar represents 100 nm.*

Imaging of the DMPC liposome–HFIP mixtures after a delay of 30 minutes generally revealed an absence of smooth particles which suggests that the particulates could have been imaged before DMPC-HFIP equilibrium conditions had been attained.



At the highest HFIP concentration of 0.38 M, the appearance of the DMPC liposomes changed considerably, with liposomes taking on an unusually smooth morphology and forming aggregates or clusters.

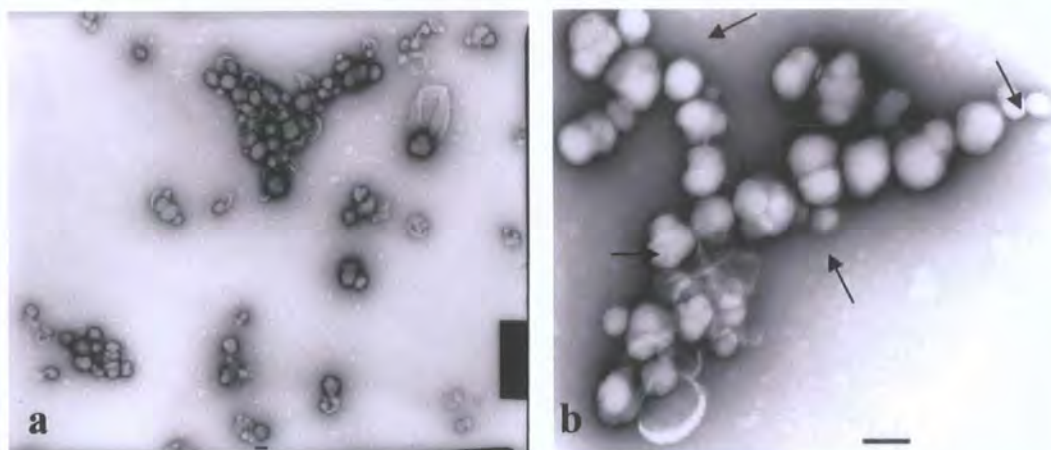


*Figure IV.1.24. DMPC liposomes in a 0.38 M HFIP- pure water solution imaged by TEM at magnifications of: a, x 22 000 and b, x 46 000. The arrows show appearance of blebbing in the liposomal structures*  
*The scale bars represent 100 nm.*

The very clear change in appearance of the sample strongly suggests that HFIP may have integrated in to the lipid membrane and affected the physical properties of the bilayer by forming mixed HFIP-lipid structures which on closer examination show signs of blebbing in many of the individual liposomal structures.

Similar experiments were carried out on DOPC liposomes in order to assess the effect of HFIP on the monounsaturated phospholipid, but the more fluid membranes did not submit as well as the saturated DMPC liposomes to the harsh drying out conditions of the TEM vacuum; it was more difficult to distinguish the effects of HFIP on the DOPC liposomes and therefore the data from these experiments was not included in this study.

In order to assess whether there were any artifacts present in the samples under observation, which could be due to the staining process, TEM images of both the stain solution and the stain with 0.38 M HFIP-water were examined.

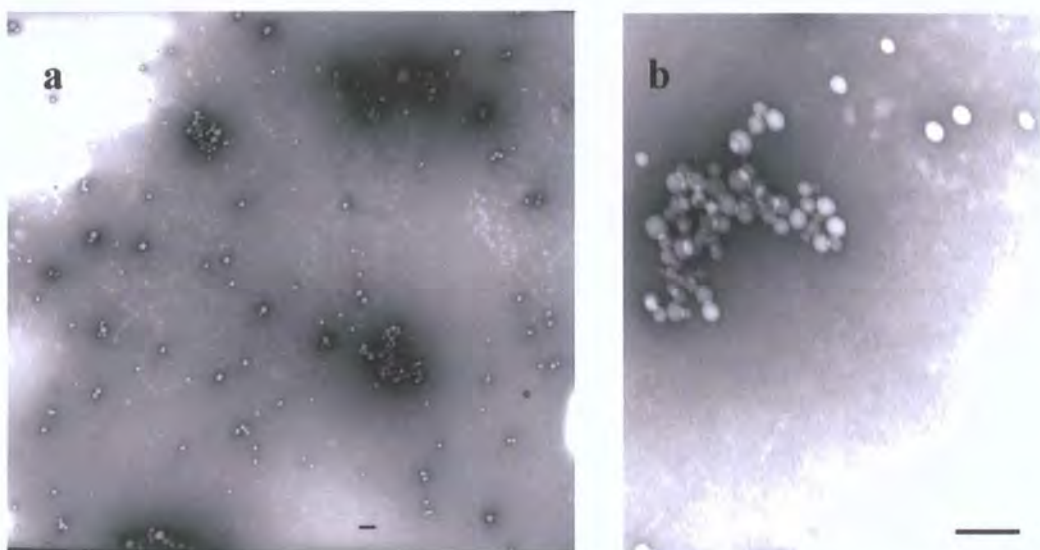


*Figure IV.1.25. TEM images of HFIP (0.38 M) - pure water mixtures (mag. a, x 46 000 and b, x 100 000). Scale bars represent 100 nm.*

The stain solution on its own only revealed a featureless background with occasional patches of higher density stain, but the HFIP-water mixtures produced small particulate structures, many of which formed discrete clusters. The individual particles had a mean diameter of  $29 \pm 16$  nm.

An explanation for the emergence of particulate structures and clusters from HFIP-water solutions may lie in the fact that fluorocarbons have a strong capacity to self aggregate into discrete molecular assemblies and to form a hydrophobic microenvironment when dispersed in an aqueous solution. The observation of these structures, which would be expected to have evaporated under the instrument vacuum, could be due to impressions left by the HFIP structures on the grid, in the stain and the formvar film.

The purity of all materials, especially HFIP was rigorously checked and all equipment involved in the experimental procedure was thoroughly cleaned, to eliminate any possibility that these structures were produced by some contaminant in the system. Scanning electron microscopy (SEM) was also used to image the



samples prepared for TEM and confirmed that the results obtained by TEM were reproducible.

Samples of HFIP-water mixtures were analysed by light scattering in order to check for the presents of particulates or clusters in solution. At the higher HFIP concentration of 0.38 M, clusters within the same average size range as those observed by TEM at this concentration, were measured reproducibly.

Experimental evidence of the presence of similar structures in trifluoroethanol-water mixtures have also been obtained from laser light scattering experiments and a range of other studies on bulky fluorinated and non fluorinated alcohols, using X-ray scattering and molecular modeling techniques, have strongly indicated self assembly of the alcohols in aqueous media with the formation of discrete clusters.<sup>3,42,43</sup>



#### IV.1.9. Conclusion.

An understanding of the effects of hexafluoroisopropanol on phospholipid membranes could lead to a more efficient use of its properties, in particular for solvation of the synthetic amphiphilic cyclic peptides, discussed in chapter II of this thesis and in general to a greater understanding of the interactions of this fluorinated alcohol with the cell membrane; interactions of small molecules with the cell membrane are of considerable importance for a number of biological applications, such as drug and metabolite uptake or passive transport across the membrane.

The effect of HFIP on the integrity, stability, packing, size and morphology of phospholipid membranes has been investigated using a wide range of experimental techniques, including  $^{19}\text{F}$  NMR; marker release experiments on EPC unilamellar vesicles containing carboxyfluorescein; differential scanning calorimetry and small angle x-ray scattering; monolayer experiments, transmission electron microscopy and light scattering analysis.

$^{19}\text{F}$  NMR was used to estimate partition coefficients values for the saturated, DMPC and the monounsaturated, DOPC phospholipids. The extent of the HFIP interactions with phospholipid membranes, would depend on the affinity of the fluorinated alcohol for the lipid bilayer and hence on its ability to partition in to phospholipid membranes.<sup>5</sup> The values estimated for the partition coefficients were very large, which shows that the HFIP molecule has a high affinity for the phospholipid environment with a marked preference for partitioning in to the more fluid monounsaturated bilayers.<sup>8</sup>

Marker release experiments, performed on EPC vesicles encapsulating a fluorescent marker, have confirmed previous reports that HFIP induces bilayer leakage and hence affects acyl chain order at very low concentrations. All alcohols are thought to affect lipid membranes, but HFIP has been shown to have a much stronger affect than most common alcohols.<sup>6</sup>

Differential scanning calorimetric analysis of multilamellar vesicles of DMPC showed a marked decrease in the main transition temperature of the bilayer on addition of HFIP over a range of concentrations, from 0.002 M to 0.05 M. This effect can be attributed to a significant decrease in fluidity of the bilayer and would result from considerable disruption to the packing of the saturated phospholipid monomers in the bilayer.

Small angle X-ray scattering data, obtained for multilamellar vesicles of both DMPC and DOPC, revealed a significant difference in the effect of HFIP on the saturated and unsaturated lipids. The intensity of both the first and second order reflections was greatly reduced and a significant broadening occurred in the case of the saturated, DMPC lipid. These results show that HFIP, over the range of concentrations considered, greatly disrupts the periodicity of the bilayer system which can be attributed to the creation of areas within the membrane with different concentrations of HFIP; this would result in loss of bilayer periodicity and would correspond to a decrease in intensity of the reflections. The substantial broadening observed in the DMPC-HFIP systems is indicative of increasing instability in the bilayer as a function of HFIP concentration, which would result from stress produced by high localized concentrations of HFIP on the bilayer structure.

The effects of HFIP were considerably less marked for the unsaturated, DOPC lipid, which shows that the more fluid and hence less densely packed membrane could accommodate the bulky fluorinated alcohol with less disruption to the unsaturated bilayer system.<sup>9</sup>

Further investigation of the behaviour of these HFIP-phospholipid systems was performed by recording pressure-area isotherms of phospholipid monolayers over HFIP-water subphases, which again provided support for strong HFIP-phospholipid interactions with considerable disruption to the saturated systems; the decrease in lift off areas and in collapse pressures was clearly indicative of an increase in monolayer fluidity and instability respectively for both phospholipid monolayers examined. Once more the saturated lipid, DMPC behaved differently to the monounsaturated lipid, DOPC by showing an increase in collapse area up to what appears to be a critical concentration for these systems and then decreasing substantially at higher HFIP subphase concentrations. These results add to an

overall interpretation of the HFIP-phospholipid systems which reveal the significant role that the degree of saturation of the lipid has in HFIP-lipid interactions.

Examination of the size (light scattering) and morphology (TEM) of phospholipid unilamellar vesicles in presence of HFIP have shown that HFIP affects the diameter of the saturated lipid vesicles to a much greater extent than that of the monounsaturated lipid vesicles. Electron microscopy of DMPC-HFIP mixtures has helped shed some light on the activity of HFIP in phospholipid membranes and together with the findings from the other techniques has lead to the following proposition of a mechanism for HFIP integration and perturbation of saturated phospholipid DMPC membranes:

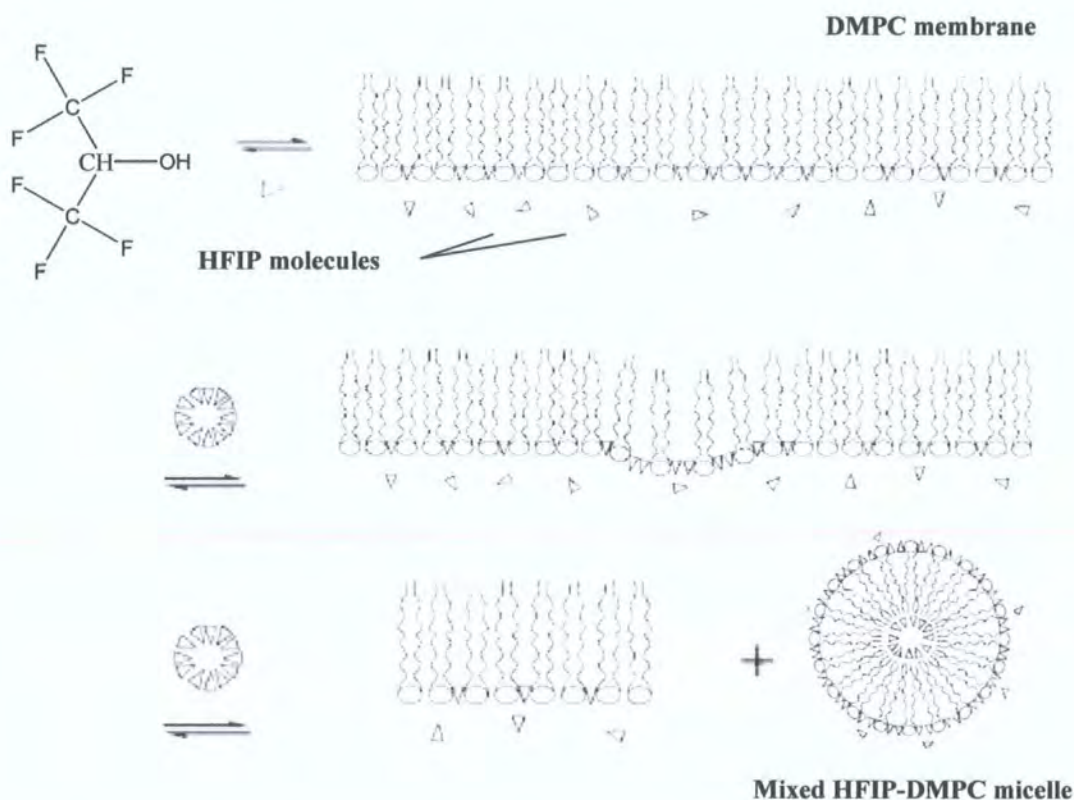


*Figure IV.1.26. Schematic model describing a mechanism for the interaction of HFIP with DMPC membranes.*

The HFIP induced perturbation in saturated DMPC membranes (DSC and SAXS data) is believed to arise through localized concentration of the HFIP molecules in the membrane, which produces areas richer and others poorer in HFIP (SAXS and Monolayer experiments). The membrane becomes unstable under the strain produced by the localized high concentration of HFIP (SAXS data), which would induce rearrangement of the membrane with loss of material in the form of mixed HFIP-lipid micelles (Light Scattering and TEM experiments) to produce a more stable membrane, poorer in HFIP.

Further investigations of a range of fluorinated and non fluorinated bulky alcohols on phospholipid membranes would add considerably to this work and could possibly provide some support for the proposed mechanism of HFIP interaction with DMPC membranes.

## **IV.2. Materials and Methods.**

### **IV.2.1. Materials.**

Phospholipids: 1,2-Dimyristoyl-*sn*-glycerol-3-phosphocholine (DMPC) was obtained from Bachem Ltd. (UK); 1,2-Dioleoyl-*sn*-glycerol-3-phosphocholine (DOPC) and Egg phosphatidylcholine (EPC) were purchased from Sigma. All phospholipids were used without further purification. HPLC grade water was from Fisher Scientific, and ultrapure water was purified using a Milli-Q purification system (Waters).

5(6)-Carboxyfluorescein (CF), Sodium Chloride, Sodium Fluoride and tris(hydroxymethyl)aminomethane (Tris) were obtained from Lancaster Synthesis. 1,1,1,3,3,3-hexafluoroisopropanol (HFIP) was purchased from Apollo Scientific and further purified by distillation at 58 to 60 °C.<sup>44</sup>.

### **IV.2.2. Methods.**

#### **IV.2.2.1. <sup>19</sup>F NMR experiments.**

Multilamellar vesicles of both DOPC and DMPC were prepared by evaporating a solution of lipid (30 mg) in CHCl<sub>3</sub> (1 ml) to dryness under vacuum to form a thin film. The film was then hydrated with deuterated water (300 µl) (D<sub>2</sub>O) to form a lipid suspension (containing 9 % w/v lipid by weight). Lipid/water partition coefficients were measured for HFIP/lipid ratios of 1:2 and 1:1, by addition of varying concentrations of liposomes to solutions of HFIP (0.09 M) in D<sub>2</sub>O containing NaF (0.3 M) as an internal reference and monitoring the intensity of the <sup>19</sup>F signal of HFIP by NMR at 376 MHz using a Varian Mercury-400 spectrometer. The intensity of the <sup>19</sup>F signal arising from the free HFIP was

measured as a function of lipid concentration with the intensity of the  $F^-$  signal used as a reference. Experiments were performed at 20 °C.

#### **IV.2.2.2. Marker release experiments.**

Unilamellar vesicles of EPC encapsulating CF were prepared by evaporating a solution of EPC in  $\text{CHCl}_3$  (1 mg  $\text{ml}^{-1}$ ) to dryness under vacuum to form a thin film and hydrating the film with 1 ml of a solution of CF (35 mM) and NaCl (150 mM) in Tris buffer (10 mM, pH 7.4). The solution was vortexed until complete lipid dispersal had been achieved and then submitted to 5 cycles of freeze-thawing between -195 and 30 °C. The solution was then extruded 10 times through a laser etched polycarbonate membrane (Whatman) with a pore size of 100 nm in diameter using a thermobarrel extruder (Lipex Biomembranes) at a temperature of 30 °C. The EPC liposome solution was then passed through a sephadex G10 column (Pharmacia PD10) equilibrated with an isotonic solution of NaCl (150 mM) in Tris buffer (10mM, pH 7.4). The ionic strength of the buffers were measured using a cryoscopic osmometer (Osmomat 030) and adjusted by addition of NaCl. Fluorescence experiments were performed immediately after CF-liposome preparation in Tris (10 mM)-NaCl (150 mM) buffer (pH 7.4) at a lipid concentration of 0.05 mg  $\text{ml}^{-1}$ . Fluorescence emission was measured at 518 nm following excitation at 491 nm using a Spex Fluorolog SpectrACQ instrument. Emission and excitation slit widths were both set at 1 mm.

#### **IV.2.2.3. Differential Scanning Calorimetry, DSC.**

DMPC (50 mg) dissolved in  $\text{CHCl}_3$  (1 ml), was dried on a rotary evaporator to a thin film and stored under vacuum for at least 3 hours to ensure complete removal of solvent. The DMPC film was hydrated with 200  $\mu\text{L}$  of HPLC grade water and vortexed for 30 mins to ensure all the lipid was dispersed. The lipid suspension was submitted to 5 cycles of freeze-thawing and divided into 10  $\mu\text{L}$  aliquots which were thoroughly mixed with HFIP at concentrations up to 0.05 M. The HFIP-DMPC samples were sealed in aluminum pans and weighed. Each sample was subjected to repeated heating/cooling cycles and scanned a minimum of 3 times to

allow for equilibration on a Perkin Elmer Pyris 1 differential scanning calorimeter (DSC),. The scanning temperature range was between 4 °C and 30 °C at a rate of 2 °C min<sup>-1</sup>. Data was processed using the software Origin (Microcal, version 6).

#### **IV.2.2.4. Small Angle X-ray Scattering, SAXS.**

Multilamellar vesicles of DMPC and DOPC were prepared, by the method detailed above (section IV.2.2.3) for the DSC experiments, at a lipid concentration of 100 mg ml<sup>-1</sup> in pure water.

HFIP was added to the MLV suspension over a range of concentrations up to 0.04 M. and then thoroughly mixed for about 15 mins before any measurements were taken. Samples were injected into a quartz capillary with a micro syringe and placed in the sample holder in the path of the beam. The beam path was evacuated (vacuum pump) and the position of the sample was optimised by measuring the intensity of scattered transmission (using a glassy carbon) through the sample. Scattering data for each of the samples were collected for one hour at 20 °C on a NanoStar (Anton Paar, Graz) distributed by Bruker SAXS. The X-ray source was a Kristalloflex 760 generator (Cu K<sub>α</sub>, 0.3 x 0.3 mm<sup>2</sup> source point, operated at 40 Kv and 35 mA) and the detector was a 2-D Position-Sensitive gas Detector (PSD). The path length from the X-ray source and sample to the detector was set at 64 cm and the program Origin (Microcal, version 6) was used to analyze peak areas.

#### **IV.2.2.5. Monolayer experiments.**

The experiment was carried out on a Nima Langmuir film balance Type 601 (programme Nima 516) with a total area of 540 cm<sup>2</sup>. The instrument was placed on a granite slab and the Teflon trough was filled with a HFIP/ultra pure water subphase with a HFIP content up to 4 % (v/v). The HFIP and water were thoroughly mixed before being poured into the trough and pressure-area isotherms were obtained for each subphase, prior to monolayer formation, to check for impurities (a flat isotherm corresponding to a clean surface).



Monolayers were prepared by drop wise addition of a  $1 \text{ mg ml}^{-1}$  solution of lipid in chloroform to the subphase surface. After a period of 15 min following spreading, Pressure-Area Isotherms were obtained by compression of the monolayer at a barrier speed of  $50 \text{ cm}^2 \text{ min}^{-1}$ .

#### **IV.2.2.6. Light Scattering Analysis.**

Unilamellar vesicles of DMPC and DOPC were prepared by evaporating a lipid solution in  $\text{CHCl}_3$  ( $1 \text{ mg ml}^{-1}$ ) to dryness under vacuum to form a thin film. The film was then hydrated with pure water and vortexed until complete lipid dispersal had been achieved. The lipid suspension was submitted to 5 cycles of freeze-thawing between  $-195$  and  $30^\circ\text{C}$  and then extruded 10 times through a laser etched polycarbonate membrane (Whatman) with a pore size of  $100 \text{ nm}$  in diameter using a thermobarrel extruder (Lipex Biomembranes) at a temperature of  $30^\circ\text{C}$ .

Size measurements on lipid/HFIP systems were performed at a final lipid concentration of  $2 \text{ mM}$  and HFIP concentrations up to  $0.3 \text{ M}$ . Size measurements on HFIP dispersions in water were performed at concentrations up to  $0.57 \text{ M}$ . All experiments were carried out in duplicate, at  $25^\circ\text{C}$  on a Zeta Plus potential analyzer (Brookhaven Instrument Corp.), with a wavelength of  $658 \text{ nm}$  and a scattering angle of  $90^\circ$ .

#### **IV.2.2.7. Transmission Electron Microscopy.**

Unilamellar vesicles of DMPC were prepared at a lipid concentration of  $0.37 \text{ mg ml}^{-1}$ , using the method described above (section IV.2.2.6) for size measurements. DMPC liposomes were pre-mixed with HFIP at concentrations up to  $0.38 \text{ M}$  and spotted either immediately or after a 30 min mixing period, on to a carbon coated copper grid covered with a Formvar layer. After a period of 30 seconds, any excess lipid-HFIP solution was drawn off from the edge of the grid using blotting paper and then a droplet of a  $1\%$  uranyl acetate solution was deposited on to the still wet grid, with any excess solution again drawn off after 30 seconds.

The samples were observed by TEM using a Philips 400 Transmission Electron Microscope at an accelerating voltage of 80 kV. Images were recorded photographically using Kodak 4883 film.

Scanning Electron Microscopy (Hitachi S-5200 FEG), operating at an accelerating voltage of 30 KV, was also used to image samples prepared for TEM.

### IV.3. References.

- 
- 1 A. Cammers-Goodwin, T. J. Allen, S. L. Oslick, K. F. McClure, J. H. Lee and D. S. Kemp, *J. Am. Chem. Soc.*, **118**, 1996, 3082-3090.
  - 2 M. P. Krafft and J. G. Riess, *Biochimie*, **80**, 489-514.
  - 3 M. Fioroni, K. Burger, A. E. Mark and D. Roccatano, *J. Phys. Chem. B*, **105**, 2001, 10967-10975.
  - 4 S M. Ennaceur and J. M. Sanderson, *Langmuir*, **21**, 2005, 552-561.
  - 5 C. Trandum, P. Westh, K. Jorgensen and O. G. Mouritsen, *J. Phys. Chem. B*, **103**, 1999, 4751-4756.
  - 6 E. van den Brink-van der Laan, V. Chupin, J. A. Killian and B. de Kruijff, *Biochemistry*, **43**, 2004, 5937-5942.
  - 7 J. M. Sanderson and A. D. Ward, *Chem. Commun.*, 2004, 1120-1121.
  - 8 K. Verschueren, *Handbook of Environmental Data on Organic Chemicals*, 3<sup>rd</sup> ed.; John Wiley and Sons, New York, 1996.
  - 9 H. Heerklotz, *J. Phys.: Condens. Matter*, **16**, 2004, R441-R467.
  - 10 S. E. Feller, C. A. Brown, D. T. Nizza and K. Gawrisch, *Biophys. J.*, **82**, 2002, 1396-1404.
  - 11 L. L. Holte, and K. Gawrisch, *Biochemistry*, **36**, 1997, 4669-4674.
  - 12 H. Rottenberg, *Biochemistry*, **31**, 1992, 9473-9481.

- 
- 13 E. S. Rowe, *Biochim. Biophys. Acta*, **813**, 1985, 321-330.
- 14 T. J. McIntosh, H. Lin, S. Li, and C. Huang, *Biochim. Biophys. Acta*, **1510**, 2001, 219-230.
- 15 X. Wang and P. J. Quinn, *Biochim. Biophys. Acta*, **1509**, 2000, 361-372.
- 16 M. Polikandritou Lambros, E. Sheu, J.S. Lin and H. A. Pereira, *Biochim. Biophys. Acta*, **1329**, 1997, 285-290.
- 17 Y. Kobayashi and K. Fukada, *Biochim. Biophys. Acta*, **1371**, 1998, 363-370.
- 18 X. Wang and P. J. Quinn, *Biochim. Biophys. Acta*, **80**, 1999, 91-99.
- 19 X. Wang and P. J. Quinn, *Eur. J. Biochem.*, **264**, 1999, 1-8.
- 20 O. Glatter and O. Kratky, *Small Angle X-ray Scattering*, Academic press INC. (London) LTD, 1982.
- 22 S. Tristram-Nagle and J. F. Nagle, *Chem. Phys. Lipids*, **127**, 2004, 3-14.
- 23 M. C. Petty, *Langmuir Blodgett films*, Cambridge University Press, 1996.
- 24 R. Magnet-Dana, *Biochim. Biophys. Acta*, **1462**, 1999, 109-140.
- 25 G. L. Gaines, JR., *Insoluble Monolayers at liquid-gas interfaces*, Interscience publishers, John Wiley & Sons, Inc., 1966.
- 26 T. Baumgart and A. Offenhausser, *Langmuir*, **18**, 2002, 5899-5908.
- 27 A. V. Hughes, S. J. Roser, M. Gerstenberg, A. Goldar, B. Stidder, R. Feidenhans and J. Bradshaw, *Langmuir*, **18**, 2002, 8161-8171.

- 
- 28 A. V. Hughes, A. Goldar, M. Gerstenberg, S. J. Roser, and J. Bradshaw, *Phys. Chem. Chem. Phys.*, **4**, 2002, 2371-2378.
- 29 W.W. Shen, S.G. Boxer, W. Knoll and C.W. Frank, *Biomacromolecules*, **2**, 2001, 70-79.
- 30 M. Leonard-Latou, R. M. Morelis and P. R. Coulet, *Langmuir*, **12**, 1996, 4797-4802.
- 31 Y. Chunbo, W. Ying, Y. Xiaomin, L. Zuhong and L. Juzheng, *Applied Surface Science*, **103**, 1996, 531-534.
- 32 A. F. Mingotaud, L. K. Mingotaud and L. K. Patterson, *Handbook of monolayers*, San Diego, Academic press, 1993.
- 33 N. Wilke and A. M. Baruzzi, *J. Electroanal. Chem.*, **537**, 2002, 67-76.
- 34 M. F. Mora, N. Wilke and A. M. Baruzzi, *Langmuir*, **19**, 2003, 6876-6880.
- 35 V. L. Shapolavalov, E. A. Kotova, T. I. Rokitskaya and Y. N. Antonenko, *Biophys. J.*, **77**, 1999, 299-305.
- 36 D. Huster, G. Paasche, U. Dietrich, O. Zschorning, T. Gutberlet, K. Gawrisch and K. Arnold, *Biophys. J.*, **77**, 1999, 879-887.
- 37 N. Wilke and A. M. Baruzzi, *Langmuir*, **17**, 2001, 3980-3986.
- 38 T. James; K. Nowotavski; W. I. Gruszecki and T. Janas, *Acta Biochimica Polonica*, **47**, 2003, 661-673.
- 39 C. N. N'soukpoe, J. Sielewiesiuk, R. M. Leblanc, R. A. Bone and J. T. Landrum, *Biochim. Biophys. Acta*, **940**, 1988, 255-265.

- 
- 40 N. Dos Santos, K. A. Cox, C. A. McKenzie, F. van Baarda, R. C. Gallagher, G. Karlsson, K. Edwards, L. D. Mayer, C. Allen and M. B. Bally, *Biochim. Biophys. Acta*, **1661**, 2004, 47-60.
- 41 T. Janas, T. Janas and K. Walinska, *J. Membrane Biol.* **177**, 2001, 256-271.
- 42 K. Gast, D. Zirwer, M. Muller-Frohne and G. Damaschun, *Protein Sci.*, **8**, 1999, 625-634.
- 43 K. Iwasaki and T. Fujiyama, *J. Phys. Chem.*, **81**, 1977, 1908-1912.
- 44 Material safety data sheet for hexafluoroisopropanol (supplier MSDS) from Apollo scientific.

## Chapter V

### General conclusion.

**V.1. Chapter II.** A series of amphiphilic cyclic peptides were designed with the view of developing model  $\beta$ -sheet systems, which could integrate into lipid membranes and disrupt the lipid bilayer through pore formation.

The cyclic peptide synthesis was achieved using solid phase Fmoc chemistry with *in situ* cyclisation in a fully automated peptide synthesizer. The peptides were purified using RP-HPLC and analysed by MALDI mass spectrometry following optimization of the solvent systems using the fluorinated alcohol, hexafluoroisopropanol.

The cyclic amphiphilic peptides were examined using a wide range of analytical techniques in order to establish whether the cyclic amphiphilic peptides had a propensity to adopt  $\beta$ -sheet structures in phospholipid bilayers and to gain some understanding of their behaviour under different environments, aqueous and lipidic.

Circular Dichroism, which was used to examine the amphiphilic cyclic peptide structure in a range of environments, clearly demonstrated that the peptide had a propensity to adopt  $\beta$ -sheet structures in buffer-salt solutions containing over 30 % TFE and in EPC/buffer-salt solutions. The structural change from random coil to  $\beta$ -sheet is also a confirmation of the cyclic amphiphilic peptide affinity for lipid media and of its ability to form a polymeric structure in membranes.

Linear Dichroism confirmed the predisposition of the cyclic amphiphilic peptide for a  $\beta$ -sheet type structure and also provided strong evidence of peptide insertion in to phospholipid membranes, together with the direction of insertion of the peptide backbone relative to the normal of the lipid membrane. The cyclic peptide was shown to interact with phospholipid membranes by inserting into the bilayer with the peptide backbone in a perpendicular orientation to the plane of the membrane. This orientation suggests that the peptide could form a  $\beta$ -barrel type structure in



phospholipid membranes similarly to those formed by prokaryotic outer membrane proteins.

Differential Scanning Calorimetry explored the effect of the amphiphilic peptide on the cooperativity of the phospholipid phase transition. The cyclic peptide, at peptide to lipid ratios as low as 0.02, abolished the pre-transition and affected both the temperature and the enthalpy change of the main transition of DMPC and DPPC lipid bilayers. This DSC study has provided strong support for the insertion of the cyclic amphiphilic peptide into phospholipid membranes and gave comparable results to DSC investigations carried out on another cyclic  $\beta$ -sheet peptide, gramicidin S with DMPC membranes.

Transmission Electron Microscopy showed that one of the cyclic amphiphilic peptides appeared to form amyloid type fibres on precipitation from a 30 % solution of the fluorinated alcohol, HFIP in water. The fibres and bundles of twisted fibres, which were similar in size and morphology to those observed in prion diseases, are thought to be readily formed by  $\beta$ -sheet proteins that have a tendency to aggregate and do not fold rapidly to adopt their stable conformation.

**V.2. Chapter III.** A natural  $\beta$ -sheet forming protein, the C-terminal domain of the autotransporter protein BrKA from *Bordetella pertussis* was overexpressed to provide a comparison for the model  $\beta$ -sheet peptides.

The aim of this study was to gain further insight into the interactions between integral membrane proteins and phospholipid membranes, as well as to determine the protein structure by attempting to grow highly ordered 2D arrays of the protein in phospholipid membranes for structural analysis by TEM and AFM.

Although a better understanding of the interactions of the BrKA C-terminal protein with phospholipid membranes has been achieved, there are still a considerable range of options to explore, especially with regards to optimization of the protein folding and 2D crystallisation processes.

**V.3. Chapter IV.** An investigation of the effects of hexafluoroisopropanol on phospholipid membranes should lead to a more efficient use of its properties, in particular with the synthetic amphiphilic cyclic peptides, discussed in chapter II of this thesis and in general to a greater understanding of the interactions of this fluorinated alcohol with the cell membrane; interactions of small molecules with the cell membrane are of considerable importance for a number of biological applications, such as drug and metabolite uptake or passive transport across the membrane.

The effect of HFIP on the integrity, stability, packing, size and morphology of phospholipid membranes has been investigated using a wide range of experimental techniques, including  $^{19}\text{F}$  NMR; marker release experiments on EPC unilamellar vesicles containing carboxyfluorescein; Differential Scanning Calorimetry and Small Angle X-ray Scattering; Monolayer experiments, Transmission Electron Microscopy and Light Scattering analysis.

HFIP was shown to induced perturbations in saturated DMPC membranes (DSC and SAXS data), which are believed to arise through localized concentration of the HFIP molecules in the membrane; this would effectively produce areas richer and others poorer in HFIP (SAXS and Monolayer experiments). The membrane, which is then believed to become unstable under the strain produced by localized high concentrations of HFIP (SAXS data), would appear to undergo a rearrangement resulting in lose of material in the form of mixed HFIP-lipid micelles (Light Scattering and TEM experiments) to produce a more stable membrane, poorer in HFIP.

Further investigations of a range of fluorinated and non fluorinated bulky alcohols on phospholipid membranes would add considerably to this work and could possibly provide some support for this proposed mechanism of HFIP interaction with DMPC membranes.

